ATMOSPHERIC FLOW FIELDS
Theory, Numerical Methods and Software Tools

Editors
R. Cocci Grifoni, G. Latini and S. Tascini

Bentham e Books

ATMOSPHERIC FLOW FIELDS:
Theory, Numerical Methods and Software Tools

Edited by

G. Latini

Department of Energetics
Polytechnic University of Marche
Italy

R. Cocci Grifoni and S. Tascini

School of Architecture and Design "E. Vittoria"
Camerino University, Ascoli Piceno,
Italy

CONTENTS

CHAPTERS

Appendix

FOREWORD

The emissions of polluting agents in the atmosphere due to anthropogenic activities are a global threat both to the environment and to the ecosystems. From this point of view, the meteorological variables play a key role, as they can trigger forcing effects able to either worsen or improve the quality of the air.

The EC has ratified the UN Convention on climate changes and consequently acceded to the Kyoto Protocol on a reduction of polluting gases. Under these treaties the international Community has committed to comply with those policies necessary to reduce atmospheric emissions.

These policies mainly provide for a reduction of polluting emissions deriving from the use of fossil fuels *versus* incentive measures for renewable energy sources.

Monitoring the flows of polluting gases released by the anthropogenic systems has become an urgent priority in order to disperse and diffuse those gases according to the environment variables and geomorphologic characteristics of an area. In this sense, the use of mathematical models able to forecast phenomena of polluting gases release and dispersion requires the skilful utilization of atmospheric data.

The whole of harmful effects due to the action of unbalancing polluting (alteration) factors affecting the lower atmosphere, and therefore living beings, are a consequence of the byproducts of human activities dispersing into the air (factories, car exhausts, *etc.*), and natural components. A shared commitment to both reduce its causes and gain a detailed understanding of the phenomena and processes that determine an excess of polluting agents is therefore essential in order to control their impact. To forecast the atmospheric polluting phenomena it is necessary a knowledge of the dynamics of the lower part of the atmosphere where human activities take place – specifically the Planetary Boundary Layer (PBL), the interface between the surface and the free atmosphere, and therefore under the direct influence of the processes at ground level.

The issue addressed in this text is to attentively analyze the atmospheric flow fields within the PBL, and the possible influences of certain meteorological phenomena in

the presence of polluting incidents. It is common knowledge that meteorology plays a key role in dispersing the atmospheric pollutants; specifically, the development of certain mesoscale circulation phenomena can jeopardize the quality of the air in the regions involved, due to their reduced diluting capacity.

Moreover, the characteristics of a specific region make the analysis of the diffusive phenomena, and the respective atmospheric dynamics, even more complex. The presence of the sea in the Italian regions surveyed - valley-coastal areas or with a complex orography, is doubtlessly the characteristic that influences most meteorology in the areas surveyed.

This volume features a collection of useful and interesting theoretic and experimental contributions on atmospheric flows through anemological, energetic and air quality assessments regarding complex regions. These contributions acknowledge the importance of both the dispersive and diffusive phenomena in the atmosphere, but also the possible development of renewable energy sources thanks to a thorough investigation on atmospheric dynamics.

The challenging relation between energy and environment has always been emblematic: the preservation of the environment, life standards, and the very salvation of our planet have been growing momentum among the interests to be protected, and therefore drawn the line on the importance of development, particularly of fossil energy as a primary source for development itself.

The sustainable development formula has therefore been drawn up to match the development with the environment demands. This formula is partially ambiguous since it still presupposes a priority of a value – the development, *vis-à-vis* the environment is considered as a mere limit. The solution of this deep dichotomy can only come through a thorough knowledge of the meteorologic-climatic aspects and the energetic potentialities of a specific region, so that their advantageous use aiming at improving the difficult relation between energy and environment can be achieved.

Marco Pacetti

Rector of the Polytechnic University of Marche

Italy

PREFACE

This volume is a collection of lectures on practical and theoretical aspects of atmospheric flows over flat and complex terrain with applications to air pollution and wind energy.

The lectures are the result of ten years of research on the dynamical behaviour of the Planetary Boundary Layer that has a direct effect on the air quality and on the boundary layer parameterization schemes used in local, regional and global models.

It is divided into two main parts. The first, which comprises three chapters, presents the structure of the Planetary Boundary Layer with emphasis in the region adjacent to the ground, the Synoptic Mesoscale Meteorology and Coastal Air Pollution and complex terrain Meteorology. The second, Chaps. 5 to 8, discusses on the planetary boundary-layer (PBL) parameterization that is a key issue for the definition of initial wind flow fields in diagnostic models, meteorological prognostic models (RAMS, MM5, WRF), the estimation of the lower atmospheric turbulence parameters by remote sensing technique, the fundamentals of Air Pollution Mathematical Modeling, an analytical solution for the nonstationary two-dimensional advection–diffusion equation to simulate the pollutant dispersion in the planetary boundary layer (the GILTT solution of the advection–diffusion equation), the selected case studies of complex terrain meteorology and an estimation of the lower atmospheric turbulence parameters by remote sensing tools.

In the appendix, will be found a complete list of available databases and software will be followed.

The unique feature of this eBook is that beyond the theoretical treatments of the analytical and numerical techniques, it includes a number of tools where the techniques presented in the main part are implemented and can be run by the reader. These practical tools can be used to easily test selected mathematical formulation or performing a swift sensitivity analysis.

The first one, Hmix, aims to a mixing height evaluation in convective condition over land, based on the Gryning-Batcharova approach. The second tool (RD) is dedicated to the Representative Day identification. Based on the Tirabassi *et al.* approach, the representative day is constituted by the actual data of the day, in the considered period, where the sum of the mean-square differences between its monitored quantities, averaged within each hour, and the same quantities for all other days at the same hour is minimized. The third tool (Prometeo) is again around the PBL characterization by elementary measurements at surface level evaluated. Based on operational methods suggested by Holstag and Van Ulden (1983) the tool allows the evaluation of Monin-Obukhov length, fiction velocity and surface heat fluxes.

All the tools will be provided with a Windows GUI and designed with a user-friendly, interactive conception in order to minimize the required computer expertise and to be readily useful to a wider number of users.

G. Latini

Department of Energetics
Polytechnic University of Marche
Italy

R.Cocci Grifoni and S. Tascini

School of Architecture and Design "E. Vittoria"
Camerino University, Ascoli Piceno
Italy

List of Contributors

Giovanni Latini

Department of Energetics, Polytechnic University of Marche, Italy.

Marco Mazzieri

Department of Energetics, Polytechnic University of Marche, Italy.

Marco T. Vilhena

Universidade Federal do Rio Grande do Sul, Porto Alegre (RS), Brasil.

Mariano Pierantozzi

Department of Energetics, Polytechnic University of Marche, Italy.

Renato Ricci

Department of Energetics, Polytechnic University of Marche, Italy.

Roberta Cocci Grifoni

School of Architecture and Design "E. Vittoria", Camerino University, Ascoli Piceno, Italy.

Rosalba D'Onofrio

School of Architecture and Design "E. Vittoria", Camerino University, Ascoli Piceno, Italy.

Simone Tascini

School of Architecture and Design "E. Vittoria", Camerino University, Ascoli Piceno, Italy.

Tiziano Tirabassi

Institute ISAC of CNR, Bologna, Italy.

CHAPTER 1

The Structure of the Atmosphere

Giovanni Latini[1] and Roberta Cocci Grifoni[2,*]

[1]Department of Energetics, Polytechnic University of Marche, Italy and [2]School of Architecture and Design "E. Vittoria", Camerino University, Ascoli Piceno, Italy

Abstract: This first chapter is an introduction that provides all the basic information that the reader will need for a profitable use of the book. It reviews the vertical structure of the atmosphere, the surface-energy budget and concepts of atmospheric stability. The atmosphere is conventionally divided into layers based on the vertical structure of density, pressure and temperature fields. This is an important issue in understanding the dynamics of the middle atmospheric and variations of the main meteorological parameters.

INTRODUCTION

The atmosphere is separated into several distinct layers divided by narrow transition zones. All atmospheric layers are characterized by differences in chemical composition, which cause temperature variations. This explains the major changes in temperature. Being compressible, air is much denser near the surface of the Earth than at higher altitudes.

Temperature varies significantly both horizontally and vertically throughout the atmosphere (as well as temporally). However, despite horizontal temperature variations, the vertical structure of the temperature is qualitatively similar in all places, and it is therefore useful to consider a "representative" temperature profile. Fig. (**1**) shows a typical temperature profile up to about 170 km.

*Address correspondence to Roberta Cocci Grifoni: School of Architecture and Design "E. Vittoria", Camerino University, Ascoli Piceno, Italy; Tel:+39 (0)737 404279; E-mail: roberta.coccigrifoni@unicam.it
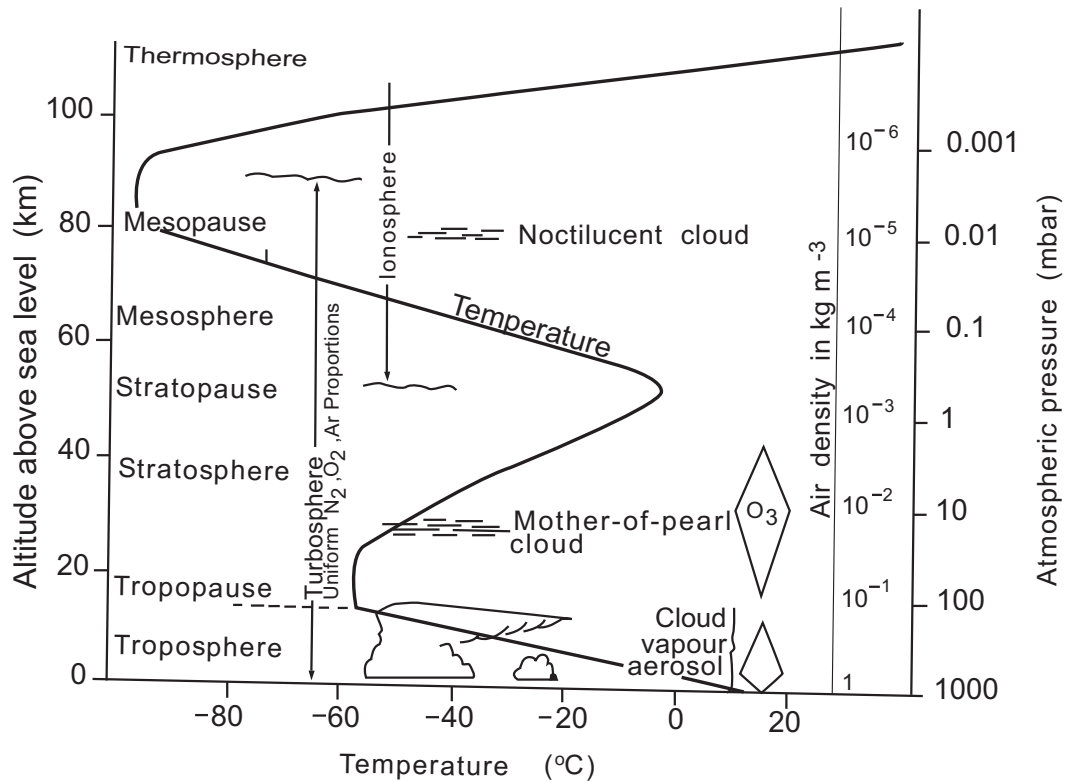
Figure 1: Vertical structure of the atmosphere.

The first layer is the troposphere. It is the atmospheric layer closest to the Earth's surface and its temperature and water vapour composition decrease rapidly with altitude.

The temperature sometimes increases rather than decreases with height in the troposphere. This phenomenon is known as temperature inversion. Temperature inversions limit or prevent the vertical mixing of air. The troposphere is denser than the layers of the atmosphere above it and contains up to 75% of the mass of the atmosphere. It is primarily composed of nitrogen (78%) and oxygen (21%), with only small concentrations of other trace gases. The troposphere also contains 99% of the water vapour in the Earth's atmosphere (Fig. **2**). Water vapour plays a central role in regulating air temperature because it absorbs solar energy and thermal radiation from the surface of our planet. Water vapour concentrations vary with latitudinal position reaching the highest concentrations in the tropics, while decreasing toward the polar regions.

The troposphere is the most variable layer of the atmosphere and it is the layer where air masses, weather fronts, and storms reside and weather occurs. Weather conditions are governed by a number of factors, including solar radiation, atmospheric circulation, water vapour and topography. However, in all cases the underlying driving force is radiant energy from the Sun.

The upper boundary of the troposphere is a narrow zone known as the tropopause, which ranges in height from 8 km near the poles to 18 km above the equator. Air temperature within the tropopause remains constant with increasing altitude.
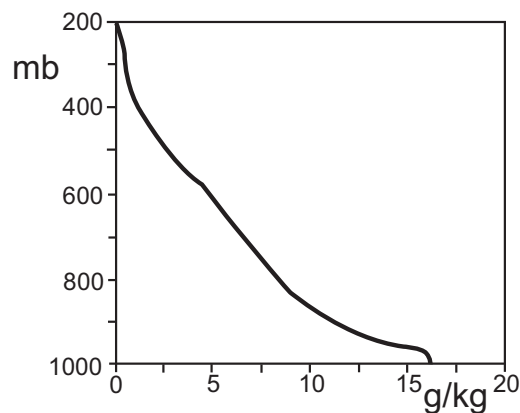
Figure 2: Global average vertical distribution of water vapour [1].

The tropopause acts as a "lid" on the troposphere, preventing air from rising upwards into the stratosphere.

The stratosphere is the second major layer of Earth's atmosphere. It lies between 10 and 50 Km above the planet's surface. The air temperature in the stratosphere remains relatively constant up to an altitude of 25 km. It then increases gradually until it reaches the stratopause. Since air temperature in the stratosphere increases with altitude, it does not allow convection, and instead has a stabilizing effect on atmospheric conditions in the region. In fact, the stability of the stratosphere helps to limit the exchange of mass between the middle atmosphere and the troposphere, since convective motions are inhibited. Due to the low content of water vapour in the stratosphere, ozone (about 90% of the ozone in the atmosphere resides in the stratosphere) is the major regulator of the thermal regime of the stratosphere. Temperature increases with ozone concentrations;

solar energy is converted into kinetic energy when ozone molecules absorb ultraviolet radiation between 0.1 and 0.3μm. At the top of the stratosphere lies the stratopause. Like the tropopause, the stratopause is an isothermal layer that separates the stratosphere from the mesosphere.

The thermosphere is located above the mesosphere, and the temperature in the thermosphere generally increases with altitude reaching 600 to 2000 K depending on solar activity. This increase in temperature is due to the absorption of intense solar radiation by both molecular and atomic oxygen, particles of which are widely separated at this extreme altitude. O_2 as well as CO_2 – the dominant IR emitter at this altitude – are photolyzed by high-energy UV rays, $\lambda < 0.1$ μm, leading to a shortage of polyatomic molecules.Because of this, loss of energy through IR is weak, so the temperature in this region becomes very high (as much as 1000 K). At these altitudes, the atmosphere becomes ionised (the ionosphere), causing the reflection of radio waves, a very important property of the upper atmosphere. The ionosphere is a special part of the atmosphere; it is not a separate layer, but an electrified field of ions and free electrons that forms part of the thermosphere.

The existence of distinct atmospheric layers and some of their properties can be qualitatively explained on the basis of radiative-convective equilibrium.

The simplest model that predicts the existence of a statically stable layer (the stratosphere) above a layer where deep convection occurs (the troposphere) is a grey-body model. This model assumes an atmosphere in radiative equilibrium, transparent to solar radiation but acting as a grey absorber for long-wave terrestrial radiation. Under these conditions, a temperature discontinuity at the surface would be observed; for realistic values of the total optical depth, the lapse rate (*i.e.* the decrease of temperature with height) in the lower atmosphere would also be above the [moist] adiabatic lapse rate, so that convection would occur. The predicted depth of the convective layer increases along with increasing surface temperature. The grey-body model is thus able to predict both the existence of the troposphere and the fact that the altitude of the tropopause increases toward the equator, but it does not predict the observed negative correlation between surface and tropopause temperatures [2]. Models including non-grey-body absorption and

the temperature dependence on water-vapour density in the atmosphere can explain this correlation [3].

## Thermal Structure of the Atmosphere

The temperature profile of the atmosphere reflects a balance between the radiative, convective and dynamical heating/cooling of the surface-atmosphere system. In particular, the vertical profile in the troposphere is the consequence of equilibrium amongst radiative processes involving aerosols, clouds and gases [4], together with the important role played by dynamical motions and moist convection [5-7]. In fact, the moist convective processes that are a characteristic feature of the troposphere include the displacement of large amounts of heat due to water evaporation and condensation. Another important difference between the troposphere and stratosphere is that the stratosphere is characterized by weak vertical motions, while vertical motions are stronger in the troposphere [8].

The thermal structure of the atmosphere can be depicted considering the radiative-convective balance. Most of the solar radiation is absorbed at the surface; the rest is absorbed by the atmosphere.

If radiative processes alone were considered, these would generate a surface temperature higher than it actually is [4]. This would happen because the atmosphere is relatively transparent to the Sun's radiation, resulting in strong heating of the surface accompanied by net radiative cooling of the atmosphere [9]. Nonetheless, the resulting convective motions remove excess heating from the surface as well as sensible and latent heat [10]. As air parcels rise they cool due to expansion, leading to a decrease in temperature with height. The lapse rate for a dry atmosphere–without moist processes and air rising rapidly enough to be unaffected by other heating/cooling sources, is close to 10ºC/km [8].

Interestingly, the lapse rate for moist air is lower than the dry adiabatic rate, because condensation from vapour to liquid or solid forms of water adds heat to the atmosphere, thus modulating the rate at which the temperature decreases with increasing altitude. Wet lapse rates can be as low as 4ºC/km in very humid atmospheres [10].

Fig. (**3**) shows that the dry lapse rate is very high. When temperatures reach the dew point (the temperature at which relative humidity is 100%), condensation takes place and a wet adiabatic rate trend (-6°C/Km) is followed.
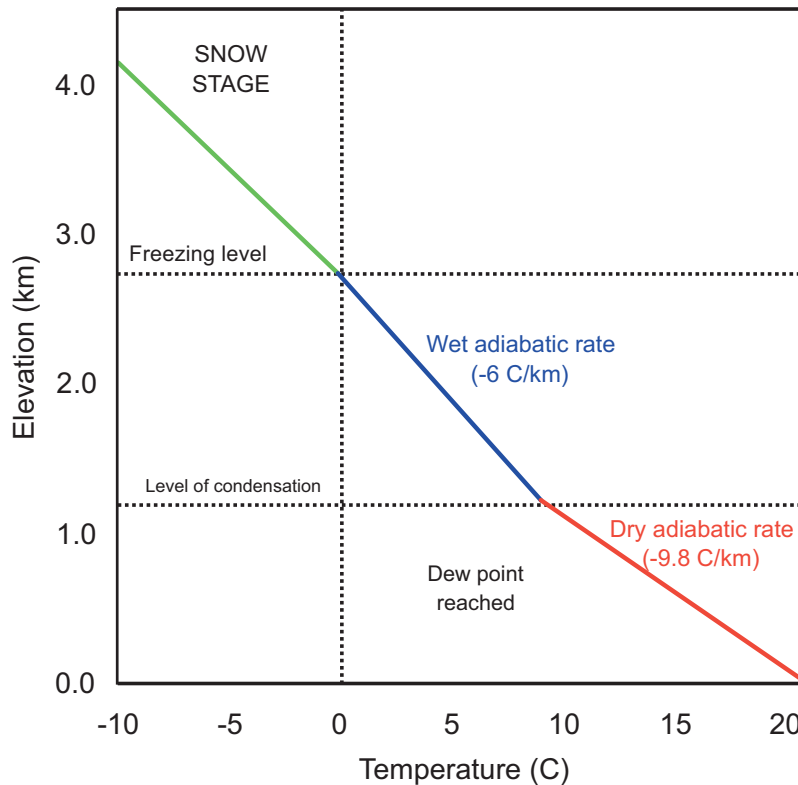
Figure 3: Adiabatic lapse rates, adopted from A.N. Strahler [12].

There are five types of lapse rate:

➢ The environmental lapse rate–(ELR) refers to the actual change in temperature with altitude for the stationary atmosphere. Sometimes also called the atmospheric lapse rate, it is usually considered to be a decrease in temperature with height.

➢ The adiabatic lapse rate (ALR) which refers to the change in temperature of air particles as they move upwards.

➢ The dry adiabatic lapse rate (DALR)is the rate at which a rising parcel of unsaturated air, such as a thermal, changes temperature.

> ➢ The moist adiabatic lapse rate (MALR), or saturated adiabatic lapse rate (SALR)varies strongly with the moisture content and weakly with pressure.

> ➢ The dew point lapse rate (DPLR)is the rate of change of the dew point temperature in an unsaturated rising air parcel.

The following Fig. (**4**) shows, in a very simple way, the lapse rates outlined above, the inversions, and the lifting condensation level (LCL), defined as the level at which a parcel of moist air lifted dry-adiabatically would become saturated.
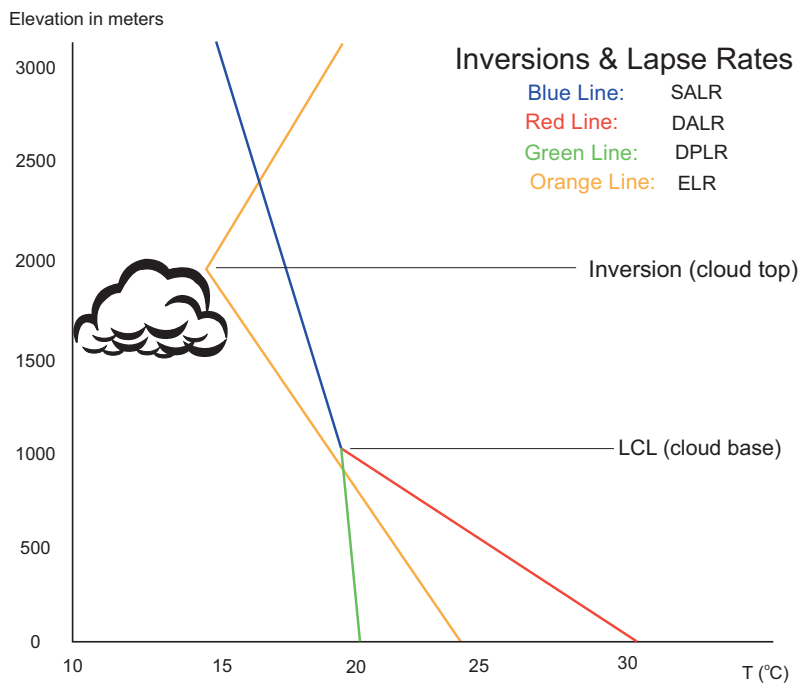
Figure 4: Lapse rates.

Real thermal profiles are more complex than the above due to the superposition of large-scale circulation and convection-cloud physical interactions [11]. For example, subtropical regions can be defined as the combination of a surface mixed layer with a trade wind boundary layer above which is the free troposphere. A thermal inversion characterizes each of the boundary layers, so that it tends to isolate the region from the layer above [13]. As stated by Hurrel [8], this denotes

limitations in assuming nominal lapse rate values uniformly from the surface to the tropopause. In the tropical upper troposphere, moisture- and cloud-related features related to convection are important aspects of the thermal profile.

In addition, interactions between radiation, moist convection, and dynamical motions determine the quantitative rate at which temperature decreases with height at any location. Large-scale dynamical mechanisms tend to result in more spatially uniform temperatures (on mean monthly and longer time scales) above the boundary layer, and over horizontal scales (Rossby radius; [14]) that vary from the planetary scale near the equator, to a couple of thousand kilometres at middle latitudes, to a few hundred kilometres near the poles. Major circulation patterns in the atmosphere, such as the Hadley and Walker circulations [5, 14], play a key role in the atmospheric energy balance in the tropics and subtropics (~30 degrees in latitude), and this crucially affects the thermal structure in those regions [15]. Lower latitudes are characterized by vertical coherence in the temperature structure, with variations in temperature of opposite signs below and above the tropopause associated with upward motion and subsidence, respectively [16]. The sense of the radiative-convective-dynamical balance above, together with the requirement for radiative balance at the top of the atmosphere (namely, equilibrium conditions wherein the net solar energy absorbed by the Earth's climate system must be balanced by the infrared radiation emitted by the Earth), can help illustrate the significance of long-lived infrared-absorbing gases in the global atmosphere.

Since specific humidity is strongly related to temperature, it is expected to rise with surface warming. The increased moisture content in the atmosphere amplifies the initial radiative heating due to the increase in greenhouse gases [9, 17]. The re-establishment of thermal equilibrium in the climate system involves the communication of the added heat input to the troposphere and the surface, leading to surface warming [4, 18]. From the preceding discussion, the lapse rate can be expected to decrease with the resultant increase in humidity, and also to depend on the resultant changes in atmospheric circulation. In general, warming occurs such that temperature changes aloft exceed those at the surface. As a consequence, the characteristic infrared emission level of the planet is shifted to a higher altitude in the atmosphere.

Having described the observed T profile, it is important to continue by discussing the associated pressure, p, and density, ρ, profiles.

Vertical Structure of the Pressure

Starting from the equation of hydrostatic equilibrium, Eq. (1) is applied to a static atmosphere, where pressure adjusts to balance gravity through a gradient force,

$$\frac{\partial p}{\partial z} + \rho g = 0 \tag{1}$$

it is common knowledge that Eq. (1) describes how pressure must decrease with height. Note that, since p must vanish as $z \to \infty$, we can obtain Eq. (2), which gives the pressure at any height

$$p(z) = g \int_0^\infty \rho \, dz \tag{2}$$

The only significant assumption made in the derivation of Eq. (1) was to ignore any vertical acceleration. This can be considered a good approximation under almost all circumstances (in the atmosphere and in the sea). On the contrary, it becomes uncertain in very energetic small-scale systems.

Using the equation of state of air, Eq. (1) can be rewritten as:

$$\frac{\partial p}{\partial z} = -\frac{gp}{RT} \tag{3}$$

If T is a constant value, T_0, we obtain the following equation:

$$\frac{\partial p}{\partial z} = -\frac{gp}{RT} = -\frac{p}{H} \tag{4}$$

where the scale height H is a constant with the value

$$H = \frac{RT_0}{g} \tag{5}$$

The solution for p is as follows, noting that by definition, $p = p_0$ and $z = 0$ at the surface,

$$p(z) = p_0 \exp\left(-\frac{z}{H}\right)$$

(6)

Alternatively,

$$z = H \ln\left(\frac{p_0}{p}\right)$$

(7)

Thus pressure decreases exponentially with increasing height.

If the temperature, T, is not constant, it is still possible to define a local scale height, $H(z) = RT(z)$,

$$H(z) = \frac{RT(z)}{g}$$

(8)

such that

$$\frac{\partial p}{\partial z} = -\frac{p}{H(z)}$$

(9)

or, written equivalently in terms of $\ln p$,

$$\frac{\partial \ln p}{\partial z} = -\frac{1}{H(z)}$$

(10)

whence the following is obtained:

$$p_z = p_0 \exp\left(-\int_0^z \frac{dz'}{H(z')}\right)$$

(11)

If $H(z) = H$, Eq. (11) reduces to Eq. (6). In fact, notwithstanding its simplicity, the isothermal result, Eq. (6), describes the real situation well; agreement between the two is generally good [1].

Vertical Structure of the Density

Air density is a function of space and time, where the vertical height dependence in particular is essential for questions concerning air pollutant diffusion.

Considering the case of an isothermal process, the density profile follows from Eq. (6):

$$\rho(z) = \frac{p_s}{RT_0} exp(-\frac{z}{H})$$

(12)

Thus, in this case, density follows the same exponential behaviour as the pressure. One consequence of Eq. (12) is that about 80% of the mass of the atmosphere lies below 10 Km [1].

For a non-isothermal process with temperature *T(z)*, it follows from Eq. (11) that

$$\rho(z) = \frac{p_s}{RT(z)} exp(-\int_0^z \frac{dz'}{H(z')})$$

(13)

For a polytropic atmosphere, *i.e.*, a model atmosphere in hydrostatic equilibrium with a constant nonzero lapse rate, the general (empirical) formulation is:

$$\frac{p}{p_0} = \frac{\rho^{n'}}{\rho_0^{n'}} = const.$$

(13a)

where *n'* is the polytropic exponent.

Using Eq. (13a) and integrating the fundamental hydrostatic equilibrium equation (1.1), the density behaviour in the isentropic atmosphere is described by:

$$\rho(z) = \rho_0(1 - \frac{n'-1}{n'}\frac{z}{H_0})^{\frac{1}{n'-1}}$$

(13b)

where H_0 is the height of the homogeneous atmosphere.

For *n'* = 1.235 and H_0 = 8434 meters, the previous equation becomes

$$\rho(z) = \rho_0(1 - 0.0000226z)^{4.25532}$$

$$(13c)$$

Another approach is the following frequently used formula [19]:

$$\rho(z) = 1.2255 - 1.1743 \cdot 10^{-4} z + 4.0267 \cdot 10^{-9} z^2$$

$$(13d)$$

Atmospheric Stability

In order to understand atmospheric stability and its role in pollution diffusion, it is important to know the mechanics of the atmosphere in relation to vertical motion.

Atmospheric stability can be defined as the "resistance" of the atmosphere to vertical motion; in fact, it is a measure of the possibility of buoyant motion.

With θ as the potential temperature and z as the height, the potential temperature is expressed as:

$$\theta = T(\frac{p_0}{p})^k$$

$$(14)$$

where $k = \dfrac{R}{c_p}$, with R as the gas constant and c_p the specific heat at constant pressure, p is the pressure, and p_0 is the pressure at reference height. For any pair of pressure and temperature values there is a corresponding value of potential temperature.

In an adiabatic atmosphere, where all processes are isentropic processes, the variation of potential temperature can be expressed as:

$$\frac{\partial \theta}{\partial z} = \left(\frac{p_0}{p}\right)^k \frac{\partial T}{\partial z} + T \frac{\partial}{\partial z}\left(\frac{p_0}{p}\right)^k$$

$$(15)$$

$$= \left(\frac{p_0}{p}\right)^k \left(\frac{\partial T}{\partial z} - \frac{kT}{p}\frac{\partial p}{\partial z}\right)$$

$$= \frac{\theta}{T}\left(\frac{\partial T}{\partial z} + \frac{Mg}{C_p}\right)$$

$$(16)$$

This is a good approximation for short-term, large-scale atmospheric motions.

We define the *T*-gradient as:

$$\gamma = -\frac{\partial T}{\partial z}$$

(17)

and the adiabatic lapse rate

$$\Gamma = \frac{Mg}{C_p} \, (= 9.8k \,/\, km)$$

(18)

Replacing these *T*-gradient and adiabatic lapse rate expressions in Eq. 16, we have

$$\frac{\partial \theta}{\partial z} = \frac{\theta}{T}(\Gamma - \gamma)$$

(19)

The vertical gradient of potential temperature gives a measure of the atmosphere's static stability, and, as previously stated, of its resistance to vertical motion.

If we consider a parcel of mass m_p within some surrounding air, the buoyancy force is given by:

$$F = m_p \frac{d^2 z}{dt^2} = (m - m_p)g$$

$$\frac{d^2 z}{dt^2} = \frac{\rho - \rho_p}{\rho_p} g$$

(20)

and

$$\frac{d^2 z}{dt^2} = \frac{T_p - T}{T} g$$

(21)

$$\frac{d^2 z}{dt^2} = \frac{(\theta_p - \theta)}{\theta} g$$

(22)

Thus, if $\partial\theta/\partial z < 0$ the stratification is statically unstable; when $\partial\theta/\partial z > 0$ it is statically stable.

The flow responds to this instability with convection motions. Air rises to the top of the unstable layer and consequently stabilizes the fluid [20].

The degree of stability or instability in an atmospheric layer is established by comparing its temperature lapse rate to the proper adiabatic rate. For example, a temperature lapse rate lower than the dry-adiabatic rate for an unsaturated parcel is considered stable because vertical motion within the parcel is discouraged. Conversely, a lapse rate higher than the dry-adiabatic rate triggers vertical motion and it is unstable. In fact, the stability of the air under vertical displacement is determined by a small change in the elevation of an air parcel.

To analyse this behaviour carefully, it is appropriate to quantify the vertical gradient of potential temperature in terms of the square of the Brunt-Väisälä frequency.

Considering a vertical displacement,

$$Z = z - z_0 = \delta z \tag{23}$$

the potential temperature can be rewritten as:

$$\theta(z + \delta z) = \theta(z_0) + \frac{\partial\theta}{\partial z}\delta z \tag{24}$$

and Eq. (22) becomes:

$$\frac{d^2 Z}{dt^2} = -\frac{g}{\theta_0}\frac{\partial\theta}{\partial z}Z \tag{25}$$

The quantity $\dfrac{g}{\theta_0}\dfrac{\partial\theta}{\partial z}$ is usually denoted by N^2, giving

$$\frac{d^2 Z}{dt^2} + N^2 Z = 0, \ N = \sqrt{\frac{g}{\theta_0}\frac{\partial\theta}{\partial z}} \tag{26}$$

The general form of the solution to this equation is

$$Z = A \, exp(\pm iNt)$$ **(27)**

where A is a constant.

For real N, this is corresponds to simple harmonic motion, with angular frequency N and period τ, given by

$$\tau = \frac{2\pi}{N}$$ **(28)**

where N is the Brunt-Väisälä frequency.

The Brunt-Väisälä frequency, or buoyancy frequency, represents the natural oscillation frequency of an air parcel displaced vertically from its equilibrium position by the buoyancy force in a stably stratified atmosphere [21].

If N is real, $N = \sqrt{\dfrac{g}{\theta} \dfrac{\partial \theta}{\partial z}}$, the solution for motion of the parcel is sinusoidal oscillation

$$Z(t) = Z(0) \, cos(Nt)$$ **(29)**

and $\partial\theta / \partial z > 0$ (*i.e.*, the atmosphere is stable).

If the atmosphere is unstable ($\partial\theta / \partial z < 0$), then the Brunt-Väisälä frequency is imaginary, and the solution for the parcel's motion is

$$Z(t) = Z(0) \, exp|N|t$$ **(30)**

In this case, the displacement grows exponentially in time, just as it would in an unstable atmosphere.

The Brunt-Väisälä frequency can also be used as a measure of stability by applying the following conditions:

N imaginary	unstable
$N = 0$	neutral
N real	stable

Perturbations of N^2 values are commonly seen in association with a variety of atmospheric phenomena, including fronts and turbulence.

Vertical motions tend to be suppressed when there is stable buoyancy stratification, but turbulence can still arise if there is enough energy in the horizontal velocity field. A useful parameter for characterizing the fluid dynamic properties is the ratio of the buoyancy timescale to the squared vertical wind shear in the flow. This ratio is defined as the Richardson number, or gradient Richardson number R_i:

$$R_i = \frac{\dfrac{g}{\overline{\theta}}\dfrac{\partial \overline{\theta}}{\partial z}}{\left[\left(\dfrac{\partial \overline{U}}{\partial z}\right)^2 + \left(\dfrac{\partial \overline{V}}{\partial z}\right)^2\right]}$$

(31)

where $\overline{U}$ and $\overline{V}$ are mean wind speeds in the zonal (east-west) and meridional (north-south) directions respectively (*i.e.*, the horizontal (x, y) velocities), θ is the mean potential temperature, and g is gravitational acceleration.

As previously stated, the Richardson number can be seen as a measure of the balance between the mechanical production of turbulent kinetic energy (TKE) and the buoyant consumption/production of TKE. Wind shear always tends to generate turbulence mechanically, while buoyancy may suppress turbulence.

It is sometimes convenient to work with the bulk form of the Richardson number:

$$R_i = \frac{\dfrac{g}{\overline{\theta}}\dfrac{\partial \overline{\theta}}{\partial z}}{\left(\dfrac{\partial \overline{u}}{\partial z}\right)^2}$$

(31a)

If this is applied to a finite layer, it is referred to as the gradient Richardson number (Eq. 31), and the mean wind can come from any direction (rather than just the *x*-direction).

Dynamic meteorology and observations show that a stably stratified fluid flow will become hydrodynamically unstable and break into a disorderly, turbulent mode when the Richardson number is smaller than some critical Richardson number, R_{ic}.

Following Pielke [22] and Nordeng [23], the critical Richardson number is given by:

$$R_{ic} = A \left(\frac{\partial z}{\partial z_0} \right)^B$$

where A and B are parameters with values $A = 0.115$ and $B = 0.175$, and z_0 is the reference height.

There are different values in the literature for the critical Richardson number. Djurić [24] found $R_{ic} = 0.21$; Lyons *et al.* [25] estimated that, near the ground, evident turbulence disappears for $R_i > 0.5$; Wanta [26] found $R_{ic} = 0.04$ for curved wind profiles. Finally, Taylor [27] concluded from perturbation theory that the value for critical Richardson number was 0.25, which is its universally accepted value.

In general, laminar flow becomes turbulent when R_i decreases below the critical Richardson number, $R_{ic} = 0.25$; turbulent flow becomes laminar when R_i increases above the termination Richardson number $R_{iT} = 1.0$, therefore marking the end of turbulence.

In conclusion, one is led to distinguish among three different degrees of stability [28]:

(1) Absolute Instability. The temperature lapse rate is higher than the dry-adiabatic lapse rate. Also known as auto-convective instability or mechanical instability. The term "absolute" is used because this applies whether or not the air is dry or saturated. Any small impulse is able to move a particle of air with increasing speed away from its original equilibrium position.

(2) Conditional Instability. The temperature lapse rate is less than the dry adiabatic lapse rate but greater than the saturation adiabatic lapse rate or pseudo-adiabatic lapse rate. If the relative humidity is high, a sufficiently strong impulse upwards may move an air particle away from its original position. Conditional instability is not significant for very dry air since the impulse required to upset the equilibrium is considered enormous.

(3) Absolute Stability. The temperature lapse rate is less than the saturation adiabatic lapse rate or the condensation adiabatic (pseudo-adiabatic) lapse rate. In this case, as in the second one, the potential temperature increases with elevation; in the first case, on the contrary, it decreases upward. It is of course possible to see from the characteristic curve if the potential temperature decreases or increases with elevation, but it is not always possible to state whether the atmosphere is conditionally unstable or absolutely stable.
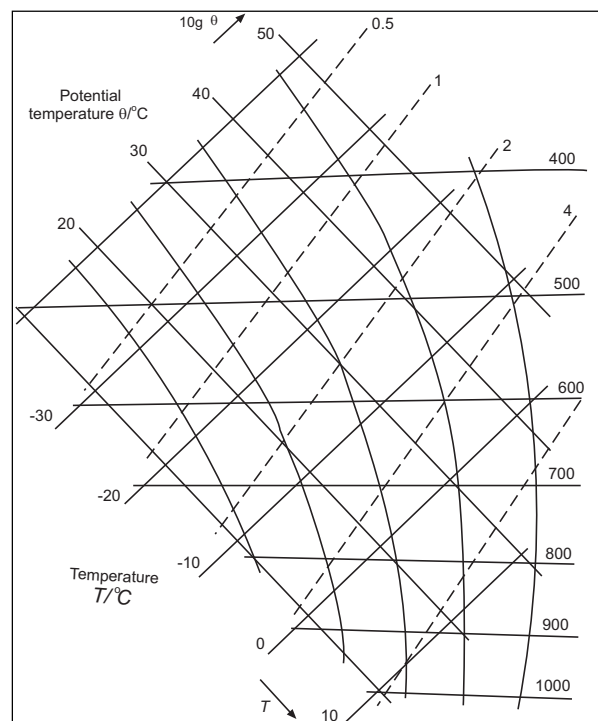
Figure 5: An example of an adiabatic chart, the tephigram, a temperature -entropy plot [29].

In general, to assist the determination of atmospheric stability, meteorologists use an adiabatic chart, *i.e.*, a thermodynamic diagram for the analysis of adiabatic processes, as a suitable tool for making stability estimates.

The basic portion of the chart is a set of temperature and pressure (or height) gridlines on which the measured temperature and moisture structure of the atmosphere can be plotted. There are several different types of thermodynamic diagrams (Stuve diagram, emagram, tephigram, Fig. (**5**) and skew-*T*/log *p* diagram).

Additional useful tools for classifying atmospheric stability are the atmospheric stability indices [30-37].

Instability indices have been developed and used to aid both research and the operational forecasting of severe weather and thunderstorms by quantifying thermodynamic instability with the use of radiosonde data [39]. In fact, in most cases stability indices are derived from the humidity and temperature data of the sounding at certain fixed levels.

Five instability indices are considered in this chapter: The Lifted Index [31], the K-index [36]), the Boyden Index [33], the Showalter Index [37] and the Total Totals index [38].

> ➢ The Lifted Index (LI) is defined as the difference between the observed temperature at 500 hPa and the temperature of a parcel (T_{parcel}) after it has been lifted pseudo-adiabatically from its original level to 500 hPa. This is done in order to capture low-level boundary layer temperature and moisture conditions while reducing diurnal effects. This hypothetical parcel is then lifted dry-adiabatically to the LCL and pseudo-adiabatically to 500 mb. The value of this index is the temperature of the environment subtracted from the temperature of the parcel at 500 mb [31]:

$$LI = T_{500hPa} - T_{parcel}$$

The Lifted Index can be calculated for any sample of air at pressure $P > 500$ hPa if the ambient temperature at 500 hPa is known. It should be noted that the Lifted Index depends on the properties of the specific air parcel used; it is not a measured quantity, but rather a parameter derived theoretically. Some authors [40, 41] observe that the Lifted Index is used as an observed static index instead of a forecast index.

Positive values imply greater stability. Values less than zero imply an unstable atmosphere; therefore, the larger the negative number, the more unstable the atmosphere is.

LI >> 0: Stable but weak convection possible for $1 < LI < 3$ if strong lifting is present.

-3 < LI < 0: Marginally unstable.

-6 < LI < -3: Moderately unstable.

-9 < LI < -6: Very unstable.

LI < -9: Extremely unstable.

➢ The Boyden Index (BI) is defined as [33]:

$$BI = Z_{700hPa-1000hPa} - T_{700hPa} - 200$$

where Z is the difference between the geo-potential height between 700 hPa and 1000 hPa.

It describes the vertical temperature profile between 1000 and 700 hPa and was initially used to assess thunderstorm risk. A threshold value equal to 94 is, in general, representative of thunderstorm activity in the troposphere [33].

➢ The K-index (KI) is a measure for thunderstorm potential based on the vertical temperature lapse rate, and the amount and vertical extent of low-level moisture in the atmosphere. The index is given by the formula:

$$KI = (T_{850hPa} - T_{500hPa}) + T_{d850hPa} - (T_{700hPa} - T_{d700hPa})$$

where KI represents a function of vertical temperature lapse rate at the 850 hPa and 500 hPa temperatures, low level moisture content at the 850 hPa dew point, and the depth of the moist layer at the 700 hPa dew point [36].

The risk of air mass thunderstorms is defined as follows:

K < 30: Thunderstorms with heavy rain or severe weather possible.

K > 30: Better potential for thunderstorms with heavy rain.

K = 40: Best potential for thunderstorms with very heavy rain.

> ➢ The Showalter Index (SI) is an index used to determine the stability of the lower half of the troposphere. It can be calculated by subtracting the environmental temperature from the parcel temperature:

$$SI = T_{env} - T_{parcel}$$

The risk of severe weather activity is defined as follows:

SI > 3 No significant activity.

1 < SI < 3 Showers possible with other sources of lift.

-2 < SI < 1 Thunderstorms possible (generally weak).

-3 < SI < -2 Thunderstorms more probable (possibly strong).

-6 < SI < -4 Strong or severe thunderstorms possible.

SI < -6 Any thunderstorms likely to be strong or severe.

It is interesting to compare the Lifted Index to the Showalter Index. When the LI is negative and the SI positive, the ABL can be considered unstable while the region just above the ABL is stable; in addition, if the LI is positive and the SI negative, the ABL can be considered stable, but the lower troposphere becomes

unstable with height. This can occur in cases where shallow polar air is in the ABL while there is an unstable air mass aloft.

When the LI and SI are both negative, it often indicates that a deep layer of unstable air in the lower troposphere is in place. On the contrary, if the LI and the SI are both positive, it often indicates that a deep layer of stable air in the lower troposphere is in place.

 ➤ The Total Totals Index [37] is a measure of thunderstorm potential and accounts for both static stability and 850 mb moisture, but it is unrepresentative in situations where the low-level moisture resides below the 850 mb level. It is defined as follows:

$$TT = T_{850} + Td_{850} - 2T_{500}$$

It is a simple index derived from the temperature lapse rate between 850 mb and 500 mb and moisture content at 850 mb. In particular, it consists of two components, the Vertical Totals (VT) and the Cross Totals (CT). The VT represents static stability or the lapse rate between 850 and 500 mb. The CT includes the 850 mb dew point.

Total Totals Index values $\geq$ +60 indicate probable moderate thunderstorms, with a possibility of scattered severe thunderstorms.

The Atmospheric Layer and the Surface Energy Budget

The concentration of atmospheric pollutants is influenced by both dispersion within the atmospheric boundary layer (ABL) and by atmospheric flow.

The atmospheric boundary layer (ABL) is the interface between the Earth's surface and the atmosphere. It is governed by the influence of the Earth's surface through friction, convective heating during the day, and radiative cooling of the ground at night. The top of ABL can be defined as the lowest level in the atmosphere at which the ground surface no longer influences meteorological variables through turbulent mass transfer [22].

The daytime ABL, namely the convective boundary layer (CBL), where air transport is driven mainly by turbulence, can usually be divided into two main sublayers:

➢ the surface layer constitutes about the lowest tenth of the whole ABL (occasionally, when the height of the lowest layer is the same height as existing surface roughness obstacles, it is treated separately as the roughness sublayer);

➢ the mixed layer above the surface layer occupies the middle of the CBL, with the formation of vigorous turbulent mixing through convection driven by buoyancy and shear effects, resulting in a vertically uniform distribution of scalars and wind speed; the upper limit of the mixed layer is the interfacial (or the entrainment) layer.

A method for classifying the various sublayers within the ABL has been previously proposed [42, 43]. However, this classification system, determined by the scaling of its turbulence characteristics, is not universal due to the complexity in establishing the atmospheric processes that characterize each sublayer and the method used for measuring its depth.

The ABL thickness is variable in time and space over land, where it can vary between hundreds of meters and a few kilometers. On the contrary, the ABL height varies very little in space and time over the sea because the sea surface temperature does not fluctuate to a great extent between day and night.

In fact, because strong cold air advection over a relatively warm sea can frequently generate extremely high fluxes of sensible and latent heat in the atmosphere, the boundary layer over the sea does not have a distinct diurnal pattern but can be stable or unstable depending on the air type that is advected relative to the sea surface temperature. For example, warm air advection over a cold sea leads to a stable ABL although this occurs infrequently.

Regarding the diurnal behavior of the ABL over land, it is mainly governed by the energy budget at the surface, which is in turn regulated by the evolution of net radiation at the surface. During the day the net radiation is partitioned primarily among three major avenues of energy exchange for the atmosphere -soil system: the heat flux into the ground, the sensible heat flux into the atmosphere, and the latent heat of evaporation. The ground heat flux can be defined as the net radiation

minus the latent heat flux plus the sensible heat flux at the soil surface (*e.g.*, Eq. 39), and is generally less than 10% of the net radiation during daytime. The fluxes are smaller at night and are less important for the atmospheric thermal balance.

Atmospheric turbulence in the ABL is produced primarily by wind shear and buoyancy. In order to describe the turbulence characteristics of the ABL, theoretical models have been developed with the use of dimensional analysis, which suggests grouping the variables into dimensionless parameters to derive universal similarity relationships [20, 44]. One of the most important arguments in the ABL similarity approach is the Monin-Obukhov (M-O) similarity [45, 46], which represents the mean gradients and turbulence characteristics as a function of important variables in the atmospheric boundary layer, such as the buoyancy variable, the kinematic surface stress, the heat flux, and the height from the ground.

The M-O similarity is based on the argument that the structure of turbulent flow in the surface layer is governed by mechanical and thermal forcing. The balance between these two components results in a length scale, the M-O scale (L), determined by the relative strength of mechanical *versus* thermal forcing, with the sign determined by the direction of the buoyancy flux. The similarity hypothesis is that the turbulent characteristics, when properly normalised, can be expressed as a universal function depending on the parameter $\xi = z/L$, where z is the height above the surface and L is the Obukhov length.

The scaling approach has been successfully verified in many atmospheric experiments and sensitivity tests, showing that atmospheric turbulence properties such as gradients, variances and co-variances, when accurately scaled, are universal functions of the stability parameter ξ [47].

Under stable stratification ($\xi > 0$), vertical transfers are not considered, and the boundary layer may be on the order of metres only. M-O parameterisation for this case often yields unsatisfactory results, and the more common case is that of nearly neutral stratification (particularly over the sea and at higher wind speeds), or unstable stratification ($\xi < 0$). In this case, the boundary layer can be considered to consist of three layers: a near surface region or wave boundary layer, a "constant flux" layer, and a mixed layer.

Turbulence is one of the most important characteristics of the ABL and it can be associated with thermal convection and friction-induced shear. It is important to remember that three basic ABL regimes can be distinguished: the convective, neutral, and stable boundary layers. It is well known that heating of the ground during the day leads to convective mixing and a deep CBL, where turbulence increases with depth, capped by a statically stable entrainment zone of discontinuous turbulence. In addition, the CBL is characterized by strong turbulence that is primarily created by buoyancy transport from the heated underlying surface. The resulting turbulence tends to mix heat, momentum, and moisture uniformly in the vertical direction. At sunset, radiative cooling of the ground leads to a shallow stable boundary layer (SBL). Finally, after sunrise the CBL develops again, destroying the SBL. In the absence of significant heating or cooling, the ABL tends to become a neutral boundary layer (NBL).

When boundary layers are advected over a surface with different surface conditions, equilibrium with the underlying surface is disturbed and an internal boundary layer (IBL) is formed [48]. It is called "internal boundary layer" because it is located within the atmospheric boundary layer and is caused by the advection of air across a discontinuity in surface temperature, surface roughness, surface humidity, or the surface flux of heat or moisture [49]. The IBL can also be defined as a constant flux layer, since the transfer of heat, momentum and mass is invariant with height.

The IBL is sometimes divided into two regions: an equilibrium zone at the surface and a transition zone between the equilibrium zone and the overlying flow (Fig. **5a**) [49].

Close to the ground, there is an equilibrium layer that is fully adjusted to the "different", or "altered", surface. Within this layer, the turbulent flux of momentum is roughly equal to its surface value. The properties differ between the top of the equilibrium layer and the top of the IBL. The upper part of the IBL is only partially adapted to the altered surface and properties within the IBL vary with increasing distance from the ground. Close to the ground the turbulent flux of momentum is roughly equal to its surface value. However, as altitude increases, the influence of the ground weakens and there is a much greater variation in the momentum flux with respect to that found at lower altitudes.
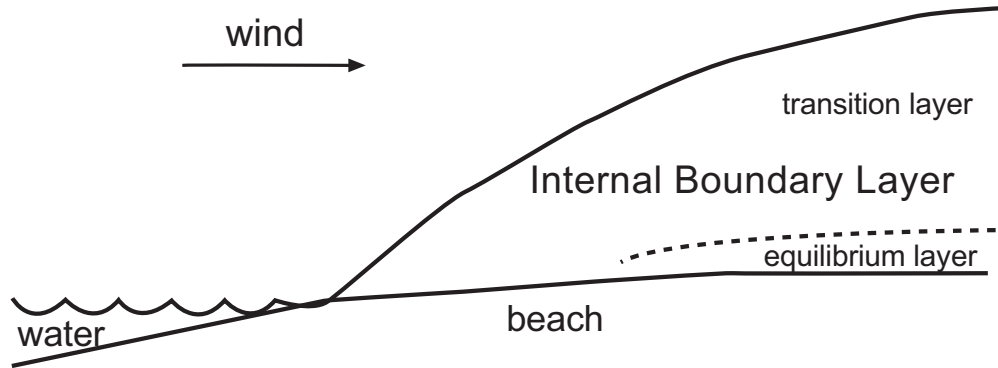
Figure 5a: Idealized time-averaged IBL structure for onshore flow.

In particular, if there is a change in surface roughness, a new equilibrium layer downwind of the line between the two roughness areas is established. The boundary layer near the ground then consists of two layers: one close to the surface, which is influenced by the new roughness, and another upper layer, which is still mainly influenced by the original roughness area. This can be represented mathematically: if the upper layer has an overall depth of at least ten times that of the roughness layer of the immediate surroundings, it can be written as a function of the fetch, x (the distance downwind of the point at which the two different surfaces meet), and the two roughness lengths z_{01} and z_{02}, the upstream and downstream roughness respectively [20]:

$$\frac{h_i}{z_{01}} = a \left(\frac{x}{z_{01}} \right)^b \tag{32}$$

The fetch, x (Fig.**5b**), has an essential influence on the height at which the change in the vertical profile takes place. The exponent $b = 0.8$ for neutral stratification, is larger for unstable stratification and smaller when stable, whereas the parameter a is defined as a function of the two roughness lengths:

$$a = 0.75 + 0.03 ln(z_{02}/z_{01}) \tag{33}$$

In general, the growth of the internal boundary layer is slow, and can be parameterised in different ways [50, 51]. For example, we can consider Carson's approach, which defines the following internal boundary layer height h_I:

$$h_I^2(x) = \frac{2(1+2A)}{U\rho c_p \gamma} \int_0^x F_0(x)dx$$

where

x is the distance from the coast in the direction of the mean wind,

U is wind speed at measurement height,

F_0 is the surface sensible heat flux,

A is a constant,

γ is the rate of increase of potential temperature with the height.

If we assume constant heat flux, we obtain

$$h_I^2(x) = \frac{2(1+2A)}{U\rho c_p \gamma} F_0 x$$

so that

$$h \propto x^{1/2}$$

Another algorithm for estimating the height of the internal boundary layer is:

$$h_i(x) = 0.1 x^{4/5} z_0^{1/5}$$

When there is a discontinuity in surface temperature or heat flux, the IBL is called a thermal internal boundary layer (TIBL). The most frequent example of a TIBL is the one produced at the coast as a result of the great temperature differences that exist between land and sea.

In fact, at the land-sea interface, a new IBL begins to develop due to mechanical and thermal effects. When the land is much warmer than the water surface and the land surface roughness is not great, thermal effects will dominate, and a TIBL begins to develop. Below the TIBL, the atmosphere is typically unstably stratified

while a stable temperature lapse rate is usually expected above the TIBL. Local circulations such as sea-land breezes as well as the TIBL are known to have a large impact on the local environment and climate and pollutant diffusion [52].
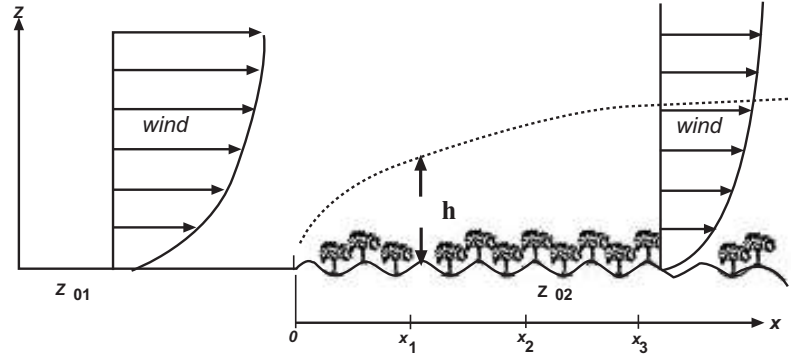
Figure 5b: Increases in the internal boundary layer height as a function of the fetch [20].

Interestingly, during sea breeze situations, a TIBL is formed over land with diffusive characteristics both inside and above the layer. Some of the more important characteristics are fumigation conditions in the presence of a TIBL, the behaviour of pollutants released inside the sea-land breeze circulation, and the presence of inversion layers. Pollutants released near the coast can become entrapped in the closed land-sea breeze circulation and the analysis of TIBL dispersion characteristics is essential for the study of the diffusion of pollutants in the presence of a TIBL.

To investigate the growth and inner structure of a stable TIBL, Garrat [49] used a mesoscale model. He formulated the following expression for the TIBL height

$$h^2 = \alpha U^2 \left(\frac{g \Delta \theta}{\theta} \right)^{-1} x$$

(34)

where:

x is the distance from the discontinuity,

g is the acceleration due to gravity,

U is the large-scale wind speed,

θ is the mean potential temperature,

$\Delta\theta$ is the difference between the temperature over land and the sea surface.

The numerical coefficient α is defined as [53]

$$\alpha = 2A_0 f(z/h) R_f C_D / \cos^3 \beta \qquad\qquad (35)$$

where $f(z/h)$ is a function of z/h, A_0 is a parameter describing the shape of the temperature profile, β is the deviation angle from the normal to the coast, and R_f represents the flux Richardson number [49]. The geostrophic drag coefficient C_D is described as

$$C_D = \frac{u_*^2}{V_g^2} \qquad\qquad (36)$$

where V_g is the geostrophic wind and $u*$ is the friction velocity.

The value α can be expressed using least square regression as follows:

$$\alpha = 0.014 \qquad\qquad (37)$$

where it depends on both the angle between the geostrophic wind and the coastline normal (β) value.

Additionally, there are several approaches to estimating the TIBL height [54]. For example, SethuRaman [55] summarized the results of a study undertaken to evaluate two coastal dispersion models using a complete coastal dispersion database. As reported by Niklas [53], SethuRaman found seven potential field databases that documented TIBL heights.

In their study, six equations to describe the TIBL height were identified in the scientific literature and compared using two experimental databases. The equations considered were attributed to Weisman [56], Plate [57], Van der Hoven [58], Peters [59], Raynor [60], and Venkatram [51].

The resulting conclusion was that the Weisman formulation gave the best prediction of TIBL heights. In fact, the report concluded that the Misra Shoreline Fumigation Model [61,62] using the Weisman equation to characterize the TIBL should be considered as the base coastal fumigation model.

The Weisman equation was developed on the basis of the following assumptions: constant over-sea temperature lapse rate, constant over-land wind profile, stable surface heat flux, and zero heat flux at the top of the TIBL, and is given as follows:

$$h = \sqrt{\frac{2H_{0,\infty}x}{\alpha C_p \rho U_L}}$$

where $H_{o,\infty}$ is the surface heat flux far inland,

α is the over-sea potential temperature vertical lapse rate (dT/dz),

U_L is the mean wind speed within the TIBL.

The prediction of complex atmospheric behaviour in coastal zones associated with thermal variations and, to a lesser extent, with surface roughness heterogeneity, generally requires three-dimensional boundary layer models that account for the interactions among all of these processes.

A meteorological situation that can generate high concentrations of pollutants in coastal environments is referred as shoreline fumigation, an example being when plumes from tall chimneys cause high ground level concentrations of pollutants further from the source than would normally occur at an equivalent inland site. This is due to the TIBL-deepening inland from the shore. Plumes that are released into the stable air near the shore can eventually be transported inland and become entrapped in the deepening unstable boundary layer. Another dispersion regime, which may occur for releases near a shoreline during on-shore flow, is plume trapping. Fig. (**5c**) illustrates these processes.

When the plume enters the TIBL, it is mixed toward the ground and can result in high ground-level concentrations of pollutants. Since this condition can persist for several hours, it cannot be considered a transient situation.
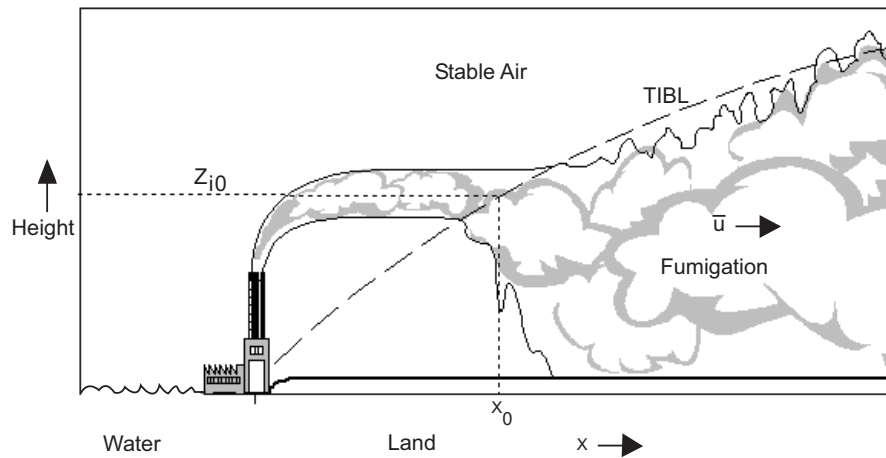
Figure 5c: A plume trapping episode associated with onshore air flow.

The TIBL may be relatively shallow in comparison to the depth of a boundary layer that would form in the absence of lake/sea effects. Hence, the vertical dispersion of pollutants released into this shallow layer will be limited in comparison to the vertical dispersion that would occur in a deeper inland boundary layer.

A case of special interest is the stably stratified internal boundary layer (SIBL), which develops as an air mass is advected from over a heated land surface to a cooler sea. The growth of the SIBL cannot be controlled by the fetch-integrated value of the surface heat flux due to the slowness of changes in surface forcing across the depth of the SIBL due to weak turbulence and the difficulty in describing its growth in terms of local parameters.

Unfortunately, there has been relatively little research in defining the parameters of a SIBL. The little data that does exist [63, 64] has been based upon dimensional arguments in order to analyse historical data.

In 1987 Garratt utilized numerical model simulations to study the SIBL structure in order to propose a simple relationship to describe the SIBL depth. Detailed observations of the SIBL structure have been presented in more recent studies (Rogers *et al.* [65, 66], Smedman *et al.* [67]). Stull [68] proposed that the growth of the nocturnal boundary layer is controlled by the time-integrated value of surface heat flux. Melas [69] extended Stull's theory to include the SIBL [70],

describing the previous phenomenon with a simple equation capable of describing the development of the SIBL as a function of downwind distance and external forcings, such as the pressure gradient force, surface roughness and potential temperature difference between the sea and land surfaces. In doing so, the author developed a simple equation capable of forecasting the SIBL depth over the sea as a function of external forcings and the distance to the coastline, and provided a parameterization of the surface heat flux over the sea with correct asymptotic behaviour. In addition, he assessed the proposed relationships by comparing the obtained results with data from the √resund experiment [71].

An additional fundamental parameter useful for determining the stability of conditions in the lower atmosphere governing the climate there is the net radiative flux of the underlying surface R_n. It is given by the difference between the absorbed radiant energy and that emitted by the underlying surface, the atmosphere, or by the Earth-atmosphere system.

It is important to remember that in advanced air pollution dispersion models, knowledge of atmospheric stability as well as surface heat fluxes and surface roughness is essential. Importantly, the surface energy balance and its components are not directly measured at meteorological stations, rendering it necessary to analyse all heat transfer processes in order to evaluate the dynamic evolution of the surface boundary layer.

The exchange of energy between Earth's surface and the atmosphere involves the absorption and emission of "natural" electromagnetic radiation by the surface, thermal conduction of heat within the ground, turbulent transfer of heat towards or away from the surface within the atmosphere, and the evaporation of water stored in the soil or condensation of atmospheric water vapour on to the surface (Fig.**6**).

The energy balance of a surface layer of finite depth and horizontal unit area can be expressed as follows:

$$\frac{dQ}{dt} = R_n - G_0 - H - LE$$

(38)

where Q is the total thermal energy stored in the surface layer, R_n is the net surface irradiance (commonly referred to as the net radiation), G_0 is the ground heat flux at the surface, H is the sensible heat flux and LE is the latent heat flux.
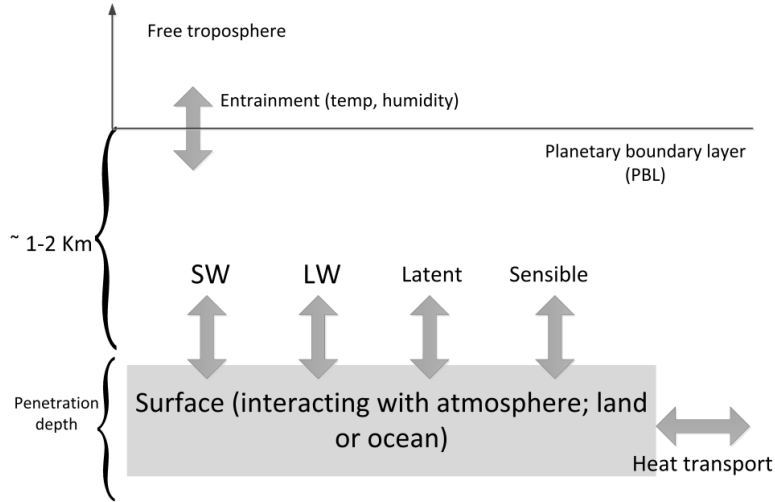
Figure 6: Energy exchange between Earth's surface and the atmosphere.

For an infinitely thin surface layer (Fig.**7**), the thermal energy stored, Q in Eq. (38), is zero and the equation reduces to

$$R_n - G_0 - H - LE = 0$$

$$R_n - G_0 = H + LE \tag{39}$$

The quantity R_n-G_0 can be considered as the available energy. To determine the surface energy balance, it is necessary to calculate the available energy as sensible or latent heat fluxes.

The way in which the available energy is dispersed can be quantified by taking the ratio of the sensible heat flux to the latent heat flux, which is known as the Bowen Ratio, B:

$$B_0 = \frac{H}{LE} \tag{40}$$

The Bowen ratio is non-dimensional and depends on the availability of water at the surface; as such, the presence of vegetation has an important effect. The Bowen ratio is small where water is freely available and it is large over arid surfaces, (in general $B_0 < 1$ for dry surfaces and $B_0 > 1$ for wet surfaces).
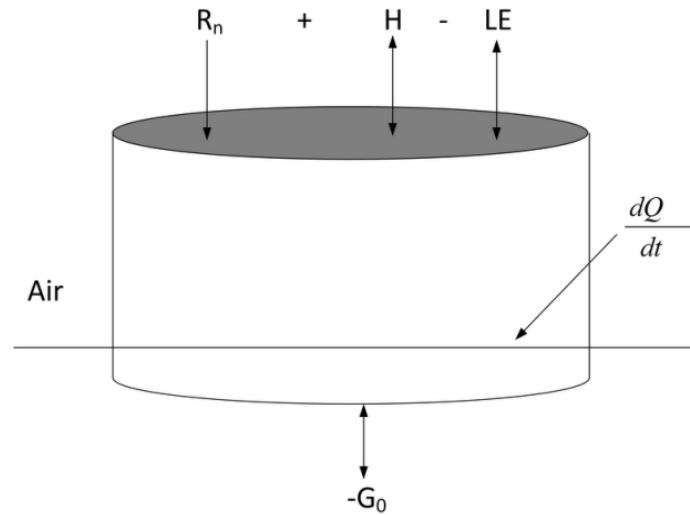
Figure 7: Surface energy balance.

Because it is based on the energy diffusion function, the Bowen ratio can be expressed as follows:

$$B_0 = \gamma \frac{\Delta T}{\Delta e}$$

(40a)

where γ is the psychrometric constant, and ΔT and Δe are the gradients of temperature and water vapour pressure in the vertical dimension.

In terms of the Bowen ratio, the surface energy balance can be written as

$$R_n - G_0 = H \frac{(1 + B_0)}{B_0}$$

$$R_n - G_0 = LE(1 + B_0)$$

(41)

The net surface irradiance is generally represented by the sum of shortwave radiative fluxes R_{ns} (mainly solar contributions) and longwave radiative fluxes R_{nl} (mainly terrestrial contributions). Consequently, the radiation balance equation is given by

$$R_n = R_{ns} + R_{nl} = (G - R_k) + (A - R_l - E)$$

(42)

where G represents the global solar irradiance, R_k is the shortwave reflected irradiance, and R_l is the longwave reflected radiation, which is negligibly small [72]. Furthermore, A represents the atmospheric downward long wave radiation component and E denotes the outgoing terrestrial long wave radiation.

Eq. 42 can be further reduced to

$$R_n = G(1-a) + R_{nl} = G(1-a) - E_{eff}$$

(43)

where

$$E_{eff} = -R_{nl} = E + R_l - A$$

(44)

and

$$a = \frac{R_k}{G}$$

(45)

In Eqs. 43 and 44, E_{eff} is the effective terrestrial radiation, while a represents the shortwave albedo.

In some reports, a is either assumed to be constant for a given surface [73-75] or estimated, for example according to Dong Dong *et al.* [76]:

$$a = 0.00158\theta + 0.386\,exp(-0.0188\theta)$$

(46)

with θ being the solar altitude.

ACKNOWLEDGEMENTS

CONFLICT OF INTEREST

The author(s) confirm that this chapter content has no conflict of interest.

REFERENCES

[1]   Marshall J, Plumb R.A. Atmosphere, Ocean and Climate Dynamics, published by Academic Press; 2008

[2]   Andrews DJ, Holton JR, Leovy C B. Middle Atmosphere Dynamics' Academic Press Inc; 1987.

[3]   Paltridge GW, Platt CMR. Radiative Processes in Meteorology and Climatology. Elsevier Scientific Publishing Company;1976.

[4]   Goody RM, Young YL. Atmospheric Radiation (Theoretical basis), 2'nd ed., Oxford Univ. Press; 1989

[5]   Holton JR. An introduction to dynamic meteorology, 3rd ed. New York: Academic Press; 1992.

[6]   Held IM. On the height of the tropopause and the static stability of the troposphere. J Atmos Sci 1982, 39: 412-417

[7]   Kiehl JT. Atmospheric general circulation modeling. Climate System Monitoring. Cambridge University Press 1992, UK,

[8]   Hurrell JW, Ramaswamy V, Meehl GA. Temperature Trends in the Lower Atmosphere: Steps for Understanding and Reconciling Differences. Thomas R. Karl, Susan J. Hassol, Christopher D. Miller, and William L. Murray, editors. A Report by the Climate Change Science Program and the Subcommittee on Global Change Research, Washington, DC. Chap.1, 2006

[9]   Manabe S, Wetherald R. Thermal equilibrium of the atmosphere with a given istribution of relative humidity. J Atmos Sci 1967; 24: 241-259.

[10]   Ramanathan V, Coakley JA. Climate modeling through radiative-convective models. Rev Geophys Space Phys 1978; 16: 465-489

[11]   Houghton JT. The Physics of Atmospheres. Cambridge University Press, UK; 1977.

[12]   Strahler AN. The Earth Sciences, Harper and Row, New York;1963.

[13]   Sarachick ES. A simple theory for the vertical structure of the tropical atmosphere. Pure Appl Geophys 1985; 123: 261-271.

[14]   Hartmann D L. Global Physical Climatology. Academic Press, 1994.

[15]   Trenberth K E, Stepaniak D P. Seamless poleward atmospheric energy transports and implications for the Hadley circulation. J Clim 2003; 16: 3705-3721.

[16]   Trenberth K E, Smith L. The vertical structure of temperature in the tropics: Different flavors of El Nino. J Clim 2006; 19: 4956-4973.

[17]   Ramanathan V. The role of ocean-atmosphere interactions in the CO_2 climate problem. J Atmos Sci 1981; 38: 918-930.

[18]   IPCC, Intergovernmental Panel Climate Change, First Assessment Report, 1990-92.

[19]   Dobesh H, Kury G. Basic Meteorological Concepts and Recommendations for the Exploitation of Wind Energy in the Atmospheric Boundary Layer. Working report. ENAIRGY, Vienna; 1999.

[20]   Stull RB, 1988. An introduction to boundary layer meteorology, Kluwer Academic Publishers, Dordrecht, The Netherlands

[21]   Yuhh-Lang Lin, Mesoscale Dynamics, Cambridge University Press 2007, UK.

[22]   Pielke RA. Mesoscale meteorological modeling. 2nd Edition, Academic Press 2002, San Diego, CA.

[23]   Nordeng TE. Parameterization of physical processes in a three-dimensional numerical weather prediction model, Norwegian Meteorological Institute Technical Report No. 65, 1986, Oslo, Norway.

[24]   Djurić D. Weather analysis, Prentice Hall, Englewood Cliffs, New Jersey, 1994.

[25]   Lyons R, Panovsky HA, Wollaston S. The critical Richardson number and its implication for forecast problems. J Appl Meteor 1964; 3: 136.

[26]   Wanta R C. The onset of turbulence in an elevated layer near sunrise. Quart J R Met Soc 1953; 79: 398.

[27]   Taylor GI. Effect of variation in density on the stability of superposed layers of fluid. Proc Roy Soc 1931; A (132): 499.

[28]   Rossby CG. Thermodynamics applied to air mass analysis. Massachusetts Institute of Technology Meteorological Papers, vol. i, no.3, 1932 Cambridge.

[29]   Houghton J. The Physics of Atmospheres. Cambridge University Press 2001.

[30]   Showalter A K. A stability index for thunderstorm forecasting. Bull Am Met Soc 1953; 34: 250-252.

[31]   Galway J G. The lifted index as a predictor of latent instability. Bull Am Met Soc 1956; 37: 528-529.

[32]   Rackliff P G. Application of an instability index to regional forecasting, Meteor Magazine 1962; 91:113-120.

[33]   Boyden CJA. Simple instability index for use as a synoptic parameter. Meteorol Mag 1963; 92: 198– 210.

[34]   Jefferson G J. A modified instability index. Meteor Magazine 1963; 92: 92-96.

[35]   Jefferson G J. A further development of the instability index. Meteor. Magazine 1963; 92: 313-316.

[36]   George JJ.Weather Forecasting for Aeronautics. Academic Press 1960

[37]   Peppler R A. A review of static stability indices and related thermodynamic parameters, Illinois State Water Survey Misc Publ 1988; 104

[38]   Stone H M.: The Energy Index for Stability. Preprints 10th Conf. Weather forecasting and Analysis. Amer Meteor Soc, Clearwater Beach, Fl 1984; pp550 – 554

[39]   Chrysoulakis N, Spiliotopoulos M, Feidas H, Domenikiotis C. and Dalezios N R. Estimation of atmospheric static stability with the use of satellite remote sensing. In: Proceedings of 7th Panhellenic (International) Conference of Meteorology, Climatology and Atmospheric Physics. Hellenic Meteorological Society, Cyprus Meteorological Association, Cyprus Meteorological Service, University of Cyprus, Nicosia 2004

[40]   Peppler R A, Lamb P J. Tropospheric static stability and central North American growing season rainfall. Mon Weather Rev 1989; 117: 1156–1180.

[41]   Huntrieser H, Schiesser H, Schmid W, and Waldvogl A. Comparison of traditional and newly developed thunderstorm indices for Switzerland. Wea. Forecasting 1997; 12: 108–125

[42]   Holtslag AAM, Nieuwstadt FTM. Scaling the atmospheric boundary layer. Bound Layer Meteor 1986; 36: 201–209.

[43]   Dayana U, Rodnizkib J. The Temporal Behavior of the Atmospheric Boundary Layer in Israel, J Appl Meteorol 1999; 38 (6) 830-836.

[44]   Arya SPS. Introduction to Micrometeorology. 2nd Ed. San Diego: Academic Press 2001.

[45]   Monin AS, Obukhov AM. Basic laws of turbulent mixing in the atmospheric near the ground. Tr Akad Nauk, SSSR Geophiz Inst 1954; 24(151).

[46]   Kader B A, Yaglom A M. Mean field and fluctuation moments in unstably stratified turbulent boundary layers. J Fluid Mech 1990; 212: 637-662.

[47]   Brutsaert W. Aspects of Bulk Atmospheric Boundary Layer Similarity under Free-Convective Conditions. Rev Geophys 1999; 37: 439–451.

[48]   Carlsson M. The stable boundary layer over the ice covered Bothnian Bay. Uppsala University, Dept. of Meteorology, 2000 Sweden.

[49]   Garrat J R. The internal boundary layer – A review. Boundary Layer Meteorol 1990; 50.

[50]   Carson DJ. The development of a dry inversion-capped convectively unstable boundary-layer. Quart J Roy Met Soc 1973; 99: 450-467.

[51]   Venkatram A. A model of internal boundary-layer development, Boundary Layer Meteorol 1977; 11: 419-437.

[52]   Barthelmie R J, Grisogono B, Pryor SC. Observations and simulations of diurnal cycles of near-surface wind speeds over land and sea. J. Geophys Res Atmospheres 1996; 101 (D16): 21327-21337.

[53]   Niklas S. The wind field in coastal areas, Examensarbete vid Institutionen för geovetenskaper 2002. ISSN 1650-6553 Nr 28.

[54]   Venkatram A. The role of meteorological inputs in estimating dispersion from surface releases. Atmos Environ 2004; 38(16): 2439-2446.

[55]   SethuRaman S. Analysis and evaluation of statistical coastal fumigation models, U.S. EPA, Research Triangle Park, NC, EPA-450/4-87-002, 1987.

[56]   Weisman B. Response to: On the Criteria for the Occurrence of Fumigation Inland from a Large Lake. Atmos Environ 1976;12: 172–173.

[57]   Plate EJ. Aerodynamic characteristics of atmospheric boundary layers. United States Atomic Energy Commission 1971.

[58]   Van der Hoven I. Atmospheric transport and diffusion at coastal sites, Nucl Safety 1967; 8: 490-499.

[59]   Peters LK. On the criteria for the occurrence of fumigation inland from a large lake. Atmos Environ 1975; 9: 809–816.

[60]   Raynor GS, Michael P, Brown R M, SethuRaman S. Studies of atmospheric diffusion from a near shore oceanic site. J Appl Meteor 1975;14: 1080-1094.

[61]   Misra PK. Dispersion from tall stacks into shoreline environment. Atmos Environ 1980; 14: 396-400.

[62]   Misra PK. Verification of a shoreline dispersion model for continuous fumigation. Bound Layer Meteor 1980;19: 501-507.

[63]   Mulhearn P J. On the formation of a stably strati_ed internal boundary layer by advection of warm air over a cooler sea. Boundary Layer Meteorol 1981; 21: 247-254.

[64]   Hsu S A. On the growth of a thermally modi_ed layer by advection of warm air over a cooler sea, J Geophys Res 1983;88: 771-774.

[65]   Rogers DP, Johnson DW, Friehe CA. The stable internal boundary layer over a coastal sea. Part I: Airborne measurements of the mean and turbulence structure. J Atmos Sci 1995; 52: 667-683.

[66]   Rogers DP, Johnson DW, Friehe CA. The stable internal boundary layer over a coastal sea. Part II: Gravity waves and the momentum balance. J Atmos Sci 1995; 52: 684-698.

[67]   Smedman A, Bergström H, Grisogono B. Evolution of stable internal boundary layers over a cold sea. J Geophys Res 1997;102: 1091-1099.

[68]   Stull RB. A Heat-flux-history Length Scale for the Nocturnal Boundary Layer. Tellus 1983; 35A: 219-230.

[69]   Melas D. The temperature structure in a stably internal boundary layer over a cold sea, Boundary Layer Meteorol 1989; 48: 361- 375.

[70]   Melas D. The depth of the stably strati_ed internal boundary layer over the sea, Geophys Res Lett 1998; 25(13): 2261-2264.

[71]   Gryning S E. The Oresund experiment - A Nordic Mesoscale Dispersion Experiment over a Land-Water-Land area. Bull Am Meteorol Soc 1985; 66: 1403-1407.

[72]   Iziomon MG, Mayer H, Matzarakis A. Empirical Models for Estimating Net Radiative Flux: A Case Study for Three Mid-Latitude Sites with Orographic Variability, Astrophys Space Sci 2000; 273(1-4): 313-330.

[73]   Sterlin J, Crabtree Jr, Kjerfve B. Radiation balance over a salt marsh. Boundary Layer Meteorol 1978; 14: 59–66.

[74]   Allen RG, Smith M, Pereira LS, Perrier A. An update for the calculation of reference evapotranspiration, ICID Bulletin 1994; 43(2): 1–10.

[75]   Snyder RL, Duce P, Spano D, Eching S. Hourly estimation of net radiation over grass, in: Proc. 23rd Conf. on Agriculture and forest Meteorology Nov. 2–6, 1998 Albuquerque, New Mexico. American Met Soc 1998:139–140.

[76]   Dong A, Grattan SR, Carroll JJ, Prashar CRK. Estimation of daytime net radiation over well-watered grass. J of Irrig and Drain 1992; 118 (3): 466–479.

Synoptic and Mesoscale Circulations

Simone Tascini[*]

School of Architecture and Design "E. Vittoria", Camerino University, Ascoli Piceno, Italy

Abstract: Atmospheric dynamics is governed by complex mathematical relationships that have been extensively modeled and discussed in recent decades. The aim of this chapter is to quickly recall the basic governing equations along with their main applications in order to better understand Modeling references. In the bibliography, a set of reference handbooks is provided for an exhaustive presentation of these topics.

Keywords: Advection, baroclinic condition, barotropic condition, circulation, conservation of momentum, Coriolis force, cyclostrophic flow, divergence, geopotential height, governing equation, gradient flow, isentropic coordinate, lapse rate, natural coordinate system, omega function, potential temperature, Rossby number, s-coordinate system, thermal wind, wind velocity.

RECALLING THE BASIC LAWS

Atmospheric dynamics is governed by a well-known set of budget equations (Eqs. 1–3) related to the conservation of momentum, mass and thermodynamic energy. These equations are characterised by the presence of derivatives of continuous functions (in both space and time) and by the consequent difficulty in finding their analytical roots. Quantities that vary continuously in space and time are called field variables and may be represented by a vector (temperature, pressure, density, circulation) or a scalar field (velocity, vorticity). A vectorial form of these governing equations is given by:

$$\frac{d\mathbf{U}}{dt} = -2\mathbf{\Omega} \times \mathbf{U} - \frac{1}{\rho}\nabla p + \mathbf{g} + \mathbf{F} \tag{1}$$

*Address correspondence to Simone Tascini: School of Architecture and Design "E. Vittoria", Camerino University, Ascoli Piceno, Italy; Tel: +39 (0)737 404279; E-mail: simone.tascini@unicam.it

$$\frac{1}{\rho}\frac{d\rho}{dt}+\nabla\cdot\mathbf{U}=0 \tag{2}$$

$$\rho\frac{dE}{dt}=-p\nabla\cdot\mathbf{U}+\rho J \tag{3}$$

where Ω is the angular velocity vector, and $\mathbf{F}$ is the force due to friction; other variables hold their standard meanings.

Due to their complexity, and in order to perform a detailed analysis, the above relations are subject to different levels of simplification. Since simplification is based on neglecting terms, it is necessary to know the magnitude of each term involved in the equation, *i.e.*, scale analysis, and the magnitude of all related derivatives.

Knowledge of the scale of each contribution leads to a classification of motions and phenomena regarding the ability to analyse or predict them. Special importance is given to the horizontal scale, since most types of motion are strongly dependent on this parameter. The table below presents a classification of motion based on the horizontal scale [1].

Type of motion	Horizontal scale
Molecular mean free path	10^{-7}
Minute turbulent eddies	10^{-2}-10^{-1}
Small eddies	10^{-1}-1
Dust devils	1-10
Gusts	10-10^2
Tornadoes	10^2
Thunderclouds	10^3
Fronts	10^4-10^5
Hurricanes	10^5
Synoptic cyclones	10^6
Planetary waves	10^7

The scale analysis technique has proved to be very useful in identifying the physics of the phenomena to be studied. A variety of different approximations have been developed and applied, and are well documented in the literature.

Starting with Eq. 1, the most simple is the geostrophic relationship, which includes only the pressure gradient and Coriolis force. Of course, only in mid-latitude and synoptic-scale perturbation conditions may be assumed as a valid approximation. A prognostic version of the geostrophic equation, obtained by retaining the acceleration term (time derivative of velocity):

$$\frac{D\mathbf{V}}{Dt} + f\,\mathbf{k}\times\mathbf{V} = -\frac{1}{\rho}\nabla p \tag{4}$$

where $\mathbf{V}$ is the horizontal velocity vector. An additional parameter, the Rossby number, $Ro = U/(f_0 L)$, represents an index of the quality of the geostrophic approximation: the smaller the number, the better the approximation.

Further approximations of the motion equations are called the *inertial flow* approximation and the *cyclostrophic flow* approximation. The first deals with a uniform geopotential field on an isobaric surface and is based on the balance of the Coriolis and centrifugal forces (Eq. 5). The second looks at a small horizontal scale of disturbance (the Coriolis force is neglected), where motion is due to a balance between the pressure gradient and the centrifugal force (Eq. 6).

$$\frac{D\mathbf{V}}{Dt} + f\,\mathbf{k}\times\mathbf{V} = 0 \tag{5}$$

$$\frac{D\mathbf{V}}{Dt} = -\frac{1}{\rho}\nabla p \tag{6}$$

Equation Parameterization

In order to better understand these relationships, it is useful to switch the reference coordinate system from Cartesian coordinates to so-called *natural* coordinates. The natural coordinate system is defined by three orthogonal axes identified by the unit vectors $\mathbf{t}$, $\mathbf{n}$, and $\mathbf{k}$. The first one is tangent to the velocity at each point; both $\mathbf{n}$ and $\mathbf{k}$ are normal to $\mathbf{t}$ but $\mathbf{n}$ lies in the horizontal plane while $\mathbf{k}$ points in the vertical direction.

Noting that

$$\frac{D\mathbf{V}}{Dt} = \mathbf{t}\frac{DV}{Dt} + \mathbf{n}\frac{V^2}{R}$$

where the terms on the right hand side describe tangential and centrifugal acceleration, we can rewrite all of the relationships presented in Eqs. 4–6. For geostrophic flow:

$$\frac{DV}{Dt} = -\frac{\partial\Phi}{\partial s} \tag{7}$$

$$\frac{V^2}{R} + fV = -\frac{\partial\Phi}{\partial n} \tag{8}$$

where *s(x,y,t)* is the curve traced out by the unit air mass and Φ is the geopotential.

Inertial flow and cyclostrophic flow is represented by:

$$\frac{V^2}{R} + fV = 0 \tag{9}$$

$$\frac{V^2}{R} = -\frac{\partial\Phi}{\partial n} \tag{10}$$

When all three major contributions (pressure gradient, Coriolis force, and centrifugal force) are considered and the tangential acceleration is null (horizontal motion parallel to height contours), the case is referred to as *gradient flow.*

The geopotential parameter (Φ) has been introduced in the simplified motion laws. This quantity, along with the correlated *geopotential height* presented below, requires a few words of introduction, since it plays an important role in meteorology.

The geopotential is defined as a potential function representing gravity according the relationships:

$$\frac{d\Phi}{dz} = g \ , \ \Phi(z) = \int_0^z gdz \tag{11}$$

The geopotential $\Phi(z)$ is therefore the work required by the air unit mass to be elevated to a height z.

As mentioned in the previous chapter, in static conditions, the pressure gradient force and gravity are balanced in the atmosphere. This is the well-known hydrostatic approximation. Hydrostatic balance is a good approximation for real atmospheres where medium- and large-scale systems are considered, far from complex terrain and convective layers (where most air pollution episodes are defined). Non-hydrostatic conditions imply integrating the pressure up to the top of the atmosphere $p(z) = \int_z^\infty \rho g dz$ which introduces mathematical complexity and computational load into the simulation.

From (11) and the equation of state for an ideal gas, it is possible to rewrite the hydrostatic balance equation in terms of geopotential height:

$$d\Phi = -\frac{RT}{p} dp \tag{12}$$

and, consequently,

$$\Phi(z_2) - \Phi(z_1) = R \int_{p_1}^{p_2} \frac{T}{p} dp \tag{13}$$

Eq. 13 is called the *hypsometric* equation. It allows an additional parameter to be introduced, called the *geopotential height,* which is defined as

$$Z \equiv \frac{\Phi(z)}{g_0} \tag{14}$$

where g_0 is the global average of gravitational acceleration at mean sea level. The hypsometric equation then becomes

$$Z_2 - Z_1 = \frac{R}{g_0} \int_{p_1}^{p_2} \frac{T}{p} dp \tag{15}$$

where $Z_T = Z_2 - Z_1$ represent the distance between two isobaric levels with respect to the temperature of the interposed layer.

In summary, geopotential height is a way of viewing the pressure as a vertical coordinate, in which the dependency of air density (or rather specific volume) on temperature is considered. Model initialization data (as will be discussed in more detail later), such as global observations and reanalysis in addition to general circulation model simulations, almost always provide pressure fields as geopotential height fields.

A further question is related to these equations: the parameterization of the vertical coordinate. In fact, in the equations presented above in the natural coordinate system, the presence of the geopotential is due to the implicit introduction of vertical pressure coordinates. The hydrostatic balance equation describes pressure that decreases monotonically with increasing height and, under most circumstances pertaining large scale motions, the fact that density vanishes is a distinct advantage. Applying pressure coordinates (in the form of the geopotential) to the approximate motion equation (Eq. 4) leads to

$$\frac{D\mathbf{V}}{Dt} + f\,\mathbf{k}\times\mathbf{V} = -\nabla_p\Phi \tag{16}$$

where the ∇_p operator is the horizontal gradient with constant pressure. It is important to note that in this equation, the vertical component of velocity, w, has been replaced by the *omega function* defined as $\omega = \frac{Dp}{Dt}$; likewise $w = \frac{Dz}{Dt}$. Of course, the omega function also replaces the vertical component of velocity in the continuity equation (Eq. 2) and thermodynamic equation (Eq. 3) as well. For large-scale motion in geostrophic conditions (*i.e.*, small Rossby number) the motion is described by

$$f\,\mathbf{V}_g = \mathbf{k}\times\nabla_p\Phi \tag{17}$$

where $\mathbf{V}_g$ is the geostrophic horizontal wind vector. As such, a constant geopotential gradient results in a geostrophic wind field that is independent of height. In turn, a constant pressure gradient would lead to variable geostrophic wind depending upon density variations.

On the other hand, constant pressure determines the null divergence of geostrophic wind: $\nabla_p\cdot\mathbf{V}_g = 0$.

From a general point of view, any biunivocal monotonic function of height may be applied as vertical coordinate. A very common and useful parameter in synoptic/regional models is the normalized pressure,

$$\sigma \equiv \frac{p(x,y,z,t)}{p_s(x,y,z,t)} \tag{18}$$

where p_s is the pressure at the surface. This treatment is especially useful when the pressure varies rapidly in both space and time, and allows the ground to be a surface within the coordinate system ($\sigma = 1$). These are also called σ-coordinate systems. Strong topographic variations are very common boundary conditions in coastal valley pollution assessments.

Normalization may be applied to regulate the z Cartesian coordinate. The benefit is the same but simplifies the geostrophic wind mentioned above.

One last consideration regarding coordinate systems and the formulation of the governing equations is isentropic coordinates. This kind of vertical coordinates are useful in true synoptic conditions when motions are quasi-adiabatic outside regions of active precipitation; this concept will become clear after a few definitions are presented.

First of all it is necessary to recall the definition of *potential temperature:*

$$\theta = T\left(\frac{p_s}{p}\right)^{\frac{R}{c_p}} \tag{19}$$

Potential temperature represents the temperature a unit volume of dry air would have if adiabatically compressed to the surface pressure (usually chosen as the reference pressure). As mentioned above, θ is a quasi-conserved quantity in quasi-adiabatic processes [2].

Furthermore it easy to show that variations in potential temperature are proportional to variations in entropy according to

$$c_p \frac{D \ln \theta}{Dt} = \frac{Ds}{Dt}$$

where *s* is the entropy. This relationship defines conditions isentropically, retaining θ as a constant field; it is more often related to isentropic surfaces.

Nonetheless, potential temperature allows for the definition of a *lapse rate* through the equation

$$\Gamma \equiv -\frac{\partial T}{\partial z} = \frac{g}{c_p} - \frac{T}{\theta}\frac{\partial \theta}{\partial z} \tag{20}$$

and an *adiabatic lapse rate*, which follows from the previous equation:

$$\Gamma_d \equiv \frac{g}{c_p} \tag{21}$$

These quantities, and moreover their difference $\Gamma_d - \Gamma = \frac{T}{\theta}\frac{\partial \theta}{\partial z}$, are generally employed as the main indicator of atmospheric stability.

A particularly strong constraint is represented by the sub-adiabatic condition ($\Gamma_d - \Gamma > 0$), which determines a statically stable or *stably stratified* atmosphere. In such conditions, the potential temperature is a biunivocal monotonic function of height and may thus be employed as an independent vertical coordinate. This leads to a vertical velocity:

$$\theta' = \frac{D\theta}{Dt} \tag{22}$$

This coordinate is particularly interesting since adiabatic motions (commonly pertaining to the synoptic scale) are two-dimensional if represented in an isotropic coordinate system.

All of the above-mentioned systems are not mutually exclusive. Modeling systems designed to be suitable on a significant range of horizontal scales (those employed for atmospheric dispersion dynamics) are based on hybrid coordinate frames that integrate different representations. This approach has the distinct

property of approximating equations depending upon the actual scale of motion, thereby resulting in optimized computational loads.

Regarding dynamic meteorology, two outstanding hypotheses need to be mentioned: *baroclinic* and *barotropic* conditions.

Barotropicity is a (theoretical) state in which surfaces of constant pressure and temperature coincide at all levels. In a barotropic atmosphere, isobaric surfaces are also isopycnic (constant density) surfaces. The atmosphere cannot sustain development, and thickness gradients are zero. If thickness contours are widely spaced (a realistic state), the atmosphere is said to be quasi-barotropic. Following from the coincidence of isobaric and isothermal surfaces (*via* the thermal wind equation), the geostrophic wind is independent of height. Hence the motions of a rotating barotropic fluid are strongly constrained.

On the other hand, baroclinity is a measure of the stratification in a fluid. A baroclinic atmosphere is one in which the density depends on both the temperature and the pressure. Barotropic zones are generally found in the central latitudes, or tropics, while baroclinic zones are generally found from the mid-latitudes to the polar regions.

Baroclinity is proportional to $\nabla p \times \nabla \rho$ which is proportional to the angle between surfaces of constant pressure and surfaces of constant density. Thus, as mentioned above, in a barotropic atmophere (in which baroclinity is zero), these surfaces are parallel.

Areas of high atmospheric baroclinity are characterized by the frequent formation of cyclones.

Parameter Budget (Vorticity and Circulation)

In principle, the set of basic governing equations, when solved in the computational domain, give a complete description of the thermodynamic behaviour of the portion of the atmosphere under consideration. Unfortunately the equation set is complex enough that only rarely may an analytical (exact) solution be found. On the other hand, the approximations mentioned above imply a

comprehensive knowledge of the boundary conditions that are applicable and consistent.

For this reason, it is sometimes useful to sidestep the problem by employing new derived variables for the governing equations. In other words, conservation laws of particular quantities are often widely applicable and significantly easier to handle. A derived quantity that is conserved allows the fundamental variable (under necessarily different constraints) to provide a synthetic snapshot of the motion.

One of the most stringent constraints follows from fluid dynamics and concerns the application of angular momentum conservation to fluids. The related derived parameter is called vorticity and is defined as the vector resulting from the curl of the velocity:

$$\omega = rot(\mathbf{U}) = \nabla \times \mathbf{U} \tag{23}$$

where $\mathbf{U}$ is the velocity vector [3, 4].

The second derived quantity is known as *circulation*, which is derived from vorticity through Stokes' theorem:

$$\iint_A \omega \cdot n \, dA = \int_C u \cdot dr = C \tag{24}$$

This relationship states that the flux of vorticity through an open surface, *A*, bounded by a closed curve, *C*, is equal to the integral of the velocity component tangent to the curve along the whole curve, namely the *circulation* of the velocity **u**. By convention, circulation is taken to be positive when $C > 0$ for clockwise integration around the closed loop.

Defined in this way, circulation represents a synthetic index of the rotation of a fluid. Analogously, vorticity represents another measure of motion. The two parameters differ substantially: the first is a scalar quantity and the second is a vector. Furthermore, while circulation gives an overall indication of fluid motion, vorticity describes the local behaviour of the fluid. Again we can talk about synthetic and analytic parameters.

It is now necessary to recall some other relationships and results regarding circulation and vorticity in order to better understand their applications and usefulness.

The first is Kelvin's theorem,

$$\frac{DC_a}{Dt} = \frac{D}{Dt} \int U_a \cdot dl = -\int \frac{1}{\rho} \cdot dp \tag{25}$$

where *a* stands for *absolute,* meaning that it is set in a coordinate system external to the Earth. The second term of the equation is called the *solenoidal term* and isnull in a barotropic atmosphere. Hence, in barotropic conditions, absolute circulation is a conserved quantity.

From the previous expression it can be shown that

$$\frac{DC}{Dt} = -\int \frac{1}{\rho} \cdot dp - 2\Omega \frac{DA_e}{Dt}$$

where A_e is the projection of the circulation surface on the equatorial plane. This is a formulation of relative circulation expressed as the difference between the absolute circulation and Earth circulation. Thus another interesting consequence results for barotropic conditions, wherein circulation varies with respect to the enclosed curve and latitude changes as follows:

$$C_2 - C_1 = -2\Omega \left(A_2 \sin \varphi_2 - A_1 \sin \varphi_1 \right).$$

Let us now consider the implications of vorticity. Defining $\omega = \nabla \times \mathbf{U}$ in terms of components:

$$\begin{cases} \omega_x = \dfrac{\partial w}{\partial y} - \dfrac{\partial v}{\partial z} \\[2mm] \omega_y = \dfrac{\partial u}{\partial z} - \dfrac{\partial w}{\partial x} \\[2mm] \omega_z = \dfrac{\partial v}{\partial x} - \dfrac{\partial u}{\partial y} \end{cases} \tag{26}$$

However, in large scale motion only the vertical component of vorticity is of importance, and we will refer to the absolute and relative vorticity with, respectively:

$$\eta \equiv \mathbf{k} \cdot \left(\nabla \times \mathbf{U}_a \right)$$
$$\zeta \equiv \mathbf{k} \cdot \left(\nabla \times \mathbf{U} \right) \tag{27}$$

A relationship between the two quantities that is analogous to the one introduced for circulation is the following:

$$\eta = \zeta + f \tag{28}$$

where f is Earth's vorticity arising from its rotation; $f = 2\Omega \sin \varphi$.

In natural coordinates, the relative vorticity becomes

$$\zeta = \frac{V}{R_s} - \frac{\partial V}{\partial n} \tag{29}$$

which highlights a twin contribution for the vorticity. The first term on the right hand side describes turning along a streamline V/R_s, and is called *curvature vorticity*; the second term, depicting the variation of wind speed along the direction normal to the motion, is called *shear vorticity*. The presence of the latter term indicates a very interesting feature of wind motion: even straight-line motion (the first term is null) can cause vorticity if the wind speed changes in a direction normal to the flow direction.

Knowing the distribution of vertical vorticity is a very useful diagnostic tool in dynamic meteorology. For example, in the Northern Hemisphere, cyclonic storms are associated with positive vorticity (symmetrically, the opposite consideration may be made for the Southern Hemisphere). In addition vorticity is a quasi-conserved quantity in optimal conditions and thus may be used in approximated forecast models.

More than vorticity, another parameter plays an important role in approximated models. Under adiabatic conditions, following from Kelvin's theorem of

circulation and the definition of potential temperature, potential vorticity may be defined in isentropic coordinates as

$$P \equiv \left(\zeta_\theta + f \right) \left(-g \frac{\partial \theta}{\partial p} \right) = \text{const} \tag{30}$$

where the minus sign allows for a positive value of P in the Northern Hemisphere.

Potential vorticity may be seen as a measure of the interdependence between vorticity and the vortex depth. In fact, since their product is a constant, every increase in vorticity determines a reduction in depth of the vortex layer and *vice versa*. In this case, the layer is defined between two isentropic surfaces that are a distance δp apart in pressure coordinates.

Eq. (30) provides a simple and powerful constraint to large-scale motions. An outstanding example may found in the extremely different character of easterly and westerly winds. Looking at Eq. (30), it is easy to see that since P depends on a Coriolis parameter, a dependence on latitude can be found, as well; a change in f with latitude is necessary to compensate changes in the relative vorticity or lapse rate. It is easy to prove that, under isentropic conditions, a zonal wind may or may not be conservative for potential vorticity depending on whether it moves west- or eastward. An even more interesting phenomenon may be found when zonal winds cross wide transverse mountain ridges. Following the stretching in an adiabatic layer (changes in $-g\,\partial\theta/\partial p$), it is easy to find anomalous behaviour for westerly winds that have cyclonic curvature and continue on a wavelike trajectory, conserving vorticity, and alternating troughs and ridges (neglecting dissipation phenomena, of course). Easterly winds start cyclonic curvature as well as westerly ones approaching a mountain as soon as the lapse rate decreases. But changes in the Coriolis parameter, f, soon compensate so that absolute vorticity is conserved and anticyclonic curvature is exhibited until the depth of the layer is established again and the wind flows along its previous trajectory. Therefore, easterly winds show stronger horizontal stability due to different influences of the Coriolis parameter. These concepts are extremely enlightening when applied to zonal winds in which the described effects are maximized the same concepts are, of course, generally applicable.

A more general constraint based on vorticity may be derived by manipulating the equations of motion in order to express them as a function of the vertical vorticity, ζ. The resulting equation is called the *vorticity equation* and may be written as follows:

$$\frac{D}{Dt}(\zeta + f) = -(\zeta + f)\left(\frac{\partial u}{\partial x} + \frac{\partial v}{\partial y}\right) - \left(\frac{\partial w}{\partial x}\frac{\partial u}{\partial z} - \frac{\partial w}{\partial y}\frac{\partial v}{\partial z}\right) + \frac{1}{\rho}\left(\frac{\partial \rho}{\partial x}\frac{\partial p}{\partial y} - \frac{\partial \rho}{\partial y}\frac{\partial p}{\partial x}\right) \quad \textbf{(31)}$$

This conservation law remains valid under general conditions (non-adiabatic) and presents an inertial term for vorticity. The three terms on the right hand side are called, respectively, the *divergence* term, the *tilting/twisting* term, and the *solenoid* term. Their contributions are quite evident; in fact, the divergence term (the most important one in synoptic motions) states that vorticity decreases as the area swept out by a parcel of air increases (divergence of motion). The second describes the generation of vorticity due to a field of nonuniform vertical motion and the last term is just a local expression of the solenoid term in Kelvin's theorem.

By analyzing the scale of the vorticity equation, it is possible to determine that the last two terms are small (10^{-11} s^{-2}) with respect to the first term and with respect to the vertical advection of vorticity, $w(\partial\zeta/\partial z)$, deriving from the development of the absolute derivative on the left side of the equation. The other terms are on the order of 10^{-10} or higher. The approximated equation for synoptic scale then becomes

$$\frac{D_h}{Dt}(\zeta + f) = -f\left(\frac{\partial u}{\partial x} + \frac{\partial v}{\partial y}\right) \quad \textbf{(32)}$$

The *h* in the absolute derivative operator stands for *horizontal* (since the vertical component has been neglected). Furthermore, vorticity has been neglected in the divergence term because it is small with respect to the Coriolis parameter. Consequently, as mentioned above, synoptic-scale vorticity is generated depending upon the divergence of horizontal motion. Of course, this condition is not always valid, with an outstanding example being in frontal zones where the scale of the tilting and solenoid contributions has the same order of magnitude as

the others. Such special assets of motion scales over wide areas (~100 km) are approached specifically as mesoscale motions.

Considering the barotropic model, it easily to show that the vorticity equation yields

$$\frac{D_h}{Dt}\left(\zeta_g + f\right) = 0 \tag{33}$$

which is called the *barotropic vorticity equation*. Such a relationship, valid when horizontal divergence is negligible, provides a simple but powerful forecasting model since mid-troposphere synoptic motions are practically non-divergent; it is, of course, better employed in short-term forecasting.

In order to complete the survey of vorticity applications for the synoptic scale, a potential vorticity conservation equation valid in baroclinic conditions must be mentioned. However, its discussion is beyond the scope of this chapter.

ACKNOWLEDGEMENTS

CONFLICT OF INTEREST

The author(s) confirm that this chapter content has no conflict of interest.

REFERENCES

[1]   Haltiner GJ, Williams RT. Numerical weather prediction and dynamic meteorology. Wiley, New York 1980.
[2]   Iribarne JV, Godson WL. Atmospheric Thermodynamics. 2nd ed. Reidel, Dordrecht, Netherlands 1981.
[3]   Brown RA. Fluid Dynamics of the Atmosphere. Academic Press New York. 1991.
[4]   Williams and Elder. Fluid Physics for Oceanographers and Physicists. Pergamon New York 1989.

CHAPTER 3

Coastal Air Pollution Meteorology and Meteorological Models

Simone Tascini[1,*] and Mariano Pierantozzi[2]

[1]*School of Architecture and Design "E. Vittoria", Camerino University, Ascoli Piceno, Italy and* [2]*Department of Energetics, Polytechnic University of Marche, Italy*

Abstract: The role of orography in a complex area is of great importance, even more so when the study area comprises a coastal region where there is a critical need for topographical information due to the presence of the sea (or, in general, large water masses). The surface boundary condition is generally defined by means of a Digital Elevation Model (DEM), which provides information about terrain heights in the area of interest. Both DEM and computational domains are discrete representations of reality, and need algorithms capable of translating the continuous reality into a discrete model. This study illustrates the care that must be taken when defining the surface boundary condition in order to avoid significant misinterpretation.

Keywords: Boundary Conditions, Coast valley breeze, coastline modeling, Complex orography, Dew point profile, Digital Elevation Model, dispersion patterns, Initial Conditions, mechanical forcing, Mesoscale Models, Nesting, ozone, Planetary boundary layer physics, raob data, Spatial Discretization, thermal gradient, THOES, Time Integration, VOC, wind rose.

SPATIAL DISCRETIZATION

The surface boundary condition is generally defined by means of a Digital Elevation Model (DEM), which provides information about terrain heights in the area of interest. Both DEM and computational domains are discrete representations of reality, and require algorithms capable of translating the continuous reality into a discrete model. A further complexity in the modeling process is that algorithm-derived discrete points generally do not match, and often refer to different geographical representations. Thus, requiring one to discretize the terrain again in order to make the information provided by the grid more representative.

---

*Address correspondence to Simone Tascini: School of Architecture and Design "E. Vittoria", Camerino University, Ascoli Piceno, Italy; Tel: +39 (0)737 404279; E-mail: simone.tascini@unicam.it

From a simplified point of view, discretization can be described as the superimposing of a pre-defined mesh over the terrain, after which a representative height for each mesh cell is assigned. Following from this definition, one may understand discretized data to be a synthesis of related analog data resulting from a process that is intrinsically irreversible. For example, it is always possible to reduce terrain data to a coarser computational grid but the contrary is never possible. Therefore, the grid spacing does not simply represent the quality of the representation, but also the scale of information retained.

In the case of coastline modeling, the influence of horizontal spacing is very strong (see Fig. **1**). Coastline modeling is similar to local breeze modeling. A very fine resolution must be applied when weak stable breezes are analyzed. Additionally, the coarse definition of land/water interfaces leads to a poor definition of the thermal gradients driving all breeze effects.
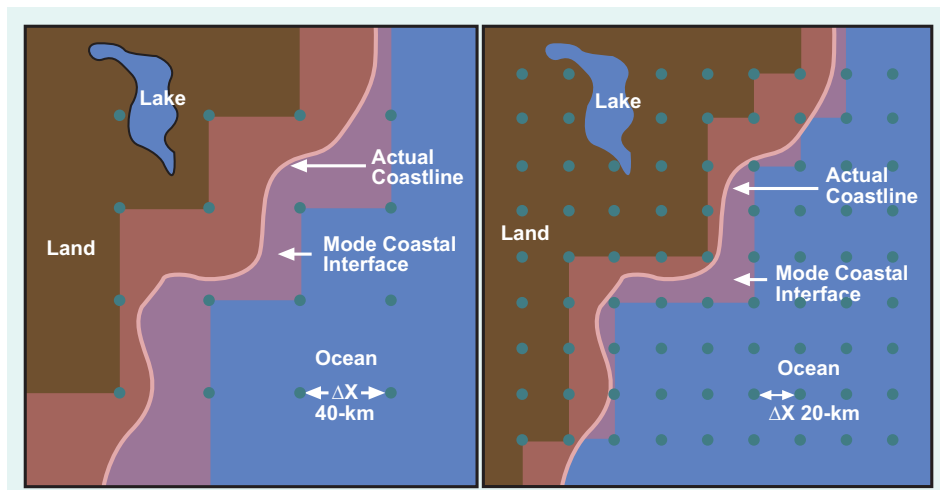
Figure 1a, 1b: A coastal region discretized using different meshes.

The lower limits imposed based on these considerations provide the starting resolution of the DEM. In order to achieve reliable simulations of thermal breezes, we implemented a specific DEM of local studies from detailed orography provided by regional authorities. The DEM realized is based on a 3" horizontal resolution and is shown in Fig. (**2**) as a 3D representation. Beyond exaggeration of the vertical scale, which is necessary to appreciate orographic complexities, it is

evident that much of the information pertaining to the lower boundary condition would be neglected when basing the simulation on the standard US Geological Survey (USGS) 30" orography (Fig. **1b**). The 10' simulation (Fig. **1a**) is shown as a comparison.
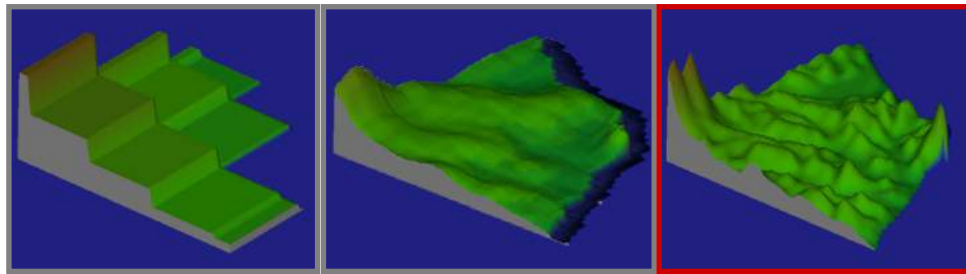
Figure 2: The Conero Promontory area. Three different horizontal resolutions for terrain discretization are shown: (a) 10' resolution; (b) 30" resolution; (c) 3" resolution.

Details of the differences in terrain information are provided for a cross-section from the Adriatic Sea to the Apennine Mountains in Fig. (**3**).
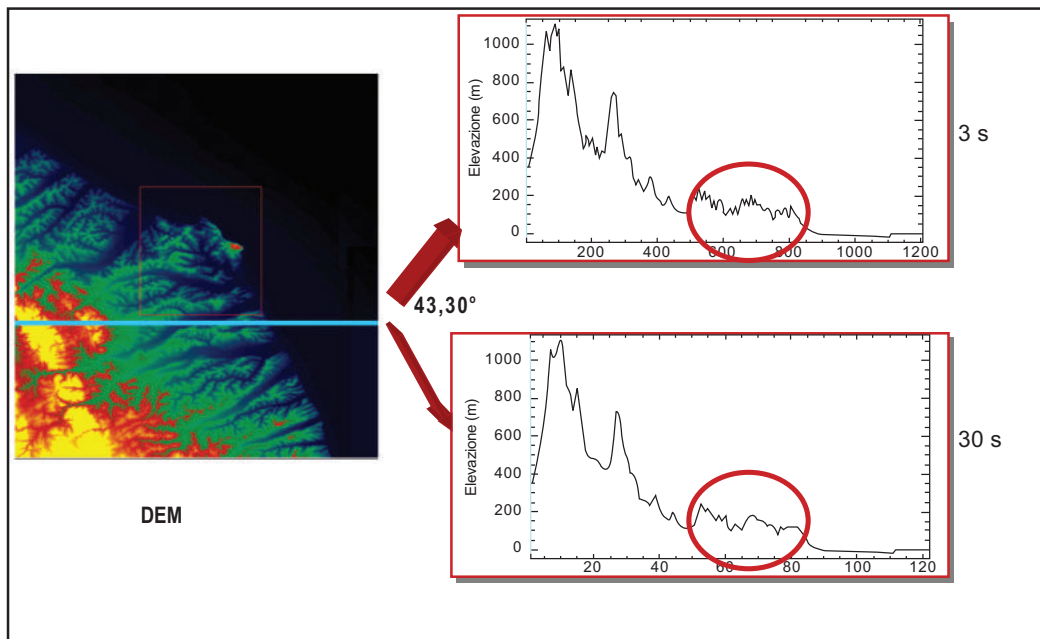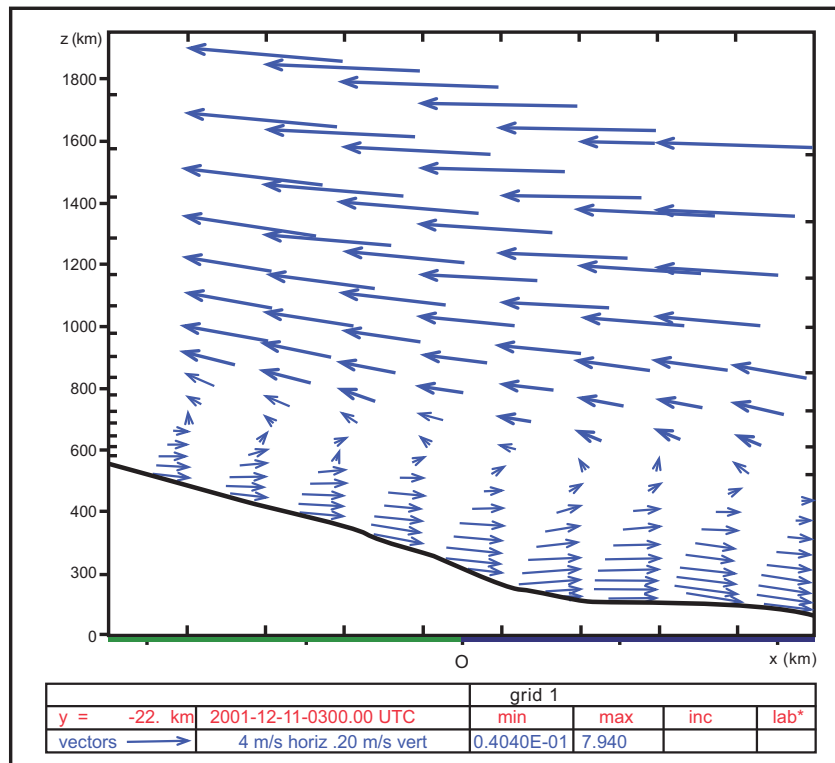

Figure 3: Terrain cross-section illustrating the differences in scale-dependent information provided.

Complex Orography

The role of orography in a complex area is of great importance, even more so when the study area consists of a coastal region where there is a critical need for topographical information due to the presence of the sea (or, in general, large bodies of water). Therefore, the two factors influencing forcing in relation to local meteorological phenomena in a coastal area are the orographical factor, which takes into consideration upslope acceleration (mechanical forcing), and the variable local radiation budget, which is responsible for breezes (thermal forcing). Although these forcing principles are pertinent to all atmospheric conditions, their influence is amplified in more complex areas.

		grid 1			
			min	max	inc	lab*
y = -22. km	2001-12-11-0300.00 UTC				
vectors	4 m/s horiz .20 m/s vert	0.4040E-01	7.940		

Figure 4: A vertical section of the wind field in the area of the Conero promontory. It is very clear that a well-formed convection cell developed a few kilometres inland. Green and blue lines at the base represent the land/sea interface.

Before further pursuing the role of orography, the simulation of local scale phenomena, *e.g.*, breezes, should first be considered, since the study area is highly influenced by such phenomena. The authors have significant experience in local

breeze simulation since it has been the first and preeminent aspect in studies of the surrounding area. The following Figs. (**4** and **5**) show how, even on a cold (relative to central Italy) winter night, breezes are omnipresent due the coastal nature of the study area.
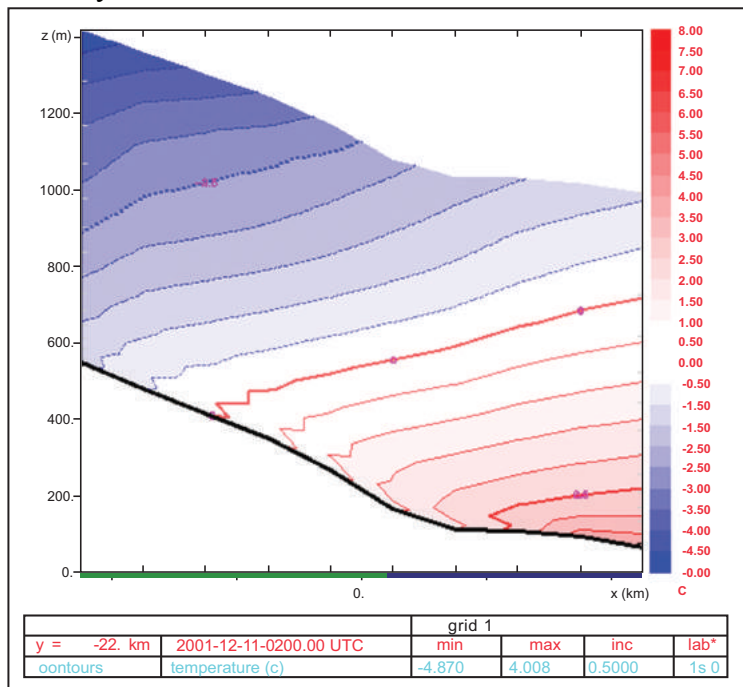
Figure 5: A vertical section of the thermal field in the area of the Conero promontory. A developed temperature gradient across the land/sea interface is evident. Coloured solid lines represent isotherms.

In order to show how this factor may affect such simulation domains, a comparison run has been carried out in a test area: the mouth of the Esino river.

The simulation is centred on the small village of Moie (lat. 43.500 deg N, long. 13.114 deg E). The computational domain covers a 70x70 square-km area with a spatial resolution of 35 cells (2 km/cell) per side. Two parallel nested grids have been set up using a 22x22 cell grid with 500 m/cell on each side. Note the 1:4 stretching ratio.

The choice of two nested grids enables testing of the model behavior both in the steep mountain region as well as in the smoother hill area found close to the sea.

Two villages where ground observations are available have been chosen for comparison, running the above-specified configuration in the Regional Atmospheric Modeling System (RAMS) twice. In the first simulation, a USGS topography dataset with 30' resolution (about 1000 m off the ground) was employed. In the second simulation, local topography information was used. Official data from regional authorities was converted and discretized into a digital elevation model. The dataset was then compiled in the RAMS proprietary format. This new orography dataset has 3' resolution (about 100 m off the ground).

In order to understand the influence of topography in the vertical direction, several profiles will now be studied. The graphs shown below are representative profiles of the dew point (Fig. **6**) and the temperature (Fig. **7**) relative to the centre of the grid where coarse and fine topography are compared. Unfortunately, the results have only a qualitative significance, since no soundings are currently available for that area. Regardless, an interesting divergence is highlighted, although this type of quantity is more affected vertically by thermal forcing. In order for solar radiation to have a minimal impact on the comparison, measurements were taken at 7:00 am. This aspect should also be considered, for example in terms of land use resolution.
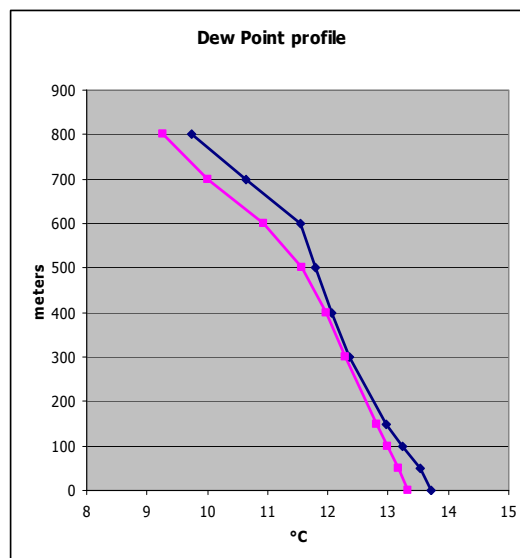
Figure 6: The dew point profile at 8:00 am. The violet line represents 1 km orography while the blue line represents 100 m orography.
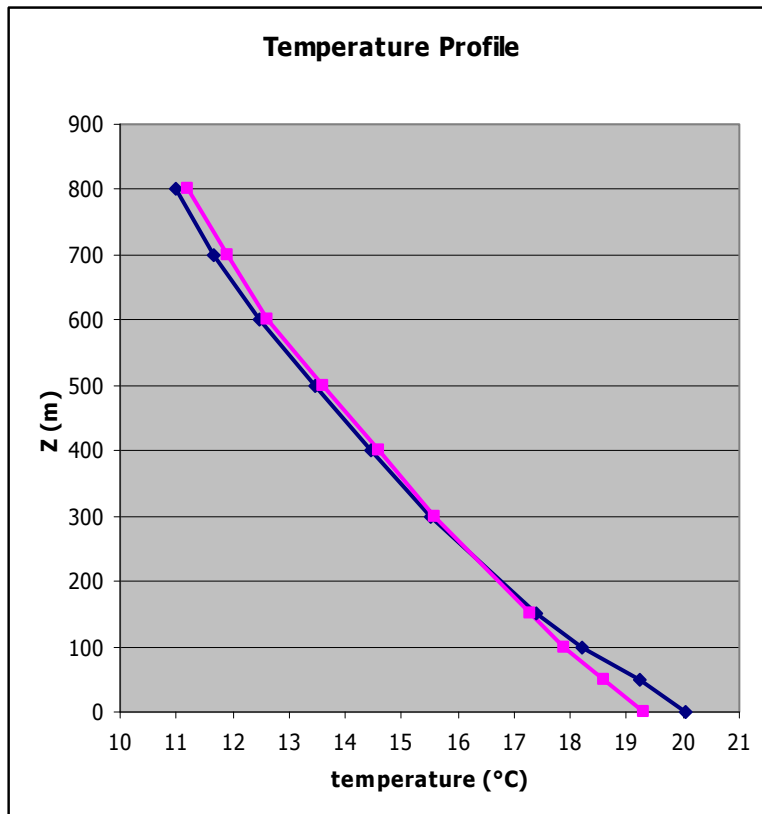
Figure 7: The behaviour of temperature.

The "Jesi" Simulation

This 24-hr simulation was performed during the 24 hours from 10–11 December 2001, and the nested grid is centred on 43.52°N, 13.24°E. In contrast to the above profiles, the results are compared to observed values (Figs. **8–10**). In all figures, the solid line represents observed data; the dashed line, fine resolution; and the dotted line, coarse resolution.

It must be noted that Jesi is located 30 km from the Adriatic Sea in the middle of the Esino valley. Therefore, the influence on local dynamics due to sea breezes is negligible, though valley breezes are always present. Moreover, at the point where Jesi is located, the Esino valley is very smooth and large with respect to the mountains. Under such conditions, the observed differences in wind speed for the two surface boundary resolutions are outstanding (Fig. **8**).

Figure 8: Wind speed behaviour.
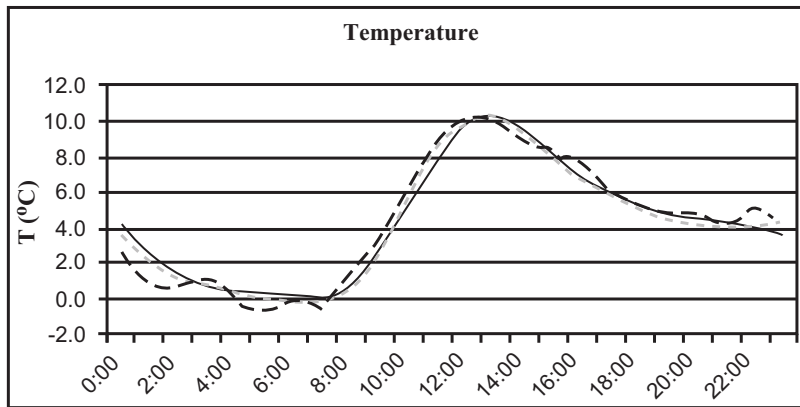
Figure 9: Temperature behaviour.
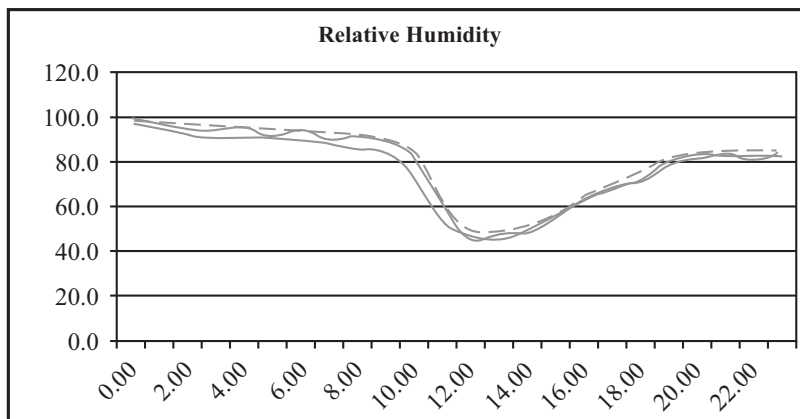
Figure 10: Relative humidity behaviour.

The "Chiaravalle" Simulation

The following results are taken from the 3 December 2001 simulation in Chiaravalle, 22 m above MSL and at precisely 43.60°N, 13.31°E.

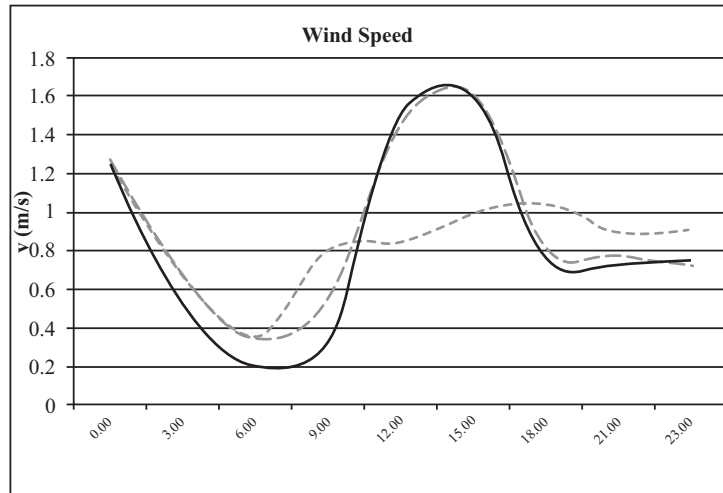In contrast to Jesi, Chiaravalle is located in close proximity to the sea (less than 10 km inland); sea breezes are dominant all year long, while the valley effect is negligible due to the "flatness" at the mouth of the river. Here we find a strong dependence on the grid resolution, even stronger than in the previous case. The wind speed, surface temperature and relative humidity are plotted as before (Fig. **11–13**).
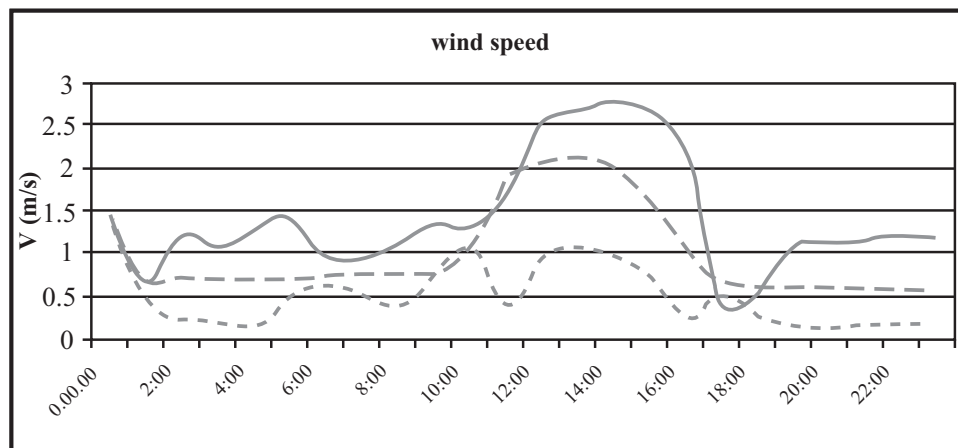
Figure 11: Wind speed behaviour.

Fig. (**11**) illustrates an interesting behavioural aspect of the model. From a qualitative point of view, all three curves show a similar trend, with certain dynamical phenomena showing significant differences between the two simulations. First of all, it should be noted that both computer-simulated value sets underestimate the observed data. This may be due to the coarse definition of surface roughness around the observation station, which is unfortunately located in the middle of an urbanized area.

As expected, the fine orography simulation is much closer to the observed data than the coarse orography simulation. It may be added that this simulation has better illustrated the local breeze dynamics as well. This is suggested by both the slight wind velocity and the times at which the speed increases or decreases.
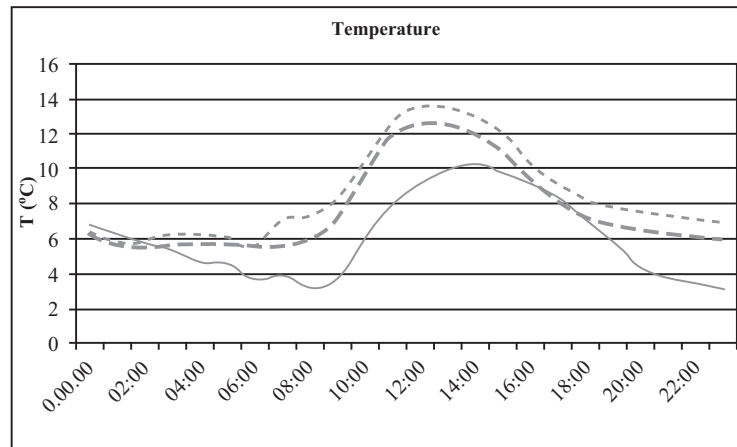
Figure 12: Temperature behaviour.
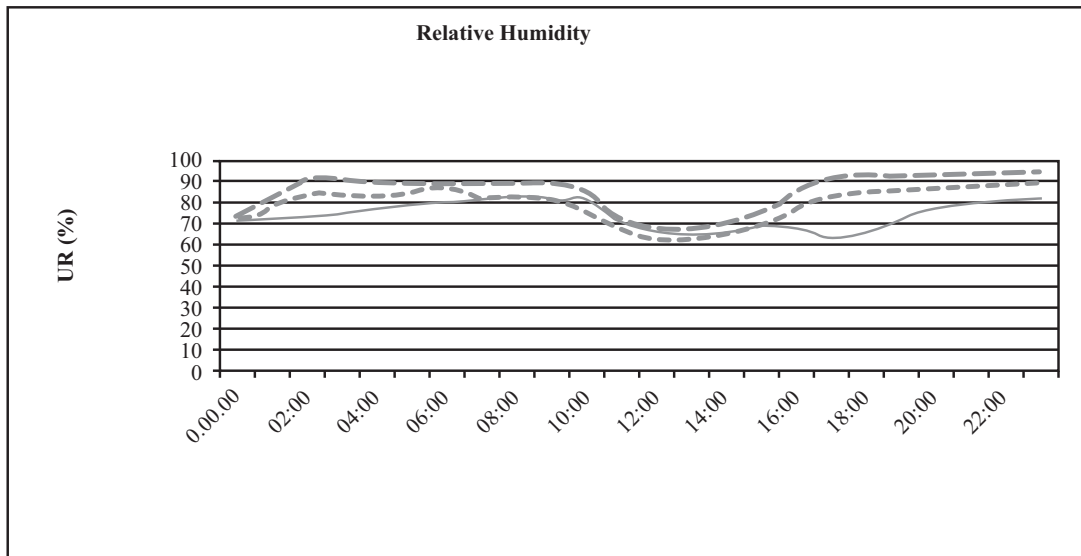
Figure 13: Relative humidity behaviour.

In the following figures, a 3D comparison of the coarse and fine orography simulations is depicted. In addition to the issues pointed out previously, a further aspect becomes evident here: the definition of coastlines. From a thermodynamics point of view, this issue pertains to the definition of thermal response areas on the surface.

In terms of quantities, we show results from a sample simulation (summer time) where a thermal response delay is observed due to a different definition of the

boundary condition (land-sea surface). Fig. (**14**) shows a vertical cross-section of wind streamlines at 10:00 am with the fine orography simulation on the left. It is evident that a convection cell has been triggered by the thermal gradient on the left (although not perfectly represented by the vis5D viewer), while on the right parallel streamlines flow seaward.
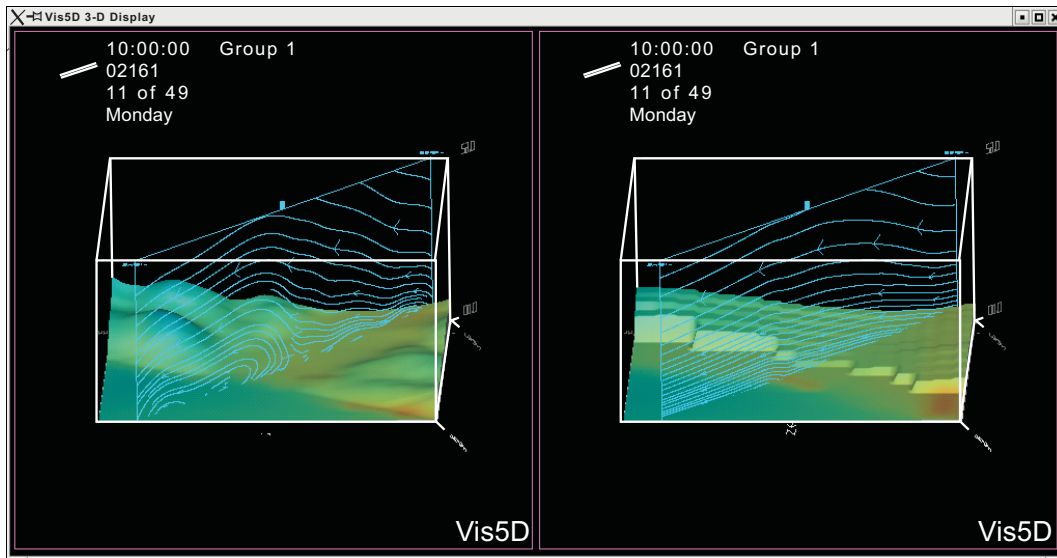
Figure 14: A vertical cross-section of streamlines at the mouth of the Esino valley (on the Adriatic Sea). Left: terrain with 100 m resolution; right: terrain with 1 km resolution. Terrain colour mapping (from blue to red) depicts the thermal field on the surface.

Two hours later (Fig. **15**), a convective pattern appears in the second simulation as well. The previous breeze cell is better developed and affects a deeper layer of the lower atmosphere.

The breeze situation in the middle of the valley (at Jesi) is shown in Fig. (**16**). Once again, development of the valley breeze is delayed due to a weak thermal gradient. In fact, as may be noticed by the lighter coloration of high terrain in Fig. (**16a**), the surface temperature is noticeably lower at greater heights due to the greater wind speed.

This phenomenon could not be simulated in the second run because of the compressed orography resulting from a coarser definition. To this end, it should be mentioned that RAMS includes a *reflected envelope* computational scheme,

allowing the user to maintain the orography "silhouette" along with a land mass balance, which results in a very efficient algorithm.
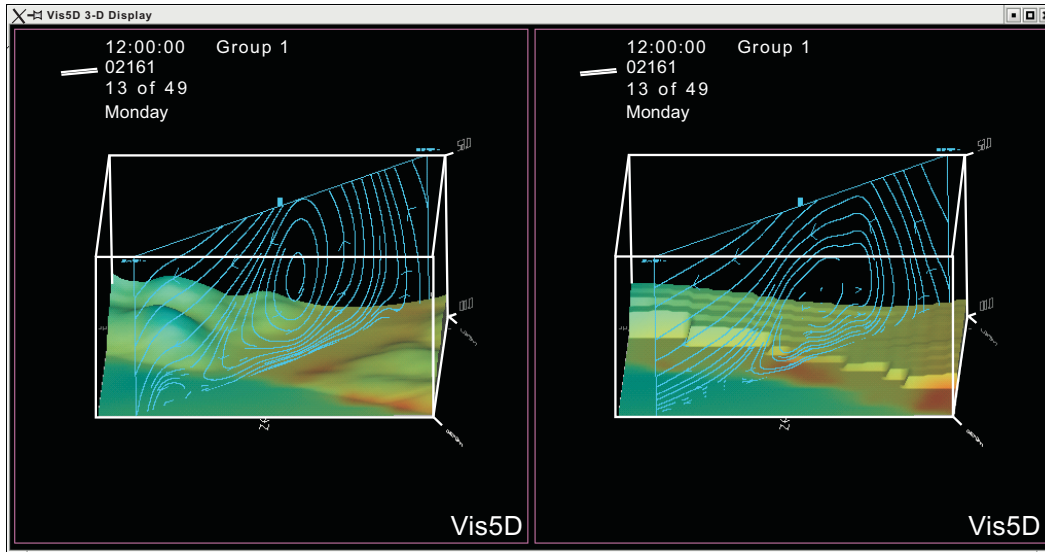
Figure 15: Images of the breeze in successive hours for fine (left) and coarse (right) grids show a sea-cell starting in the coarser grid, too.

This study illustrates the care that must be taken when defining the surface boundary condition in order to avoid significant misinterpretation.
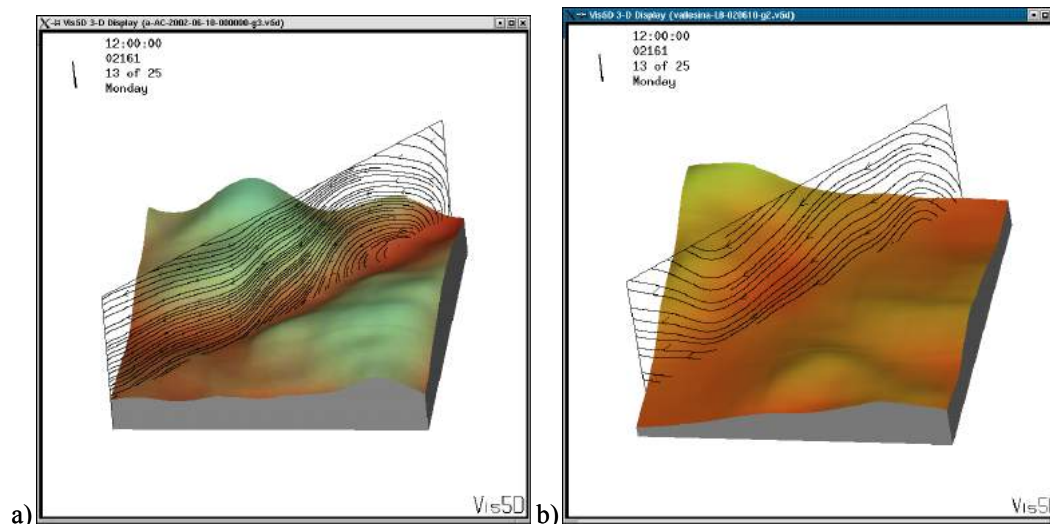
Figure 16: Breeze phenomena along the inner valley are very weak, especially in the central segment where the valley is wide and slopes gently.

MESOSCALE MODELS: A QUICK OVERVIEW

In this section, a brief survey of current meaningful references in the field of mesoscale models is presented. Focus is placed on three models that represent the current state of the field: the Regional Atmospheric Modeling System (RAMS), the Fifth Generation Penn State/NCAR mesoscale model (MM5), and the Weather Research and Forecasting model (WRF).

RAMS and MM5 followed the evolution of atmospheric dynamics modeling. They were developed based on several specific research-oriented models in the academic environment, and implement research advances of the last twenty years in parameterization and computational techniques. Both systems rely on a user community that develops model enhancements and disseminates results; the RAMS community is smaller than the MM5 community, but this is easily ascribable to the fact that RAMS was not freely available until the end of 2003.

WRF represents something different since it was designed as a well-planned project through a huge effort by a wide group of institutions that took account of all past experience. It appears to be destined to be a unique reference in the future.

All of these models are now freely downloadable from public web sites and are provided as open-source code. Code is mainly written in FORTRAN 90 and developed primarily for UNIX-based machines. These technical aspects are important since they imply some consequences: software portability is, of course, maximized since users compile the executable on their own machines; the computer skills of the user are maximized as well! This consideration is coupled to the absence of a graphical interface so a certain familiarity with the operating system is required. Naturally, once these first obstacles have been overcome, the possibility of delving deep in the code and eventually applying the desired modifications is a great opportunity, especially from the research point of view.

Regarding the latter point, a very critical role is played by the documentation available, which may be classified on a scale of complexity: tutorial, user's guide, test-case data, technical documentation (involving physical and mathematical aspects), and code documentation (main program flow, function and procedure

synopses). The lack of documentation or its poor maintenance needlessly increases the model complexity. RAMS is particularly weak on this point, although simpler model management partly compensates the difference.

In the operational aspect, the main difficulty for all three resides in data acquisition and input if the user is operating outside the USA. In fact, all three models have been developed and used primarily in the USA and so US standards and data formats are used overall. The wider the community, the more format compatibilities are overcome. So currently, even if it is not automatic, upper air or surface observations are no longer a serious problem. When these models were employed for the first time, gridded global data retrieval and input were also serious problems. The arrival of the Internet has blown away all communication difficulties.

RAMS

RAMS is the acronym for Regional Atmospheric Modeling System, which is a piece of software dedicated to atmospheric dynamics modeling, implemented and supported by ATMET (www.atmet.com). It consists of several different modules (Fig. **17**) that are able to manage atmospheric simulation (both diagnostic and prognostic) from data preparation to output representation. Specifically, there are three main parts in RAMS: ISAN, the RAMS model, and REVU.

The ISAN package performs the initial data objective analysis (according to the Barnes scheme) on a polar-stereographic grid. As a vertical coordinate, a hybrid σ-isentropic coordinate is used. Initial data are provided by general circulation models (*e.g.*, those provided by NCEP or ECMWF), which are then blended and interpolated with rawinsondes (*raob* data) and surface observations. Specific user-defined options are dedicated to data analysis management.

The main unit is the RAMS model, a module that simulates the evolution of atmospheric fields within the defined time bounds. A specific section deals with the governing equations. Along with the basic thermodynamic equations, a number of optional parameterization features are available: microphysics computation, radiation, precipitation, vegetation modeling (LEAF sub-model), *etc.*

The last module is REVU (RAMS Evaluation and Visualization Utility), which is used for output post-processing and results analysis. It is able to compute a large number of parameters and to prepare output in different standard visualization formats: Vis5D, GRADS, NCAR graphics, ASCII tables, *etc.* It also allows the user to inspect the resulting fields in different ways: 3D fields, soundings, specific points, *etc.*

There is no theoretical limit to RAMS' application, so it has been successfully applied from synoptic to micro-scale phenomena. The two-way grid nesting technique permits the use of very small mesh/cell size according to the required spatial resolution. While local phenomena are resolved on the finest grids, larger-scale phenomena are simulated on coarser ones (which are employed as fine-grid boundary conditions).

At present, the OLAM model has been specifically implemented for large-scale purposes.

The RAMS system derives from previous models developed for research in environmental modeling, and particularly for the simulation of the convective motion of clouds, mesoscale convective systems, precipitation, *etc.* RAMS parent codes were developed around 1980 at Colorado State University (Department of Atmospheric Science), elaborating on three existing models: a cloud mesoscale model [1], a hydrostatic cloud model [2], and a sea breeze model [3]. The current version of RAMS results from the merger of these three models.

The first versions of code were written in FORTRAN 77 with some C code in order to facilitate I/O procedures and dynamic memory allocation. It was implemented and supported primarily on UNIX systems. Presently (version 6), all RAMS code has been ported to FORTRAN 90 and has been widely compiled on LINUX and Windows systems as well. The Linux OS in particular has allowed the diffusion of parallel versions of the code.

The original machines employed for RAMS simulation computation were CRAY-1 (at NCAR). Afterwards, many other systems have been used, following computer development. Nowadays, it is easy to find RAMS running on a parallel

machine (*e.g.*, SGI, IBM, Sun) or even on a PC-cluster parallel machine. As computational capabilities have increased, newer features have been implemented in the model code.

For further details visit http:\\www.atmet.com.
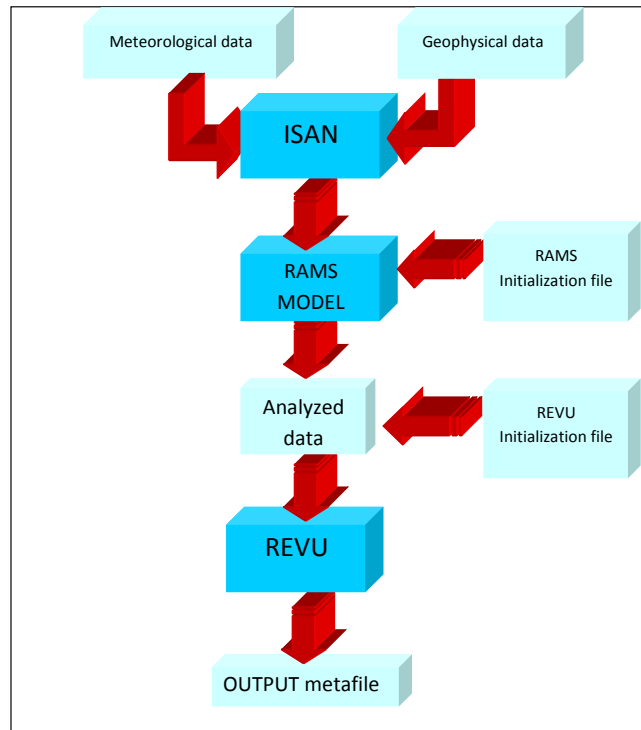
Figure 17: RAMS modules and data flow chart.

MM5 Modeling System

The Mesoscale Model version 5 (MM5) is a modeling system originally developed at Penn State University [4] and then continued at the NCAR (National Center for Atmospheric Research), featuring further capabilities in each new version.

MM5 is a very versatile model ranging from small to large scales of motion based on non-hydrostatic equations and multiple grid nesting (which makes approaching small scales possible). Furthermore, four-dimensional data assimilation is performed along with several optional parameterizations.

These characteristics make MM5 and RAMS absolutely comparable systems that represent the recent state of the art for atmospheric modeling. Grand expectations within the international modeling community are now directed toward the recently created WRF project (discussed briefly in the next section).

MM5 is not merely software, but rather a suite of utilities (Fig. **18**) around a main integration module, which are referred to as the MM5 modeling system. The utilities cover all of the necessary operations to set up a simulation: boundary conditions (from terrain gridding to atmospheric lateral and upper bounds), initial condition (3D first-guess fields, upper air soundings, and surface observations), analysis post-processing, and result representation. The modules distributed within the MM5 system are:

- TERRAIN: performs the horizontal interpolation of terrain elevation data (with a specific map projection, *e.g.*, polar stereographic). This model also processes land use data.

- REGRID: performs the horizontal interpolation of isobaric meteorological data (from global or regional models). It consists of two sub-modules, *pregrid* and *regridder*, which are responsible for the two-dimensional analysis. Vertical interpolation is postponed to a later step in the MM5 modeling chain (*interpf*).

- RAWINS and little_r: these modules enhance the initial 3D fields with observations (rawinsondes and surface) according to the Cressman technique or a multi-quadratic scheme.

- INTERPF: performs the vertical interpolation in σ-coordinates, which follow the terrain near the ground and tend to isobars in higher levels.

- MM5: after all previous steps are completed, the MM5 core module is ready to start the simulation.

- NESTDOWN: a module dedicated to generating data for finer grids.

- INTERPB: performs the *interpf* operations 'backward'. It produces pressure-level fields from the σ-coordinate fields. It can also produce "virtual observations" for *rawins* and *little_r*.

- GRAPH/RIP: a basic graphic output unit based on NCAR graphics libraries for viewing the results.

Along with the official modules, many small and large utilities have been developed by the international user community. For example, output is possible in GRADS or VIS5D format (which currently represent two scientific standards).

All modules are written in FORTRAN 77 or 90 and are developed and supported on UNIX machines (Linux is extensively employed of course). Naturally, a suitable code has been developed to allow this system to run on parallel machines, with both shared and distributed memory architectures.

For further details refer to http://www.mmm.ucar. edu/mm5.
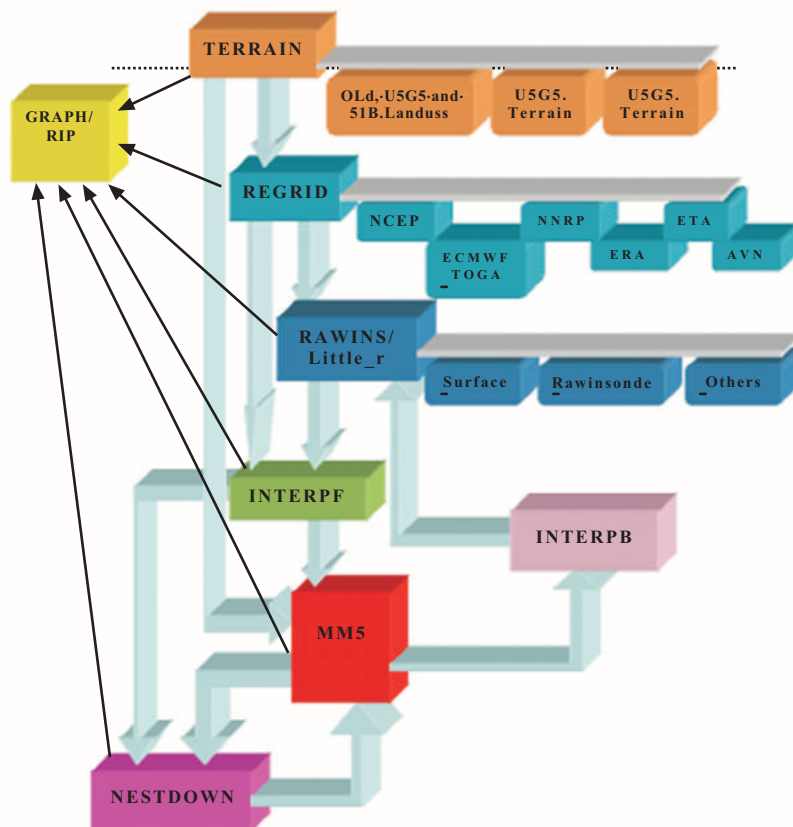
Figure 18: The MM5 modules.

WRF

The Weather Research and Forecasting modeling system (WRF) is the result of a coordinated knowledge-sharing project among all major US scientific and governmental agencies interested in dynamic meteorology. WRF represents the current state of the art in meteorological modeling.

The driving idea was to set up a main framework encompassing several different modules for parameterization, data assimilation, graphical output, *etc.*, as well as different integration cores.

This approach has been chosen in order to allow the broader user community to continuously test the model, developing new code or enhancing the existing one. Furthermore, a faster transfer of information and tools from research to operations is enabled.

The WRF Software Framework (WSF, [5, 6]) currently includes two documented support cores (Fig. **19**): the ARW (Advanced Research WRF solver, originally referred to as the Eulerian Mass, or EM, solver) which is developed, maintained and supported by NCAR; and the NMM (Non-hydrostatic Mesoscale Model) solver developed at NCEP, which is documented and supported by the Developmental Testbed Center (DTC). The fundamental purpose of the DTC is the transfer of new science and technology to the operational community, which may benefit from DTC testing to highlight the strengths and weaknesses.

Along with supported cores, the WRF framework includes several physics packages (integrated through the *Standard Physics Interface*) for parameterization research: WRF-var, which is a module dedicated to variational data assimilation [7], and programs related to initialization. Further post-processing and data conversion programs are currently under development (*e.g.*, from WRF to GRADS /VIS5D).

WRF is a very flexible structure based on a system of multiple (and moving) nested grids capable of simulations ranging from meters to thousands of kilometres. The widest applications are foreseen: from operational numerical weather prediction to basic input for air quality models; downscaling climate

simulations, atmosphere-ocean coupling, or idealized simulations (*e.g.*, boundary-layer eddies, convection, baroclinic waves).

Along with all of these objective capabilities (better summarized in tables below), the impressive participation of official US institutions makes WRF a special and important experiment, which will benefit the worldwide scientific community for years into the future. The institutions involved, other than NCAR (Mesoscale and Microscale Meteorology Division) and NCEP, are: the Forecast System Laboratory, the Air Force Weather Agency (AFWA) of the Department of Defense, the Naval Research Laboratory (NRL), the Center for Analysis and Prediction of Storms (CAPS) at the University of Oklahoma, and the Federal Aviation Administration (FAA), along with the participation of a number of university scientists.
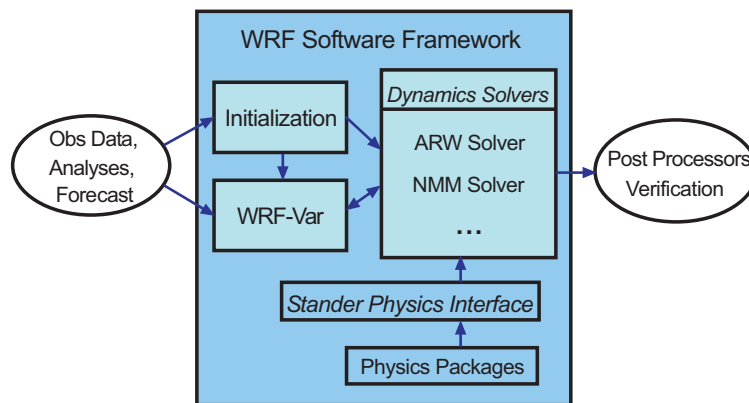
Figure 19: WRF system components.

The WRF modeling system is very well documented, so any information on running the ARW modeling system and any other details may be found on the Web:

http://wrf-model.org (the WRF project home page)

http://www.mmm.ucar.edu/wrf/users (the WRF -ARW user page maintained at NCAR)

http://www.dtcenter.org/wrf-nmm/users (WRF -NMM user page maintained at DTC)

Table 1: Governing Equation

Aspect\Model	RAMS	MM5	WRF
Equations	Standard non-hydrostatic Reynolds-averaged primitive equations.	Fully compressible, Euler non-hydrostatic.	Fully compressible, Euler non-hydrostatic with a run-time hydrostatic option available. Conservative for scalar variables.
Prognostic Variables	Horizontal velocity components u and v, vertical velocity w, perturbation potential temperature, Exner function. Optionally, turbulent kinetic energy and any number of scalars such as water vapour mixing ratio, rain/snow mixing ratio, and cloud water/ice mixing ratio.	Horizontal velocity components u and v, vertical velocity w, perturbation temperature, and perturbation surface pressure of dry air.	Horizontal velocity components u and v, vertical velocity w, perturbation potential temperature, perturbation geopotential, and perturbation surface pressure of dry air. Optionally, turbulent kinetic energy and any number of scalars such as water vapour mixing ratio, rain/snow mixing ratio, and cloud water/ice mixing ratio.
Vertical Coordinates	Terrain-following system, with vertical grid stretching permitted. Top of the model is exactly flat.	Terrain-following hydrostatic-pressure, with vertical grid stretching permitted. Top of the model is a constant pressure surface.	Terrain-following hydrostatic-pressure, with vertical grid stretching permitted. Top of the model is a constant pressure surface.
Horizontal Grid	Arakawa C-grid staggering.	B-grid staggering.	Arakawa C-grid staggering.
Time Integration	Time-split integration using a first-order forward/backward, leapfrog, or hybrid scheme. A smaller time step is used for acoustic and gravity wave modes.	Time-split integration using a semi-implicit Klemp-Wilhemson scheme, or leapfrog scheme. A smaller time step is used for acoustic and gravity wave modes.	Time-split integration using a third-order Runge-Kutta scheme with smaller time steps for acoustic and gravity wave modes.
Spatial Discretization	Two schemes available: - second- and fourth-order leapfrog - second- and sixth-order forward [8] advection in horizontal and vertical.	second-, fourth-, and sixth-order forward [8] advection in horizontal and vertical.	second- to sixth-order advection options in horizontal and vertical.
Turbulent Mixing and Model Filters	Deformation-based parameterization and turbulent kinetic energy parameterization.	Deformation-based parameterization and turbulent kinetic energy parameterization.	Sub-grid-scale turbulence formulation in both coordinate and physical space. Divergence damping, external-mode filtering, vertically implicit acoustic step off-centering. Explicit filter option also available.

Table 1: contd...

Domain Definition	RAMS	MM5	WRF
Initial Conditions	Three -dimensional for real data; various observational datasets are combined and processed by a mesoscale isentropic data analysis package.	Three-dimensional for real data: upper air and surface observations; global/regional models analysis.	Three-dimensional for real data, and one-, two- and three-dimensional for idealized data. A number of test cases are provided.
Lateral Boundary Conditions	Basic radiative conditions.	Sponge and nudging boundary conditions, moisture variables.	Periodic, open, symmetric, and specified options available.
Top Boundary Conditions	Wall ($w = 0$), Klemp and Durran gravity wave radiative condition, absorbing layer (Rayleigh damping).	Klemp and Durran and Bougeault gravity wave radiative condition.	Gravity wave absorption (diffusion or Rayleigh damping). Top boundary condition $w = 0$ at constant pressure level.
Bottom Boundary Conditions	Physical.	Physical.	Physical or free-slip.
Earth's Rotation	Full Coriolis terms included.	Coriolis terms optionally included.	Full Coriolis terms included.
Mapping to Sphere	Rotated polar stereographic projection.	Three map projections are supported: polar stereographic, Lambert-conformal, and Mercator. Curvature terms included.	Three map projections are supported for real-data simulation: polar stereographic, Lambert-conformal, and Mercator. Curvature terms included.
Nesting	One-way, two-way.	One-way, two-way, overlapping moving grids.	One-way, two-way, and moving nests.

Model Physics	RAMS	MM5	WRF
Microphysics	Bulk schemes ranging from simplified physics suitable for mesoscale modeling to sophisticated mixed-phase physics suitable for cloud -resolving modeling.	Bulk schemes ranging from simplified physics suitable for mesoscale modeling to sophisticated mixed-phase physics suitable for cloud -resolving modeling.	Bulk schemes ranging from simplified physics suitable for mesoscale modeling to sophisticated mixed-phase physics suitable for cloud -resolving modeling.
Cumulus parameterizations	Modified Kuo scheme.	- Anthes-Kuo - Grell - Kain-Fritsch - New Kain-Fritsch (including shallow convection physics) - Betts-Miller - Arakawa-Schubert	Adjustment and mass-flux schemes for mesoscale modeling, including NWP.

Surface physics	Multi-layer land surface models ranging from a simple thermal model to full vegetation and soil moisture models, including snow cover.	Fluxes of momentum, sensible and latent heat, ground temperature prediction using the energy balance equation, variable land use categories, 5-layer soil model, OSU land-surface model (V3.1–V3.5), Noah land-surface model (since V3.6), Pleim-Xiu land-surface model (V3 only).	Multi-layer land surface models ranging from a simple thermal model to full vegetation and soil moisture models, including snow cover and sea ice.
Planetary boundary layer physics	Turbulent kinetic energy prediction.	Bulk formula, Blackadar scheme, Burk-Thompson (Mellor-Yamada 1.5-order/level-2.5 scheme), Eta TKE scheme (Janjic, 1990, 1994), MRF scheme (Hong and Pan 1996), Gayno-Seaman scheme (Gayno 1994).	Turbulent kinetic energy prediction or non-local K schemes.
Atmospheric radiation physics	Longwave and shortwave schemes, with (Marher and Pielke) or without cloud effects (Chen and Cotton).	Simple cooling; Dudhia's long- and short-wave radiation scheme, NCAR /CCM2 radiation scheme, and RRTM long-wave radiation scheme.	Longwave and shortwave schemes with multiple spectral bands and a simple shortwave scheme. Cloud effects and surface fluxes are included.

GOVERNING EQUATIONs

RAMS

Grid Structure and Staggering

The staggering scheme adopted in the RAMS modeling system refers to Messinger and Arakawa [9]. In this scheme, all thermodynamic quantities are defined, along with velocity components (u, v, and w) with a stagger of ½ Δx, ½ Δy, and ½ Δz, where Δx, Δy, and Δz are the grid-cell widths in the x, y, and z directions, respectively.

A rotated polar-stereographic projection is adopted in order to minimize the distortion of the main area of interest (rotation of the projection pole near the domain centre).

Regarding the adopted coordinates, a terrain-following system is set up using the σ_z coordinate [10-12]. This is a coordinate system with a "flat" top to the domain

and the lowest level adhering exactly to the terrain. The coordinates are defined as such:

$$\begin{cases} x^* = x \\ y^* = y \\ z^* = H\left(\dfrac{z - z_g}{H - z_g}\right) \end{cases}$$

where H is the height of the highest level of the grid and z_g is the topographic height as a function of (x, y).

The vertical level may be introduced into the model in two different ways: a complete specification of each level height, or by defining a stretching ratio between two succeeding levels along with the height of the first level. The latter option easily allows for the definition of a higher vertical resolution near the ground.

Equations of Motion

For horizontal motion:

$$\frac{\partial u}{\partial t} = -u\frac{\partial u}{\partial x} - v\frac{\partial u}{\partial y} - w\frac{\partial u}{\partial z} - \theta\frac{\partial \pi'}{\partial x} + fv + \frac{\partial}{\partial x}\left(K_m\frac{\partial u}{\partial x}\right) + \frac{\partial}{\partial y}\left(K_m\frac{\partial u}{\partial y}\right) + \frac{\partial}{\partial z}\left(K_m\frac{\partial u}{\partial z}\right)$$

$$\frac{\partial v}{\partial t} = -u\frac{\partial v}{\partial x} - v\frac{\partial v}{\partial y} - w\frac{\partial v}{\partial z} - \theta\frac{\partial \pi'}{\partial y} + fu + \frac{\partial}{\partial x}\left(K_m\frac{\partial v}{\partial x}\right) + \frac{\partial}{\partial y}\left(K_m\frac{\partial v}{\partial y}\right) + \frac{\partial}{\partial z}\left(K_m\frac{\partial v}{\partial z}\right)$$

and for vertical motion:

$$\frac{\partial w}{\partial t} = -u\frac{\partial w}{\partial x} - v\frac{\partial w}{\partial y} - w\frac{\partial w}{\partial z} - \theta\frac{\partial \pi'}{\partial z} - \frac{g\theta_v'}{\theta_0} + \frac{\partial}{\partial x}\left(K_m\frac{\partial w}{\partial x}\right) + \frac{\partial}{\partial y}\left(K_m\frac{\partial w}{\partial y}\right) + \frac{\partial}{\partial z}\left(K_m\frac{\partial w}{\partial z}\right)$$

In the equations above, u, v, and w are the east-west, north-south, and vertical wind components, respectively; θ is the potential temperature, and K_m is the eddy viscosity coefficient for momentum.

The first three terms on the right hand side represent advection; the fourth term contains π', which is the Exner function, a function of pressure. The Coriolis terms, f_u and f_v, are given in terms of the f-coefficient (the Coriolis parameter), and the three last terms describe turbulent mixing.

We can define the quantity π' as

$$\pi' = c_p \left(\frac{P}{P_0} \right)^k$$

where

c_p is the specific heat of dry air ($1004 \ \text{J K}^{-1} \ \text{kg}^{-1}$)

P is the pressure at the point considered

k is a constant equal to 0.286

P_0 is the reference pressure (10000 mbar)

Heat Equation

$$\frac{\partial \theta_{il}}{\partial t} = -u \frac{\partial \theta_{il}}{\partial x} - v \frac{\partial \theta_{il}}{\partial y} - w \frac{\partial \theta_{il}}{\partial z} + \frac{\partial}{\partial x} \left(K_h \frac{\partial \theta_{il}}{\partial x} \right) + \frac{\partial}{\partial y} \left(K_h \frac{\partial \theta_{il}}{\partial y} \right) + \frac{\partial}{\partial z} \left(K_h \frac{\partial \theta_{il}}{\partial z} \right) + \left(\frac{\partial \theta_{il}}{\partial t} \right)_{rad}$$

Here, θ_{il} is the potential temperature of ice water and K_h is the eddy viscosity coefficient for heat and moisture. The *rad* subscript denotes the tendency for radiation parameterization.

Water Species Mixing Ratio Continuity Equation

$$\frac{\partial r_n}{\partial t} = -u \frac{\partial r_n}{\partial x} - v \frac{\partial r_n}{\partial y} - w \frac{\partial r_n}{\partial z} + \frac{\partial}{\partial x} \left(K_h \frac{\partial r_n}{\partial x} \right) + \frac{\partial}{\partial y} \left(K_h \frac{\partial r_n}{\partial y} \right) + \frac{\partial}{\partial z} \left(K_h \frac{\partial r_n}{\partial z} \right)$$

where r_n is the water species mixing ratio of total water, rain, pristine crystals, aggregates and snow.

Mass Continuity Equation

$$\frac{\partial \pi'}{\partial t} = -u \frac{R\pi_0}{c_v \rho_0 \theta_0} \left(\frac{\partial \rho_0 \theta_0 u}{\partial x} + \frac{\partial \rho_0 \theta_0 v}{\partial y} + \frac{\partial \rho_0 \theta_0 w}{\partial z} \right)$$

where ρ is the density.

MM5

Coordinate System

The vertical coordinate is defined as a function of pressure as follows:

$$\sigma = \frac{(p_0 - p_t)}{(p_s - p_t)}$$

where p_s and p_t are the pressure at the surface and the upper bound of the reference level, which are time-independent. The total pressure for a chosen grid point is given by

$$p = p*\sigma + p_t + p',$$

where $p*(x,y) = p_s(x,y) - p_t$.

All equation presented are in their advective form.

Equations of motion

For horizontal motion:

$$\frac{\partial p*u}{\partial t} = -m^2 \left[\frac{\partial p*uu/m}{\partial x} + \frac{\partial p*vu/m}{\partial y} \right] - \frac{\partial p*u\dot{\sigma}}{\partial \sigma} + uDIV +$$

$$- \frac{mp*}{\rho} \left[\frac{\partial p'}{\partial x} - \frac{\sigma}{p*} \frac{\partial p*}{\partial x} \frac{\partial p'}{\partial \sigma} \right] + p*fv + D_u \tag{1}$$

$$\frac{\partial p*v}{\partial t} = -m^2 \left[\frac{\partial p*uv/m}{\partial x} + \frac{\partial p*vv/m}{\partial y} \right] - \frac{\partial p*v\dot{\sigma}}{\partial \sigma} + vDIV +$$

$$- \frac{mp*}{\rho} \left[\frac{\partial p'}{\partial y} - \frac{\sigma}{p*} \frac{\partial p*}{\partial y} \frac{\partial p'}{\partial \sigma} \right] - p*fu + D_v \tag{2}$$

and for vertical motion:

$$\frac{\partial p^* \omega}{\partial t} = -m^2\left[\frac{\partial p^* u\omega/m}{\partial x} + \frac{\partial p^* v\omega/m}{\partial y}\right] - \frac{\partial p^* \omega\dot{\sigma}}{\partial \sigma} + \omega DIV +$$

$$+ p^* g\frac{\rho_0}{\rho}\left[\frac{1}{p^*}\frac{\partial p'}{\partial \sigma} + \frac{T_v'}{T} - \frac{T_0 p'}{T p_0}\right] - p^* g[(q_c + q_r)] + D_\omega$$

(3)

The pressure is given by

$$\frac{\partial p^* p'}{\partial t} = -m^2\left[\frac{\partial p^* u p'/m}{\partial x} + \frac{\partial p^* v p'/m}{\partial y}\right] - \frac{\partial p^* p'\dot{\sigma}}{\partial \sigma} + p' DIV +$$

$$- m^2 p^* \gamma p\left[\frac{\partial u/m}{\partial x} - \frac{\sigma}{mp^*}\frac{\partial p^*}{\partial x}\frac{\partial u}{\partial \sigma} + \frac{\partial v/m}{\partial y} - \frac{\sigma}{mp^*}\frac{\partial p^*}{\partial y}\frac{\partial v}{\partial \sigma}\right] +$$

$$+ \rho_0 g\gamma p\frac{\partial \omega}{\partial \sigma} + p^* \rho_0 g\omega$$

(4)

and the temperature is

$$\frac{\partial p^* T}{\partial t} = -m^2\left[\frac{\partial p^* u T/m}{\partial x} + \frac{\partial p^* v T/m}{\partial y}\right] - \frac{\partial p^* T\dot{\sigma}}{\partial \sigma} + TDIV +$$

$$+ \frac{1}{\rho c_p}\left[p^*\frac{Dp'}{Dt} - \rho_0 g p^* \omega - Dp'\right] + p^*\frac{\dot{Q}}{c_p} + D_T,$$

(5)

where

$$DIV = m^2\left[\frac{\partial p^* u/m}{\partial x} + \frac{\partial p^* v/m}{\partial y}\right] - \frac{\partial p^* \dot{\sigma}}{\partial \sigma},$$

and

$$\dot{\sigma} = -\frac{\rho_0 g}{p^*}\omega - \frac{m\sigma}{p^*}\frac{\partial p^*}{\partial x}u - \frac{m\sigma}{p^*}\frac{\partial p^*}{\partial y}v.$$

All other symbols represent the usual quantities.

In the MM5 model, it is possible to include all of the negligible components of the Coriolis force. The complete Coriolis force implies a small acceleration directed upward (downward) in westerly (easterly) fluxes and a deviation rightward (leftward) in horizontal fluxes in the Northern (Southern) Hemisphere. The Coriolis parameter is introduced *via f* (defined as $2\Omega sin\varphi$ where φ is the latitude) along with the angular difference between the *y*-axis and true north. This angle is given by the following relationship:

$$\tan\theta = -\cos\phi \frac{\partial\lambda/\partial y}{\partial\phi/\partial y},$$

where ϑ is the longitude.

WRF

The ARW dynamics solver integrates the compressible, non-hydrostatic Euler equations. The equations are cast in flux form using conserved variables, following the philosophy of Ooyama [13]. The equations are formulated using a terrain-following mass vertical coordinate [14].

The Vertical Coordinate and Variables

The ARW solver currently supports three projections: the Lambert conformal, polar stereographic, and Mercator projections, which are described in Haltiner and Williams [15]. These projections, and the ARW implementation of the map factors, assume that the map factor transformations for *x* and *y* are identical at a given point; that is, the transformation is isotropic. Anisotropic transformations, *e.g.*, a latitude-longitude grid, can be accommodated by defining separate map factors for the *x* and *y* transformations.

The ARW equations are formulated using a terrain-following hydrostatic-pressure vertical coordinate denoted by η and defined as

$$\eta = (p_h - p_{ht})/\mu \qquad\qquad\qquad (6)$$

where $\mu = p_{hs} - p_{ht}$

The hydrostatic component of the pressure is p_h, and p_{hs} and p_{ht} refer to values along the surface and top boundaries, respectively. The coordinate definition (Eq. 6), proposed by Laprise [16], is the traditional σ-coordinate used in many hydrostatic atmospheric models. The quantity η varies from a value of 1 at the surface to 0 at the upper boundary of the model domain. This vertical coordinate is also called a mass vertical coordinate.

Since $\mu(x, y)$ represents the mass per unit area within the column at (x, y), the appropriate flux-form variables are

$$V = \mu v = (U, V, W)$$
$$\Omega = \mu \dot{\eta}$$

$$\Theta = \mu \theta$$

The covariant velocities–are represented by $v = (u, v, w)$ while $\omega = \dot{\eta}$ is the contra-variant 'vertical' velocity. Again, θ is the potential temperature. As will be seen below in the ARW governing equations, the non-conserved variables $\phi = gz$ (the geopotential, or pressure) and $\alpha = 1/\rho$ (the inverse density) also appear.

Governing Equations

Using the variables defined above, the flux-form Euler equations can be written as

$$\partial_t U + (\nabla \cdot Vu) - \partial_z \left(p\phi_\eta\right) + \partial_\eta \left(p\phi_x\right) = F_U \tag{7}$$

$$\partial_t V + (\nabla \cdot Vv) - \partial_y \left(p\phi_\eta\right) + \partial_\eta \left(p\phi_y\right) = F_V \tag{8}$$

$$\partial_t W + (\nabla \cdot Vw) - g\left(\partial_\eta p - \mu\right) = F_W \tag{9}$$

$$\partial_t \Theta + (\nabla \cdot V\theta) = F_e \tag{10}$$

$$\partial_t \mu + (\nabla \cdot V) = 0 \tag{11}$$

$$\partial_t \phi + \mu^{-1}\left[(V \cdot \nabla\phi) - gW\right] = 0 \tag{12}$$

along with the diagnostic relation for the inverse density,

$$\partial_\eta \phi = -\alpha \mu$$

and the equation of state:

$$P = P_0 \left(R_D \theta / P_0 \alpha \right)^\gamma$$

In Eq. (7) – (8), the subscripts x, y, and ∂ denote differentiation,

$$\nabla \cdot Va = \partial_x (Ua) + \partial_y (Va) + \partial_\eta (\Omega a)$$

and

$$\nabla \cdot Va = U\partial_x a + V\partial_y a + \Omega\partial_\eta a$$

where a represents a generic variable. $\gamma = c_p/c_v = 1.4$ is the ratio of the heat capacities for dry air, R_d is the gas constant for dry air, and p_0 is a reference pressure (typically 10^5 Pa). The terms F_U, F_V, F_W, and F_θ represent forcing terms arising from the model physics, turbulent mixing, spherical projections, and the Earth's rotation.

The prognostic equations (7) – (12) are cast in conservative form except for (12), which is the material derivative of the definition of the geopotential. Eq. (12) could be cast in flux form, but we find no advantage in doing so since $\mu\phi$ is not a conserved quantity. We could also use a prognostic pressure equation in place of Eq. (12), [14], but pressure is not a conserved variable, and we could not use a pressure equation and the conservation equation for θ (Eq. 10) because they are not linearly independent. Additionally, prognostic pressure equations have the disadvantage of containing a mass divergence term multiplied by a large coefficient (proportional to the speed of sound), which makes spatial and temporal discretization problematic. It should be noted that the relation for hydrostatic balance (Eq. 12) does not represent a constraint on the solution, but is rather a diagnostic relation that is a formal part of the coordinate definition. In the hydrostatic counterpart to the non-hydrostatic equations, Eq. (9) replaces the vertical momentum equation (Eq. 9) and becomes a constraint on the solution.

Moisture

In formulating the moist Euler equations, we retain the coupling of dry air mass to the prognostic variables, and we retain the conservation equation for dry air (Eq. 7), as opposed to coupling the variables to the full (moist) air mass and hence introducing source terms in the mass conservation equation (Eq. 7). Additionally, we define the coordinate with respect to the dry air mass. Based on these principles, the vertical coordinate can be written as

$$\eta = (p_{dh} - p_{dht}) / \mu_d \tag{13}$$

where μ_d represents the mass of the dry air in the column and p_{dh} and p_{dht} represent the hydrostatic pressure of the dry atmosphere and the hydrostatic pressure at the top of the dry atmosphere. The coupled variables are defined as

$$\mathbf{V} = \mu_d \mathbf{v} \tag{14}$$

$$\Omega = \mu_d \dot{\eta} \tag{15}$$

$$\Theta = \mu_d \theta \tag{16}$$

With these definitions, the moist Euler equations can be written as

$$\partial_t U + (\nabla \cdot \mathbf{V} u)_\eta + \mu_d \alpha \partial_z p + (\alpha / \alpha_d) \partial_\eta p \partial_x \phi = F_U \tag{17}$$

$$\partial_t V + (\nabla \cdot \mathbf{V} v)_\eta + \mu_d \alpha \partial_y p + (\alpha / \alpha_d) \partial_\eta p \partial_y \phi = F_V \tag{18}$$

$$\partial_t W + (\nabla \cdot \mathbf{V} \omega)_\eta - \left[g(\alpha / \alpha_d) \partial_\eta p - \mu_d \right] = F_W \tag{19}$$

$$\partial_t \Theta + (\nabla \cdot \mathbf{V} \theta)_\eta = F_\Theta \tag{20}$$

$$\partial_t \mu_d + (\nabla \cdot \mathbf{V})_\eta = 0 \tag{21}$$

$$\partial_t \phi + \mu_d^{-1} \left[(\mathbf{V} \cdot \nabla \phi) - gW \right] = 0 \tag{22}$$

$$\partial_t Q_m + (\mathbf{V} \cdot \nabla q_m)_\eta = F_{Q_m} \tag{23}$$

where the diagnostic equation for dry inverse density is

$$\partial_\eta \phi = -\alpha_d \mu_d$$

and the diagnostic relation for the full pressure (vapour plus dry air) is

$$p = p_0 \left(R_d \theta_m / p_0 \alpha_d \right)^\gamma$$

In these equations, α_d is the inverse density of the dry air $\frac{1}{\rho_d}$ and α is the inverse density, which takes into account the full parcel density $\alpha = \alpha_d(1 + q_v + q_c + q_r + q_i + \cdots)$ where q are the mixing ratios (per mass of dry air) for water vapour, clouds, rain, ice, *etc.* Additionally, $\theta_m = \theta \left(1 + \left(\frac{R_v}{R_d} \right) q_v \right) \cong (1 + 1.61 q_v)$, and $Q_m = \mu_d q_m; q_m = q_v, q_c, q_i \ldots$.

Dispersion Sensitivity to Vertical Meteorological Profiles

The following case study aims to highlight the effect of meteorological fields on pollution dispersion. The models employed for the analysis are RAMS (as the meteorological processor), presented previously, and AERMOD (as the Gaussian dispersion model).

THE FALCONARA CASE STUDY

AERMOD relies on the AERMET module to complete the necessary input data. AERMET is a general-purpose meteorological pre-processor. It is necessary for the organization of available meteorological data into a format suitable for use by AERMOD as well as for the estimation of the necessary boundary layer parameters for dispersion calculations. AERMET is able to process hourly National Weather Service (NWS) surface observations, NWS twice-daily upper-air soundings, and data from on-site stations.

The NWS upper-air soundings are column datasets that can be used to characterize the vertical development of a meteorological field. The idea of vertical development of a meterological field is a key issue in accurate dispersion modeling. Since the areas under study can be on the magnitude of tens of kilometres, it is essential to choose the best starting dataset. There are also other

factors that can strongly influence the sounding selection. In addition to dataset selection, terrain conditions can also have a strong influence on the output. Modeling based on information in prognostic fields may also influence the dataset choice. Selection of the virtual sounding must also be considered. Therefore, when selecting an upper-air sounding, careful consideration must be put into selecting the most representative sounding for the task; this is particularly important when the amount of available data is limited. Limited data is a frequent problem in Italy, and the Marche region is no exception.

In other words, even the most advanced Gaussian model, such as AERMET/AERMOD, responds very well if applied to rather uniform terrain with sufficient data to balance eventual terrain anomalies; but complex orography presents a challenging limiting condition.

The case study is located on the Adriatic coast at the mouth of the Esino River near the town of Falconara Marittima. The study area is a river valley with a dominant breeze regime all year long. The pollutant source of interest is a cluster of fourteen stacks belonging to an important local refinery. Table **1** summarizes the source characteristics (all point sources) adopted in the simulations. The pollutant considered is nitrogen oxide (NO_x).

Table **2** shows a synoptic description of mentioned models concerning adopted equations and approximations, domain definition techniques and physical phenomena sub-modeling.

Table 2: Emission sources considered in the case study.

Source	Emission [g/s]	Height [m]	Gas temperature [°K]	Gas speed [m/s]	Diameter [m]
stck1	2.63	60	473	3.5	3.1
stck2	1.31	52	470	3.5	2.7
stck2	1.31	35	714	28.9	1.1
stck3	0.8	54	811	5.9	1.3
stck4	1.31	60	501	4.3	1.7
stck5	3.94	60	463	20.9	1.1
stck6	1.31	55	637	10.9	1.2
stck7	0.8	22	640	5.5	1.2
stck8	0.92	50	657	3.5	1.6

Table 2: contd....

stck9	0.53	28	553	2.3	1.4
stck10	1.05	54	523	3.7	2.3
stck11	1.18	54	523	3.6	2.5
stck12	5.25	15	773	5.9	0.6
stck13	39.44	50	393	11.4	8
stck14	0.3	50	423	2.1	3.5

The simulation area is shown in Fig. (**20**). The upper-air datasets are located 15 kilometres from the pollution source: one is at the very end of the valley (at the mouth of the small river) and the other is a few kilometres inland. The locations were chosen based upon the presence of surface monitoring stations, which allowed for validation of the meteorological simulations.
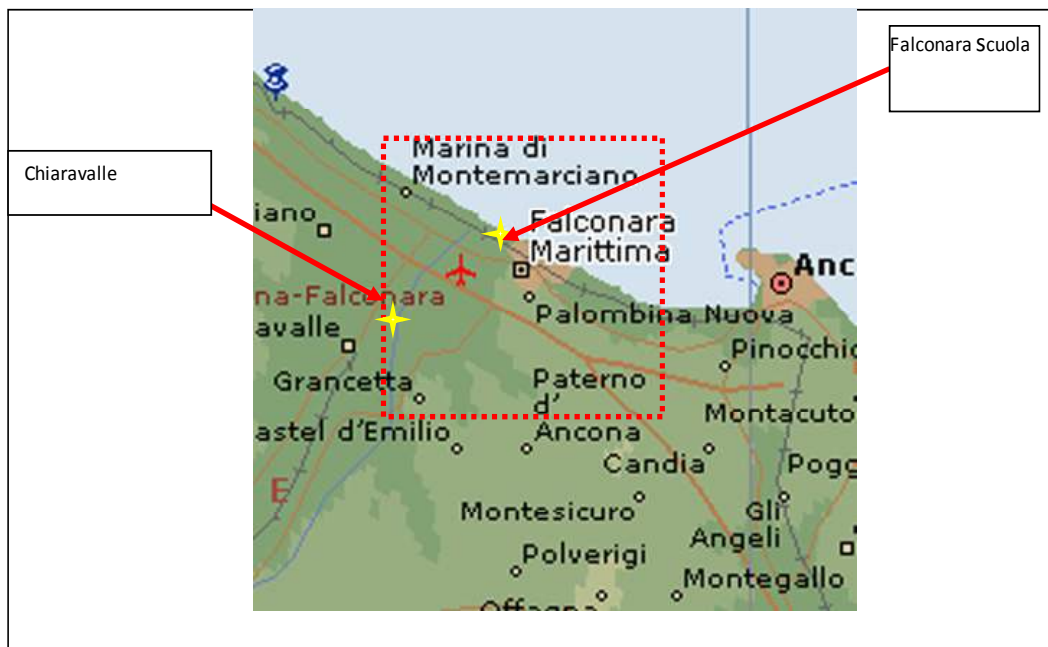
Figure 20: The simulation territory showing the location of the "forecasted sounding".

The simulation was set up with 400 surface receptors uniformly distributed on a square receptor grid. The following figures summarize the simulation results from Falconara Marittima (Fig. **21**) and Chairavalle (Fig. **22**) in terms of report receptor final concentrations.
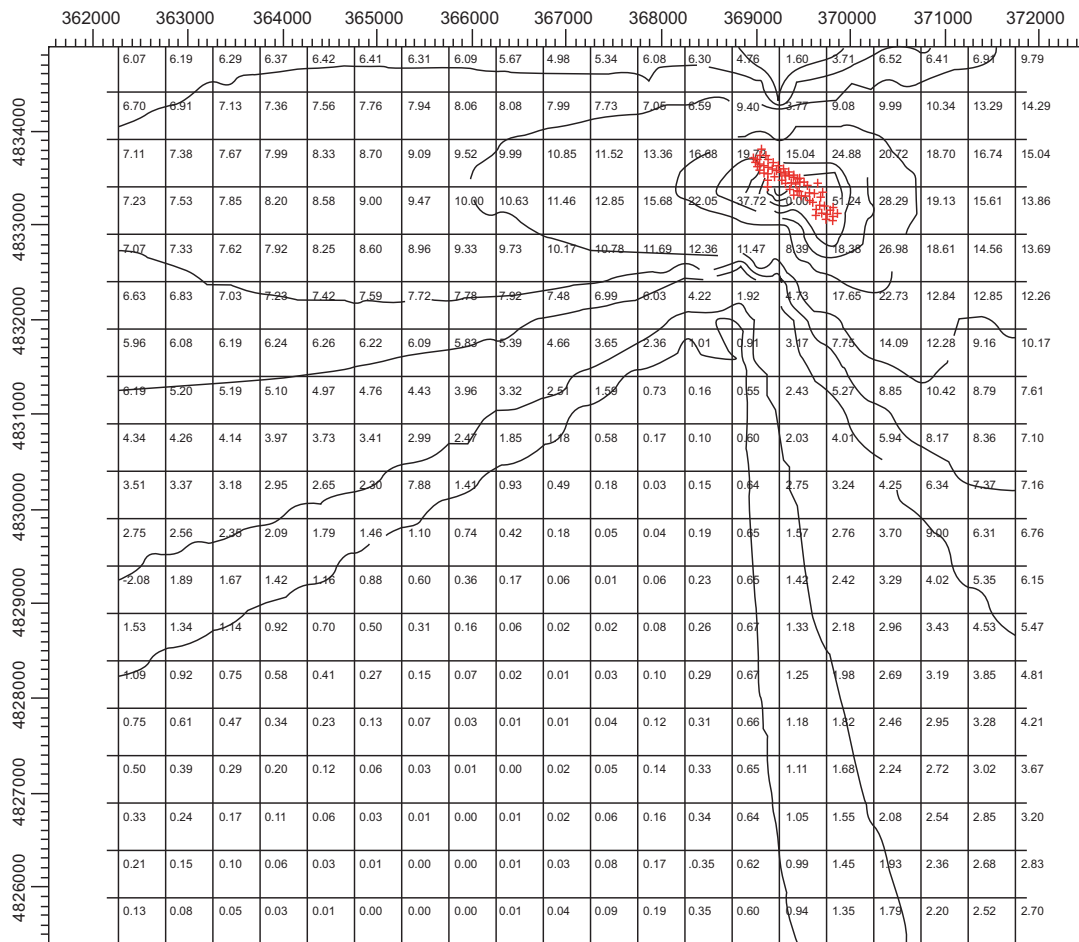
Figure 21: Receptor values during a simulation averaged over 24 hours. The upper-air sounding is located in Falconara Marittima and the maximum recorded value is 79.12 μg/m^3 (NO$_x$).

It is interesting to note that the distribution patterns (Figs. **21** and **22**) at the two sites are very dissimilar. Observations from the Falconara Marittima site show very low values on the valley side (south-west corner) and more significant values on the seaward side (northeast corner). Meanwhile, the opposite is true at the Chiaravalle site. The different dispersion patterns can be attributed to both the different vertical profile data as well as differences in the wind direction at the survey area. Values are low (with respect to warning thresholds) making this result even more interesting, since differences by of factor of six are observable between the two simulations. The invariability of the maximum value is due to calm weather conditions that allowed the plume to settle close to the source.
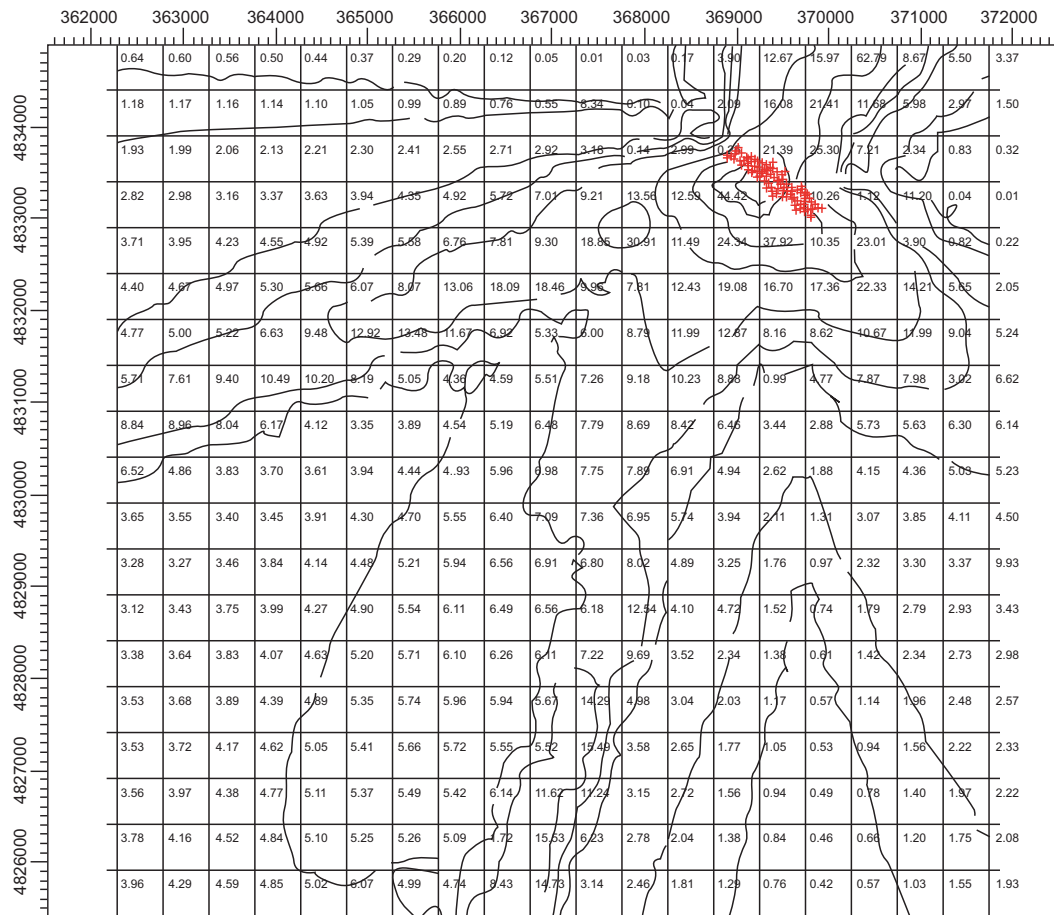
**Figure 22:** Receptor values related to a simulation averaged over 24 hours. The upper-air sounding is located in Chiaravalle and the maximum recorded value is 77.74 μg/m3 (NO_x).

Since the wind direction strongly influences the local pollutant concentrations, it was considered in greater depth. Fig. (**23**) provides the wind roses for both locations during the 24-hour survey period. As is evident from the wind rose for seaside town of Falconara Marittima (Fig. **23a**), there is a strong influence on the dominant alongshore circulation driving the mean wind in the southeast direction. On the other hand, the Chiaravalle station (Fig. **23b**) is influenced by valley-breeze-driven circulation, which is dominant in the northeast direction. As previously mentioned, in both locations the observed wind speed values are generally extremely low (0.5–1.5 m/s). Only at the Chiaravalle site is there some incidence of wind speeds up to 3.3 m/s.
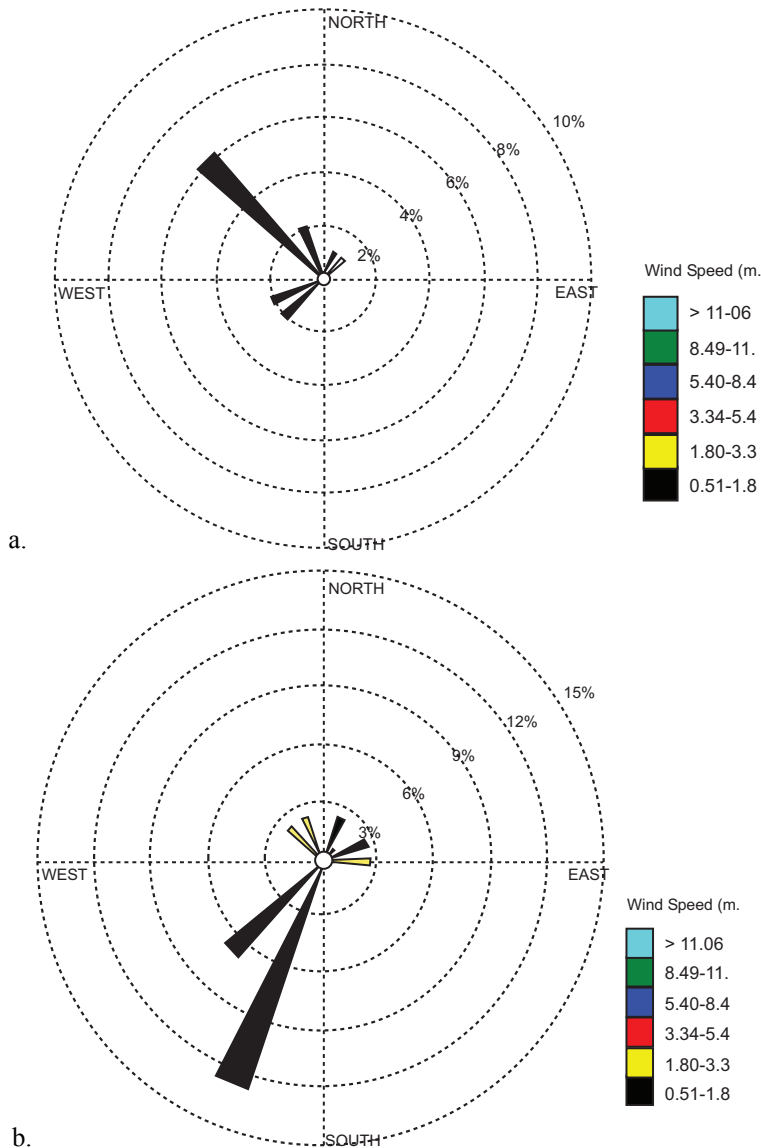
Figure 23: Wind roses for the period studied at the Falconara Marittima (a) and Chiaravalle (b) sites.

Hence, as a general procedure for approaching a complex terrain domain, a preliminary meteorological study is necessary in order to examine such aspects. It is necessary to highlight non-homogeneities in the time-averaged wind field as well as make a sensitivity analysis of a peculiar site to characterize the upper-air data.

Further considerations may also be made regarding precautionary choices: *e.g.*, opting for data providing the worst condition, *etc.*

The points highlighted above are even more relevant if the data pertaining to the meteorological conditions are not gathered on-site but are rather predicted by a mesoscale model. In fact, the literature contains a variety of reports based on studies coupling mesoscale and dispersion models. One example is that of Isakov and collaborators [16], who published a comparison of AERMOD simulations using a variety of meteorological inputs with data taken from onsite observations, 10-km NWS site data, the Eta model (coarsely resolved), and MM5 (quite finely resolved). The results demonstrate that more-comprehensive models, such as Eta and MM5, provide the best meteorological input data for dispersion models such as AERMOD. Furthermore, the poorest forecasts were those of wind direction for Wilmington, California, a shore town.

Again, topographical factors have a strong impact on the accuracy of model-generated predictions. Therefore, high spatial resolution is strongly recommended. The reliability of wind-direction-field predictions (provided by mesoscale models) depends on the accuracy of internal thermal boundary layer simulations (growing with the distance to the sea). This is particularly important in instances of higher release. The internal thermal boundary layer can be simulated for shoreline applications only by adequately resolved models. In such cases, it is strongly recommended that the computational grid resolution be coupled to a comparable resolution of orography information.

In conclusion, the acquisition of highly resolved meteorological models is necessary for generating accurate dispersion models. As we have shown, in addition to the use comprehensive models, wind direction data taken from on-site observations is crucial to achieving a truly representative model. Dispersion models generated for onshore sites in zones of complex orography are even more complex. Contrary to Mass and colleagues [17], we propose a much finer resolution then the generally recommended resolution [18], which ranges from 5 km to 1 km in complex terrain. As discussed previously, we propose a 0.1 km horizontal resolution for maximum accuracy in such situations.

Meteorology and THOES: a case study

The Summer 2000 Episode

During the summer of 2000, the Ancona provincial monitoring network recorded a severe transient high ozone event (THOE) in Falconara Marittima.

The event was so strong that drastic measures were taken in order to reduce the pollutant concentration, including a forced reduction of road traffic and a forced stoppage of plants and productive activities.

The selected study area is a typical coastal area located in the middle of Italy. Topography in this area is fairly complex and its proximity to the coast implies significant interaction between sea and valley breezes. The sea-breeze/land-breeze circuit is a mesoscale circulation of air caused by the differential heating and cooling of the land and sea surfaces in the coastal zone. The climate in this area, in fact, is classified as subcoastal, where there is a year-round sea breeze. During the summer, sea breezes combine with upslope winds to create re-circulations along the coast with residence times on the order of days.

Air pollution dynamics and associated meteorological processes in this area were analyzed. Our aim is to show the meteorological aspects and complementary modeling results to help interpret the observed ozone cycles.

The Area Studied and the Monitoring Network

The Falconara Marittima municipal area, though located on the shoreline, involves an area of about 25 km^2, presenting a rather complex orography. It extends from nearly flat land in the north to a hilly area toward the south. Moreover the Esino River passes through the area, with its mouth close to the town; a very important national route (SS16), a highway (A14), a large refinery, and an airport are all located in this area.

The region is subject to breezes that are dominant during the warmest period of the year. Due to the moderate steepness of the Esino Valley, valley breezes are very slight, although they have a synergistic effect on nocturnal land breezes (the mountain breezes act likewise on the sea breezes).

Air quality monitoring is performed by means of the integrated monitoring network of the Provincial Authorities, and a mobile lab is available in the event of severe episodes. At present, there are three monitoring stations within the Falconara municipal area, identified as:

"Falconara Scuola", located near the refinery and the sea;

"Falconara Acquedotto", close to the refinery but at a higher altitude;

"Falconara Alta", located in the historical town centre, several kilometres from the refinery and the sea.

The three monitoring stations–collect meteorological data along with air quality values.
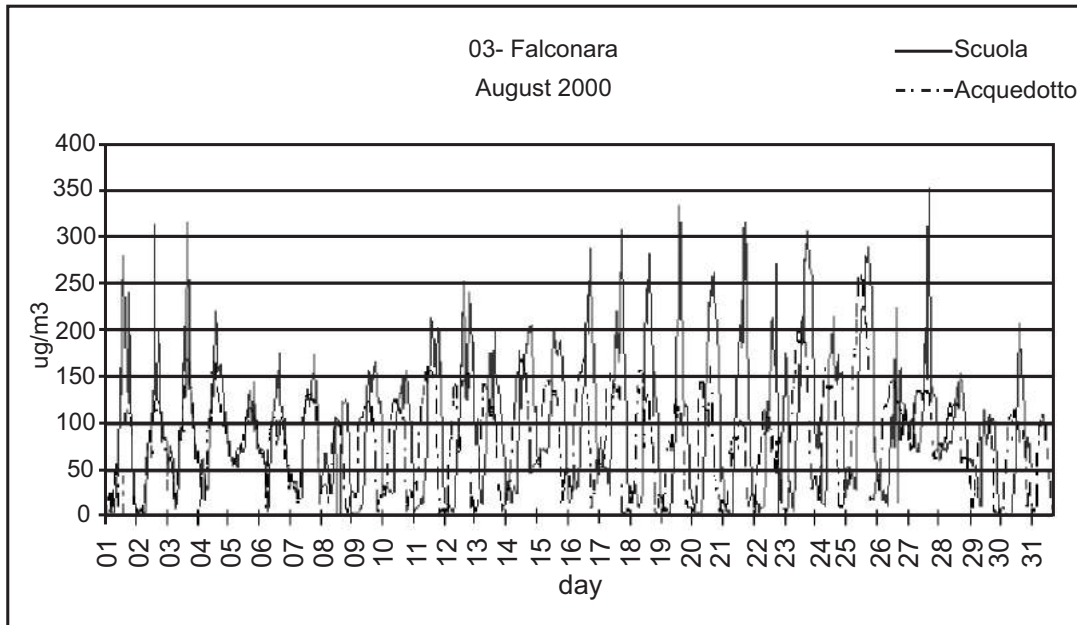
Figure 24: The ozone trend in Falconara during summer 2000.

In Fig. (**24**), the ozone trends from station 1 (Falconara Scuola) and station 2 (Falconara Acquedotto) are shown. It is easily to see how high the ozone peaked during that summer (200 µg/m^3 is the legal limit for hourly averaged observations). Solar activity was high (Fig. **25**) but not exceptional for the area.
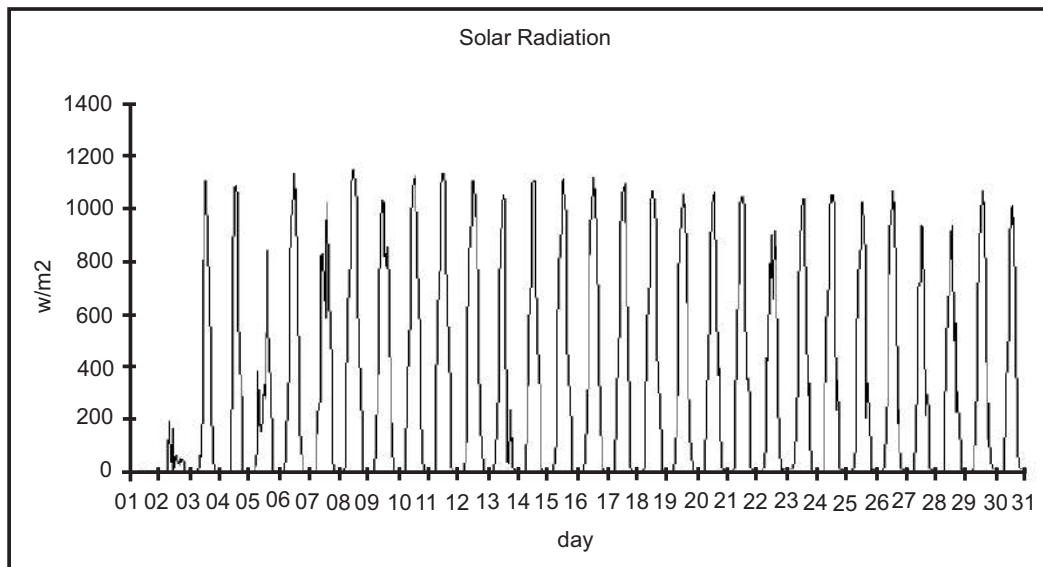
Figure 25: The solar radiation trend in Falconara during summer 2000.

Local Meteorology: Simulation for August 2000

The RAMS model was used to simulate the local-scale meteorology (running on a parallel machines to shorten the calculation time).

The whole period was fragmented into 36- or 48-hour simulations. Each simulation started from the results of the previous one, introducing further ground observations related to the period.

The simulation involved basic RAMS microphysics in order to evaluate cloud formation. The computational domain consists of four nested regular grids, as shown in Fig. (**26**), with the following characteristics:

Number of nodes in the *x*-direction per grid: 18, 17, 17, 17, 37;

Number of nodes in the *y*-direction per grid: 18, 17, 17, 17, 37;

Number of nodes in the *z*-direction per grid: 30, 30, 30, 30, 30;

Number of soil layers: 11;

Coarsest grid specification:;

Adopted projection: polar stereographic;

Cell width in the *x*-direction: 50000 m;

Cell width in the *y*-direction: 50000 m;

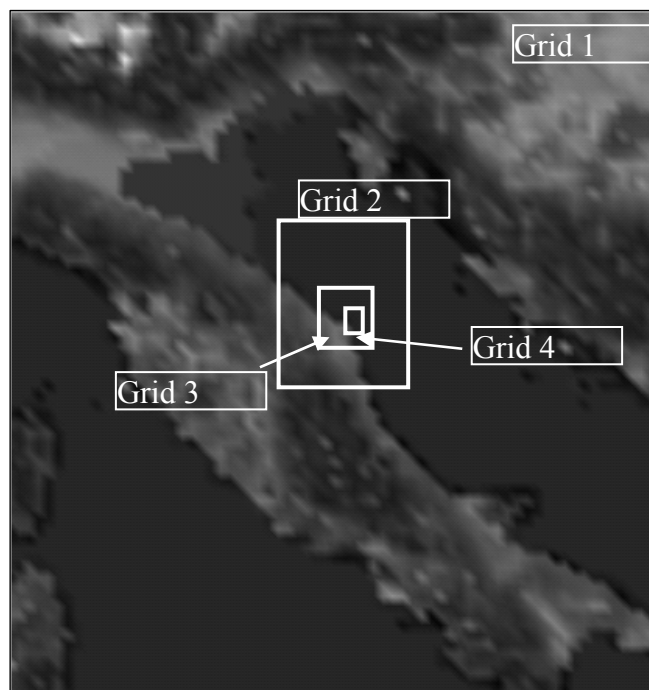Spatial nesting ratio for each grid level in both (*x* and *y*) directions: 1:5:5:5;

Height of first cell layer: 50 m;

Vertical stretching ratio: 1.15;

Max vertical height: 1500 m;

Time nesting ratio for each grid level: 1:5:5:5;

Figure 26: The RAMS simulation domain.

Upper air data: from the European Centre for Medium-range Weather Forecasts (ECMWF) with 0.5° horizontal resolution;

Surface data: from the Ancona provincial authority monitoring network;

Orography data: from the regional cartography service with 100-m horizontal resolution;

Land use and sea surface temperature: from the USGS–with 1-km horizontal resolution.

We expected to find slight breezes in the early morning and late evening, and their total absence at night when land and sea temperatures are closer. All simulations confirmed the theoretical predictions.

The first examination that should be made concerns the conditions that foster ozone formation. The literature clearly states that this is influenced by three major atmospheric properties: pressure, insolation (and indirectly the surface temperature), and horizontal wind velocity [19, 20].

High Pressure

Observations lead us to consider that every ozone episode occurs in conditions of high atmospheric stability, which implies synoptic high pressure. Looking at the Mediterranean basin, this situation is typically verified throughout the summer season, which is characterised by the presence of an anticyclone system involving the entire Mediterranean Sea. On the other hand, a strong reduction in ozone dynamics has been recorded at the first stage of development of low pressure or during the transition between two different high pressures within the same season [7].

The simulations confirmed the persistence of a high-pressure system throughout the area in August 2000.

Surface Temperature and Solar Radiation

The strong correlation between daily surface-temperature maxima and ozone episodes is well known from the literature; on the contrary, there is no specific correlation with daily mean values. In fact, the major forcing is irradiation, and correct statistical parameters may be the radiation-period duration or the daily maximum surface radiation. Unfortunately all of these data were unavailable.

In agreement with seasonal values, the solar radiation was constantly high throughout the month (see Fig. **25**).

Horizontal Wind Field

Ozone episodes are almost always recognisable under conditions of slight horizontal wind fields, which normally reduce pollutant dispersion. Furthermore, the scarce contribution of synoptic circulation allows local meteorological regimes (*e.g.*, breezes) to develop.

Fig. (**27**) shows that a stable sea breeze developed on 23 August; it is representative of the general behaviour throughout the month.
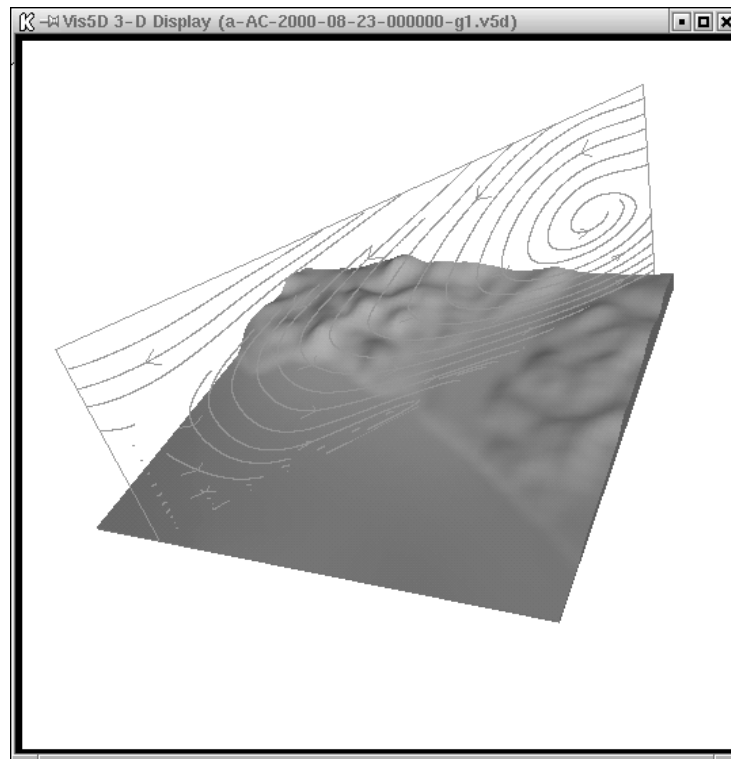
Figure 27: Extended convective cell of a sea breeze.

Moreover, the simulations showed how the breeze system was persistent and well-formed, performing a complete rotation. In the morning, breezes become intense between 9:00 and 10:00 (local time, LT) and come from the east, nearly

parallel to the coastline. At later hours, they tend to rotate clockwise, becoming ever stronger until 14:00 LT, when they are perpendicular to the coast. As night approaches, the breezes weaken and flow in a direction opposite to that in the morning, while they completely cease around 21:00 or 22:00 LT. During the twelve sunny hours, there is a rotation of 180°, which is completed by a further 180° rotation in the nocturnal land breeze phenomenon. A complete rotation of 360° was discovered in a 24-hr period on all critical days.

The persistence of breezes (only few days are characterised by absent or unstable breezes) was an initial confirmation to our hypotheses about ozone episodes in August 2000.

Several authors, such as Liu *et al.* [7, 20, 21] confirm the generally accepted conclusion that breezes, as well as other PBL-related phenomena, always lead to a worsening of air quality conditions [22, 23]. In fact, these phenomena can trigger the recirculation or stagnation of pollutants due to small-scale whirling motions, which are thermally induced by temperature gradients or mechanically induced by terrain roughness and natural obstacles. Examples of potentially dangerous situations for pollutant accumulation are katabatic winds along mountain versants, or whirls formed on the downwind side of an obstacle (*e.g.*, a ridge).
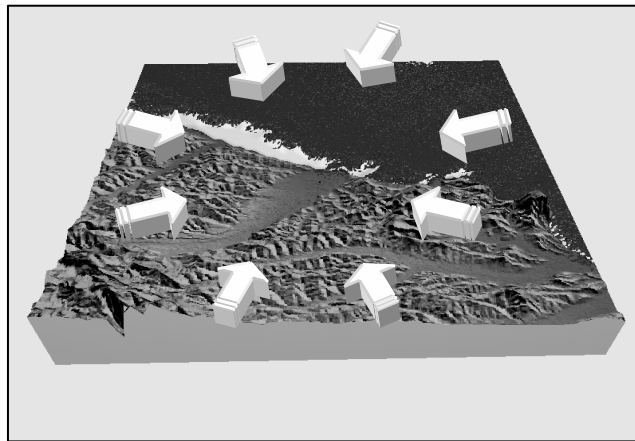
Figure 28: Breeze directions throughout the day in Falconara Marittima.

Figs. (**29**) and (**30**) show the vertical humidity profile for two different times on day 12 Falconara some kilometres off the coast. In Fig. (**29**), it is immediately

evident that the relative humidity (RH) is higher near the sea surface, while the upper layers remain substantially constant during the night.
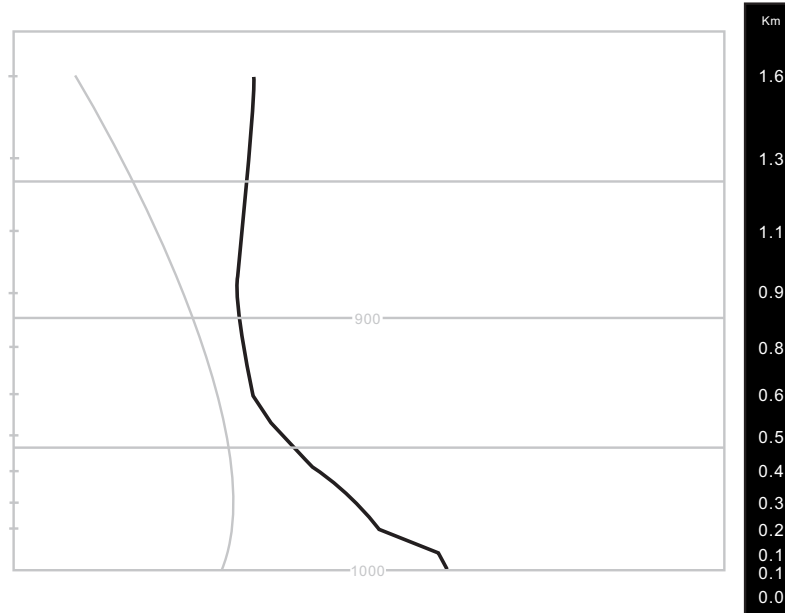
Figure 29: Relative humidity (dark line) and temperature (light line) profiles at few kilometres offshore at 6:00 am on 12 August 2000.
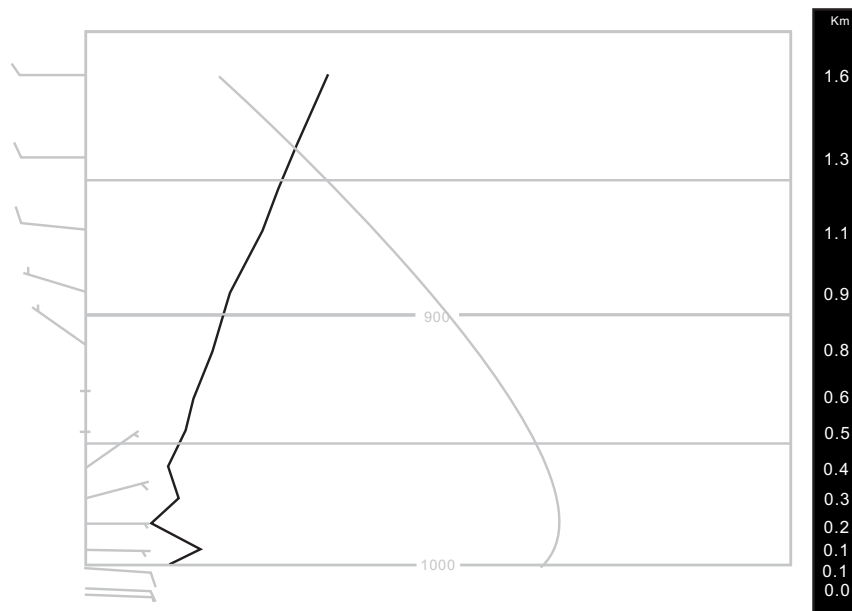
Figure 30: Relative humidity (dark line) and temperature (light line) profiles a few kilometres off the shore at 15:00 am on 12 August 2000.

A higher surface humidity over the sea at night (Fig. **31** is a further representation of the RH field) is an important point in the ozone evolution puzzle we are trying to piece together, as explained in the next section.

06:00:00
00222
8 of 25
Wednesday

Vis5D
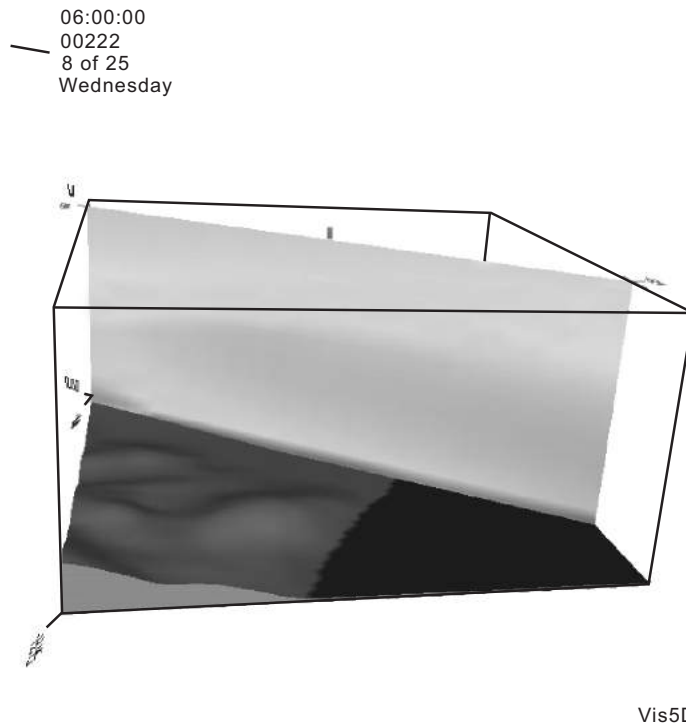
Figure 31: Relative humidity distribution (from black, maximum, to white) in a vertical section along the axis of the valley axis at 7:00 am on 9 August 2000.

Observed wind vectors at locations in the coastal area obviously show diurnal variation with changeover between the land and sea breezes. During the day, photochemical processes are very active and result in very high ozone concentrations. NO_x concentrations decrease and reach a low level at noon due to photochemical loss and the increase of the mixing layer. At night and in the early morning, the land breeze transports the precursors and photochemically produced ozone over the sea. In the daytime, the accumulated ozone over the sea returns to land with the sea breeze and contributes significantly to high-ozone episodes in clean coastal areas.

Moreover, the light land breeze that develops at night (generally weaker than the diurnal breeze) moves ozone [17, 23] over the marine surface, where high

nocturnal humidity inhibits dry deposition. The observations also show a similar trend. According to our hypotheses, this dangerous recirculation phenomenon occurred several times, persisting for 2–3 days, and dramatically affected ozone concentration values. This process is analysed in detail in the next section.

DISCUSSION AND CONCLUSIONS

The episode depicted in Fig. (**32**) is a well-known ozone pollution event characterizing the area under investigation. The whole process is radiation-triggered. This aspect is easily observable by following the dotted line representing the solar radiation evolution during this two-day sample. As soon as the Sun is high enough to heat the Earth's surface (one hour after dawn), the temperature increases and the most important element fostering this complex system is released into the atmosphere. In fact, it is conceivable that volatile organic compounds (VOCs) contained in tanks at the nearby refinery, due to a malfunction in the tanks' floating cover, increased their evaporation rate, and their concentration in the surrounding area grew higher and higher.
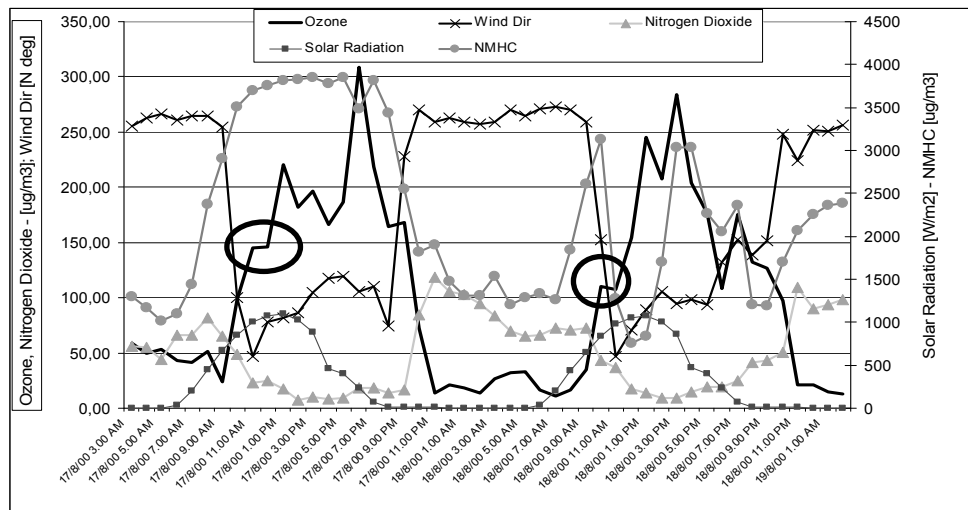
Figure 32: A sample period showing a typical 48-hr evolution of ozone, its precursors, and major meteorological forcing (17–18 August).

This area is easily recognizable as being VOC -limited with respect to the precursor balance for ozone formation. The rapid release of the limiting precursor

allows the secondary pollutant to form. Observing the graph, the role played by nitrogen dioxide, which is contextually depleted by the ozone formation process, is evident.

The process continues after the radiation peak (between 1:00 and 2:00 pm), due to the high air and surface temperature reached during the day, and we find a sustained level of ozone until one hour after sunset.

In these terms, the ozone dynamics is, as previously mentioned, well known. The point in scenarios like the present one is to understand the role played by breezes.

Looking at Fig. (**32**) and (**33**), we have a snapshot of a very strong daily periodicity and, furthermore, of a strict correlation or anti-correlation between the implied quantities. The thermal nature of breezes points to a direct correlation with radiation, which seems to imply that, although triggered by the same forcing of ozone, breezes act as simply a meteorological background for the pollution phenomenon.

More likely, breezes provide regimes of light but stable wind with little latency with respect to solar activity. The first consideration is that wind, however weak, should foster pollution dispersion, but the observed velocity rarely exceeds 4 m/s. More important is the geographical placement of pollutant sources in the mouth of the valley. In fact, the refinery is located on the eastern side of both the town and major roadways, which are the major sources of nitrogen oxides (due to combustion processes) in the summer. When the sea breeze starts a few hours after dawn, the volatile organic compounds dispersed over the refinery are most likely transported toward the town, thereby modifying the chemical equilibrium of the precursors and triggering the dynamical formation of ozone. In the opposite case, when the breeze blows from inland (just a couple of hours after sunset), volatilised hydrocarbons depleted by the decrease in temperature-are definitively blown back eastward beyond the shoreline.

Along with VOCs, ozone is subject to advection as well. It is transported over the sea where, affected by the presence of residual VOCs and the high humidity, it remains suspended over the sea and is recirculated with the changing breeze.

It is very difficult to estimate this contribution without the help of both monitoring stations over the sea and a photochemical model, but our hypothesis is substantiated by the observation of a systematic variation in the slope of the ozone curve (highlighted by the circles in Fig. **32** and **33**). Specifically, we observe a greater steepness in the first hours followed by a visible change where the increase of ozone is reduced.

Since this happens around midday, we cannot attribute the variation to a simple reduction of ozone activity. Conversely, the presence of an external contribution which is then quickly depleted is questionable.
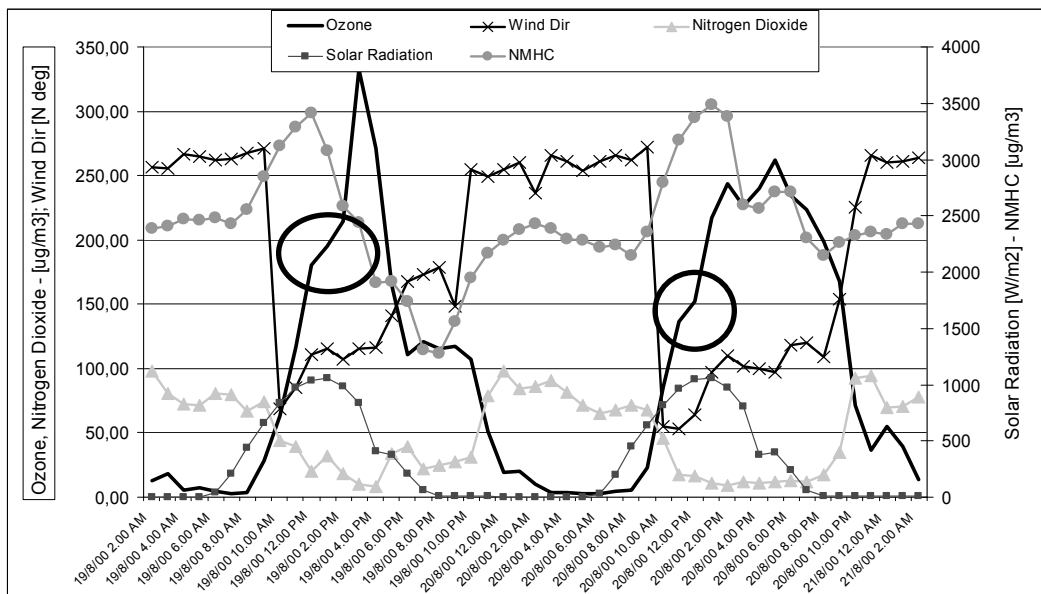
Figure 33: A sample period showing a typical 48-hr evolution of ozone, its precursors, and major meteorological forcing (19–21 August).

All of the simulations executed have underscored a meteorological situation strongly influenced by local breezes capable of triggering advection phenomena. In these conditions, ordinary ozone -depletion dynamics may be affected by the "bouncing" of air masses between land and sea. This may also affect the ozone/precursor ratio at certain times. Of course we lack upper-air soundings in order to have a complete and clear idea of the boundary-layer dynamics, above all the mixed-layer height and its evolution.

Much effort has been made to understand breeze cycles since this phenomenon is very important in the area under investigation; however, the most significant result comes from the comparison between the simulations shown and those related to some particular periods. In fact, we found only two days characterized by weak insolation (probably cloudy days) and no breeze development. In correspondence with these two periods, we could clearly recognize the consequent strong depletion of ozone.

Another interesting aspect is related to experimental evidence: there is a delay of about 12 hours between breeze cessation and ozone abatement.

These last observations and considerations strongly encourage us to sustain the hypothesis that breezes are a major forcing factor in coastal ozone episodes.

One final observation is reported for the acute episode of 12 August: an explanation can be found for the establishment of a breeze front, as can be seen in Fig. (**34**). In this situation, the breeze convective cell is compressed by air coming out from the inland mixed layer, which is heated more than the coastal one.

This scenario is not stable, but is particularly dangerous since a strong convergence motion is produced and coupled to recirculation dynamics.

Figure 34: A convective cell of sea breeze compressed by the inland turbulent boundary layer. The terrain colour scale indicates the surface temperature.

ACKNOWLEDGEMENTS

CONFLICT OF INTEREST

The author(s) confirm that this chapter content has no conflict of interest.

REFERENCES

[1]   Tripoli G J. and Cotton W R. The Colorado State University three-dimensional cloud /mesoscale model: General theoretical framework and sensitivity experiments. J. de Rech. Atmos. 1982; no.16, 185–220.

[2]   Tremback C J. Numerical simulation of a mesoscale convective complex: model development and numerical results. Ph.D. dissertation, Atmospheric Science Paper no. 465, Colorado State University, Dept. of Atmospheric Science, Fort Collins, Colorado 1990.

[3]   Mahrer Y and Pielke R A. A numerical study of the airflow over irregular terrain. Beitrage zur Physik der Atmosphare. 1977; 50, 98–113.

[4]   Anthes, R.A, and Warner T T. Development of hydrodynamic models suitable for air pollution and other mesometeorological studies. Mon. Wea. Rev. 1978; 106, 1045–1078.

[5]   Michalakes J, Dudhia J, Gill D, Klemp J, and Skamarock W. Design of a next-generation regional weather research and forecast model. Towards Teracomputing, World Scientific, River Edge. New Jersey 1999;117–124.

[6]   Michalakes J, Dudhia J, Gill D, Henderson T, Klemp J, Skamarock W, and Wang W.The Weather Research and Forecast Model: Software Architecture and Performance. Proceedings of the Eleventh ECMWF Workshop on the Use of High Performance Computing in Meteorology. Reading, U.K., Ed. George Mozdzynski. 25–29 October 2004.

[7]   Barker D.M, Huang W, Guo Y-R, Bourgeois A, and Xiao X. N,: A Three-Dimensional Variational Data Assimilation System for MM5: Implementation and Initial Results. Mon. Wea. Rev. 2004; 132, 897–914.

[8]   Tremback C J, Tripoli G J, and Cotton W R. A regional scale atmospheric numerical model including explicit moist physics and a hydrostatic time-split scheme. Preprints of the Conference on Numerical Weather Prediction, Montreal Quebec. 1985 June 17–20.

[9]   Mesinger F and Arakawa A. Numerical methods used in atmospheric models. GARP publication series. WMO/ICSU joint Organization Committee. 1976; no. 14, 64 pp.

[10]   Gal-Chen T and Somerville R. C. J. On the use of a coordinate transformation for the solution of the Navier-Stokes equations. J Comput Phys. 1975; no. 17, 209–228.

[11]   Clark T L. A small dynamic model using a terrain-following coordinate transformation. Journal of Computational Physics. 1977; no. 24, 186–215.

[12]   Ooyama K V. A thermodynamic foundation for modeling the moist atmosphere. J. Atmos. Sci. 1990; 47, 2580–2593.

[13]   Klemp JB, and Wilhelmson RB. Simulations of three-dimensional convective storm dynamics. J. Atmos. Sci. 1978; 35, 1070–1096.

[14]   Williams RT and Haltiner G J. Numerical Prediction and Dynamic Meteorology. John Wiley and Sons, New York 1980.

[15]   Isakov V, Venkatram A, Touma JS, Koracin D, and Otte TL. Evaluating the use of outputs from comprehensive meteorological models in air quality modeling applications. Atmospheric Environment 2007; Vol. 41 Issue 8, 1689–1705, ISSN 1352-2310.

[16]   Mass CF, Ovens D, Westrick K, and Colle BA. Does increasing horizontal resolution produce more skillful forecasts? Bulletin Of the American Meteorology Society. 2002; 83, 407–430.

[17]   Cairns MM and Corey J. Mesoscale model simulations of high-wind events in the complex terrain of Nevada. Weather Forecasting. 2003; 18, 249–263.

[18]   Arakawa A and Schubert W H. Interaction of a cumulus cloud large scale environment. Part I. J. Atmos. Sci. 1974; 31, 674–701.

[19]   Banta RM, Senff CJ, White AB, Trainer M, McNider RT, Valente RJ, Mayor SD, Alvarez RJ, Hardesty R.M, Parish DD, and Fehsenfeld FC. Daytime buildup and nighttime transport of urban ozone in the boundary layer during a stagnation episode. Journal of Geophys. Res. 1998; 103, 22, 519–522, 544.

[20]   Liu K-Y, Wang Z, and Hsiao L-F. A modeling of the sea breeze and its impacts on the ozone distribution in Northern Taiwan. Environmental Modeling and Software. 2002; 17, 21–27.

[21]   Blackadar A K. Modeling the nocturnal boundary layer. Preprints of Third Symposium on Atmospheric Turbulence and Air Quality. Raleigh, NC, 19–22 October 1976, Amer. Meteor. Soc., Boston, 46–49.

[22]   Blackadar A K. High-resolution models of the planetary boundary layer. Advances in Environmental Science and Engineering. 1979; 1 Pfaflin and Ziegler Eds., Gordon and Breach Publ. Group, Newark, 50–85.

[23]   Chen C and Cotton W R. A one-dimensional simulation of stratocumulus-capped mixed layer, Boundary-Layer Meteorology. 1983; no. 25, 289–321.

CHAPTER 4

Selected Applications of Coastal Valley Meteorology

Roberta Cocci Grifoni[1,*] and Giovanni Latini[2]

[1]*School of Architecture and Design "E. Vittoria", Camerino University, Ascoli Piceno, Italy and* [2]*Department of Energetics, Polytechnic University of Marche, Italy*

Abstract: The atmospheric boundary layer (ABL) height a fundamental parameter characterising the structure of the lower troposphere. It is one of the important parameters requested by different dispersion models as input data for forecasting air quality. The aim of this chapter is to review various methods for the mixed layer height estimate in a complex coastal valley area and compare them to achieve critical awareness of their application. In this chapter, selected case studies of complex terrain meteorology are presented.

Keywords: Atmospheric boundary layer, coastal breeze, coastal valleys, eddy fluxes, GPS_MET, GRAS, Ionospheric term, mixing height, Monin-Obukhov length, Pasquill classification, Planetary Boundary Layer, Prognostic methods, RASS, refractivity index, Scattering term, signal-to-noise ratio, synoptic winds, turbulent diffusion, vertical gradients, Wind profilers.

INTRODUCTION

The ABL is commonly divided into two main sublayers: the shallow, adiabatic-sensitive surface layer, and the convective boundary layer, identified by the vertical thermal structure controlling the height up to which pollutants are generally well mixed.

Holtslag and Nieuwstadt [1] suggested a method for classifying the various sublayers within the ABL,-determined by the scaling of its turbulence characteristics. However, their definition of the various ABL sublayers is not all-encompassing due to the inherent complexity in both determining the governing atmospheric process prevailing within each sublayer and choosing the method used to measur its depth.

---

*Address correspondence to Roberta Cocci Grifoni: School of Architecture and Design "E. Vittoria", Camerino University, Ascoli Piceno, Italy; Tel: +39 (0)737 404279; E-mail: roberta.coccigrifoni@unicam.it

A number of alternative definitions of the ABL exist, each lending itself to different approaches to derive the ABL height. The definitions are based on either the turbulence characteristics of the atmosphere or the vertical structure of one or more meteorological variables. Most diagnostic analyses determine the height from temperature profiles, although wind is occasionally used. Of considerable current interest is a class of methods based on the Richardson number criteria. Prognostic methods calculate the time evolution of the top of the ABL from a rate equation.

In 1997, Beyrich, [2] proposed a definition for the mixed layer depth in which concentration profiles are exclusively determined by either convection or mechanical turbulence, although they noted that these are not always the only dispersion processes. Therefore, determination of layer depths is commonly based on mean meteorological parameters such as temperature profiles.

The determination of this parameter is important in applications ranging from meteorological modeling and forecasting to atmospheric pollutant dispersion problems. Several studies describing the spatial–temporal distribution over coastal valley areas of the free convection layer (FCL), the mixed layer, the entrainment layer, and the stable boundary layer have been conducted [3-6]. However, as pointed out by Builtjes [7], the weakest point in meteorology data is still the determination of the height of the mixed layer.

In summary, there are two basic possibilities for the practical determination of the mixing height: its derivation from profile data and its parameterisation using simple equations or models. A number of commonly used methods of both types are reviewed below, along with considerations regarding their applicability to various types of meteorological data and atmospheric conditions.

The classical way of describing the structure of the ABL is through the use of similarity theories. It is assumed that the structure of the ABL depends on the height of the ABL, the height above ground, and turbulence parameters such as momentum and heat fluxes, which are combined into the Monin-Obukhov length scale [4,8]. The Monin-Obukhov length roughly equals the height at which the production of mechanical and convective turbulence is equal.

STABILITY, MIXING HEIGHT, AND INVERSIONS

The ABL was initially divided into domains, each characterised by a set of scaling parameters [1,9] where the basic dimensionless scaling parameters are taken as h/z and L/h. The scaling parameter h was considered a simple hupper boundary for use in Gaussian dispersion models or simple box models [10], and was assigned a constant value (usually 1000 m for atmospheric unstable conditions). Atmospheric stability was described by the famous Pasquill stability classification [11], which, contrary to the Monin-Obukhov length, can be determined from very simple, standard meteorological measurements.

Subsequently, the Monin-Obukhov length gradually replaced the Pasquill classification for the description of atmospheric stability and models appeared in which the vertical inhomogeneity of turbulence characteristics within the ABL is considered both as a function of L/h and of h/z [12]. Parameterised profiles were used for quantities such as standard deviations of turbulence wind velocity fluctuations and these, in turn, were related to atmospheric dispersion processes. The mixing height is no longer just the parameter that limits the dispersion in the vertical direction; it is also taken into account in the parameterisation of turbulence within the ABL.

The main diagnostic formulae for the evaluation of mixing height are reported in Table **1**.

Table 1: Diagnostic formulae for the mixing height calculation (where u_{10} is wind speed (10m), f is the Coriolis parameter, $u*$ is the roughness wind speed, and L is the Monin-Obukhov Length).

Reference	Mixing height equation	Range of use (PGT)
Zilitinkevich (1972) $c_2 \approx 0,4$	$h = c_2 \left(\dfrac{u_* L}{f} \right)^{1/2}$	E,F
Arya (1981) $a = 0,43 \quad b = 29,3$	$h = a \left(\dfrac{u_* L}{f} \right)^{1/2} + b$	D-F
Arya (1981)	$h = 0,89 \dfrac{u^*}{f} + 85,1$	D-F
Mahrt (1982)	$h = 0,06 \dfrac{u^*}{f}$	D-F

Nieuwstadt (1984)	$h = 28u_{10}^{3/2}$	D-F
Benkley & Schulman (1979)	$h = 125u_{10}$	D-F
H van Dop	$0,263L\left[1+\left(2,28\dfrac{u^*}{fL}\right)\right]^{1/2}$	E-F
Dierdorff	$h = \left[\dfrac{1}{30L}+\dfrac{f}{0,4u^*}\right]^{-1}$	D-F

In recent years, three-dimensional numerical models of the atmosphere have become increasingly popular tools. In fact, regional patterns of the mixing height can be derived from mesoscale model output (*i.e.*, CSU-RAMS, The Colorado State University Regional Atmospheric Modeling System). Models have been used to estimate the mixing height over extended complex areas.

When detailed output from mesoscale models is not readily available, or available only on a grid that is too coarse to resolve the mixing height in sufficient detail, modeling of the mixing height is almost entirely based on so-called slab-type models [13,14]. These models describe the rate of growth of the daytime unstable boundary layer, for which diagnostic expressions have thus far proved unsatisfactory. Slab models, also known as jump or integral models, assume that mean values of variables such as the temperature, are constant with height within the unstable boundary layer and that the entrainment layer can be represented as a infinitesimally thin layer across which there is a discontinuous jump in the value of a variable. The effects of latent heating, horizontal advection, divergence of the radiative heat flux, and large-scale vertical velocities are treated as negligible. The first approach considered only surface heating as the driving force for the growth of the convective boundary layer. The effect of mechanical turbulence was later discussed by Driedonks [15], Yordanov and Batchvarova [16], and Gryning and Batchvarova [6].

For neutral to stable conditions, a number of expressions based on similarity theory exist for estimating the top of the ABL. Van Ulden and Holtslag [17] review several of these methods. A major advantage of surface flux-based methods is the relatively limited amount of data required: surface momentum and heat fluxes and surface-

layer scaling parameters such as the friction velocity $u*$ and the Monin-Obukhov length, L. These quantities can be derived from readily available surface observations using the similarity flux-profile equilibrium relations.

The slab approach has been used extensively in air pollution and dispersion modeling due to its efficiency and simplicity [18,19]. The method assumes that the vertical distribution of potential temperature within the boundary layer is uniform with a strong capping inversion.

The formation of capping inversions exists when the air flows over an abrupt change in surface conditions. The traditional example is the internal boundary layer that forms downwind of a coastline in onshore flow. The abrupt change from water to land conditions produces an internal boundary layer, which begins at the shoreline and grows in depth with distance inland. Because the land surface is generally warmer than the sea, the internal boundary layer is convective.

THE BATCHAROVA-GRYNING MODEL

The derivation of the prediction equation for the height of the internal boundary layer as function of downwind distance is given by the Gryning and Batcharova approach [6].

A reasonable parameterization of the top-layer temperature flux, as a function of the surface flux, the friction velocity and the convective boundary layer height results in a simple equation for the evolution of the mixing height, h:

$$\left\{ \left[\frac{h^2}{(1+2A)h - 2BkL} \right] + \left[\frac{C u_*^2 T}{\gamma g \left[(1+A)h - BkL \right]} \right] \right\} \frac{\Delta h}{\Delta t} = \frac{\left(\overline{w'\theta'} \right)_s}{\gamma} \tag{1}$$

where

$$L = -u*^3 T \big/ Kg \overline{(w\theta')} \tag{2}$$

is the Monin-Obukhov length, T is a representative convective boundary layer temperature, g is gravitational acceleration, and K is the Von Karman constant.

The parameters $A = 0.2$, $B = 5$, and $C = 8$ are experimentally determined, and a typical value of 0.007 K/m is used for the temperature gradient, γ, above the planetary boundary layer.

Considering the simplicity of the models, a one-dimensional model can be developed for the estimation of hourly mixing height values from routinely measured surface meteorological data.

A simple code [20] can be used in convective situations (Fig. **1**), in which only data series are available and vertical sounding is not possible.

This is a preliminary algorithm that can be tested against the measured data and will be improved in the future.
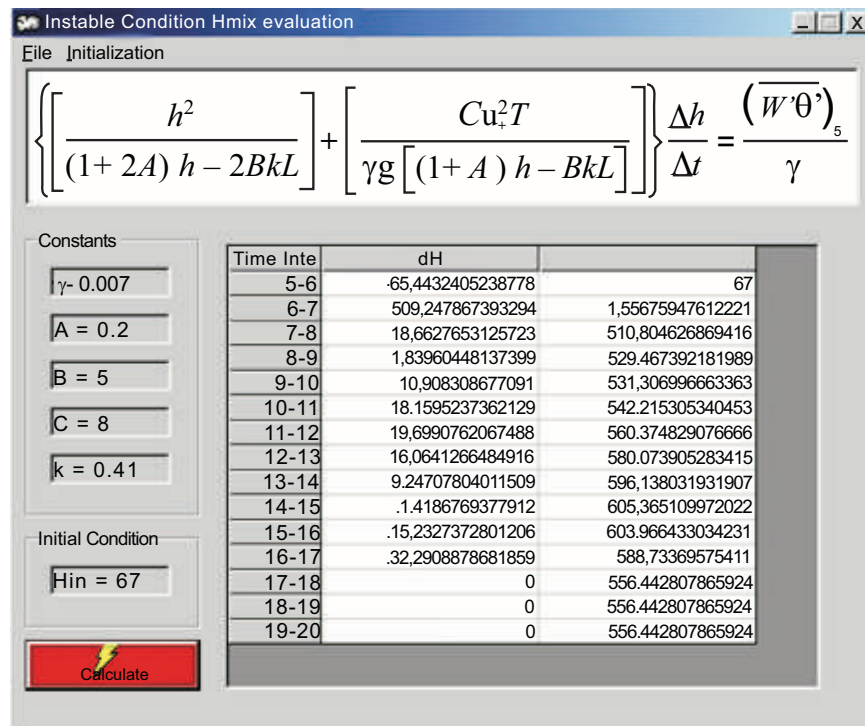

Figure 1: Main window showing mixing height values (see Appendix A).

The model for the development of the internal boundary layer in a complex coastal area was evaluated in Latini *et al.* [20] and compared with measurements from the literature and several different estimates.

The authors initially tested the described approach in a complex coastal area (Esino Valley) in central Italy (Marche). This area covers 20 km inland from the coast and is 20 km wide. The Esino Valley is characterised, like most Italian valleys, by a riverbed that is roughly perpendicular to the coast in a NE direction. The valley is surrounded by hillsides that gradually increase in height the further removed they are from the coast. The climate in this area is classified as subcoastal. There is a year-round sea breeze of variable intensity that is influenced by a heavy component from the NW. This gives way to a meandering current along the coast with a component parallel to the coast caused by the synoptic winds.

The component perpendicular to the coast is called the *coastal breeze* or *sea breeze* according to the wind origin. In the presence of a discontinuity, as in the case of the hillsides situated at the entrance of the valley, the sea breeze forces the breeze to come from the valley. The sea breeze is most intense during the warmer daytime hours and decreases in intensity during the night.

A simulation was run for the temporal evolution of the planetary boundary layer over the coastal valley. The simulation starting point was set at sunrise when the heat flux becomes positive. The simulation was based on hourly averages of the input parameters: temperature, Monin-Obukhov length, friction velocity and the vertical kinematic heat flux.

The meteorological output data is derived from hourly measurements performed by the Italian Air Force Weather Station in Falconara Marittima, which is located 2 km from the coast, more or less in the middle of the Esino Valley. Information concerning both frequencies and the monthly/seasonal distribution of speed, direction and directional persistence of wind, atmospheric stability and air temperature is provided.

THE RICHARDSON NUMBER

The top of the boundary layer can also be determined by calculating the gradients between successive levels from the surface upwards until the critical Richardson number (see Chapter 1) is exceeded.

The flux Richardson number, R_{if}, which is related to the production of turbulent kinetic energy (TKE), is

$$R_{if} = \frac{g}{\theta} \frac{<w'\theta'>}{<u'w'>\frac{\partial u}{\partial z} + <-v'w'>\frac{\partial v}{\partial z}} \qquad (3)$$

where g is gravitational acceleration, $\bar{\theta}$ is a reference potential temperature, $\langle w'\theta' \rangle$ is a vertical kinematic eddy heat flux, $\langle u'w' \rangle$ and $\langle v'w' \rangle$ are vertical kinematic eddy fluxes of the u and v momentum, and $\partial u/\partial z$ and $\partial v/\partial z$ are the vertical gradients of the u and v wind components, respectively. For unstable flows, R_{if} is negative; for neutral flows it is zero; and for statically stable flows, R_{if} is positive. Richardson proposed that $R_{if} = 1$ is a critical value, and at any $R_{if} < 1$, static stability is not strong enough to prevent the mechanical generation of turbulence [21]. For negative values of R_{if}, buoyancy generation of turbulence is a dominant process. Employment of a flux-gradient scheme for the parameterization of turbulent fluxes yields the gradient Richardson number, R_i:

$$R_i = \frac{g}{\theta} \frac{\frac{\partial \theta}{\partial z}}{\left(\frac{\partial u}{\partial z}\right)^2 + \left(\frac{\partial v}{\partial z}\right)^2} \qquad (4)$$

Substituting the gradients in (2) with finite differences in the coordinate frame used leads to

$$R_i = \frac{g(z_j - z_{j-1})}{\bar{\theta}} \frac{\theta_j - \theta_{j-1}}{\left(u_j - u_{j-1}\right)^2 + \left(v_j - v_{j-1}\right)^2} \qquad (5)$$

The algorithm of Eq. (3) computes R_i over layers of approximately 20 metres.

This approach requires highly resolved vertical temperature and wind data so that the derivatives can be computed accurately, a condition that is not commonly met by either observational profiles or forecast model data. The Richardson number calculated in this manner is sensitive to small changes in temperature profiles. The smoothing of gradients by using finite differences also results in the need to use larger critical R_i values than can be justified theoretically [21]. As an example, a recent application found that using an ABL criterion of $R_i = 0.25$ underestimated the boundary layer height, while values closer to 0.55 produced reasonable results depending on the thickness of the successive layers [22].

Note, in fact, that (3) is not commonly used in practice. Instead, the formulation proposed and applied by Mahrt [23], Troen and Mahrt [24], Sørensen [25], Seibert *et al.* [26], Gryning and Batchvarova [27, 28], Zilitinkevich and Baklanov [29], *etc.* is the bulk Richardson number:

$$R_{iB} = \frac{gz(\theta_v(z)-\theta(s))}{\theta_v(s)(u(z)^2+v(z)^2)} \tag{6}$$

The quantities $\theta_v(s)$ and $\theta_v(z)$ are the virtual potential temperatures at the surface [30], taken at the lowest model level and height z, respectively, and $u(z)$ and $v(z)$ are the horizontal wind components (usually easterly and northerly) as a function of height.

The wind speed at the surface is taken to be zero. The main weakness of Eq. (4) in describing turbulence effects is that it might not sense the most energetic relevant eddies, thus contributing to errors in the model. Moreover, turbulence does not have to be a single-valued function of R_i alone. The main advantage and the reason for the widespread use of Eq. (4) is in the definition of H, which is an integral property that relates surface processes to processes higher in the ABL, and thus should embed non-local effects. The surface is assumed to be the main source of turbulence, with fluxes mainly driven by surface heat and friction. When calculating H, we actually determine the height of the layer that is under direct influence of the surface.

Vogelezang and Holtslag [17] suggested a Richardson number where wind is defined with respect to the lowest model level, and a term that accounts for surface friction has been added:

$$R_{iB} = \frac{gz(\theta_v(z)-\theta_v(s))}{\theta_v(s)\left[(u(z)-u(s))^2+(v(z)-v(s))^2+bu_*^{\,2}\right]} \tag{7}$$

where b is a parameterisation constant recommended to be set equal to 100.

The inclusion of these terms improves the estimate of the Richardson number by determining shear production from the region of the ABL above the surface layer. The bu^{*2} term accounts for turbulence production due to surface friction, which is

non-negligible for neutral boundary layers at which both elevated shear and buoyancy contributions may be small.

In practice, the Richardson number is computed using all model or observed levels greater than z until the critical value is exceeded. The value of h is then determined by linear interpolation between that level and the next lowest one. The use of the bulk Richardson number to obtain h has recently been shown to yield good results for a variety of atmospheric conditions, with the results relatively insensitive to the exact choice of z. The results do depend on the choice of the critical number, although common values are between 0.25 and 0.30. The main weaknesses of the Richardson number approach are the requirement for sufficiently resolved vertical profiles of wind and temperature and the uncertainty in the best value of the critical Richardson number.

Sørensen [30] and Vogelezang and Holtslag [17] made an empirical estimate for the value of the critical Richardson number. Despite their differences in the formulation of the bulk Richardson numbers, both studies found a value of 0.25 for the critical Richardson number to be adequate [31].

Under unstable conditions (defined as upwards turbulent heat flux from the mast, *i.e.*, $z = L < 0$), it is generally sufficient to consider only vertical profiles of temperature and humidity. The base of the inversion, or jump, in virtual potential temperature, θ_v, and/or specific humidity, q, determines the height of the ABL. Above h, a significant layer (*i.e.*, of a depth of a few hundred metres) with a quasi-homogeneous lapse rate has been identified. The information regarding this layer is used to determine the background stratification into which the ABL should rise. This background stratification can be used to compute the Brunt-Väisälä frequency (see Chapter 1):

$$N = (g\beta\gamma)^{1/2}, \text{ where } \gamma = \left(\partial\theta/\partial z\right)_{z>h}.$$

For stable conditions, the observed surface inversion is an indication of an absolute maximum for the ABL height, h, since the inversion is determined by both turbulent and radiative cooling. Therefore, the stable ABL height is identified by inspecting the data regarding wind, humidity, and R_i profiles for

clear changes below this inversion height, which would indicate a change in the structure of the lower atmosphere. The criteria adopted were a wind maximum, a change in either the wind direction or humidity profiles slope, and/or persistent large departures of R_i values beyond a critical value of about 1.

THE ATMOSPERIC BOUNDARY LAYER HEIGHT

In the absence of turbulence profiles, as is generally the case, the determination of the ABL height from profiles of mean quantities contains a certain amount of subjectivity. This, compounded with other uncertainties embedded in data sets, makes the evaluation of various models somewhat uncertain. On the other hand, this is partly reduced by the fact that the present subjective analysis is applied concomitantly to different profiles (wind, temperature, humidity and R_i), thus forcing the results towards some converging physical criterion. Even so-called objective algorithms such as threshold values can misinterpret certain profile features if they do not undergo a subjective check [26].

The ABL height varies between 60 and 730 m under stable conditions with a mean of 281 m. Under unstable daytime conditions ($z = L < 0$), the ABL height varies between 190 and 1080 m with a mean of 588 m.

Numerous other approaches for estimating the height of the atmospheric boundary layer can be found in the literature. Apart from temperature -based methods, h can be determined from vertical wind profile criteria, using definitions such as the height of the maximum low-level wind speed, the height of the maximum east-wind wind speed, or the lowest level of negligible vertical wind shear.

Latini *et al.* [32] inferred the depth of the ABL from a semi-empirical estimate of boundary layer parameters like the Monin-Obukhov length, L, and the roughness length z_0.

With positive heat flux at the ground (sunny conditions) and some wind, there exists both mechanical turbulence and heat convection, but it is well known from the turbulence energy budget that the generation of mechanical turbulence decreases rapidly with increasing height, since it is proportional to the vertical heat flux at the surface. In contrast, the generation of heat convection varies very little with height.

A simple equation for h_{mix} under convective conditions can be derived from the thermal energy budget [33]:

$$h_{mix}(t) = \frac{T(t) - T_0}{\Gamma - \Lambda} \tag{8}$$

where Γ is the adiabatic lapse rate and Λ is the lapse rate at sunrise.

In Italy, the lapse rate at sunrise is not easily available and so the value of $\Gamma - \Lambda$ is computed as K_t/L_0, with L_0 equal to the Monin-Obukhov length at sunrise and $K_t = K_1 + K_2/\sin\varphi$ (K_1 and K_2 are constants and φ is the maximum solar elevation). The central application of this methodological approach is mainly in estimating the mixing height of the coastal valley while attempting the development of a suitable method that considers only two parameters, $T(t)$ and z_0:

$$h_{mix} = \frac{T(t) - T_0}{\alpha K_i {}^1/_L} \tag{9}$$

where $1/L = az_0{}^b$ with a and b constants from [34] and α another constant.

It is adequate to estimate the surface roughness length, z_0, using tables that give typical z_0 values based on land use [16]. A grid with appropriate refinement of space discretisation is used for the ground roughness z_0 estimate. This semi-empirical estimate was developed for a resolution of nxn km^2 (n = 1,2,40) grid squares, depending on the single evaluation, or measurements, and corresponding survey map.

The parameter α, which represents the correlation coefficient between the mixing height and stability conditions, has been determined for different scenarios. The night-day transition can be characterised by neutral conditions or slightly unstable conditions. In the first case, the α parameter assumes a unitary value. In the second one, it may assume different values depending on the different meteorological conditions present during the day and at night [20].

A mathematical software code was developed for the evaluation of α-values from the elevation of the Sun, wind speed, cloud cover, and ceiling height. The α-

parameter was determined on an hourly basis for various periods from the data in Table **2**).

Table 2: α-parameter values.

	Night-time slightly stable	Night-time Neutral	Night-time very stable
Daytime unstable	$0.2 \leq \alpha \leq 0.3$	$0.4 \leq \alpha \leq 0.6$	$0.3 \leq \alpha \leq 0.4$
Daytime very unstable	$0.2 \leq \alpha \leq 0.3$	$0.4 \leq \alpha \leq 0.6$	$0.2 \leq \alpha \leq 0.3$
Daytime slightly unstable	$0.6 \leq \alpha \leq 0.8$	$0.6 \leq \alpha \leq 0.8$	$0.3 \leq \alpha \leq 0.4$

The mixing height prognostic routine was compared with modeled and observed mixing heights. The authors generally found good agreement despite the simplicity of the method. The results obtained indicate that this semi-empirical method gives reliable information regarding mixing height evolution over complex coastal areas.

GPS_MET

Another interesting approach to estimating the height of the atmospheric boundary layer is to use remote sensing measurements that provide many atmospheric parameters.

In satellite remote sensing, vertical profiles of temperature and water vapour are usually derived from passive observations of radiances. Several instruments on different satellite platforms are able to provide such data.

One of them is GPS_MET (GPS/Meteorology), which consists of a modified GPS receiver onboard a micro satellite (MicroLab 1) in a 740 km circular orbit with a 70° inclination.

The GPS_MET experiment has provided researchers with high-quality meteorological data [35,36]. Even though many GPS_MET soundings have failed to penetrate the 5 km of the troposphere in the presence of significant water vapour, Rocken *et al.* [37] demonstrate 1 K mean temperature agreement with the

best correlative data sets (TOVS, MLS, HALOE, radiosondes and global analysis data from NCEP and ECMWF) between 1 and 40 km. Standard deviations are generally found to be less than 2–3 K.
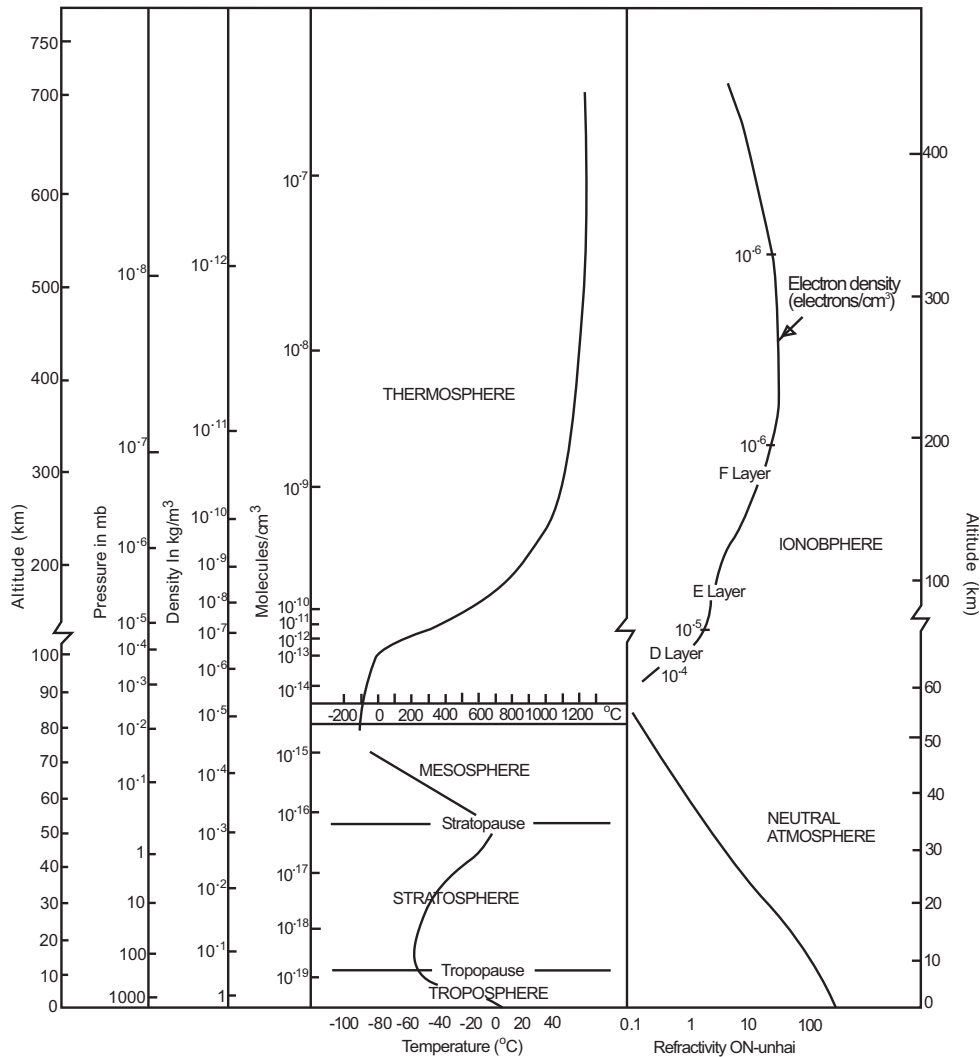
Figure 2: The mean vertical structure of Earth's atmosphere, showing temperature, refractivity and electron density distributions (adapted from Rocken *et al.* [39]).

Early results from GPS_MET [38] suggest that it can measure temperature as a function of pressure to an accuracy of 1 K or less with a vertical resolution on the order of 1 km at and near the tropopause. This suggests that the technique may play a special role in determining atmospheric data within this altitude range.

Fig. (**2**) provides an overview view of the mean vertical temperature and refractivity distribution in the atmosphere and the electron density distribution in the ionosphere as well as the nomenclature used for the different spheres and layers.

Further studies [36] have addressed the accuracy of GPS_MET retrievals compared with that of other sensors, namely radiosondes providing comparable *in situ* measurements, and with various weather-prediction models. The comparison made among about 114 retrieved temperature profiles, ECMWF analysis, and radiosonde data indicates that above an altitude of about 3 km, GPS occultation temperature profiles are accurate to better than 2 K on average (Fig. **3**) with a standard deviation of about 1–2 K.

ECMWF analyses are one of the best available global analyses of atmospheric temperature structure below 30 mbar.
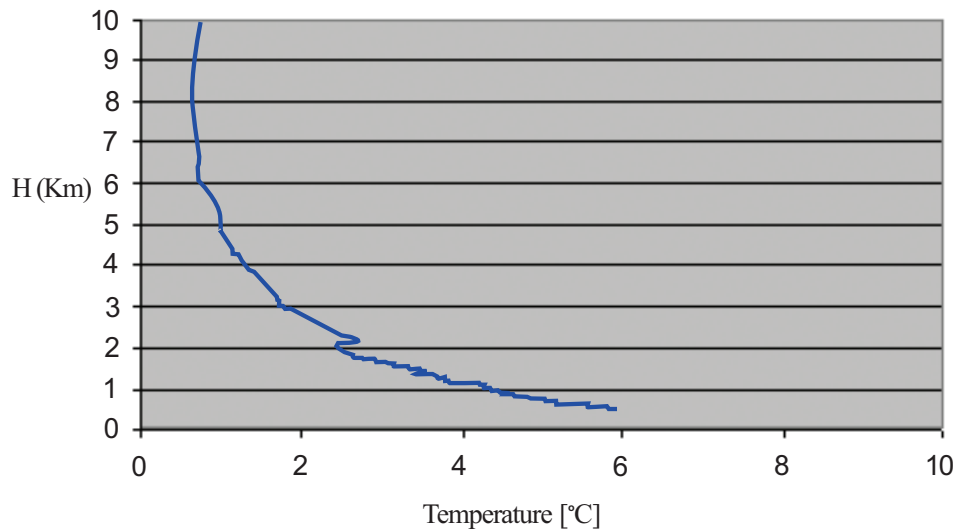
Figure 3: Temperature profile accuracy.

Accurate knowledge of GPS orbits comes from an overall solution involving all 24 GPS satellites and a global network of ground receivers. The LEO orbit is determined by use of other links tracking non-occulting GPS satellites.

The refractivity, *N,* is related to atmospheric quantities [40]:

$$N = (n-1) \cdot 10^6 = 77.6 \frac{P}{T} + 3.73 \cdot 10^5 \frac{P_w}{T^2} - 40.3 \cdot 10^6 \frac{N_e}{f^2} + 1.45W \qquad \textbf{(10)}$$

where

P is the total pressure,

T is the temperature,

P_w is the water vapour partial pressure,

N_e is the electron density,

f is the operating frequency,

W is the liquid water content.

Thus, in the Earth's atmosphere there are four sources of refractivity disturbing the passage of GPS signals. These are referred to as the dry term [(a) in Eq. 3] moist term (b), ionospheric term (c), and scattering term (d). The dry term is due to the polarizability of molecules in the atmosphere and the moist term is due to the large permanent dipole moment of water. The dry term dominates for altitudes between 0 and 90 km, the contribution from water vapour becoming important in the lower atmosphere. The ionospheric term is essentially due to free electrons in the ionosphere, and the scattering term, owing to water droplets suspended in the atmosphere, can be considered small compared to the dry and moist terms.

The approximate equation for the low atmosphere is [35]:

$$N = 77.6 \frac{P}{T} + 3.73 \cdot 10^5 \frac{P_w}{T^2} \qquad \textbf{(11)}$$

As a result, atmospheric parameters of interest are linked by a simple mathematical relation to the refractive index. This allows for their reconstruction with the help of the well-known gas law and equation for hydrostatic equilibrium (Chapter 1):

$$P = \frac{\rho RT}{m} \qquad \textbf{(12)}$$

$$\frac{\partial P}{\partial h} = -g\rho \tag{13}$$

where

R is the gas constant,

m is the gas molecular weight,

h is the vertical height,

g is gravitational acceleration.

Due to the superimposition of temperature and water vapour effects in the resulting refractivity, its accuracy can be negatively influenced by abundant water vapour in the lower troposphere. Another problem in this region may be the loss of signal lock due to limited sensitivity of the receiver.

The next generation of space-borne GPS receivers (*i.e.*, GRAS) will lead to much stronger performance. GRAS observations combine high vertical resolution and high absolute accuracy with global coverage and good long-term stability. These features complement the existing and planned meteorological observation systems very well.

The GRAS instrument on MetOp, as part of the EPS system, will provide an unrivalled set of high-quality atmospheric sounding data with a vertical accuracy ranging from 1 km down to 100 m at low altitudes. In addition, GRAS provides a unique opportunity to establish the height of the tropopause with a vertical accuracy better than 1 km.

An estimate of the error associated with temperature profiles and mixing height evaluations has been computed from the well-known law

$$\Delta h_{mix} \approx \left. \frac{df(T)}{dT} \right|_{T=T_0} \Delta T$$

and, as a consequence,

$$\frac{\Delta h_{mix}}{h_{mix}} = 0.0581$$

The expected accuracy of radio occultation temperature retrievals, their long term stability, and the physical simplicity of the observables are key factors that suggest that these observations may be useful for the assessment of mixing height evolution in typically complex areas such as coastal valleys.

An example of this methodology is the evaluation of the mixing height behaviour in Fairbanks, Alaska (USA) located 358 miles north of Anchorage, approximately in the centre of the state.

In the winter the climate is harsh, with temperatures averaging 20°C below zero, and there are correspondingly harsh summer conditions with temperatures up to 35°C. The shortest day in winter has less that 3 hours of sunlight while the longest day of summer has 21 hours of sunlight.

Fig. (**4**) shows an example of a temperature profile at dawn derived from measurements made on 13 February 1997 during a GPS occultation. This profile has been used to evaluate the mixing height (the bold lines in the figure).

The region between the two bold lines is the evaluated range of mixing height based on the estimated accuracy of GPS-MET data; the dashed line is the mixing height evolution calculated using the Monin-Obukhov length method [32].

It is clear from the figure that agreement between the two data sets is good, with mean differences generally less than 40 m.

A similar approach to estimating the mixing height suggests profile measurements, as previously stated, either *in situ* or by remote sounding (sodar, clear-air radar, lidar, RASS, wind profile, airborne microwave temperature profiler [MTP], *in situ* aircraft data, *etc.*). As a particular example, in the acoustic sounding system (RASS), signals emitted by a sodar are scattered by temperature inhomegeneities characterized by the structure parameter of the acoustic refractive index. According to observations, the backscattered signal has a secondary maximum at the top of the mixing layer [2]. Emeis and Turk [41] detected the

mixing height from the sodar data by employing two different criteria. According to the first a sharp decrease in the acoustic backscatter intensity indicates the top of the turbulent layer; the second diagnoses the secondary maxima of the backscatter profile. The search is preformed separately using both criteria, and the lower height is chosen to denote the mixing height.
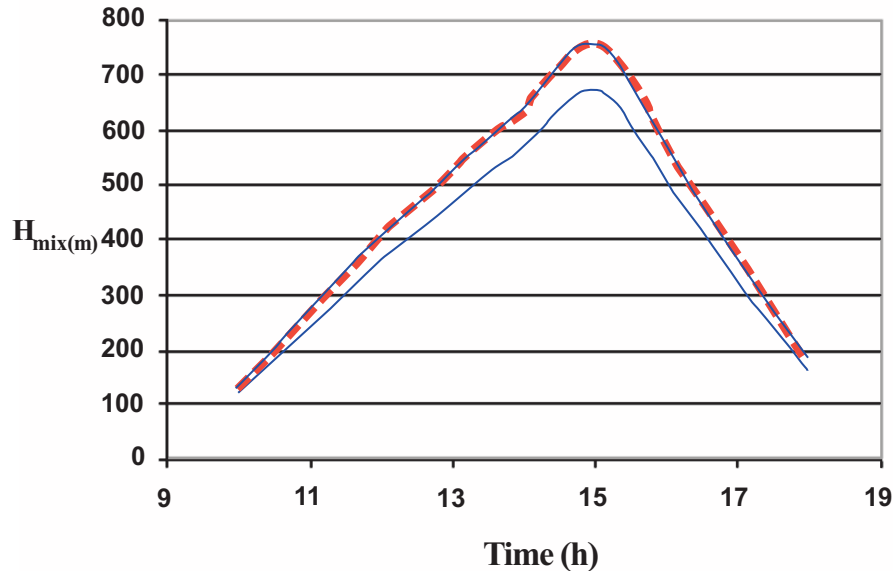
Figure 4: The mixing height behaviour.

The mixing height can also be determined by a wind profiler from the signal-to-noise ratio (SNR). The return signal is received primarily from the inhomogeneities in the radio refractive index [42]. These inhomogeneities essentially depend on fluctuations of the temperature and especially on the moisture fields [43].

Since there is often a humidity gradient between the mixing layer and the free atmosphere, a peak can be seen in the wind profiler backscatter profile at the top of the mixing layer and the SNR [44].

Radiosonde systems measure profiles of temperature, pressure, and relative humidity as they ascend through the atmosphere, and these measurements are sent to ground receivers. Mixing height estimates determined from radiosonde systems depend on the atmospheric constituent used for the analysis. Wind profilers

measure vertical variations in the refractive index, and lidar systems observe the distribution of particulate matter in the mixing height. MTP systems measure the thermal emissions and absorption from oxygen molecules in the atmosphere. *In situ* instruments on aircraft often make measurements of temperature, humidity, wind speed, wind direction, and concentrations of various species from which the mixing height can be determined.

Among remote sensing methods, a significant one is the ceilometer [45] based on the lidar-technique, which measures the aerosol concentration profile. Since aerosol concentrations are generally lower in the free atmosphere than in the mixing layer, where most sources of aerosols are located, it can be expected that the mixing height is associated with a strong gradient in the vertical back-scattering profile. This can be considered a new technique to lower the inherent uncertainty involved in the determination of the mixing height.

Considering the complexity of the coastal valley region, the three-dimensional mesoscale model (CSU-RAMS, for example) performs reasonably well in evaluating the mixing height, and particularly well in the complex coastal area.

Sea and land breezes, mountain valley winds, and winds generated due to other types of land surface variability (*e.g.*, urban-rural differences, snow cover variability, vegetated areas adjacent to less vegetated regions, *etc.*) also contribute to differential wind and turbulence fields. These mesoscale atmospheric features develop due to horizontal surface gradients in surface sensible and latent turbulent heat fluxes. They are described in a wide variety of sources including Atkinson, [46], and Pielke [47]. Even if differences in surface turbulent fluxes are not strong enough to create distinct mesoscale circulation, they can significantly affect the vertical structure of the atmospheric boundary layer and, in turn, atmospheric dispersion. These effects were demonstrated by simulating atmospheric dispersion over a series of land patches with different soil water content [48].

The CSU-RAMS modeling system [49] is a versatile modeling system capable of simulating flows on scales from a global hemisphere to a building with several options, including multiple nesting and convective and boundary layer parameterisations. It is assembled around the full set of primitive dynamical

equations that govern atmospheric motions, and supplements these equations with optional parameterisations for turbulent diffusion, solar and terrestrial radiation, moist processes (including the formation and interaction of clouds), and sensible and latent heat exchange between the atmosphere and multiple soil layers. Prognostic soil-vegetation relationships are used to calculate the diurnal variation of temperature and moisture at the ground-atmosphere interface. Turbulence sensible heat, latent heat, and momentum fluxes in the surface layer are based on similarity equations.

This model can be used under complicated meteorological and topographical conditions; it is not a model of internal boundary layer depth, but gives output from which the depth can be derived.

It has been found that the success of the RAMS model relies on the correct reproduction of the local wind field. This is generally a difficult task near the coast due to an inability to capture various sub-grid features, as well as the added complexity during the morning transition hours from land breeze to sea breeze.

In fact, a coastal region is influenced by many meteorological phenomena due to interactions between breezes and large-scale wind systems. Mesoscale air flows in coastal regions are mainly determined by the land-sea temperature contrast driving land-sea breezes and by the orography driving mountain-valley breezes, while the shape of the coastline has an effect on mesoscale wind flow.

All of these phenomena strongly influence various scalar fields, including moisture, mixing height and consecutively air pollution concentrations. The improved capability of mesoscale models to reproduce physical complexity nowadays allows accurate simulations for use in planetary boundary layer parameterizations. Mesoscale models also help to understand–processes by allowing full control over environmental parameters. Hence, it is possible to determine factors steering phenomena as well as test their sensitivity to changes in environmental conditions.

In general, current parameterizations of surface and boundary layer processes in RAMS, as well as in other mesoscale models, are based on scaling laws valid strictly for flat topography and uniform land cover. Some studies have been performed [50] in order to investigate whether this limits the applicability of

RAMS in steep, inhomogeneous terrain. RAMS captures many of the observed boundary layer characteristics within the steep valley. This model can qualitatively simulate the wind field, temperature structure, and convective boundary layer height in the valley, but the horizontal temperature structure across and along the valley may be less homogeneous in the model than in the actual observed situation.

ACKNOWLEDGEMENTS

The authors kindly thank their respective universities for their support.

CONFLICT OF INTEREST

The author(s) confirm that this chapter content has no conflict of interest.

REFERENCES

[1]   Holtslag AAM, Nieuwstadt FTM. Scaling the atmospheric boundary layer. Bound Layer Meteor 1986; 36 (24): 201–209.
[2]   Beyrich F. Mixing height estimation from sodar data – a discussion. Atmos Environ 1997; 31: 3941–3953.
[3]   Dayan U, Rodnizki J. The Temporal Behavior of the Atmospheric Boundary Layer in Israel. J Appl Meteorol 1999; 38: 830-836.
[4]   Obukhov AM. Turbulence in an Atmosphere with a Non-uniform Temperature. Boundary Layer Meteorol 1946; 2: 7-29.
[5]   Batchvarova E, Cai X, Gryning SE, Steyn D. Modeling Internal Boundary- Layer Development in a Region with a Complex Coastline. Boundary Layer Meteorol 1999; 90,1-20.
[6]   Gryning SE, Batchvarova E. Analytical Model for the Growth of the Coastal Internal Boundary Layer during Onshore Flow. Quart J Roy Meteorol Soc 1990; 116: 187- 203.
[7]   Builtjes P J H. Major Twentieth Century Milestones in Air Pollution Modeling and Its Application. In: Air Pollution Modeling and Its Application XIV, S.E. Gryning and F. Schiermeier (eds.), Kluwer Academic/Plenum Publishers, New York, 2001; pp 3-16.
[8]   Monin AS, Obukhov AM. Basic Laws of Turbulence Mixing in the Ground Layer of the Atmosphere. Akad Nauk SSSR, Geofiz Inst Trudy 1954; 151: 163-87.
[9]   Gryning SE, Holtslag AAM, Irwin JS, Sivertsen B. Applied Dispersion Modeling Based on Meteorological Scaling Parameters. Atmos Environ 1987; 21: 79-89.
[10]   Turner DB. Workbook of Atmospheric Dispersion Estimates, Office of Air Programs Publication, A-P 26, Environmental Protection Agency, Research Triangle Park, 1970.
[11]   Pasquill F. Atmospheric Diffusion. 2nd ed. Chichester, Ellis Horwood Ltd 1974.
[12]   Gryning SE, Holtslag AAM, Irwin JS, Sivertsen B. Applied Dispersion Modeling Based on Meteorological Scaling Parameters. Atmos Environ 1987; 21: 79-89.

[13]   Tennekes H, Driedonks A G M. Basic Entrainment Equations for the Atmospheric Boundary Layer. Boundary Layer Meteorol 1981; 20: 515-531.

[14]   Carson DJ. The development of a dry inversion-capped convectively unstable boundary layer. J R Met Sot 1973; 99: 450-467.

[15]   Driedonks AGM. Dynamics of the Well-mixed Atmospheric Boundary Layer. KNMI Sci Rep WR De Bilt 1981; 81 (2): 189

[16]   Yordanov D, Batchvarova E. Über die höhe der internen thermischen grenzschicht bei see-wind. Z Meteorol 1988; 38: 145-149.

[17]   Vogelezang D, Holtslag A. Evaluation and Model Impacts of Alternative Boundary-Layer Height Formulations. Boundary Layer Meteorol 1996; 81: 245-269.

[18]   Taha H, Bornstein R. Urbanization of meteorological models and implications on simulated heat islands and air quality', In: R. J. de Dear, J. D. Kalma, T. R. Oke and A. Auliciems, Eds.: Biometeorology and Urban Climatology at the Turn of the Millenium. Selected Papers from the Conference ICB-ICUC '99, Sydney, Australia, 8-12 Nov. 1999.

[19]   EPA. A User's Guide for the CALMET Meteorological Model, EPA-454/B-95-002, U.S. Environmental Protection Agency, Research Triangle Park, NC, 1995.

[20]   Latini G, Cocci Grifoni R, Passerini G. Dependency of mixing height as function of Monin-Obukhov length on stability conditions, Air Pollution VIII, 2000, WIT Press, Southampton (GB), pp.623-632,

[21]   Stull R B. An Introduction to Boundary Layer Meteorology, Kluwer Academic Press, 1988

[22]   Straume AG, Koffi EN'D, Nodop K. Dispersion Modeling Using Ensemble Forecasts Compared to ETEX Measurements. J Appl Met 1998; 37: 1444-1456

[23]   Mahrt L. Modeling the depth of the stable boundary layer. Bound Layer Meteorol 1981; 21: 3–19.

[24]   Troen IB, Mahrt L. A simple model of the atmospheric boundary layer; sensitivity to surface evaporation. Bound Layer Meteorol 1986; 37: 129–148

[25]   Sørensen J H, Rasmussen A, Svensmark H. Forecast of atmospheric boundary-layer height for ETEX real-time dispersion modeling. Phys Chem Earth 1996; 21: 435–439.

[26]   Seibert P, Beyrich F, Gryning SE, Joffre S, Rasmussen, Tercier A. Review and interscomparison of operational methods or the determination of the mixing height. Atmos Environ 2000; 34: 1001–1027.

[27]   Gryning, S E, Batchvarova E. Marine boundary layer and turbulent fluxes over the Baltic Sea: measurements and modeling. Bound.-Layer Meteorol. 2002, 103: 29–47.

[28]   Gryning S E, Batchvarova E. Marine atmospheric boundary layer height estimated from NWPmodel output. Int J Environ Pollut 2003; 20 (1/2/3/4/5/6): 147–153.

[29]   Zilitinkevich S, Baklanov A. Calculation of the height of the stable boundary layer in practical applications. Bound Layer Meteorol 2002; 105: 389–409.

[30]   Sørensen J H. Sensitivity of the DERMA Long-Range Gaussian Dispersion Model to Meteorological Input and Diffusion Parameters. Atmos Environ 1998; 24: 4195- 4206.

[31]   Gryning S E. The height of the atmospheric boundary layer during unstable conditions REPORT, Risø-R-1536(EN), 2005.

[32]   Latini G, Cocci Grifoni R, Passerini G, Tirabassi T. Evaluation of mixing Height over Complex Coastal Terrain, in Air Pollution VII, 1999, WIT Press, Southampton (GB), pp. 697-706.

[33]   Panofsky, H. A. and Dutton, J. Atmopheric Turbulence. John Wiley and Sons, 1984.

[34]   Liu M, Durran P, Mundkur P, Yocke M, Ames J. The Chemistry, Dispersion, and Transport of Air Pollutants Emitted from Fossil Fuel Plants in California: Data Analysis and Emission

Impact Model, Final Report to Air Resources Board, contract no. ARB 4-258, Sacramento, California, 1976.

[35] Kursinski ER, Hardy R, Hajj GA, Schofield JT, Linfield K. Observing Earth's atmosphere with radio occultation measurements using the Global Positioning System, J Geophys Res 1997;102 (23):429-465.

[36] Hardy KR, Hajj GA, Kursinski ER. Accuracies of atmospheric pro les obtained from GPS occultations. Int J Satell Commun 1994;12: 463-473.

[37] Rocken C, Anthes R, Exner M, *et al.* Analysis and validation of GPS_MET data in the neutral atmosphere, J Geophys Res 1997; 102(29): 849-860.

[38] Kursinski E R. Initial results of radio occultation observations of Earth's atmosphere using the global positioning system (GPS), Science 1996; 271: 1107-1110.

[39] Gorbunov M E, Gurvich A S, Bengtsson L. Advanced algorithms of inversion of GPS/MET satellite data and their application to reconstruction of temperature and humidity. Report No. 211, Max-Planck Institute for Meteorology, Hamburg, 1996.

[40] Thayer G D. An improved equation for the radio refractive index of air. Radio Science1974; 9 (10): 803-807.

[41] Emeis S, Türk M. Frequency distributions of the mixing height over an urban area from SODAR data, Meteorologische, 2004.

[42] Angevine W, White A, Avery S K. Boundary layer depth and entrainment zone characterization with a boundarylayer profiler. Boundary Layer Meteorol 1994; 68: 375–385.

[43] White A B, Fairall C W, Thomson D W. Radar observations of humidity variability in and above the marine atmospheric boundary layer. J Atmos Oceanogr Technol 1991; 8: 539–558.

[44] Cohn S A, Angevine W M. Boundary layer height and entrainment zone thickness measured by lidars and wind-profiling radars. J Appl Meteorol 2000; 39: 1233–1247.

[45] Eresmaa N, Karppinen A, Joffre SM, Räsänen J, Talvitie H. Mixing height determination by ceilometer. Atmos Chem Phys 2006; 6: 1485–1493.

[46] Atkinson B W. Meso-scale Atmospheric Circulations. London: Academic Press, 1981.

[47] Pielke R A. Mesoscale Meteorological Modeling. New York: Academic Press, 1984.

[48] Pielke R A, Uliasz M. Influence of landscape variability on atmospheric dispersion. J Air Waste Manage Assoc 1993; 43: 989-994.

[49] Pielke R A, Cotton WR, Walko RL, *et al.* A comprehensive meteorological modeling system, RAMS. Meteorol. Atmos Phys 1992; 49: 69-91.

[50] Latini G, Cocci Grifoni R, Passerini G, Tascini S. Modeling the interactions between sea breezes and valley breezes, Proceedings of 12th Conference on Interactions of the Sea and Atmosphere, American Meteorological Society, 2002.

<div style="text-align:right">

CHAPTER 5
</div>

Fundamentals of Air Pollution Mathematical Modeling

Roberta Cocci Grifoni[*] and R. D'Onofrio

School of Architecture and Design "E. Vittoria", Camerino University, Ascoli Piceno, Italy

Abstract: A dispersion model is essentially a computational procedure for predicting pollutant concentrations downwind of a source. Current models are based on knowledge of the emission characteristics (stack exit velocity, plume temperature, stack diameter, *etc.*), terrain (surface roughness, local topography, nearby buildings), and state of the atmosphere (wind speed, stability, mixing height, *etc.*). The main purpose of this chapter is to provide an overview of different dispersion models. The objective of dispersion Modeling is to predict the rate of spread of the pollutant cloud, and the consequent decrease in mean concentration. The model must be able to predict diffusion rates based on measurable meteorological variables such as wind speed, atmospheric turbulence, and thermodynamic effects. Therefore, algorithms at the heart of air pollution models are based on mathematical equations describing these various phenomena, which, can be used to predict concentration distributions downwind of a source when combined with empirical (field) data.

Keywords: AERMOD, AERSCREEN, atmospheric downwash, atmospheric turbulence, Box Model, CALPUFF, coastal-area meteorology, Dense Gas Models, dispersion models, emission, Gaussian Models, Lagrangian Models, land/sea breeze, Mesoscale models, MM5, New-generation Models, OCD, plume fumigation, pollutant concentration, Screening Models.

DISPERSION MODELS

Dispersion models require input data, which includes meteorological conditions such as wind speed and direction, the amount of atmospheric turbulence (as characterized by what is called the "stability class "), the ambient air temperature, and the height to the bottom of any inversion aloft that may be present.

Meteorological data is used by the model to help simulate plume transport and

---

*Address correspondence to Roberta Cocci Grifoni: School of Architecture and Design "E. Vittoria", Camerino University, Ascoli Piceno, Italy; Tel: +39 (0)737 404279; Tel: roberta.coccigrifoni@unicam.it

dispersion. Data quantifying the wind direction and speed, ambient temperature, mixing height, and atmospheric stability are used as input to the model. The meteorological data recorded hourly by nearby representative National Weather Service stations are often used as input to refined models. Use of actual meteorological data recorded at representative locations allows for the prediction of both short- and long-term pollutant concentrations.

Source/emission parameters define how emissions are released into the atmosphere. For example, for pollutants that are vented from stacks, emission information needed by the models includes the temperature and velocity of gases exiting the stack, the height and diameter of the stack, and the emission rates of the pollutants to be addressed. Models may also require the dimensions of adjacent buildings if estimating pollutant concentrations due to downwash (entrainment of pollutants into building wakes and cavities).

The rate at which a plume disperses and eventually reaches ground level is affected by the degree of urbanization of the surrounding area. Therefore, terrain elevations at the source and receptor locations as well as land use information are also important input parameters in dispersion Modeling. Greater plume dispersion is generally found in urban environments due to enhanced mechanical and thermal turbulence. Land use near the facility is used to determine whether the area should be defined as urban or rural.

In general, there are two levels of sophistication of models. The first level consists of relatively simple estimation techniques that normally use preset, worst-case meteorological conditions to provide conservative estimates of the air quality impact of a specific source or source category. These are called screening techniques or screening models. Meanwhile, more complex situations may require a more advanced level of Modeling sophistication, which can be obtained from the use of refined models.

Screening techniques are relatively simple calculations that provide conservative estimates of the air quality impact from a specific source. The purpose of screening is to eliminate the need for further detailed Modeling of sources that clearly will not cause or contribute to ambient concentrations in excess of specific

air quality criteria. If the predicted maximum impact from the screening model exceeds the specified criteria, then more sophisticated models may be applied.

Refined models consist of analytical techniques that provide more detailed treatment of physical and chemical atmospheric processes. These complex models accordingly require more detailed and precise input data, and provide more specialized concentration estimates. In theory, refined models give a more accurate estimate of source impact and the effectiveness of control strategies. These models can also be used to evaluate proposed engineering changes (*e.g.*, stack height or location) that may, for example, bring the source into compliance.

There are five types of air pollution dispersion models: Gaussian, Box, Lagrangian, Eularian, and Dense Gas models that, along with their hybrids, are discussed in more detail below.

Gaussian Distribution

Historically, the most frequently used dispersion models have been based on the Gaussian (or normal) distribution where the air contaminant concentration profile through the plume follows a normal bell curve in both the vertical and lateral directions. The concentration is greatest at the plume centreline, and decreases with distance from the centreline. More recent models account for pollutant dispersion due to wind force, which result in non-Gaussian vertical distributions. In such models, the rate at which the plume spreads as it travels downwind is a function of atmospheric turbulence. Nonetheless, the results of Gaussian models generally agree with experimental data and have undergone extensive validation.

The Box Model

The box model is the simplest model. It assumes the airshed (*i.e.*, a given volume of atmospheric air in a geographical region) has the shape of a box. It also assumes that air pollutants inside the box are homogeneously distributed and uses that assumption to estimate the average pollutant concentrations anywhere within the airshed. Although useful, this model is very limited in its ability to accurately predict the dispersion of air pollutants over an airshed, because the assumption of homogeneous pollutant distribution is overly simplified.
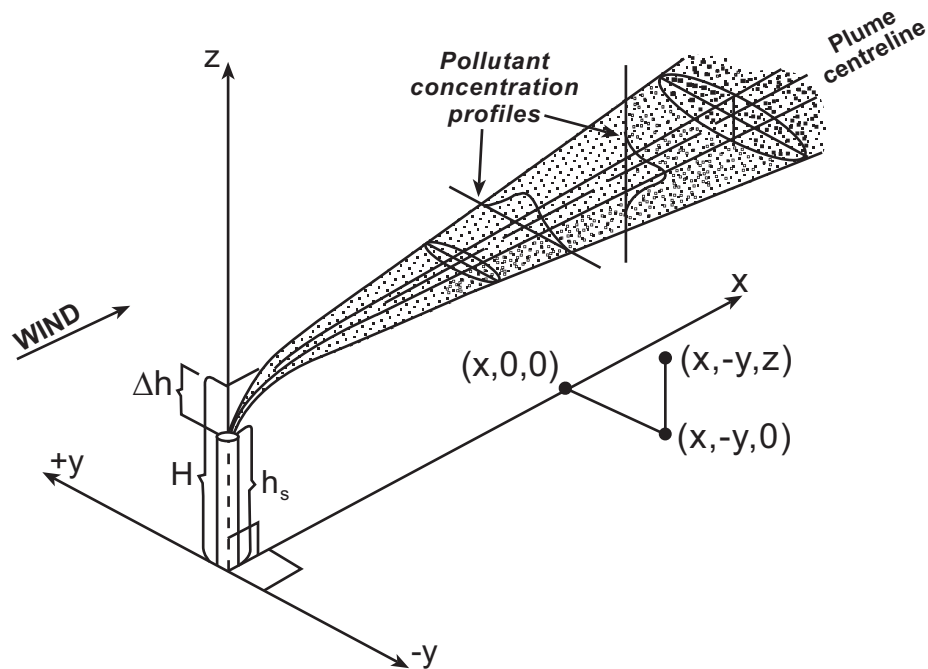
Figure 1: A plume dispersing in a normal (Gaussian) distribution along two axes –crosswind and vertically. The plume movement downwind is dependent on wind speed and hence, dispersion in this direction is not Gaussian.

Lagrangian Dispersion

The Lagrangian dispersion model mathematically follows pollution plume parcels (also called particles) as the parcels move in the atmosphere; it models the motion of the parcels as a random walk process. The Lagrangian model then calculates the velocity of the particles as a random (stochastic) process. Furthermore, the model is able to describe particle dispersion through statistical analysis based on the trajectories of a large number of particles.

Eulerian Dispersion

The Eulerian dispersion model is similar to the Lagrangian model in that it also tracks the movement of a large number of pollution plume parcels as they move away from their initial location. The most important difference between the two models is that the Eulerian model uses a fixed three-dimensional Cartesian grid as a frame of reference rather than a moving frame of reference.

Dense Gas Models

Finally, dense gas models are models that simulate the dispersion of dense gas pollution plumes (*i.e.*, pollution plumes that are heavier than air).

Gaussian models are the most widely used for regulatory purposes. The Gaussian model disperses emissions in the horizontal and vertical planes using Gaussian (bell-shaped for normalized) pollutant concentration distributions (see Fig. **1**). A plume's shape over time depends largely upon the wind speed and the atmosphere's tendency to become well mixed or unstable. When the atmosphere is unstable, a plume spreads out and disperses more quickly than when the atmosphere is stable.

Even if the turbulence is considered homogeneous as a first approximation, the presence of a solid boundary at ground level must be allowed for in order to conserve mass. The ground is usually assumed to be a perfect reflector and its presence is represented by a mirror image source placed below ground.

If the effective source height is assumed to be at an elevation *h*, the concentration can be estimated through the superposition:

$$C(x,y,z;H) = \frac{Q}{2\pi u \sigma_y \sigma_z} exp\left[-\frac{y^2}{2\sigma_y^2}\right]\left\{exp\left[-\frac{(z-h)^2}{2\sigma_z^2}\right] + exp\left[-\frac{(z+H)^2}{2\sigma_z^2}\right]\right\}$$

(1)

If the source is located at the ground (*z* = 0), this reduces to:

$$C(x,y,0;H) = \frac{Q}{\pi u \sigma_y \sigma_z} exp\left[-\frac{1}{2}\left(\frac{y^2}{\sigma_y^2} + \frac{H^2}{\sigma_z^2}\right)\right]$$

(2)

The following implicit assumptions must be considered for the previous formulation:

1) Continuous emission or emission times equal to or greater than travel times to the downwind position of interest, so that diffusion in the direction of travel can be ignored.

2) The material diffused is a stable gas or aerosol (<20 mm diameter), which remains suspended in the air over long periods of time.

3) Mass is conserved through reflection at surfaces.

4) Steady-state conditions are assumed during the time interval for which the model is used, usually one hour.

5) Constant wind speed, *u*, with height is assumed.

6) Constant wind direction with height is assumed.

7) The wind shear effect on horizontal diffusion is not considered (effect becomes large beyond ~10 km).

8) The dispersion parameters are assumed to be independent of *z* and functions of *x*.

9) The averaging times of all quantities (*u*, σ_y, σ_z, *C*) are assumed to be the same.

Some of these limitations can be overcome through the use of a Gaussian "puff" model. With this model, puffs are integrated in time, allowing for variable winds, although they are still invariant with height.

Plume Fumigation

We consider a tall stack in a coastal area located on a shoreline that emits a narrow plume towards land (Fig. **2**). The plume is embedded in the stable boundary layer and is intercepted by a growing thermal internal boundary layer (TIBL) over land. The height of the TIBL increases with solar heating of the land surface. Convective mixing over land can rapidly bring elevated pollutants to the ground, causing local high ground-level concentrations. Unlike fumigation events associated with the erosion of nocturnal ground-based inversions (see section), coastal fumigation may persist for several hours, and in the same location.

Fumigation was described first by Hewson and Gill [1]. The equations for estimating concentrations with these conditions have been given by Holland [2], Hewson [3], Gifford [4], Bierly and Hewson [5], and Pooler [6].
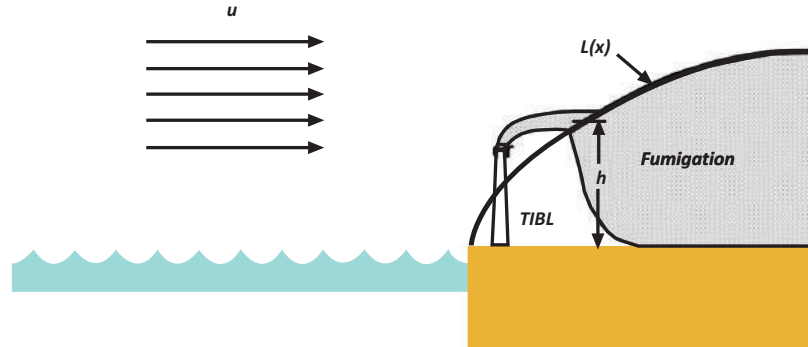
Figure 2: Coastal fumigation.

Coastal fumigation is an important issue in a coastal valley area. The potential effect of coastal fumigation should be considered carefully, especially when dealing with a large source located on a coastline. Several steady-state Gaussian - plume models have been developed by the Western Australia Department of Environmental Protection, in addition to, for example, the US EPA OCD (Offshore and Coastal Dispersion) model, that contain algorithms to model TIBL effects, which may be appropriate tools if coastal fumigation is identified as a significant issue at a particular site.

The pollutant concentration can be estimated by using the following expression:

$$C_{sl}(x,y,0) = \frac{Q}{2\sqrt{2\pi}u\sigma_y L(x)}\left\{1 + \mathrm{erf}\left[\frac{L(x)-H}{\sqrt{2}\sigma_{zs}}\right]\right\}\exp\left(-\frac{y^2}{2\sigma_y^2}\right) \tag{3}$$

where:

C_{sl} = ground-level concentration due to shoreline fumigation (*mass / volume*)

h = effective stack height (*length*)

$L(x)$ = height of the TIBL (*length*) $\approx Ax^{1/2}$ for small x (A = constant)

Q = emission rate (*mass / time*)

x, y = coordinates of ground-level receptor (*length*)

u = wind speed (*length / time*)

σ_y = standard deviation of lateral spread of plume in TIBL (*length*)

σ_{zs} = standard deviation of vertical spread of plume in stable layer (*length*)

In a complex meteorological situation, an in-depth analysis shows cases of fumigation and inversion break-up fumigation (see Fig. **3**) along with the retention of pollutants in the airshed caused by land/sea breeze effects.
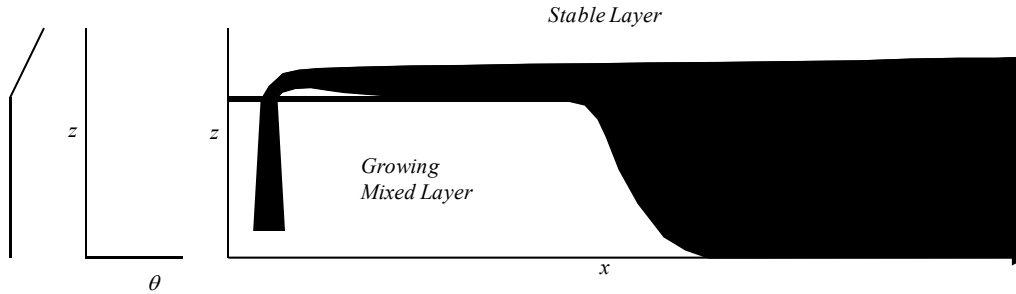
Figure 3: Fumigation and inversion break-up fumigation.

To assess ground level concentrations under inversion break-up fumigations, it is necessary to assume that the plume was initially emitted into a stable layer. As a result, values of σ_y and σ_z characteristic of stable conditions must be selected for the particular distance of interest.

The expression to estimate the ground level concentration when the inversion has been eliminated to a height, hi, is estimated with (Fig. **4**) [7]:

$$C_{ib}(x, y, 0; H) = \frac{q}{\sqrt{2\pi} u \sigma_{yf} h_i} \exp\left(-\frac{y^2}{2\sigma_{yf}^2}\right) \tag{4}$$

where

C_{ib} is the ground level concentration due to inversion breakup fumigation,

H is the effective stack height,

h_i is the height through which inversion has been eliminated,

q is the portion of emission in the mixed layer,

σ_{yf} is the standard deviation of lateral plume spread at ground level during inversion breakup,

σ_z is the standard deviation of vertical plume spread at ground level in a stable layer.
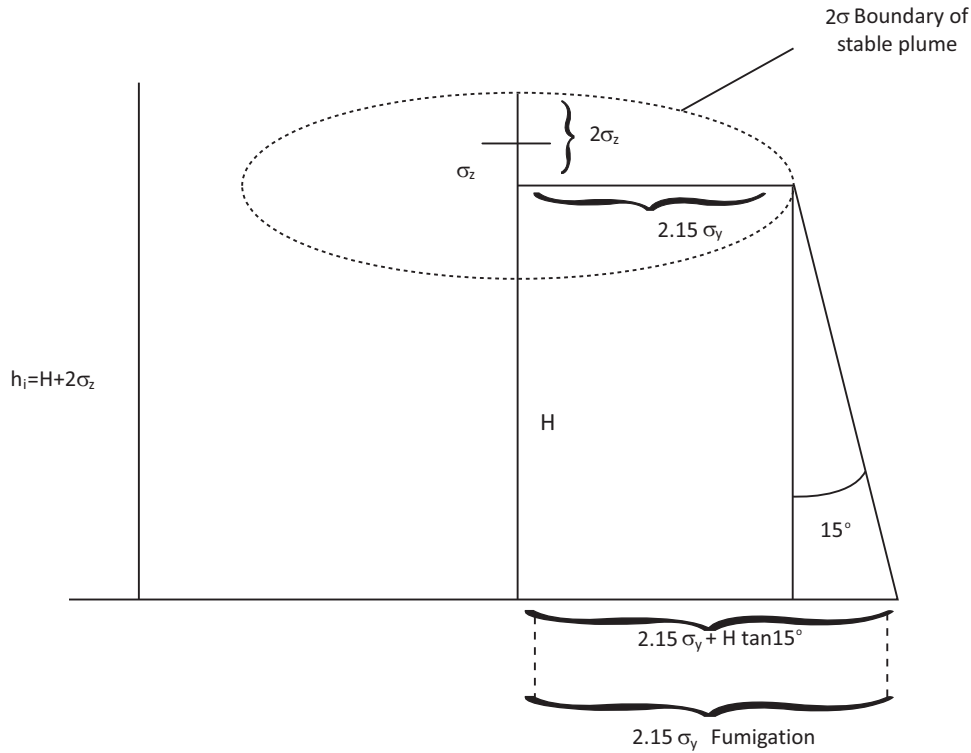
Figure 4: Diagram showing assumed height h_i and σ_y during fumigation [7].

In general, steady-state models are not effective for simulating high ground-level concentrations in the TIBL. However, advanced models, such as CALPUFF or new-generation Gaussian models such as AERMOD, which provide more realistic representations of the coastal-area meteorology, are arguably the most suitable for simulating the fumigation process.

AERSCREEN

The first set of models, known as screening models, are usually more general, relatively simple, and do not require as much time or data from the user. Screening models can be useful for identifying emissions sources that clearly will or will not cause or contribute to ambient concentrations in excess of air quality standards.

Since many screening tools use worst-case scenarios to model pollutant concentrations, they are generally a safe and conservative first estimate of project-level emissions.

AERSCREEN can be considered an example of a new-generation screening model. The AERSCREEN model retains many of the simplicities of SCREEN3 while including many of the more sophisticated features found in the US EPA's new-generation refined model, AERMOD. AERSCREEN is a relatively simple interactive program that can quickly perform single source, short-term calculations, including:

- Single point source calculations;

- Building wake effects for either attached or detached stacks;

- Incorporating the effects of building downwash on maximum concentrations for both near-wake and far-wake regions;

- Site-specific meteorology based on surrounding surface characteristics;

- Site-specific terrain elevations based on 1-degree digital elevation maps;

- Overall maximum impact as a function of distance;

- Automatic scaled impacts for 3-hour, 8-hour, 24-hour and annual averages.

However, if a screening model produces results indicating that a source may, in fact, exceed air quality standards, a model of greater sophistication must be used to provide results with greater resolution.

As previously stated, more complex models are sometimes referred to as refined models. These models require greater data input, but in return provide more refined estimates of emission source impacts. For most analyses, it is recommended that a screening model be used first, followed by a more refined model when necessary.

AERMOD

Nowadays new-generation air-quality dispersion models are often used for regulatory air quality Modeling. An important feature of these models is the use of boundary layer and surface energy flux parameterizations to provide turbulence parameters for estimating diffusion rates. These models are, in fact, based on principles of new generation meteorology, which employs continuous variables to characterise atmospheric conditions rather than the fixed number of categories used by traditional Gaussian models. An example of a new-generation model is AERMOD. Some studies [8] have demonstrated that it can be successfully applied over complex coastal areas comprising valleys, hills, urban zones, and an industrial zone.

AERMOD is a Gaussian steady-state plume dispersion model for the assessment of pollutant concentrations from point, volume, and area sources. Sources may be located in rural or urban areas, and receptors may be located in simple or complex terrain. The complex terrain capabilities of AERMOD are of particular interest. Complex terrain is defined as terrain in which ground elevations are above the stack tip or release height.

Special features of AERMOD include its ability to treat the vertical non-homogeneity of the planetary boundary layer, surface releases, sources with irregularly shaped areas, a three-plume model for the convective boundary layer, a limitation on vertical mixing in the stable boundary layer, and fixing of the reflecting surface at the stack base. AERMOD also includes an improved treatment of dispersion in the presence of complex terrain.

AERMOD requires the use of two pre-processor modules to develop the necessary components of the model.

1. AERMET (AERMOD Meteorological Pre-Processor)

AERMET is the meteorological pre-processor for AERMOD. Input data may come from hourly cloud cover observations, surface meteorological observations, and upper-air soundings. The output includes surface meteorological observations and parameters and vertical profiles of several atmospheric parameters.

2. AERMAP (AERMOD Terrain Pre-Processor)

The AERMAP pre-processor is a terrain pre-processor designed to simplify and standardize the input of terrain data for AERMOD. Input data includes receptor terrain elevation data. Terrain data may be in the form of digital data available from the US Geological Survey. For each receptor, the output includes the location and height scale value, namely the elevation used for the computation of airflow around hills.

AERMOD simulates transport and dispersion from multiple point area, or volume sources based on an up-to-date characterization of the atmospheric boundary layer. Sources may be located in rural or urban areas, and receptors may be located in simple or complex terrain. The model employs hourly sequential pre-processed meteorological data to estimate concentrations for averaging on timescales from one hour to one year. Specifically, it is appropriate for the following applications:

➢ Point, area, and volume sources;

➢ Surface, near-surface, and elevated releases;

➢ Rural or urban areas;

➢ Simple or complex terrain;

➢ Transport distances over which steady state assumptions are appropriate, up to 50 km;

➢ 1-hour to annual averaging times;

➢ Continuous toxic air emissions.

AERMET organizes data from both the upper air and hourly surface observation stations and then estimates the necessary parameters for dispersion calculations.

Representative climatological variables such as albedo, the Bowen ratio, and surface roughness reflect the surface characteristics; they are representative of the

Modeling domain, and are therefore used by the model. The effects of changes in land use parameters and various complex orography on the modelled design concentrations in AERMOD are extremely complex. Choosing the correct AERMOD input data is an all-important first step in the successful assessment of pollutant concentrations.

Reasonably accurate estimates of these characteristics [9] are necessary for AERMOD to provide accurate results.

In addition, in a coastal valley area, an initial sensitivity analysis should be performed to assess the importance of topographic information. AERMOD assumes that the concentration at a receptor is the weighted combination of two concentration estimates: a purely horizontal plume and a plume that is vertically displaced by the terrain. For an assessment of the needs and potential of the model, the coast of Marche Region (Italy) was selected as a study area [8] because of the presence of different types of topographically influenced flow patterns. Results from a series of sensitivity experiments indicated significant topographical forcing, although synoptic forcing was quite strong in this valley.

Another interesting property of AERMOD is that it offers the possibility of incorporating the current understanding of dispersion and micrometeorology in order to model the impact of sources at short distances. Amongs its capabilities, it can make use of more advanced meteorological information such as that produced by a mesoscale model, namely RAMS [10]. RAMS is capable of Modeling weather systems such as land/sea breezes and mountain circulations, and it is suitable for Modeling meteorological conditions in a complex coastal area. In the study mentioned, the authors considered a set of AERMOD runs using RAMS data as input and compared the results with AERMOD runs made using surface and upper air data from the Local Airbase Station.

From the results, it is readily apparent that the two models predict short-term average concentrations in a similar fashion (when using identical input data). The positions of concentration maxima are almost identical. The value predicted using RAMS -AERMOD is slightly higher and therefore the most likely to be exact. This could be attributed to the evident capability of RAMS to model PBL parameters and its structure.

According to the most recent findings by the US EPA [11], AERMOD can be considered the most accurate dispersion model available for regulatory applications. This substantiation is based upon a number of tests that have been performed by the US EPA and others [12] to compare AERMOD to other dispersion models, such as the Industrial Source Complex (ISC3) and the Complex Terrain Dispersion Model PLUS unstable algorithms (CTDMPLUS).

As of November of 2005, AERMOD incorporates the effects of building downwash, the common name for the effect buildings have on plume movement and subsequent ground-level pollutant concentrations.

In summary, AERMOD has a built-in screening tool (AERSCREEN), a surface characteristic pre-processor (AERSURFACE), meteorological data pre-processor (AERMET) and terrain data pre-processor (AERMAP), all of which are available for free download from the US EPA website (http://www.epa.gov/scram001).

CALPUFF

The CALPUFF Modeling system [13] is a Lagrangian puff model.

Pollutant releases can be represented by a series of puffs of material, which are also transported by model winds. Each puff represents a discrete amount of pollution, whose volume increases due to turbulent mixing. Puff models are far less computationally expensive than particle models, but are not as realistic in their description of pollutant distribution. However, they are often more than adequate, and are used for regulatory purposes.

CALPUFF is programmed to simulate continuous puffs of pollutants emitted from a source into the ambient wind flow. As wind flow changes from hour to hour, the path of each puff changes to the new wind flow direction. Puff diffusion is Gaussian, and concentrations are based on the contributions of each puff as it passes over or near a receptor point.

A sufficiently large number of puffs is necessary to adequately reproduce the plume solution at near-field receptors. Fig. (**5**) shows how a puff model treats a continuous emission point source as a series of puffs. The puffs are represented

diagrammatically by interlocking circles that become increasingly larger as they move further away from the source. The course of the circles changes direction, moving up and then down, to show how the model tracks the actual course of the plume downwind.

+ Release point
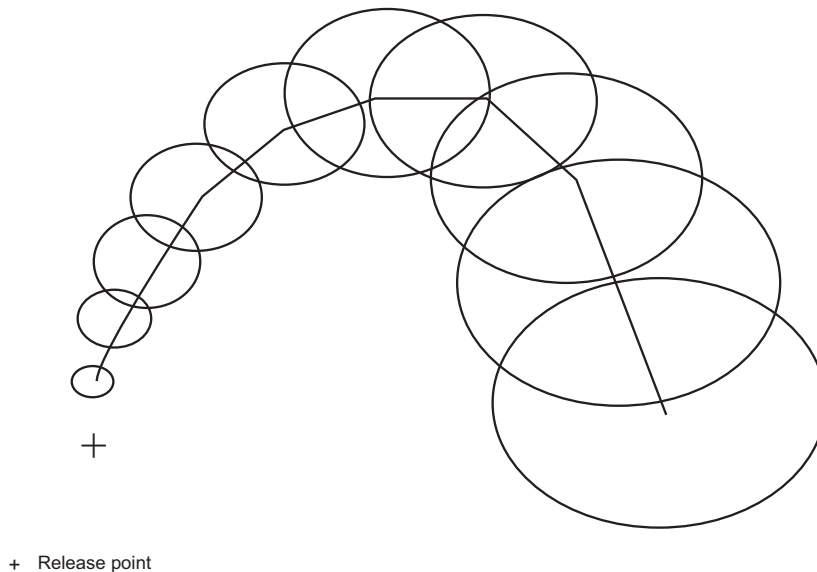
Figure 5: Continuous emission point source subdivided as a series of puffs.

CALPUFF is designed to handle the complexities posed by complex terrain, large source -receptor distances, chemical transformation, and deposition.

It includes algorithms for near-field effects such as building downwash, transitional buoyant and momentum plume rise, partial plume penetration, subgrid scale terrain and coastal interaction effects, as well as terrain impingement. It also treats longer-range effects such as pollutant removal due to wet scavenging and dry deposition, chemical transformation, vertical wind shear, over-water transport, plume fumigation, and visibility effects due to particulate matter.

CALPUFF was originally designed for mesoscale applications and treated emissions as integrated puffs. As features were added to the model for handling local-scale applications, it was realized that use of the integrated puff approach was inefficient. Therefore, a more efficient approach was developed to treat emissions as a slug, in which the slug is stretched so as to better characterize local

source impacts. The slug can be visualized as a group of overlapping circular puffs having very small separation distances. When run in slug mode, the hourly averaged pollutant mass is spread evenly throughout the slug.

The Modeling system consists of three main components and a set of pre-processing and post-processing programs. The three main components of the modeling system include:

1. CALMET (a diagnostic three-dimensional meteorological model);

2. CALPUFF (an air quality dispersion model);

3. CALPOST (a post-processing package).

Each of these programs has a graphical user interface (GUI). In addition to these components, there are numerous other processors that may be used to prepare geophysical (*i.e.*, land use and terrain) data, meteorological data (surface, upper-air, precipitation, and buoy data), and interfaces to other models such as the Penn State/NCAR Mesoscale Model (MM5), the National Centers for Environmental Prediction (NCEP) ETA model, and the RAMS meteorological model. These are all available for free download from the US EPA website (http://www.epa.gov/scram001).

This model is also able to deal with typical sea/land transition situations, even if they are complex conditions to simulate.

In fact, the interaction of the production and dissipation of turbulence in coastal valley regions are very complex. In the case of a sea breeze, when marine air flows over warmer land, mechanical shear and buoyancy forces both act to increase turbulence energy. However, when air flows over the colder sea surface in a land breeze, mechanical turbulence interacts with the stably stratified flow to dissipate turbulence energy. Thus, the interaction between turbulence and stratification is an important factor in the growth of a thermal internal boundary layer near the coast.

CALPUFF evaluates turbulence and dispersion characteristics that are consistent with the land use properties of each cell grid, whether the cell is classified as water or land, for the gridded meteorological fields provided by CALMET.

An example of how CALPUFF can be used to evaluate changes in dispersion with land use properties is when a puff inside the marine layer enters the mixed layer and its growth changes. In this case, the growth of the puff is modified from one appropriate for the marine boundary layer to one appropriate for the overland boundary layer.

Once a puff crosses a coastline from water to land during conditions favorable to the TIBL formation, the increased mixing height for the puff grows with distance along the trajectory of the puff.

OCD

When modeling the dispersion of pollutants from a source located near the coast, the effects of coastal fumigation may be simulated in either:

a) a Gaussian -plume model, which has the ability to handle this specific effect (*e.g.*, DISPMOD, OCD, AERMOD or US EPA 's SCREEN 3); or

b) an advanced model (CALPUFF), which gives a realistic representation of the meteorology in the coastal area.

One of the most-used models for simulating the effects of offshore emissions from point, area, or line sources on the air quality of coastal areas is the Offshore and Coastal Dispersion (OCD) model [14, 15].

This model includes special algorithms that account for overwater plume transport and dispersion, as well as the changes that take place as the plume crosses the shoreline. The model also includes parameterizations for the development of the thermal internal boundary layer (TIBL), plume fumigation, overwater surface boundary layer, plume dispersion over complex terrain, and platform downwash. The model was specifically evaluated with field experiments conducted in coastal areas [15].

OCD requires meteorological data measured in the overwater layers in order to characterize the overwater boundary layer. One of the mandatory variables is the

overwater mixing height, which is not routinely measured. Because of this, if the data are missing, OCD assigns a constant 500 m to the overwater mixing height [16].

OCD was initially designed to simulate the effects of offshore sources on coastal regions. As a result, the model has a sophisticated procedure to determine the timing for an offshore plume to enter the TIBL. At the transition, the model uses the virtual source technique to account for the change in dispersion regimes (from over water to over land) in polar coordinates. OCD also properly handles cases when sources and receptors are both over water or over land. However, a close review of the code shows that OCD does not correctly calculate impacts on offshore areas from coastal sources. For example, in subroutine CALC, due to an insufficiency in the program logic, when a land-based plume travels to over-water areas, the change in dispersion regime is not triggered and the code continues to perform dispersion calculations as if the plume were still over land. This highlights the need for the OCD code to be carefully reviewed and modified to ensure that the land-to-water as well as water-to-land pathways are correctly treated [16].

ACKNOWLEDGEMENTS

CONFLICT OF INTEREST

The author(s) confirm that this chapter content has no conflict of interest.

REFERENCES

[1]   Hewson E W, Gill G C. Meteorological investigations in Columbia River Valley near Trail, B.C., pp 23-228 in repoter submitted to the Trail Smelter Arbitral tribunal, Bur. Of Mines Bull.453, Washington: Govt. Print. Off 1944.
[2]   Holland J Z. A meteorological survey of the Oak Ridge area. Report ORO-99, Atomic Energy Comm Washington 1953.
[3]   Hewson E W. Stack heights required to minimize ground concentrations. Trans. ASME 77 1955: 1163-1172.
[4]   Gifford F A. Atmospheric dispersion calculations using the generalized Gaussian plume model. Nucl Saf 1960; 2 (2): 56-59, 67-68.

[5]   Bierly EW, Hewson EW. Some restrictive meteorological conditions to be considered in the design of stacks. J Appl Meteorol 1962;1 (3): 383-390.

[6]   Pooler F. Potential dispersion of plumes fron large power plants. PHS publ. 1965.

[7]   Turner D B. Workbook of atmospheric dispersion estimates, Environmental Protection Agency, Office of air program, North Carolina: Research Triangle Park 1970.

[8]   Latini G, Cocci Grifoni R, Passerini G. Application of new generation models over complex coastal areas, Coastal Environment IV, 2002, WIT Press, Southampton (GB), pp. 385-394.

[9]   Latini G, Cocci Grifoni R, Passerini G. The Optimal Choice of AERMOD Input Data in Complex Areas, Air Pollution Modeling and its Applications, 2002, Kluwer Academics Plenum, pp. 513-514.

[10]   Cocci Grifoni R, Latini G, Passerini G, Tascini S. Applications of Rams and Aermod models to evaluate pollution dispersion in a coastal valley, Air Pollution Modeling and its Applications, 2004, Kluwer Academic / Plenum, pp. 627-631.

[11]   EPA, Guideline on Air Quality Models. US Environmental Protection Agency 2005.

[12]   EPA, AERMOD: Latest Features and Evaluation Results. Research Triangle Park, NC 2003:.

[13]   Scire JS, Strimaitis DG, Yamartino RJA, User's Guide for the CALPUFF Dispersion Model (Version 5.0). Earth Tech, Inc., 196 Baker Avenue, Concord, MA 01742, 2000.

[14]   Hanna SR, Schulman LL, Paine RJ, Pleim JE, Baer M. Development and Evaluation of the Offshore and Coastal Dispersion (OCD) Model. Japca J Air Waste Ma 1985; 35: 1039-1047.

[15]   Hanna SR, Di Cristofaro DC. Development and Evaluation of the OCD /API Model. Final Report, API Pub. 4461, Washington (D.C): American Petroleum Institute1988.

[16]   Chang J C, Fernau M E, Scire J S, Strimaitis D G. A Critical Review of Four Types of Air Quality Models Pertinent to MMS Regulatory and Environmental Assessment Missions. U.S: Department of the Interior New Orleans Minerals Management Service, Gulf of Mexico OCS Region 1998.

CHAPTER 6

Advection-Diffusion in the Atmosphere: Equations and Solutions

Tiziano Tirabassi[1,*] and Marco T. Vilhena[2]

[1]Institute ISAC of CNR, Bologna, Italy and [2]Universidade Federal do Rio Grande do Sul, Porto Alegre (RS), Brasil

Abstract: Analytical solutions of equations are of fundamental importance in understanding and describing physical phenomena. We provide a short review of the analytical solutions of the advection-diffusion equation. Two new solutions are presented, adopting novel analytical approaches named Generalized Integral Laplace Transform Technique (GILTT) and Advection Diffusion Multilayer Model (ADMM). The GILTT method is an analytical series solution of the advection-diffusion equation including the solution of an associate Sturn-Liouville problem, expansion of the pollutant concentration in a series in terms of the attained eigefunction, replacement of this expansion in the advection-diffusion equation and, finally, taking moments. This procedure leads to a set of differential ordinary equations that is solved analytically by Laplace transform technique. The ADMM method is an analytical integral solution of the advection-diffusion equation based on a discretization of the PBL in N sub-layers; in each sub-layers the advection-diffusion equation is solved by the Laplace transform technique, considering an average value for eddy diffusivity and the wind speed.

Keywords: Advection-diffusion equation, Analytical solutions, Integral transform, air pollution modeling, atmospheric boundary-layer, atmospheric dispersion, atmospheric turbulence, air quality management.

INTRODUCTION

The management and safeguard of air quality presupposes knowledge of the state of the environment. Such knowledge involves both cognitive and interpretative aspects. Monitoring networks and measurements in general, together with an inventory of emission sources, are of fundamental importance for the construction of the cognitive picture, but not the interpretative one. In fact, air quality control

*****Address correspondence to Tiziano Tirabassi:** Institute ISAC of CNR, Bologna, Italy; Tel: + 39 (0) 51 6399601; E-mail: t.tirabassi@isac.cnr.it

requires interpretative tools that are able to extrapolate in space and time the values measured by analytical instrumentation at field sites, while environmental improvement can only be obtained by means of a systematic planning of reduction of emissions, and, therefore, by employing instruments (such as mathematical models of atmospheric dispersion) capable of linking the causes (sources) of pollution with the respective effects (pollutant concentrations).

The processes governing the transport and diffusion of pollutants are numerous, and of such complexity that it would be impossible to describe them without the use of mathematical models. Such models therefore constitute an indispensable technical instrument of air quality management.

The theoretical approach to the dispersion in the atmosphere assumes different forms. In the K approach, diffusion is considered, at a fixed point in space, proportional to the local gradient of the concentration of the diffused material. Consequently, it is fundamentally Eulerian since it considers the motion of fluid within a spatially fixed system of reference.

Lagrangian models differ from Eulerian ones in adopting a system of reference that follows atmospheric motions. This class includes all models that decomposes the pollutant cloud into discrete "elements", such as segments, puffs or computer particles. In particle lagrangian models pollutant dispersion is simulated through the motion of computer particles whose trajectories allow the calculation of the concentration field of the emitted substance. The underlying hypothesis is that the combination of the trajectories of such particles simulate the paths of the air particles situated, at the initial moment, in the same position

In this chapter we take in consideration the Eulerian approach

Eulerian Approach: K Models

Eulerian models are the most suitable for tackling problems of greater complexity, for example, the dispersion of pollutants over complex terrain or the diffusion of non-inert pollutants. They are based on the resolution, on a fixed spatial-temporal grid, of the equation of mass conservation of the pollutant chemical species, expressed in terms of concentration $c(x, y, z, t)$ [1]:

$$\frac{\partial c}{\partial t} = -u \cdot \nabla c + D\nabla^2 c + S \tag{1}$$

In (1) u is the wind speed vector, of the components u, v, w; $D\nabla^2 c$ is the molecular diffusion term (generally neglected), with D the molecular diffusion coefficient; S is the term referring to the source, measuring the emission intensity and representing the pollutant removal kinetic; ∇ is the gradient operator; ∇^2 is the Laplacian.

In order to resolve (1) it is necessary to know the wind field u, something that is not possible since it is extremely variable in space and time, from the scale of centimeters to kilometers. Consequently, wind is divided into two parts:

$\bar{u}$ the so-called ensemble average

u' the turbulent fluctuations of wind at mean nil

Thereupon the wind speed is expressed as the sum of the two components, mean and turbulent:

$$u = \bar{u} + u' \tag{2a}$$

with $u = \bar{u} + u' = 0$

The same considerations can be made for c. Therefore:

$$c = \bar{c} + c' \tag{2b}$$

with $\bar{c'} = 0$

The ensemble average refers to the mean value obtained by the repetition of many experiments in the same meteorological and emission conditions.

The new u and c are introduced into (1); after several calculations and hypothesising a wind with divergence nil, the following is obtained:

$$\frac{\partial \bar{c}}{\partial t} = -\bar{u} \cdot \nabla \bar{c} - \nabla \cdot \overline{c'u'} + D\nabla^2 \bar{c} + \bar{S} \tag{3}$$

This equation includes some new variables (those with an apex) whose values are unknown. The appearance of new terms in equations for mean quantities leads to a number of unknowns greater than the number of equations. Thus, the system of equations is not closed and is therefore unresolvable. To close it, in fact, new equations of variance and covariance (second order moments) would be required, but this would only shift the problem to a higher order since it would yield further unknown quantities that are third order moments. Now, if it were decided to find equations for the third order moments, this would yield unknowns of a higher order, *i.e.* fourth order moments, requiring the introduction of new equations. Iterating the procedure, the conclusion would be reached that the number of unknowns is always greater than the number of equations. A solution to this problem consists of utilizing only a finite number of equations, relative to a certain number of unknowns, parameterizing the remaining ones in terms of known quantities.

The most classic and widely used approach to obviate this problem is the parameterization of second order moments, assuming a hypothetical analogy between molecular diffusion and the turbulent transfers. Such approach is referred to as the K-theory or flux-gradient theory, as it assumes that the flow of a given field is proportional to the gradient of an appropriate mean variable. This is a first order closure of the set of equations under examination, since it conserves the equations relative to the first moments and parameterizes the second moments:

$$\overline{c' u'} = -K \nabla \overline{c} \tag{4}$$

where K is the eddy diffusivity coefficient.

The simplicity of the K-theory of turbulent diffusion has led to its widespread use as the mathematical basis for simulating urban, photochemical pollution. However, K-closure has its own limits. In contrast to molecular diffusion, turbulent diffusion is scale-dependent. This means that the rate of diffusion of a cloud of material generally depends on the cloud dimensions and the intensity of turbulence. As the cloud grows, larger eddies are incorporated in the expansion process, so that a progressively larger fraction of turbulent kinetic energy is available for the cloud expansion. However, eddies much larger than the cloud

itself are relatively unimportant in its expansion. Thus, the gradient-transfer theory works well when the dimension of dispersed material is much larger than the size of turbulent eddies involved in the diffusion process, *i.e.* for ground-level emissions and for large travel times. Strictly speaking, one should introduce a diffusion coefficient function not only of atmospheric stability and emission height, but also of the travel time or distance from source. However, such time-dependence makes it difficult to treat the diffusion equation in a fixed-coordinate system where multiple sources have to be treated simultaneously. Otherwise, one should limit the application of the gradient theory to large travel times [2]. A further problem is that the down-gradient transport hypothesis is inconsistent with observed features of turbulent diffusion in the upper portion of the mixed layer, where countergradient material fluxes are known to occur [3].

In addition, unlike molecular diffusion, turbulent diffusion is not a property of fluids, but of the turbulence itself or of flows, and it may vary greatly from one flow to another and from one region to another of the same flow. The above relations are essentially based only on a qualitative analogy between molecular and turbulent diffusion. For the first order closure to be realistic, the mean concentration field must have a much larger scale time than that of turbulent transport.

Despite these well known limits, the K-closure is widely used in several atmospheric conditions, because it describes the diffusive transport in a Eulerian framework, where almost all measurements are Eulerian in character. It produces results that agree with experimental data as well as any more complex model, and it is not as computationally expensive as higher order closures.

The reliability of the K-approach strongly depends on the way the eddy diffusivity is determined on the basis of the turbulence structure of the PBL, and on the model's ability to reproduce experimental diffusion data. A great variety of formulations exist [4]. Most of them are based on similarity theory, and give different results for the same atmospheric stability, as well as discontinuities and jumps at the transition between different stability regimes of the PBL.

The tensor K (3x3) of turbulent diffusion, whose elements can be extrapolated from experimental measurements, is introduced in equation (3). Then, by also applying the following approximations:

- the **K** tensor is diagonal,

- the molecular diffusion is negligible,

- c represents the concentration of a non-reactive pollutant (thus $\bar{S}$ =S),

equation (3) can be written in the form:

$$\frac{\partial \bar{c}}{\partial t} = -\bar{u} \cdot \nabla \bar{c} + \nabla \cdot K \nabla \bar{c} + S \qquad \textbf{(5)}$$

Equation (5) can be integrated (analytically or numerically) if input data for u, K and S are provided, together with the initial and boundary conditions for $\bar{c}$.

Eulerian models and K models mainly differ in the functions utilised for the K coefficients and the techniques used for the integration of (5).

Equation (5) can be resolved in two ways:

i.   with analytic methods, obtaining exact solutions;

ii.   with numerical methods, obtaining approximate solutions.

In this chapter we take in consideration analytical solutions.

Analytical formulae are of fundamental importance in understanding and describing physical phenomena. Analytical solutions or approximations (as opposed to numerical ones) explicitly take into account all the parameters of a problem, so that their influence can be reliably investigated and it easy to obtain the asymptotic behavior of the solution, which is usually difficult to generate through numerical calculations. Moreover they are fast, simple and generally, do not require complex meteorological inputs.

Analytical Solutions

Analytical solutions of equations are of fundamental importance in understanding and describing physical phenomena. Analytical solutions (as opposed to numerical ones) explicitly take into account all the parameters of a problem, so that their influence can be reliably investigated and it easy to obtain the

asymptotic behavior of the solution, which is usually difficult to generate through numerical calculations.

There are analytical solutions of the two-dimensional advection-diffusion equation [5, 6]:

$$u \frac{\partial C}{\partial x} = \frac{\partial}{\partial z}\left(K_z \frac{\delta C}{\delta z} \right) + S \tag{6}$$

where u is mean velocity (the wind is assumed along x axis, while z is the height), C is the mean concentration, S is the source term, and K is the vertical eddy exchange coefficient. Moreover, as usual, the along-wind diffusion was neglected because considered little in respect to the advection. Although, very recently a steady state mathematical model for dispersion of contaminants in low winds by taking into account the longitudinal diffusion in the advection-diffusion equation was formulated [7].

The best-known solution is the so-called Gaussian solution, where both wind and turbulent diffusion coefficients are constant with height. So it is not a realistic solution of the equation of transport and diffusion in the atmosphere. In the so-called Gaussian models, the solution is forced to represent real situations by means of empirical parameters, referred to as "sigmas". They can be either stationary (the time- independent plume models) or time-dependent (puff models). The name given to these models is derived from the fact that the pollutant distribution, both vertical and transversal to wind direction, is described by the famous curve discovered by the physicist-mathematician Gauss. The various versions of Gaussian models essentially differ in the techniques utilised to calculate the sigmas as a function of atmospheric stability and the downwind distance from the emission source. Gaussian models are fast, simple and do not require complex meteorological inputs. For these reasons they are still widely used by the environmental agencies all over the world for regulatory applications.

However, there are models based on non-Gaussian analytical solutions.

Roberts (1923) presented a bi-dimensional solution, for ground-level sources only, in cases where both the wind speed and vertical diffusion coefficients follow power laws as a function of height. That is:

$$u = u\left(z / z_1\right)^{\alpha} \tag{7a}$$

$$K = K_1\left(z / z_1\right)^{\beta} \tag{7b}$$

where z_1 is the height where u_1 and K_1 are evaluated.

Rounds [8] obtained a bi-dimensional solution valid for elevated sources, but only for linear profiles of K_z. Smith [9] resolved the bi-dimensional equation of transport and diffusion with u and K_z power functions of height with the exponents of these functions following the conjugate law of Schmidt (*i.e.*, 'wind exponent' = 1-'K_z exponent').

Smith [10] also presented a solution in the case of constant u, but K_z following:

$$K_z = K_0 z^a\left(h - z\right)^b \tag{8}$$

where K_0 is a constant and a and b can be:

a $\geq$ 0 and b = 0

a = 0 and b> 0 for 0 $\leq$ z $\leq$ h

a = 1 and b > 0 for 0 $\leq$ z $\leq$ h

a = 1 and b = 0 for 0 $\leq$ z $\leq$ h/2; a = 0 and b = 1 for h/2 $\leq$ z $\leq$ h

where h is the height of the atmospheric boundary layer.

Scriven and Fisher [11] proposed a solution with constant u and K_z as:

$$K \equiv z \text{ for } 0 \leq z \leq z \tag{9a}$$

$$K_z = K_z\left(z_s\right) \text{ for } z_s < z \leq h \tag{9b}$$

where z_s is a predetermined height (generally, the height of the surface layer). This solution allows (as boundary conditions) a net flow of material towards the ground:

$$K_z \cdot \frac{\partial C}{\partial z} = V_g C \qquad\qquad\qquad (10)$$

where V_g is the deposition velocity. The Scriven and Fisher solution [11] has been used in the United Kingdom for long range transport of pollutant. In Fisher [12] the deposition of sulphur over the United Kingdom, Sweden and the rest of Europe was compared and it was found that the British contribution to deposition over rural Sweden was about one half of the Swedish contribution.

Yeh and Huang [13] and Berlyand [14] published bi-dimensional solutions for elevated sources with u and K following power profiles, but for a unbound atmosphere. That is:

$$K_z \cdot \frac{\partial C}{\partial z} = 0 \ \text{ at } z = \infty \qquad\qquad\qquad (11)$$

Demuth [15] put forward a solution with the same conditions, but for a vertically limited boundary layer. That is:

$$K_z \cdot \frac{\partial C}{\partial z} = 0 \ \text{ at } z = \text{h} \qquad\qquad\qquad (12)$$

The solutions of Yeh and Huang, Berlyand and Demuth are used in the air pollution model KAPPAG [16-18].

By applying the Monin-Obukhov similarity theory to diffusion, van Ulden [19] derived a solution for vertical diffusion from continuous sources near the ground only with the assumption that u and K_z follow power profiles. His results are similar to Roberts', but he provided a model for non-ground level sources, but applicable to sources within the surface layer. SPM [20] is a model that utilizes the solution proposed by van Ulden.

Nieuwstadt [21] presented a solution, which was a particular case of Smith's [10] solution noted above. Subsequently, Nieuwstadt and Haan [22] extended that solution to the case of a growing boundary layer height. Catalano [23], in turn, extended the latter solution to the case of non-zero mean vertical wind profiles.

Chrysikopoulos *et al.* [24] presented a three-dimensional atmospheric dispersion - deposition model for a ground-level area source.

Lin and Hildemann [25] extended the solution of Demuth [15] with boundary conditions suitable for simulating dry deposition to the ground.

Recently, Brown *et al.* [26] derived from the solution of Yeh and Huang [13], equations for point source releases for the first four moments of the vertical concentration distribution and the magnitude and downwind location of the maximum ground concentration.

Sharan and Yadav [27] obtained a three-dimensional solution (with u and Kz constanat) for low wind condition where the diffusion coefficients are function of down-wind distance from the source. Sharan and Modani [28] presented a two-dimensional solution with Kz constant and function of down-wind distance from the source, with a power low wind profile and for a finite boundary layer.

Essa *et al.* [29] obtained an analytical solution with dry deposition to the ground with any vertical function of wind and eddy coefficients but for a fixed vertical shape of contaminant concentrations.

$$c(x,z) = F(x)\left(1 - \frac{z}{h}\right)^2 \tag{13}$$

where F(x) is any function of x.

Using ADMM (Advection-Diffusion Multilayer Method) approach, Vilhena *et al.* [30] proposed a general solution for any wind and eddy coefficient profiles, but represented by a steep function in z.

Finally Wortmann *et al.* [31] and Moreira *et al.* [7], applaing GILTT technique (Generalized Integral Laplace Transform Technique), found a general two-dimensional steady state solution for any profiles of wind and eddy coefficient diffusions and a limited PBL.

GILTT Approach

It is presented the construction of the two-dimensional analytical solution for the advection-diffusion-deposition equation to simulate pollutant dispersion in

atmosphere with deposition to the ground, valid for any variable vertical eddy diffusivity coefficients and wind profile. That is, solution of:

$$u(z)\frac{\partial C(x,z)}{\partial x} = \frac{\partial}{\partial z}\left(K_z(z)\frac{\partial C(x,z)}{\partial z}\right) \tag{14}$$

subjected to the boundary conditions:

$$K_z(z)\frac{\partial C(x,z)}{\partial z} = V_g C(x,z) \text{ at } z = 0 \tag{14a}$$

$$K_z(z)\frac{\partial C(x,z)}{\partial z} = 0 \text{ at } z = h \tag{14b}$$

and a continuous source condition:

$$u(z)C(0,z) = Q\delta(z - H_s) \text{ at } x = 0 \tag{14c}$$

Here, C denotes the pollutant concentration, Kz is the turbulent eddy diffusivity coefficient assumed to be a function of the variable z, u is the mean wind oriented in the x direction and function of the variable z, Vg the deposition velocity, h is the height of PBL, Q the emission rate, Hs the height of the source and δ is the Dirac-Delta function. The two-dimensional equation is equivalent to concentrations from an infinite line source, or cross-wind integrated concentration from a point source.

To solve the problem by the GILTT method, Eq. (14) is rewritten as:

$$u(z)\frac{\partial C(x,z)}{\partial x} = K_z(z)\frac{\partial^2 C(x,z)}{\partial z^2} + K'_z(z)\frac{\partial C(x,z)}{\partial z} \tag{15}$$

where it should be noted that the first term on the right hand side satisfies the following Sturm-Liouville problem:

$$\zeta''_i(z) + \lambda_i^2 \zeta_i(z) = 0 \text{ at } 0 < z < h \tag{16}$$

$$-K_z(z)\zeta'_i(z) + V_g\zeta_i(z) = 0 \text{ at } z = 0 \tag{16a}$$

$$\zeta'_i(z) = 0 \ \text{at } z = h \tag{16b}$$

where the symbols " $'$ " and " $''$ " mean first and second derivative respect z, respectively.

The solution of problem (16) constitutes a well known set of orthogonal eigenfunctions $\zeta_i(z) = \cos(\lambda_i(h - z))$ whose eigenvalues fulfill the ensuing transcendental equation:

$$\lambda_i(z)\tan(\lambda_i(z)h) = H_1 \tag{16c}$$

where $H_1 = \dfrac{V_g}{K_z(z_0)}$

For more details see the work of Özisik [32]. The eigenvalues are obtained from Eq. (16c) using the Newton-Raphson solving technique. Kz is not evaluated at z = 0, but at z_0 (the roughness length) where Vg is defined also [1]. In fact the lower boundary condition implies that the flux near the ground must be equal to the deposition rate, where also Vg is defined. Arya [1] following van Ulden [19] suggest $z = z_0$ as a good actual approximation of z = 0.

It is now possible to apply the GILTT approach. For this purpose, the pollutant concentration is expanded in the series [7, 31]:

$$C(x,z) = \sum_{i=0}^{\infty} \overline{c}_i(x)\zeta_i(z) \tag{17}$$

where $\zeta_i(z)$ comes from the well known solution of the Sturm-Liouville problem given in problem (16) and $\overline{c}_i(x)$ is the solution of the transformed problem. The solution of $\overline{c}_i(x)$ is given below.

Replacing the above equation in Eq. (14) and taking moments, the following is obtained:

$$\sum_{i=0}^{\infty}\left[\overline{c}_i(x)\int_0^h K'_z(z) \ \zeta'_i(z)\zeta_j(z) \ dz - \lambda_i^2\overline{c}_i(x)\int_0^h K_z(z)\zeta_i(z)\zeta_j(z) \ dz - \overline{c}'_i(x) \int_0^h u(z) \ \zeta_i(z)\zeta_j(z)dz \right] = 0 \tag{18}$$

The above equation can be written in matrix fashion as:

$$Y'(x) + F.Y(x) = 0 \tag{19}$$

where Y(x) is the column vector whose components are $\overline{c}_i(x)$, the matrix F is defined as $F = B^{-1}E$ and the entries of the matrices B and E are written by:

$$b_{i,j} = -\int_0^h u(z)\zeta_i(z)\zeta_j(z)dz \tag{20}$$

and

$$e_{i,j} = \int_0^h K_z'(z)\zeta'_i(z)\zeta_j(z)dz - \lambda_i^2 \int_0^h K_z(z)\zeta_i(z)\zeta_j(z)dz \tag{21}$$

Following the procedure of Wortmann *et al.* [31] and Moreira *et al.*[7], one obtains the following solution for problem (19):

$$Y(x) = X.G(x).\xi \tag{22}$$

where X is the eigenfunction matrix of F, G is the diagonal matrix whose entries have the form $e^{-d_i x}$, *di* are the eigenvalues of F and ξ the vector given by $\xi = X^{-1}Y(0)$. Applying the source condition (1c) transformed by the GILTT technique, the unknown vector ξ is determined by solving the resulting linear system. Therefore, the solution for the concentration given by Eq. (18) is now well determined because the vector $\overline{c}_i(x)$ is now known. For more details and recent developments, see the work of Wortmann *et al.* [31], Moreira *et al.* [7], Buske *et al.* [33, 34], Tirabassi *et al.* [35], Moreira *et al.* [36] and Tirabassi *et al.* [37].

ADMM Approach Solutions

To solve the advection-diffusion equation for non-homogeneous turbulence we must take into account the dependence of the eddy diffusivity and wind speed profile on the height variable. Therefore, to solve this kind of problem by the

Laplace Transform technique, we perform a stepwise approximation of these coefficients.

The Stepwise Approximation of the Eddy Diffusivity and Wind Speed

The height h of the PBL is discretized into N sub-intervals in such manner that inside each sub-region, and assume respectively the following average values:

$$K_n = \frac{1}{z_{n+1} - z_n} \int_{z_n}^{z_{n+1}} K_z(z)dz \tag{23}$$

$$u_n = \frac{1}{z_{n+1} - z_n} \int_{z_n}^{z_{n+1}} u(z)dz \tag{24}$$

for $n = 1:N$

On order to handle problems whereas the vertical eddy diffusivity depending on x and z, we proceeded in a similar manner. Initially, we perform the average in the z variable, namely:

$$K_n(x) = \frac{1}{z_{n+1} - z_n} \int_{z_n}^{z_{n+1}} K_z(x,z)dz \tag{25}$$

Discretizing the x-variable into M sub-intervals with length Δx, in each sub-region, we take the following averaged values:

$$K_{i,n} = \frac{1}{x_{i+1} - x_i} \int_{x_i}^{x_{i+1}} K_n(x')dx' \tag{26}$$

for $i = 1:M$.

This kind of procedure is also applied for the wind profile in the z-direction. Now we are in position to solve the advection-diffusion equation by the Laplace Transform technique for each sub-interval.

The Laplace Transform solution

In the sequel, we report the solution of the advection-diffusion equation for the following cases: one-dimensional time-dependent equation, two-dimensional steady-state equation, two-dimensional steady-state equation with longitudinal diffusion, two-dimensional time-dependent equation and two-dimensional time-dependent equation with longitudinal diffusion, vertical velocity and source term.

The One-Dimensional Time-Dependent Advection-Diffusion Equation

Let us consider the following advection-diffusion equation:

$$\frac{\partial \overline{C}}{\partial t} = K_z \frac{\partial^2 \overline{C}}{\partial z^2}$$

(27)

for $0 < z < z_i$ and $t > 0$, subject to the boundary conditions:

$$K_z \frac{\partial \overline{C}}{\partial z} = 0 \quad \text{at z = 0, h}$$

(28)

and the initial condition:

$$\overline{C}(z,0) = Q\delta(z - H_s) \quad \text{at t = 0}$$

(29)

where H_s is the source height and Q is the instantaneous emission

Assuming that the non-homogeneous turbulence is modeled by an eddy diffusivity depending on the z-variable, in order to apply the Laplace Transform technique we have to consider the stepwise approximation discussed in previous section. Therefore, after this procedure the equation (27) has the form for every sub-interval $z_n < z < z_{n+1}$:

$$\frac{\partial \overline{C}_n}{\partial t} = K_n \frac{\partial^2 \overline{C}_n}{\partial z^2}$$

(30)

for $n = 1:N$. Applying the Laplace Transform to the above ansatz we come out:

$$\frac{d^2}{dz^2}\widehat{C_n}(z,s) - \frac{s}{K_n}\widehat{C_n}(z,s) = -\frac{1}{K_n}\overline{C_n}(z,0) \tag{31}$$

Here $\widehat{C}_n(z,s)$ denotes the Laplace Transform of $\overline{C}_n(z,t)$ in the t variable, we mean $\widehat{C}_n(z,s) = L\{\overline{C}_n(z,t); t \to s\}$, which has the well known solution [38]:

$$\widehat{C}_n(z,s) = A_n e^{-R_n z} + B_n e^{R_n z} + \frac{Q}{2R_a}\left(e^{-R_n(z-H_s)} - e^{R_n(z-H_s)}\right) \tag{32}$$

where

$$R_n = \sqrt{\frac{s}{K_n}} \text{ and } R_a = \sqrt{K_n s}$$

Now, given a closer look to the solution in equation (32), we can see that exist 2N integration constants. Therefore, to make possible the determination of these integration constants we need to impose (2N-2) interface conditions, namely the continuity of concentration and flux concentration at interface. These conditions are expressed as:

$$\overline{C}_n = \overline{C}_{n+1} \text{ n = 1, 2,.(N-1)} \tag{33}$$

$$K_n \frac{\partial \overline{C}_n}{\partial z} = K_{n+1} \frac{\partial \overline{C}_{n+1}}{\partial z} \text{ n = 1, 2,.(N-1)} \tag{34}$$

Indeed, applying the boundary and interface conditions to the concentration solution given by equation (32) we obtain the system:

$$\begin{bmatrix} M_{11} & M_{12} & 0 & 0 & 0 & 0 & \cdots & 0 \\ M_{21} & M_{22} & M_{23} & M_{24} & 0 & 0 & \cdots & 0 \\ M_{31} & M_{32} & M_{33} & M_{34} & 0 & 0 & \cdots & 0 \\ 0 & 0 & M_{43} & M_{44} & M_{45} & M_{46} & \cdots & 0 \\ 0 & 0 & M_{53} & M_{54} & M_{55} & M_{56} & \cdots & 0 \\ \vdots & \vdots & \vdots & \vdots & \vdots & \vdots & \vdots & \vdots \\ 0 & 0 & 0 & 0 & M_{n-1,n-3} & M_{n-1,n-2} & M_{n-1,n-1} & M_{n-1,n} \\ 0 & 0 & 0 & 0 & 0 & 0 & M_{n,n-1} & M_{n,n} \end{bmatrix} \begin{bmatrix} A_1 \\ A_2 \\ A_3 \\ A_4 \\ \vdots \\ \vdots \\ A_{n-1} \\ A_n \end{bmatrix} = \begin{bmatrix} 0 \\ 0 \\ \vdots \\ D_{n^*} \\ D'_{n^*} \\ \vdots \\ 0 \\ 0 \end{bmatrix}$$

where $M_{i,j}$ are given by:

$$M_{11} = R_1$$

$$M_{12} = -R_1$$

$$M_{2n,2n-1} = e^{R_n z_n}$$

$$M_{2n,2n} = e^{-R_n z_n}$$

$$M_{2n,2n+1} = -e^{R_n z_n}$$

$$M_{2n,2n+2} = -e^{-R_n z_n}$$

$$M_{2n+1,2n-1} = K_n R_n e^{R_n z_n}$$

$$M_{2n+1,2n} = -K_n R_n e^{-R_n z_n}$$

$$M_{2n+1,2n+1} = -K_{n+1} R_{n+1} e^{R_{n+1} z_n}$$

$$M_{2n+1,2n+2} = K_{n+1} R_{n+1} e^{-R_{n+1} z_n}$$

$$M_{n,n-1} = R_N e^{R_N z_N}$$

$$M_{n,n} = -R_N e^{-R_N z_N}$$

and in the sub-layer of contaminant emission, D_{n_*} and D'_{n_*} are written like:

$$
\begin{cases}
D_{n_*} = \dfrac{Q}{2R_a}\left(e^{-R_n(z-H_s)} - e^{R_n(z-H_s)}\right) \\[3mm]
D'_{n_*} = \dfrac{Q}{2}\left(e^{-R_n(z-H_s)} - e^{R_n(z-H_s)}\right)
\end{cases}
$$

Solving this linear system and inverting the transformed concentration by the Gaussian quadrature scheme we finally get:

$$\overline{C}_n(z,t) = \sum_{i=1}^{k} a_i \frac{p_i}{t} \left[A_n e^{-R_n z} + B_n e^{R_n z} + \frac{Q}{2R_a} \left(e^{-R_n(z-H_s)} - e^{R_n(z-H_s)} \right) H(z-H_s) \right] \tag{35}$$

where $H(z-H_s)$ is the Heaviside function that multiplies the part that is different from zero only in the sublayer that contains the source, k is the number of the quadrature points, R_n and R_a are given by:

$$R_n = \sqrt{\frac{p_i}{tK_n}} \text{ and } R_a = \sqrt{K_n \frac{p_i}{t}}$$

a_i and p_i are the Gaussian quadrature parameters tabulated in the book of Stroud and Secrest [32]. Therefore the solution of problem (27) is expressed by equation (35). To this point it is relevant to underline that this solution is semi-analytical in the sense the only approximations considered along its derivation are the stepwise approximation of the parameters and the numerical Laplace inversion of the transformed concentration.

The two-dimensional steady-state advection-diffusion equation

The two-dimensional steady-state advection-diffusion equation reads like:

$$u \frac{\partial \overline{C}}{\partial x} = K_z \frac{\partial^2 \overline{C}}{\partial z^2} \tag{36}$$

for $0 < z < z_i$ and $x > 0$, subject to the boundary conditions:

$$K_z \frac{\partial \overline{C}}{\partial z} = 0 \text{ at } z = 0, \text{ h} \tag{37}$$

and

$$\overline{C}(0,z) = \frac{Q}{u} \delta(z-H_s) \text{ at } x = 0 \tag{38}$$

where H_s is the height source and Q is the contaminant continuous emission rate.

Proceeding in similar manner of the previous section we perform the stepwise approximation of the parameters, we apply the Laplace Transform in the x-variable, we solve the resulting set of ordinary differential equations and we apply the boundary and interface conditions to determine the integration constants. This procedure leads to the solution:

$$\bar{C}_n(x,z) = \sum_{i=1}^{k} a_i \frac{p_i}{x}\left[A_n e^{-R_n z} + B_n e^{R_n z} + \frac{Q}{2R_a}\left(e^{-R_n(z-H_s)} - e^{R_n(z-H_s)} \right) H\left(z - H_s \right) \right] \quad \textbf{(39)}$$

where

$$R_n = \sqrt{\frac{u_n}{K_n}\frac{p_i}{x}} \text{ and } R_a = \sqrt{u_n K_n \frac{p_i}{x}}$$

and the the Heaviside function multiplies the part that is different from zero only in the sublayer that contains the source

For more details regarding integration constants determination, applications and recent developments, see the works of Vilhena *et al.* [30], Moreira *et al.* [39], Costa *et al.* [40], Moreira *et al.* [41] and Vilhena *et al.* [42].

ACKNOWLEDGEMENTS

CONFLICT OF INTEREST

The author(s) confirm that this chapter content has no conflict of interest.

REFERENCES

[1]   Arya S. Air pollution meteorology and dispersion. New York, Oxford University Press, 1999.
[2]   Pasquill F, and F B Smith. Atmospheric Diffusion. New York, John Wiley & Sons, 1983.
[3]   Deardoff JW, Willis GE. A parameterization of diffusion into the mixed layer. Journal of Applied Meteorology 1975; 14, 1451-1458.

[4]   Seinfeld J H, and SN Pandis. Atmospheric chemistry and physics. New York John Wiley & Sons; 1998.

[5]   Tirabassi T. Analytical air pollution advection and diffusion models. Water Air and Soil Poll; 1989, 47, 19-24.

[6]   Tirabassi T. "Operational advanced air pollution modeling". PAGEOPH 2003; 160, 5-16.

[7]   Moreira D M, M T Vilhena, T Tirabassi, D Buske, and R M Cotta. Near source atmospheric pollutant dispersion using the new GILTT method. Atm Envirom; 2005, 39, 6289-6294.

[8]   Rounds W. Solutions of the two -dimensional diffusion equation.Trans. Am Geophys Union; 1955, 36, 395-405.

[9]   Smith FB. The diffusion of smoke from a continuous elevated poinr source into a turbulent atmosphere. J Fluid Mech; 1957a, 2, 49-76.

[10]   Smith FB. Convection-diffusion processes below a stable layer. London, Meteorological Research Committee 1957b; N. 1048 and 10739.

[11]   Scriven RA and Fisher BA. The long range transport of airborne material and its removal by deposition and washout-II. The effect of turbulent diffusion. Atmos Environ 1975; 9, 59-69.

[12]   Fisher BEA. The long range transport of sulphur dioxide. Atmos Environ 1975; 9, 1063-1070..

[13]   Yeh G. and Huang C.H. (1975), Three-dimensional air pollutant modeling in the lower atmosphere, Bound. Layer Meteor. 1975; 9, 381-390..

[14]   Berlyand MY. Contemporary problems of atmospheric diffusion and pollution of the atmosphere. Raleigh, NC U.S.A Translated version by NERC USEPA 1975..

[15]   Demuth C. A contribution to the analytical steady solution of the diffusion equation for line sources. Atmos Environ 1978; 12, 1255-1258.

[16]   Tagliazucca M, Nanni T and Tirabassi T. An analytical dispersion model for sources in the surface layer, Nuovo Cimento 1985;8C, 771-781.

[17]   Tirabassi T, Tagliazucca M and Zannetti P. KAPPA G, a non Gaussian plume dispersion model: description and evaluation against tracer measurements. JAPCA 1986; 36, 592 59.

[18]   Tirabassi T, Tagliazucca M and Paggi P. A climatological model of dispersion in an inhomogeneous boundary layer. Atmos Environ 1989; 23, 857-862.

[19]   Van Ulden, AP. Simple estimates for vertical diffusion from sources near the ground. Atmos Environ 1978; 12, 2125-2129.

[20]   Tirabassi T and Rizza U. A practical model for the dispersion of skewed puffs. J. Appl Meteor 1995; 34, 989-993.

[21]   Nieuwstadt FTM. An analytical solution of the time-dependent, one-dimensional diffusion equation in the atmospheric boundary layer. Atmos Environ 1980; 14, 1361-1364..

[22]   Nieuwstadt FTM and de Haan BJ. An analytical solution of one-dimensional diffusion equation in a non.stationary boundary layer with an application to inversion rise fumigation. Atmos Environ 1981; 15, 845-851.

[23]   Catalano GD. An analytical solution to the turbulent diffusion equation with mean vertical wind. In Proceedind of 16t Southeastern Sem. Thermal Sci Miami Fl,USA 19-21 April 1982; 143-151.

[24]   Chrysikopoulos C V, L M Hildemann, and P V Roberts. A three-dimensional atmospheric dispersion -deposition model for emissions from a ground-level area source. Atm Environ 1992; 26A, 747-757.

[25] Lin JS and Hildemann LM. A generalised mathematical scheme to analytically solve the atmospheric diffusion equation with dry deposition. Atmos Environ; 1997, 31, 59-71.

[26] Brown MJ, Arya SP and Snyder W. Plume descriptors from a non-Gaussian concentration model. Atmos Environ 1997; 31, 183- 189.

[27] Sharan M, Yadav AK. Simulation of diffusion experiments under light wind, stable conditions by a variable K-theory model. Atmosph Environ 1998; 32, 3481-3492.

[28] Sharan M and Modani M. A two-dimensional analytical model for the dispersion of air-pollutants in the atmosphere with a capping inversion. Atmosph Environ 2006; 40, 3479-3489.

[29] Essa KSM, Etman SM and Embaby M. New analytical solution of the dispersion equation. Atmospheric Research 2007; 84, 337-344.

[30] Vilhena MT, Rizza U, Degrazia GA, Mangia C, Moreira DM and Tirabassi T. An analytical air pollution model: development and evalution. Contr Atmos Phys 1998; 71, 315-320.

[31] Wortmann S, MT Vilhena, DM Moreira, and D Buske. A new analytical approach to simulate the pollutant dispersion in the PBL. Atm Environ 2005; 39, 2171-2178.

[32] Özisik M N. Heat Conduction. New York John Wiley & Sons 1980.

[33] Buske D, Vilhena MT, Moreira DM and Tirabassi T. An analytical solution of the advection-diffusion equation considering non-local turbulence closure. Environ Fluid Mech; 2007, 7, 43-54..

[34] Buske D, Vilhena MT, Moreira DM and Tirabassi T. An analytical solution of the advection-diffusion equation considering non-local turbulence closure. Environ Fluid Mech; 2007, 7, 43-54..

[35] Buske Daniela, Marco T Vilhena, Davidson M Moreira and Tiziano Tirabassi. Simulation of pollutant dispersion for low wind conditions in stable and convective Planetary Boundary Layer. Atmos Environ; 2007b, 41, 5496-5501.

[36] Moreira DM, Vilhena MT, Buske D, Tirabassi T. The state-of-art of the GLTT method to simulate pollutant dispersion in the atmosphere. Atmospheric Research 2009; 92, 1-17.

[37] Tirabassi T, Buske D, Moreira DM and Vilhena MT. A two-dimensional solution of the advection-diffusion equation with dry deposition to the ground. JAMC 2008; 47, 2096-2104.

[38] Boyce W and Di Prima. R. Elementary differential equations and boundary value problems. New York, John Wiley & Sons Inc 2001.

[39] Moreira DM, Tirabassi T, Vilhena MT and Carvalho J.C. A semi-analytical model for the Tritium dispersion simulation in the PBL from the ANGRA I nuclear power plant. Ecological Modeling 2005b; 189, 413-424.

[40] Costa CP, Vilhena MT, Moreira D M and Tirabassi T. Semi-analytical solution of the steady three-dimensional advection-diffusion equation in the planetari boundary layer. Atmos Environ; 2006, 40, 5659-5669.

[41] Moreira DM, MT Vilhena T Tirabassi C Costa and B Bodmann. Simulation of pollutant dispersion in atmosphere by the Laplace transform: the ADMM approach. Water Air and Soil Pollution 2006; 177, 411-439.

[42] Vilhena MT, Costa CP, Moreira DM.and Tirabassi T. A semi-analytical solution for the three-dimensional advection-diffusion equation considering non-local turbulence closure. Atmospheric Research 2008; 90, pp 63-69.

CHAPTER 7

Estimation of the Lower Atmospheric Turbulence Parameters by Sodar-Rass Unit and Sonic Anemometer

Renato Ricci[1], Roberta Cocci Grifoni[2,*] and Marco Mazzieri[1]

[1]Department of Energetics, Polytechnic University of Marche, Italy and [2]School of Architecture and Design "E. Vittoria", Camerino University, Ascoli Piceno, Italy

Abstract: Purpose of this chapter was to analyze the planetary boundary layer (PBL) using remote sensing tools. Sodar techniques allowed us to obtain speed and wind direction profiles from a height ranging from 30/40 m. to 1000 m. The SODAR (Sound Detection And Ranging) is, in fact, an alternative to the use of cup anemometers and offers the possibility of measuring both the wind speed distribution with height and the wind direction. In particular, these instruments play a key role both to assess the wind resource in a specific area and to estimate the alteration of the wind field caused by the complex orography of the region.

Keywords: Aerogenerator, Atmospheric Temperature Structure Parameter, complex orography, Cup Anemometer, environmental wind gallery, orographic acceleration, orographic acceleration, planetary boundary layer, RASS, remote sensing, Snodar, Sodar, Sodar calibration, speed patterns, Thermal Bubble, Ultrasonic Anemometer, Wind gallery, wind park, wind speed, wind turbines.

INTRODUCTION

It is crucial to carry out an accurate estimate of the wind speed and direction level with the axis of rotation [1]. Since the height of wind turbines are usually 80/100 m. high, and they reach 105/150 m. with the blades, measures in highly not homogeneous regions with a complex orography are fundamental: thus Sodar measures could positively substitute the anemometer towers.

As a matter of fact, using classic anemometric techniques to obtain precise information about wind speed and direction, as well as standard functions - such

───────────────────

*Address correspondence to Roberta Cocci Grifoni: School of Architecture and Design "E. Vittoria", Camerino University, Ascoli Piceno, Italy; Tel+39 (0)737 404279; Fax: roberta.coccigrifoni@unicam.it

as power law and logarithmic law for the reconstruction of the speed profile incident on the aerogenerator, could lead to wrong evaluations of the wind potential of the region studied [2].

The advantages of these new survey techniques are countless: besides the one above mentioned, it is important to highlight that these techniques have allowed us to carry out quick measurements on the very sites of the turbines, while this would have been impossible with the anemometric towers.

The first part of this work has been necessary to calibrate the Sodar system [3].

The test area included the municipalities of Serravalle di Chienti, Montecavallo and Pieve Torina, in the Marche region (middle Italy),where there is a project of a wind park of regional interest. The project has already singled out 17 sites for the installation of as many 2 MW aerogenerators.

Sodar Calibration

For the calibration we compared directly the measures of the wind field obtained with the Sodar system with the measures gathered by the anemometric tower installed near Mount Tolagna.

The correlation between the data obtained and the data gathered by the control unit set up on the tower, was rather good, yet it can be improved by increasing the statistic basis of the data available.

Actually, all studies concerning the calibration of the Sodar systems have a far greater number of data for the comparison [4]. The results deriving from the correlation between Sodar – Ultrasonic Anemometer and Sodar – Cup Anemometer, are shown in the Table **1** where N is the number of specimen and R^2 is the correlation coefficient.

Table 1: Correlation amongst Sodar, Ultrasonic Anemometer and Sodar and Cup Anemometer

	WIND SPEED Sodar Cup Anemometer	WIND SPEED Sodar Sonic Anemometer	DIRECTION Sodar Sonic Anemometer
N	181	155	253
R^2	0.83	0.87	0.97

Sodar Measurement Setup

After calibrating the instrument, the profiles of wind speed and direction have been surveyed on the very sites where the turbines are to be setup.

High quality sodar measurements require a careful selection of the sodar antenna location (away from possible sources of fixed echo), fully functioning antennas and a proper system setup for maximizing the S/N ratio. The main recommendations can be summarised as:

i). Recommended distance from obstacle (mast) should be larger than the height of the obstacle to eliminate fixed echo problems.

ii). Increased height resolution (>10 m) will increase the signal availability at all heights.

iii). Include a proper signal screening and a data averaging procedure.

The anemometric study provided information on these parameters in 10 different positions, where as many aerogenerators will be created.

The data gathered where relevant to determine how the orography of the region has an ever changing influence on the main characteristics of the wind at the altitudes interested in the installation of the aerogenerators.

The knowledge of the speed profile will allow a more focused choice of the kind of generator to be set up in a specific place and therefore a better exploitation of the wind resource.

Fig. (**1**) shows some typical speed patterns (2D) observed in one of the positions surveyed. At low altitude slight orographic effects can be detected.

Fig. (**2**) shows the same position but, as this time the wind comes from a different direction, the position is more influenced by the orography. The high orographic acceleration, compared to the logarithmic pattern, can be clearly seen at low altitudes, both from the profiles of the horizontal wind speed and from the profiles of the vertical speed *w*.
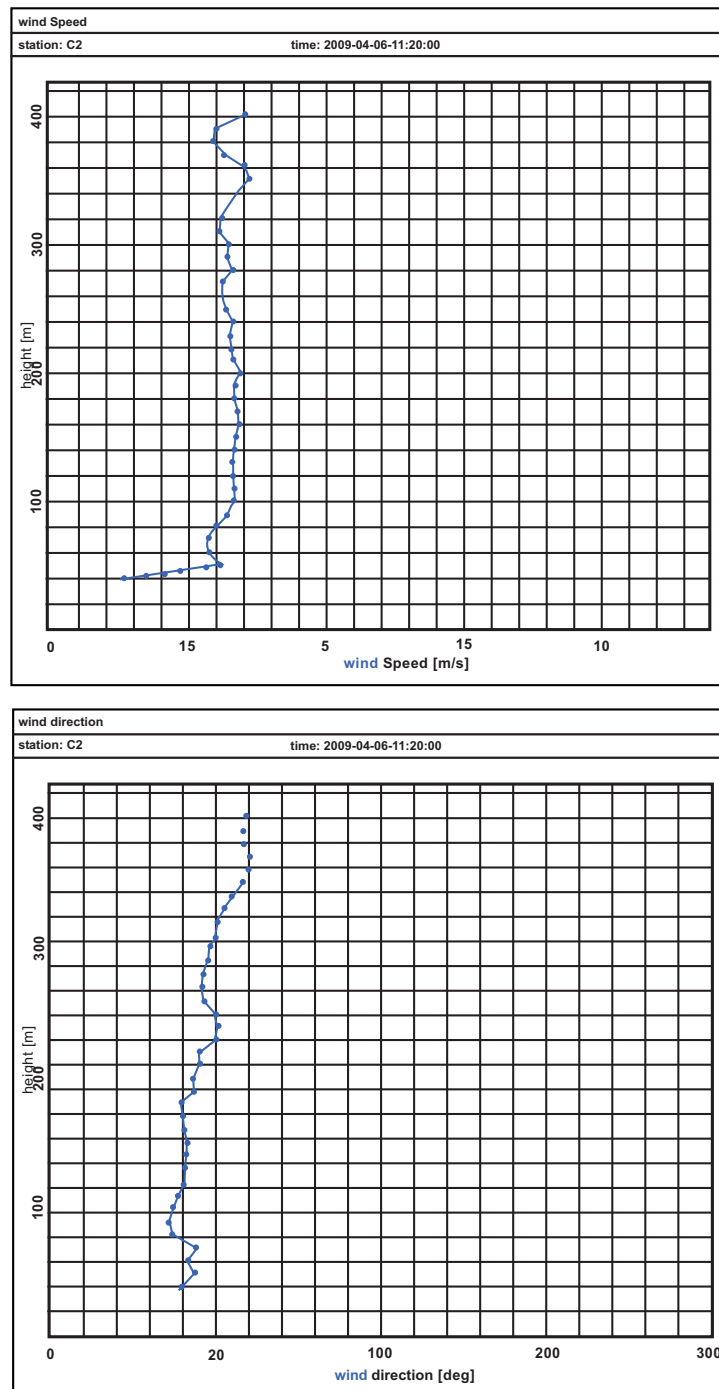
Figure 1: Aerogenerator C2 position: profiles measured April 6 2009. Typical speed and dir. patterns (2D) and with slight orographic effects at low altitudes for the direction.
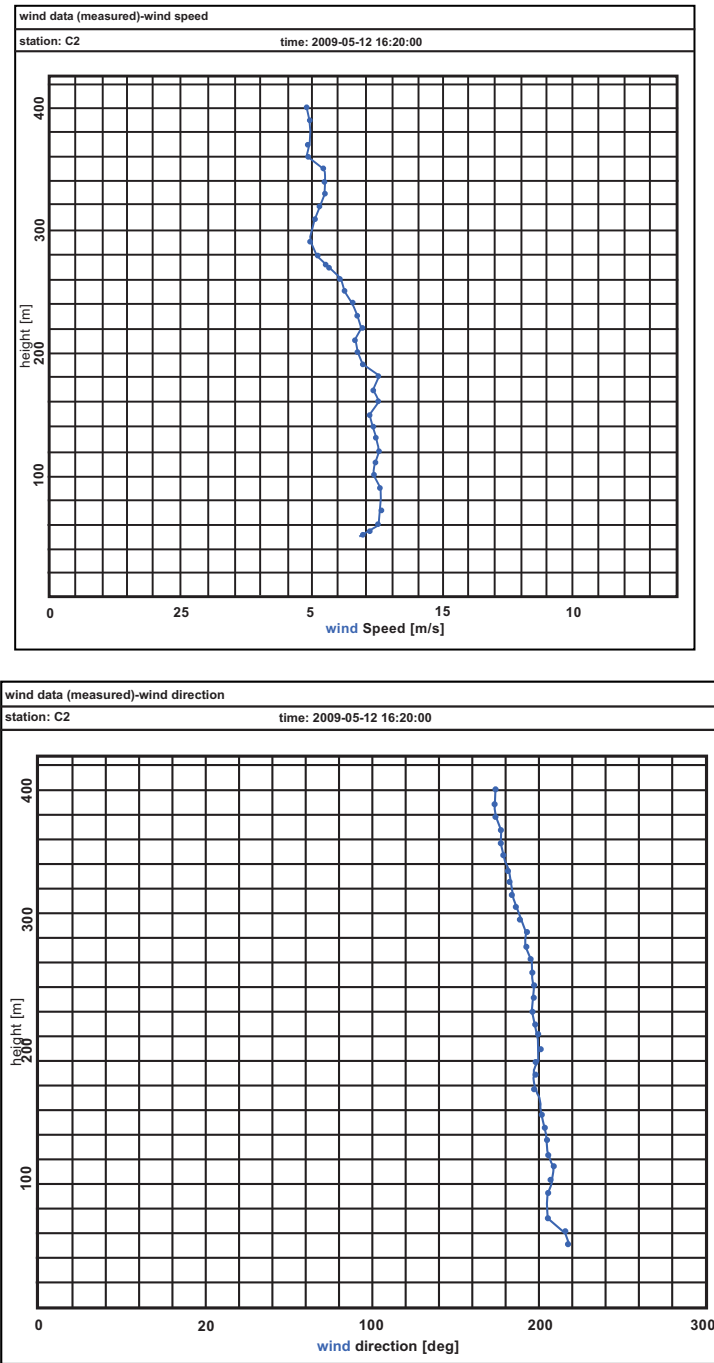
Figure 2: C2 aerogenerator position: profiles measured on May 12, 2009. Speed and direction courses (2D) typical of a strong orographic acceleration.

Fig. (**3**) shows qualitatively the original direction of the wind in position C2 in the days of measurement. It is clear that the wind blowing west/ south-west has to ascend a slope lined with trees, and this is the cause for the high orographic accelerations recorded by Sodar, during the May 2009, 12 measurements.
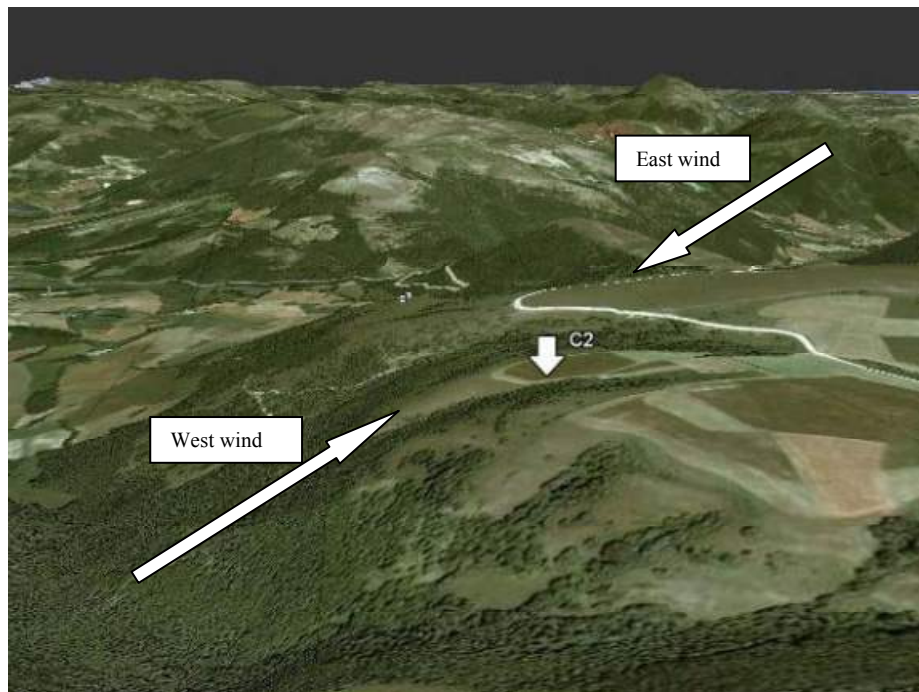
Figure 3: Wind directions on position C2, on 2 days of measurement. It clearly shows the tree-lined side that the wind blowing west/south-west must ascend on May 12.

On other occasions, to interpret speed profiles (2D) other than the regular trends, the measure of the vertical component of the wind speed vector (*w*) provided by the Sodar has been extremely useful. It is necessary to stress that it is not possible to gather information on this parameter using standard anemometric techniques. The vertical profile of the *w*, relating to that of the speed (2D), can clearly show the presence of possible convective movements.

We have also identified conditions characterized by a powerful thermal activity. Fig. (**4**) shows the comparison between *w* profiles gathered at different times during the same day. The two trends respectively highlight the progress of the convective movements and their end.
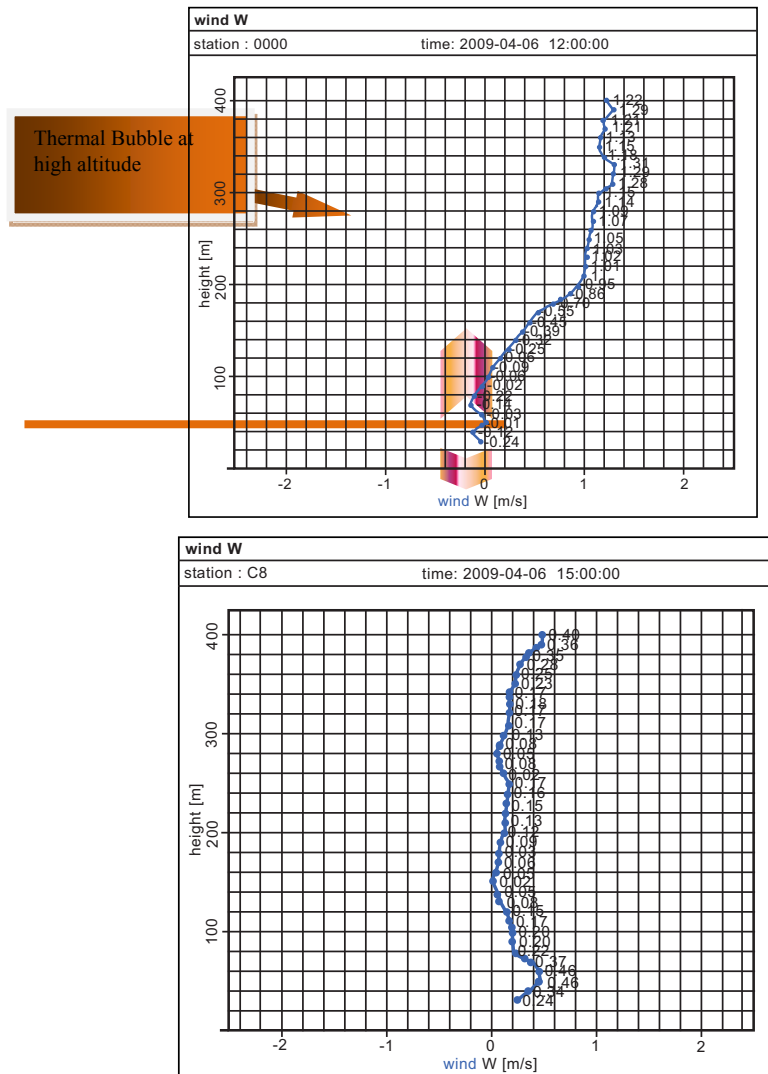
Figure 4: Profies measured: w course typical of a strong thermal activity (right) and its conclusion (left).

In the final analysis, we have compared data gathered from the tests with data gathered in the environmental wind gallery of the Marche Department of Energetic, Polytechnic University. In the test chamber we have used a scale orographic model of the area considered for the setting up of the wind site in order to obtain results that can integrate and finish those gathered through the Sodar analysis. After a thorough analysis of the different terms of comparison available, and the contrasting conditions between the test chamber and the field measures,

we chose to compare these data with logarithmic speed-up, calculated for both measurement techniques. The comparisons were performed exclusively in West-South/West configuration, and only for the turbines whose positions showed a similar wind direction in both measurement techniques.

The data obtained prove a good harmonization in most of the turbines compared. Let's not forget that the atmosphere simulated in the wind gallery presents a neutral stability (the thermal flow on the ground is ignored), whilst the real atmosphere does not.

At the end of the analysis, the conclusions were that each one of the turbines can generally present two different situations, in relation to orographic conditions met by the wind. The absence of a hill or a promontory windward determines an orographic acceleration effect due only to the mountain versant where the wind turbine is positioned. The presence of a hill windward side the one under scrutiny (in terms of wind direction), implies a double acceleration orographic effect.

Figs. (**5**) and (**6**) show the speed-up profiles in two explanatory examples of the situations just illustrated. The charts highlight the rotoric band, *i.e.* the altitude range – between 25 m and 105 m., concerning the type of aerogenerators to be set up in the wind park.
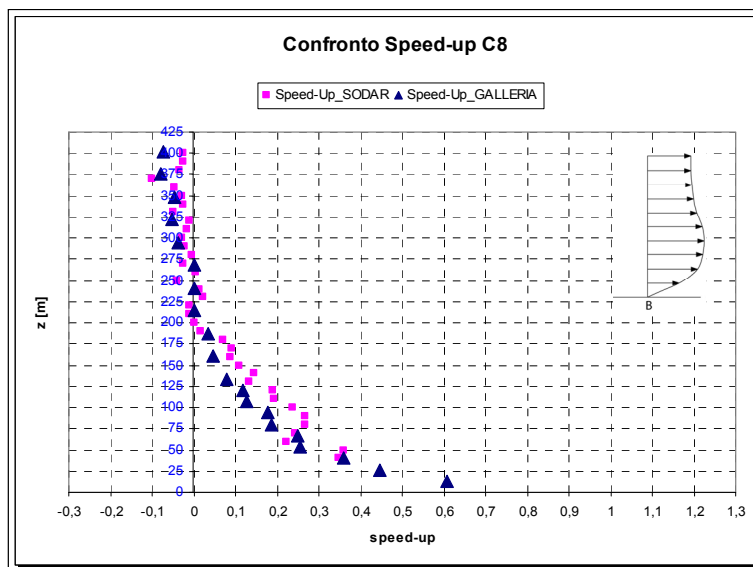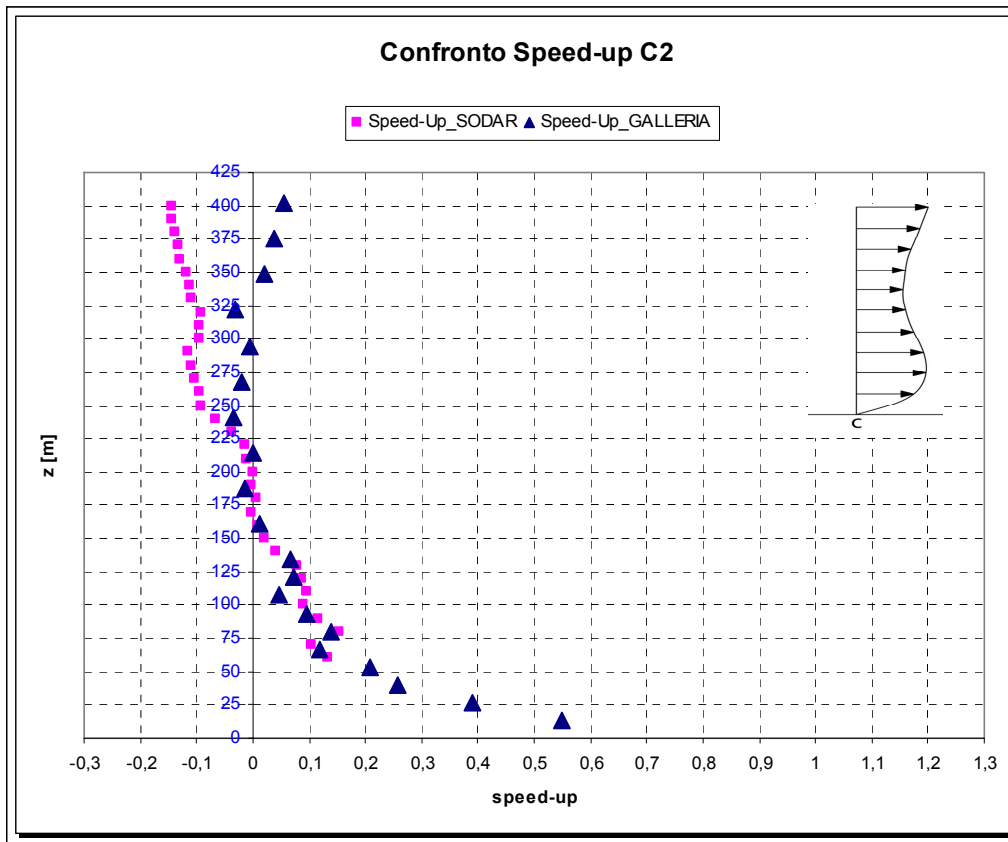

Figure 5: Speed-up course obtained: trend due to a simple orographic effect

Figure 6: Speed-up courses obtained: trend due to a double orographic effect.

The charts in Figs. (**6**) and (**7**) also show qualitatively the speed profile (2D) types to which the speed-ups refer to.

The comparisons show good qualitative concordance between the *in situ* and the laboratory measurements. These are the first step of a survey in progress at the Termofluido group of the Università Politecnica delle Marche comparing directly real situations with situations reproduced in the wind gallery. The theory work already developed and the future ones will contribute to the improvement of the assessment systems for real wind fields - with Sodar, and recreated − with the wind gallery.

The final part of this work was carried out at the University of New South Wales in Sydney, where the use of remote sensing techniques examination of the

planetary boundary layer has been studied in order to assess how atmospheric turbulences can cause changes in the astronomical images. This analysis will be essential for the siting of an astronomic site.

The search for good sites has become very important after the telescopes technology advancements; in fact not only is it necessary to choose a good site, but also to study its orientation in relation to the atmospheric currents in order to obtain the highest stability.

Thus a new tool has been tuned, the Snodar, to measure the Atmospheric Temperature Structure Parameter C_T^2, from a 5 m. of height to a minimum 100 m. with a resolution of 1 m [5].

Fig. (**7**) shows one of the first return echoes of the acoustic signal recorded by the Snodar according to the altitude.
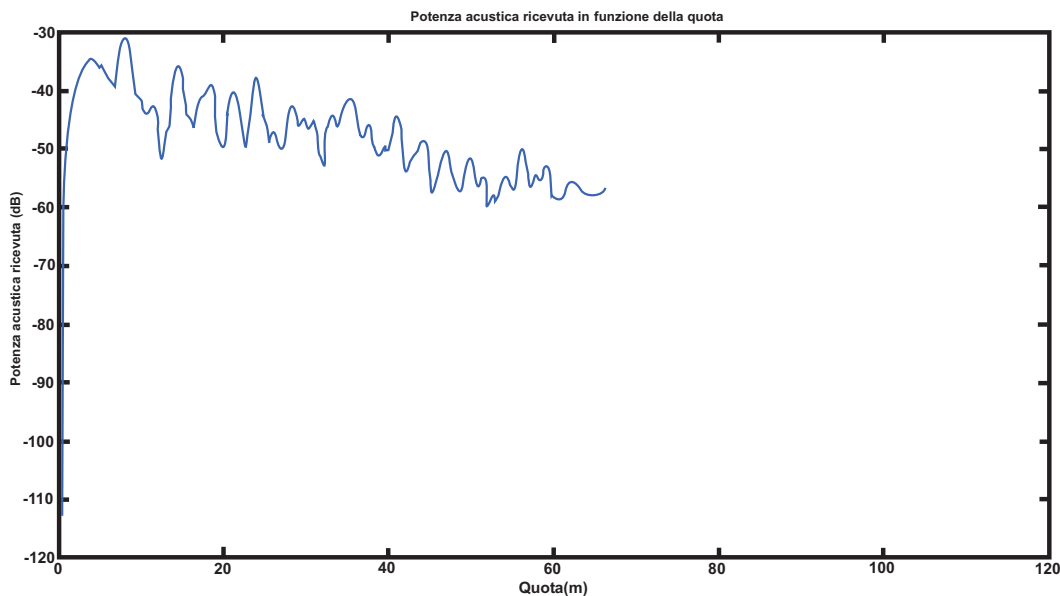
Figure 7: Backscatter signal recorded by Snodar and filtered of the background noise

The assessment of this parameter will allow us to estimate the height of the atmospheric limit layer and hence to obtain a guideline of the height in case of a telescope set up so that it won't be affected by problems in relation to the seeing.

ACKNOWLEDGEMENTS

The authors kindly thank their respective universities for their support.

CONFLICT OF INTEREST

The author(s) confirm that this chapter content has no conflict of interest.

REFERENCES

[1]   Vogt S, Thomas P. Sodar – a useful remote sounder, to measure wind and turbulence. J Wind Eng Ind Aerod 1995; 54(55): 163-172.

[2]   Sozzi R, Georgiadis T, Valentini M. Introduzione alla Turbolenza Atmosferica- concetti stime misure –Pitagora Editrice Bologna 2002.

[3]   Crescenti GH. The Degradation of Doppler Sodar Due to Noise: A Review. Atmos. Environ 1998; 32 (9).

[4]   Bradley S, Antoniou I, von Hünerbein S, Kindler D, de Noord M, and Jørgensen HSODAR. Calibration for wind energy applications.Final reporting on WP3, EU WISE project NNE5-2001-297. The University of Salford, Greater Manchester UK 2005.

[5]   Bonner C S, Ashley MCB, Cui X, Feng L, *et al.* Thickness of the Atmospheric Boundary Layer Above Dome A, Antarctica during 2009 Astronomical Society of the Pacific 2010; 122, 1122–1131.

List of Air Quality Models

ADAM (US Environmental Protection Agency, Office of Air Quality Planning and Standards [OAQPS]) -The Air Force Dispersion Assessment Model is a modified box and Gaussian dispersion model that incorporates thermodynamics, chemistry, heat transfer, aerosol loading, and dense gas effects. Release scenarios include continuous and instantaneous, area and point, pressurized and unpressurized, and liquid/vapour/two-phased options.
download

ADMS-Roads - A model for simulating dispersion of vehicular pollutant emissions from small road networks in combination with emissions from industrial plants, it handles multiple road sources as well as multiple point, line, or area emission sources and the model operation is similar to the other ADMS models.

ADMS-Screen - A screening model for rapid assessment of the air quality impact of a single industrial stack to determine if more detailed modeling is needed, it combines the dispersion modeling algorithms of ADMS models with a user interface that requires minimal input data.

ADMS-URBAN - A model for simulating dispersion on scales ranging from the street to the city or county, it handles the most relevant emission sources such as traffic, industrial, commercial, and domestic sources. It is also used for air quality management and assessments of current and future air quality *vis-à-vis* national and regional standards in Europe and elsewhere.

AERMAPUS (US Environmental Protection Agency, Office of Air Quality Planning and Standards [OAQPS]) -A terrain pre-processor for AERMOD, AERMAP processes commercially available digital elevation data and creates a file suitable for use within an AERMOD control file. This file contains elevation and hill-height scaling factors for each receptor in the air dispersion study.
download

AERMOD Modeling System (US Environmental Protection Agency, Office of Air Quality Planning and Standards [OAQPS]) - A steady-state plume model that incorporates air dispersion based on the planetary boundary layer turbulence structure and scaling concepts, it includes the treatment of both surface and elevated sources, as well as both simple and complex terrain.
download

AEROPOL (Estonia) - The AERO-Pollution model developed at the Tartu Observatory in Estonia is a Gaussian plume model for simulating the dispersion of continuous, buoyant plumes from stationary point, line and area sources over flat terrain on local to regional scales. It includes plume depletion by wet and/or dry deposition as well as the effects of buildings in the plume path.

AEROPOL is a steady-state Gaussian dispersion model, which includes plume rise (based on Briggs formulae), wet deposition (scavenging integrated along the path of precipitations in the atmosphere) and dry deposition (deposition velocity concept for gases). Multiple reflections of the gas plume off of the underlying surface and capping inversion are considered (partial adsorption at each reflection), as well as complete deposition at the underlying surface for coarse particles. Building effects on stack gas dispersion are included. Dispersion parameters (Briggs rural or urban), wind profiles and mixing heights are treated as functions of Pasquill stability. Routine ground-based meteorological information is sufficient to run AEROPOL. Concentration near the underlying surface, dry, and wet deposition flux (separately and summarised) are calculated. Annual, seasonal, or time-series averaging may be performed, computing the output values for each meteorological situation separately. Each situation in the sequence is assumed static. Area sources (*e.g.* built-up areas) are interpreted as arrays of point sources defined with the precision of a Cartesian grid cell. There are two options for - line sources: an array of point sources (highly accurate, resource-consuming) and an array of line segments (less resource-consuming).

AFTOX is a Gaussian dispersion model that handles continuous or instantaneous liquid- or gas-elevated or surface releases from point or area sources. The output consists of concentration contour plots, concentration at a specified location, and maximum concentration at a given elevation and time.
download

AP-42: Compilation of Air Pollutant Emission Factors (Mobile Sources)(US Environmental Protection Agency, Office of Mobile Sources) -The "Compilation of Air Pollutant Emission Factors, Volume II: Mobile Sources" (commonly referred to as "AP-42") contains two sections: highway vehicles and non-road mobile sources. Section I provides extensive information about the highway vehicle emission factor model, currently MOBILE5, and includes numerous tables of values used in the model and -look-up tables- of emission factors produced by the model. Section II provides emission factor information in the form of look-up tables for a wide range of non-road mobile sources (including agricultural equipment, construction equipment, lawn and garden equipment, aircraft and aircraft engines, locomotives, marine vessels, and miscellaneous types of equipment).
download

ASMUS is a diffusion and stream-flow model of urban structures. The principle of this micro scale model follows the concept shown by Röckle (1990). Beginning with an estimated starting wind field, the three-dimensional stream flow field is determined *via* a variation method. Freedom of divergence for the calculated velocity field is a necessary requirement. The quality and realism of the results of this diagnostic wind field model depend crucially on the starting conditions so the starting wind field must be given as accurately as possible. The diagnostic stream flow model does not show any direct indicator for turbulence (necessary for dispersion); it first solves a balance equation for turbulence energy that makes it possible to consider transport and diffusion as well as production and dissipation**.**

ASPEN (US Environmental Protection Agency, Office of Air Quality Planning and Standards [OAQPS]) - The Assessment System for Population Exposure Nationwide consists of both a dispersion module and a mapping module. The dispersion module is a Gaussian formulation based on ISCST3 for estimating ambient annual average concentrations at a set of fixed receptors within the vicinity of an emission source. The mapping module produces a concentration at each census tract. The input data required are emissions data, meteorological data, and census tract data.
download

AUSPLUME is the dispersion model designated as the primary model accepted by the Environmental Protection Authority (EPA) in Victoria, Australia.

AUSPUFF - A Gaussian puff model designed for regulatory use by CSIRO, AUSPUFF is a non-steady-state Gaussian puff model that was designed to become a regulatory model. Unlike AUSPLUME, it can be used in conditions with complex meteorology; it requires a 3-D met data set (diagnostically [AUSMET], or prognostically from the CSUMM model supplied with AUSPUFF). AUSPUFF can represent recirculation of pollutants by continuously releasing and following puffs and can explicitly handle simple chemical transformations.

AUSTAL2000 is an atmospheric dispersion model for simulating the dispersion of air pollutants in the ambient atmosphere. It is the official air dispersion model used in the assessment of permits for industrial sources by the German Federal Environmental Agency. The model accommodates point, line, area, and volume sources of buoyant plumes. It has capabilities for building effects, complex terrain, plume depletion by wet or dry deposition, and first order chemical reactions. It is based on the LASAT model developed by Ingenieurbüro Janicke Gesellschaftfür Umweltphysik. It simulates the dispersion of air pollutants by utilizing a random-walk process (Lagrangian simulation model)
download

BLP (US Environmental Protection Agency, Office of Air Quality Planning and Standards [OAQPS]) is a Gaussian plume dispersion model designed to handle unique modeling problems associated with aluminum reduction plants and other industrial sources where plume rise and downwash effects from stationary line sources are important.
download

BlueSky (US Department of Agriculture, Forest Service) - A modeling framework designed to predict cumulative impacts of smoke from forest, agricultural, and range fires, the BlueSky smoke-modeling framework combines emissions, meteorology, and dispersion models to generate predictions of smoke impacts across the landscape.
download

BUO-FMI (Finland) - This model was specially developed by the Finnish Meteorological Institute (FMI) to estimate the atmospheric dispersion of neutral or buoyant plume gases and particles emitted from fires in warehouses and chemical stores. It is a hybrid of a local-scale Gaussian plume model and a gradient transfer (K-theory) approach. Plume depletion by dry deposition is included, but wet deposition is not.

CAL3QHC/CAL3QHCR (US Environmental Protection Agency, Office of Air Quality Planning and Standards [OAQPS]) - CAL3QHC is a CALINE3-based CO model with queuing and hot spot calculations, and a traffic model to calculate delays and queues that occur at signalized intersections. CAL3QHCR is a more refined version based on CAL3QHC that requires local meteorological data.
download

CALINE3 (US Environmental Protection Agency, Office of Air Quality Planning and Standards [OAQPS]) is a steady-state Gaussian dispersion model designed to determine air pollution concentrations at receptor locations downwind of highways located in relatively uncomplicated terrain. CALINE3 is incorporated into the more refined CAL3QHC and CAL3QHCR models.
download

CALINE4: California LINE Source Dispersion Model (California Department of Transportation) - A modeling program used to assess air quality impacts near transportation facilities, it is based on the Gaussian diffusion equation and employs a mixing zone concept to characterize pollutant dispersion over the roadway.
download

CALPUFF Modeling System (Earth Tech Inc.) - CALPUFF is a non-steady-state meteorological and air quality modeling system for assessing the long-range transport of pollutants and their impacts on a case-by-case basis for certain near-field applications involving complex meteorological conditions. The modeling system consists of three main components and a set of pre-processing and post-processing programs. The main components of the modeling system are CALMET (a diagnostic 3-dimensional meteorological model), CALPUFF (an air quality dispersion model), and CALPOST (a post-processing package).
download

CAMEO (US Environmental Protection Agency and National Oceanic and Atmospheric Administration) - CAMEO (Computer-Aided Management of Emergency Operations) is a software suite of applications that includes CAMEO, ALOHA, and MARPLOT. It supports chemical emergency management for government and industry with chemical safety and emergency response data, digitized mapping, and air dispersion modeling.

download

CAMx - The Comprehensive Air quality Model with extensions simulates air quality over many geographic scales. It handles a variety of inert and chemically active pollutants, including ozone, particulate matter, organic and inorganic PM2.5/PM10, and mercury, as well as other toxics.

CAR: Calculation of Air pollution caused by Road traffic - This simple model was originally developed by TNO for the Netherlands only (vehicles, meteorology), but is now also available in an English version, "CAR International". CAR is used intensively in the Netherlands. The model is based on investigations in wind tunnels, theoretical considerations and dispersion measurements Only common meteorological input data is required. CAR calculates annual percentiles and averages for inert gases and NO_2. After input of the latest country-specific emission factors for CO, NOx, benzene, lead, black smoke, and existing background concentrations, CAR calculates the concentrations of pollutants according to velocity, daily traffic density (DTV), portion of heavy traffic (%), distance to the roadway (m), drive mode, type of roadway (5 different types), and tree factor (3 types).The model is an empirical screening model that makes a first appraisal of pollutant concentrations with little effort necessary.

CAR-FMI (Finland) - This model was developed by the Finnish Meteorological Institute (FMI to evaluate the atmospheric dispersion and chemical transformation of vehicular emissions of inert (CO, NO_x) and reactive (NO, NO_2, O_3) gases from a road network of line sources on a local scale. It is a Gaussian line-source model that includes an analytical solution for the chemical cycle NO-O_3-NO_2.

CAR-International (The Netherlands) - See **CAR**. The Calculation of Air pollution from Road traffic is an atmospheric dispersion model developed by

the Netherlands Organisation for Applied Scientific Research. It is used to simulate the dispersion of vehicular emissions from roadway traffic.

COMPLEX1 (US Environmental Protection Agency, Office of Air Quality Planning and Standards [OAQPS]) is a multiple-point-source screening technique with terrain adjustment that incorporates the plume impaction algorithm from the VALLEY model.
download

CONSUME (US Department of Agriculture, Forest Service) -With fuel characteristics, lighting patterns, fuel conditions, and meteorological attributes, CONSUME computes fuel consumption and emissions by combustion. CONSUME is designed to import data directly from the Fuel Characteristic Classification System (FCCS), and the output is formatted to feed other models and provide usable outputs for burn plan preparation and smoke management requirements.
download

CPB: Canyon Plume Box - This GEOMET urban canyon model makes it is possible to calculate pollutant concentrations caused by vehicles in an urban canyon. The model has three different levels. For stream flow not parallel to roadways, the model calculates an average stream flow field according to Hotchkiss and Harlow. For stream flow parallel to the roadway a Gaussian plume model is implemented, which considers reflexions off of canyon walls. Mechanically induced turbulence is then determined, and finally pollutant concentrations at receptor points are calculated with a combination of Gaussian plumes/box models. The model is valid for a height/width ratio of an urban canyon between 0.5 and 2.0.The model calculates averages and the 98%-value of chemically inert substances. NO_2 is calculated with a simple transformation of NO to NO_2 in the presence of ozone with a known concentration.

CTDMPLUS (US Environmental Protection Agency, Office of Air Quality Planning and Standards [OAQPS]) -The Complex Terrain Dispersion Model Plus Algorithms for Unstable Situations is a refined point-source Gaussian air quality model for use in all stability conditions over complex terrain.
download

CTSCREEN (US Environmental Protection Agency, Office of Air Quality Planning and Standards [OAQPS]) is a Gaussian plume dispersion model designed as a screening technique for regulatory application to plume impaction assessments in complex terrain. CTSCREEN is a screening version of the CTDMPLUS model.

download

DEGADIS (US Environmental Protection Agency, Office of Air Quality Planning and Standards [OAQPS]) –This model simulates atmospheric dispersion at ground level of nearby dense gas (or aerosol) clouds released with zero momentum into the atmospheric boundary layer over flat, level terrain. The model describes the dispersion processes that accompany the ensuing gravity-driven flow and entrainment of the gas into the boundary layer.

download

DIPCOT (Greece) - Dispersion over Complex Terrain is a model developed by the National Centre of Scientific Research "DEMOKRITOS" in Greece that simulates the dispersion of buoyant plumes from multiple point sources over complex terrain on a local-to-regional scale. It does not include wet deposition or chemical reactions.

DISPERSION21 (Sweden) - This model was developed by the Swedish Meteorological and Hydrological Institute (SMHI) to evaluate air pollutant emissions from existing or planned industrial or urban sources on a local scale. It is a Gaussian plume model for point, area, line, and vehicular traffic sources. It includes plume penetration of inversions aloft, building effects, NOx chemistry, and can handle street canyons. It does not include wet or dry deposition, complex atmospheric chemistry, or the effects of complex terrain.

DISPLAY-2 (Greece) - A vapour cloud dispersion model for neutral or denser-than-air pollution plumes over irregular, obstructed terrain on a local scale. It accommodates jet releases as well as two-phase (*i.e.*, liquid-vapour mixtures) releases. This model was developed at the National Centre of Scientific Research "DEMOKRITOS" in Greece.

DISPMOD - A Gaussian atmospheric dispersion model for point sources located in coastal regions, this model was specially designed by the Western Australian Department of Environment to simulate plume fumigation that occurs when an elevated onshore pollution plume intersects a growing thermal internal boundary layer contained within offshore air flow coming onshore.

DIWIMO: Diagnostic Wind Field Model - This wind field model calculates a low-divergence wind field using an initial three-dimensional wind field gradient field overlies the initial wind field (to balance the pressure) and the divergence of the resulting wind field is minimized. This leads to the solution of a Poisson-Equation with mixed marginal conditions. DIWIMO – uses a terrain-matched coordinate system, and the greater mathematical and programming effort results in more precise calculations. Atmospheric stability can be considered approximately with a density-weighting factor, which determines the ratio of vertical to horizontal divergence. The wind field calculated has the characteristics of a potential stream. Advection and diffusion effects (*e.g.*, dynamic stream transfer) and thermal induced flows (*e.g.* convection, drainage flows, down-slope winds) are not taken into account.

EK100W (Poland) is a Gaussian plume model used for air quality impact assessments of pollutants from industrial point sources as well as for urban air quality studies on a local scale. It includes wet and dry deposition. The effects of complex terrain are not included.

EMS-HAP (US Environmental Protection Agency, Office of Air Quality Planning and Standards [OAQPS]) - The Emissions Modeling System for Hazardous Pollutants is a processor that and lesemission inventory for input into the ASPEN model or the ISCST3 model. EMS-HAP is written in the SAS programming language and is designed to run on any UNIX workstation.
download

Emsoft Exposure Model for Soil-Organic Fate and Transport (US Environmental Protection Agency, National Center for Environmental Assessment [NCEA]) is a screening model that may be used: to determine concentrations of contaminants remaining in the soil over a given time (when the

initial soil concentration is known); to quantify the mass flux (rate of transfer) of contaminants into the atmosphere over time; and to subsequently calculate contaminant air concentrations by inputting mass flux values into atmospheric dispersion models.
download

ENVI-met– A three-dimensional micro-scale urban climate model, ENVI-met is capable of simulating interactions between micro-scale shaping of the environment (shape of buildings, *etc.*) and the microclimate in cities or rural areas. The typical scale of horizontal resolution is between 0.5 and 10m and the investigation period lasts 24 to 48 hours. The model predicts stream flow fields, temperature and humidity distribution, as well as turbulence in a three-dimensional model with a temporal resolution of 10.
download

FARM (Italy) - The Flexible Air quality Regional Model is an atmospheric dispersion model designed for the analysis of episodes and scenarios, to evaluate the effects of regional emission control policies and pollution forecasts in complex situations. It accommodates point and area sources, and includes photochemistry and plume depletion by wet and dry deposition.

FITNAH: Flow over complex Terrain with Natural and Anthropogenic Heat Sources - A three-dimensional numerical model for meteorological purposes, this model was developed at the Meteorological Institute of the University of Darmstadt and was the first meso-scale model in Germany. It is a non-hydrostatic model.

FLEXPART (Austria/Germany/Norway) is an efficient and flexible Lagrangian particle transport and diffusion model for regional and global applications, with forward and backward mode capabilities. Developed at BOKU Vienna, TU München, and NILU.

GASTAR - A model for simulating accidental releases of denser-than-air flammable and toxic gases, this model handles instantaneous and continuous releases, releases from jet sources, releases from the evaporation of volatile liquid

pools, variable terrain slopes and ground roughness, obstacles such as fences and buildings, and time-varying releases.

GOSOL Developed by Goretzki (1990 this model evaluates the solar energetic properties of a planning concept and also makes – spatial representation possible. It runs on a PC and is equipped with a CAD instrument. The model handles up to 700 trees (monthly change of foliage) and 700 predefined buildings with a maximum of 5400 walls and 3200 windows. For every building the model divides incoming solar radiation in hourly intervals for every month and calculates reflexion, diffuse, and direct solar radiation. The model considers slope and orientation of window areas as well as shade caused by vegetation, buildings, and terrain. It also calculates heating requirements, solar heating contribution and rest heating requirements for every building as well as for the whole planning area

GRAL (Austria) - The Graz Lagrangian model was developed at Graz University of Technology. It is a dispersion model for buoyant plumes from multiple point, line, and tunnel portal sources. It handles flat or complex terrain but has no chemistry or deposition capabilities.

HAVAR (Czech Republic) - A Gaussian plume model integrated with a puff model and a hybrid plume-puff model, developed by the Czech Academy of Sciences, it is intended for routine and/or accidental releases of radio nuclides from single point sources within nuclear power plants. The model includes radioactive plume depletion by dry and wet deposition as well as by radioactive decay. For the decay of some nuclides, the creation of daughter products that then grow into the plume is taken into account.

HYROAD (US Environmental Protection Agency, Office of Air Quality Planning and Standards [OAQPS]) - The Hybrid ROAD way Model integrates three modules that simulate the effects of traffic, emissions and dispersion. It is designed to determine hourly concentrations of carbon monoxide (CO) or other gas-phase pollutants, particulate matter (PM), and air toxins from vehicle emissions at receptor locations that occur within 500 meters of roadway intersections.
download

HYSPLIT (National Oceanic and Atmospheric Administration, Air Resources Laboratory) - The HYbrid Single-Particle Lagrangian Integrated Trajectory model is a new version of a complete system for computing simple air parcel trajectories in complex dispersion and deposition simulations. The result of a joint effort between NOAA and Australia's Bureau of Meteorology, the model has recently been upgraded. New features include improved advection algorithms, updated stability and dispersion equations, a new graphical user interface, and the option to include modules for chemical transformations. Without the additional dispersion modules, HYSPLIT computes the advection of a single pollutant particle, or simply its trajectory.

IBS_AIWAST- A meso-scale climate and dispersion model, Atmospheric Impulse, Heat and Mass Transport– is a numerical climate model that solves the conservation equations for mass, impulse, energy and air mixtures (*e.g.*, humidity and other ingredients) in Eulerian coordinates. The integration can also be done with a coupled system of equations in a coordinate plane following the orography. The coupling considers connections between temperature and humidity, which significantly affect the flow field. The model also considers the reflection of sunlight, the evaporation and condensation of water, and the additional transport of energy and humidity through turbulence. AIWAST works in combination with a surface model., Heat and mass flows can be modulated realistically by using a Neumann function as an edge condition.

IBS_CITY win a three-dimensional prognostic flow and dispersion model appropriate for micro-scale city climates, this model numerically solves the differential equations of impulse, heat, and mass transport. With regard to heat exchange at the borders, adherence conditions are valid on fixed borders and conductive transport disappears; disperse conditions are valid for open borders with convection prevailing. As an edge condition on the upper border, the surface-spread undisturbed wind vector is calculated either from existing data, out of the AKS, or through extrapolation with the logarithmic speed analysis or the Ekman spiral. Considering the interaction between turbulence and friction, convective and conductive transport and the construction, the speed profile is calculated in layers close to the ground Heat balance near the ground is considered. IBS_CITY uses geo-referenced data and interfaces common GI-systems. Emissions are

considered as line, point, or area sources. -loor sweep is replicated by an altitude-dependent relief with an overlying building structure.–**IBS_STÖRFALL** - A micro-scale heavy gas model, IBS_STÖRFALL is a time-dependent model for calculating the spread of heavy gases and vapours. It considers important specifics of heavy gas dispersion, *e.g.*, the ground following dispersion, the influence of temperature when defining the partial pressure gradient, the interaction between the atmosphere and heavy gases and the typical proper motion compared to atmospheric flow. The heavy gas model includes a wind field calculation considering real site structures and construction. The result is a time-dependent presentation of the dispersion rate that can be illustrated in a computer animation.

IBS_VERKEHR is a micro-scale three-dimensional prognostic flow and dispersion model. It numerically solves the differential equations of impulse, heat and mass transport. With regard to heat exchange at the borders, adherence conditions are valid on fixed borders and conductive transport disappears for pollutant transport; disperse conditions are valid for open borders with convection prevailing for pollutants. As an edge condition on the upper border, the surface-spread undisturbed wind vector is calculated either from existing data, out of the AKS, or through extrapolation with the logarithmic speed analysis or the EKMAN spiral. Considering the interaction between turbulence and friction, convective and conductive transport and the construction, the speed profile is calculated in layers close to the ground. IBS_VERKEHR uses geo-referenced data and interfaces with common GI-systems. Traffic emissions are considered as line sources. Floor sweep is replicated by a complex construction on flat terrain.

IFDM (Belgium) - The Immission Frequency Distribution Model, developed at the Flemish Institute for Technological Research(VITO), is a Gaussian dispersion model used for point and area sources dispersing over flat terrain on a local scale. The model includes plume depletion through dry or wet deposition but cannot handle building effects, chemical transformations or complex terrain.

IGEMS: Internet Geographical Exposure Modeling System (US Environmental Protection Agency, Office of Pollution Prevention and Toxics [OPPT]) - IGEMS is a modernization of OPPT's older Graphical Exposure Modeling System and PCGEMS tools. IGEMS brings together in one system

several EPA environmental fate and transport models and some of the environmental data needed to run them. IGEMS includes models and data for ambient air, surface water, soil, and ground water, and makes the models much easier to use than their stand-alone counterparts. IGEMS will have graphics and Geographical Information System (GIS) capabilities for displaying environmental modeling results.

IMMPROG2000 is a Lagrange model for mean conditions. The whole IMMPROG-package consists of the dispersion models IMMPROG-P (point source), IMMPROG-H (line source), and IMMPROG-C (urban canyon), as well as IMMPROG-G(odour model). The point source model IMMPROG-P corresponds to the Gaussian model described by the TA Luft.TSP emission or deposition calculations are also possible. Additionally, IMMPROG-P is able to consider topography as well as inversions. The model also supports calculations of emissions (vertical jets). Calculations for emissions from tunnel portals are also possible. IMMPROG-H largely corresponds to the Hiway-2-Model from the U.S. Environmental Protection Agency, but IMMPROG-H has a better correction of slow wind influence. The model improvement is primarily aligned with NOx and NO2 predication. When calculating the dispersion simulation, IMMPROG-H also considers turbulence caused by traffic. Calculations can be made for roadways on flat terrain or for terrain with small clefts. IMMPROG-C is a line model, which is based on the ―Canyon Plume Box Model (CPBM). It calculates pollutant emissions of inert gases caused by traffic in urban canyons. IMMPROG-C is particularly suitable for areas in inner cities.

INPUFF-U (Romania) - This model was developed by the National Institute of Meteorology and Hydrology in Bucharest, Romania. It is a Gaussian puff model for calculating the dispersion of radio nuclides from passive emission plumes on a local-to-urban scale. It can simulate accidental or continuous releases from stationary or mobile point sources. It includes wet and dry deposition. Building effects, buoyancy effects, chemical reactions and the effects of complex terrain are not included.

ISC3 Long-Term (US Environmental Protection Agency, Office of Air Quality Planning and Standards [OAQPS]) is a steady-state Gaussian plume model that

can be used to assess pollutant concentrations from a wide variety of sources associated with an industrial complex.

<u>download</u>

ISC3 Short-Term (US Environmental Protection Agency, Office of Air Quality Planning and Standards [OAQPS]) is a steady-state Gaussian plume model that can be used to assess pollutant concentrations from a wide variety of sources associated with an industrial complex.

<u>download</u>

ISC-PRIME (US Environmental Protection Agency, Office of Air Quality Planning and Standards [OAQPS]) is a model with building downwash incorporated into the Industrial Source Complex Short-Term Model (ISCST3).

<u>download</u>

IWAIR: Industrial Waste Air Model (US Environmental Protection Agency, Office of Solid Waste) - This model evaluates inhalation risk and estimates whether specific wastes and management practices may pose an unacceptable risk to human health.

<u>download</u>

KALM– This is a drainage flow model that uses the so-called low water equations, simplified forms of the basic stream mechanics equations, which a short calculation time and low storage requirements possible. A differential method is used with a variable number of grid points and values, *i.e.*, topography and land use must be specified at every grid point.–The model may be run on a complex grid in order to consider macro-scale influences at a high resolution in the area of interest–If no cool air reservoir forms, the calculation becomes stationary after 1 h-**KAMM** - The Karlsruher Mesoscale Model was developed by the Meteorologischen Institut in Karlsruhe. It is a non-hydrostatic three-dimensional model that can be assigned to the meso-scale models, with the typical grid from 1to 5 km.

KLIMM - The meso-scale Climate Model Mainz was developed to simulate regional climates (urban heat island, local circulation systems, *etc.*) and pollutant dispersion in regional areas.

LADM is an advanced model developed by Australia's Commonwealth Scientific and Industrial Research Organisation (CSIRO) for simulating the dispersion of buoyant pollution plumes and predicting the photochemical formation of smog over complex terrain on a local-to-regional scale. The model can also handle fumigated plumes (see the books listed in the "Further reading" section for an explanation of these plumes).

LASAT: Lagrangian Simulation of Aerosol Transport - This dispersion model calculates the dispersion of traces substances in the atmosphere by simulating the transport and dispersion of a group of representative substances after random selection. This has several advantages with respect to other models: the accuracy in a range up to a few 100m is higher than the accuracy of classical diffusion equations; a point source is treated exactly as a point source; and the user can choose the number of particles, making it possible to affect the accuracy and speed of the calculations. LASAT is a tool for experts to appraise special dispersion situations. The user can name any number of emissions sources in any number as point, line, area, grid, or volume sources.

LOTOS-EUROS (The Netherlands) - The Long Term Ozone Simulation - European Operational Smog model was developed by the Netherlands National Institute for Public Health and the Environment (RIVM. It is designed to model the dispersion of pollutants such as photo-oxidants, aerosols, heavy metals over all of Europe. It includes simple reaction chemistry as well as wet and dry deposition.

LPDM: Lagrangian Particle Dispersion Model- This model, used by the Deutscher Wetterdienst, is based on the research of Glaab (1986) and Vogel (1986). It considers pollutants as inert, and neglects the effects of gravity, considering a constant deposition velocity. The dispersion is simulated in the same way as with LASAT, based on the calculation of a very large number of representative particle trajectories.

MEMO (Greece) – An Eulerian non-hydrostatic prognostic meso-scale model for wind flow simulations, it was developed by the Aristotle University in Thessaloniki in collaboration with the Universität Karlsruhe. This model is designed to describe atmospheric transport phenomena on a local-to-regional scale

MERCURE (France) is an atmospheric dispersion modelling CFD code developed by Electricité de France (EDF) and distributed by ARIA Technologies, a French company. The code is a version of the CFD software ESTET, developed by EDF's Laboratoire National d'Hydraulique.

METDIA is a regional diagnostic stream flow model that is capable of calculating a stationary wind field over complex terrain on the basis of either wind measurements or a known macro-scale stream. METDIA is a diagnostic model based on the physical principle of mass continuity. It modifies a given initial wind field so the resultant wind field is stationary and free of divergence, and it is used to study the influence of atmospheric stratification, orography, and land use. The Poisson equation in METDIA is solved numerically *via* an L-SOR method in a coordinate system that follows topography. Non-equidistant grid spacing can be chosen in three directions.

METKAT is a drainage flow model based on a special form of the vertical integrated motion equations, the so-called low water equations. The model assumes that cool air layer near the ground is mixed homogeneously. The model calculates the horizontal distribution of the cool air layer depth and horizontal wind under considerations of ground friction, buoyancy, mixing processes at the upper margin of the cool air layer, and the local cool air production. It is also possible to consider the dispersion of emissions near the ground in the cool air layer.

METRAS was developed by the Meteorological Institute of the University of Hamburg in cooperation with the Alfred-Wegener Institutfür Polar- und Meeresforschung in Bremerhaven and the Institutfür Troposphären for schung, Leipzig. Details on this non-hydrostatic three-dimensional meso-scale chemistry, transport and stream flow model.

MIMO is a prognostic micro-scale model that describes air motion near complex building structures. Within MIMO, conservation equations for mass, momentum, and scalar quantities such as potential temperature, turbulent kinetic energy and specific humidity are solved. Non-equidistant grid spacing is allowed in all directions. The numerical calculation is based on second-order discretization applied on a staggered grid. Conservation properties are fully preserved within discrete model equations. Discrete pressure equations are solved with a fast elliptic solver in conjunction with a generalized conjugate gradient method. Advective terms are treated with an FCT scheme. Turbulent diffusion can be described with either a one- or two-equation turbulence model. Similarity theory is applied at roughness height, and Neumann or Dirichlet conditions are applied at lateral boundaries and for scalar quantities. Generalized radiation conditions are also implemented for lateral boundaries.

MISKAM is a sophisticated physical micro-scale climate and dispersion model developed by the Institutfür Physik der Atmosphäre of the University of MainzIt is a three-dimensional non-hydrostatic stream flow and dispersion model that is able to predict wind distribution and emission concentrations with – very high resolution–from roadway level up to larger parts of urban areas. It was initially developed to depict microclimate problems (Eichhorn, 1989) and is now also available in a PC version for emission prediction. MISKAM explicitly treats buildings as right-angled block structures making it possible to realistically model stream flows next to buildings As a basis, MISKAM uses the complete three-dimensional motion equations to simulate stream flow conditions as well as the advection diffusion equation of density-neutral substances for dispersion calculations, considering - sedimentation and deposition as well. Pollutant sources can be represented as any combination of point and line sources within a certain given model area.

MMSOILS (US Environmental Protection Agency, Center for Exposure Assessment Modeling [CEAM]) - The Multimedia Contaminant Fate, Transport, and Exposure Model estimates human exposure and health risk associated with releases of contamination from hazardous waste sites. The methodology consists of a multimedia model that addresses the transport of a chemical in groundwater, surface water, soil erosion, the atmosphere, and accumulation in the food chain.

Human exposure pathways considered in the methodology include: soil ingestion, air inhalation of volatiles and particulates, dermal contact, ingestion of drinking water, consumption of fish, consumption of plants grown in contaminated soil, and consumption of animals grazing on contaminated pasture.
download

MOBILE5.0a_h (US Environmental Protection Agency, Office of Mobile Sources)models highway mobile source emissions.
download

MOBILE5b (US Environmental Protection Agency, Office of Mobile Sources) models highway mobile source emissions and includes the effect of the final reformulated gasoline (RFG) rules on Nox emissions.
download

Mobile6 (US Environmental Protection Agency) - This vehicle emission modeling software determines the relative contribution of transportation sources to air quality.
download

Models-3/CMAQ - The latest version of the Community Multi-scale Air Quality model has state-of-the art capabilities for conducting urban- toregional-scale simulations of multiple air quality issues, including tropo spheric ozone, fine particles, toxins, acid deposition, and visibility degradation.

MODIM (Slovak Republic) - A model for calculating the dispersion of continuous, neutral or buoyant plumes on a local to regional scale, this integrates a Gaussian plume model for single or multiple point and area sources with a numerical model for line sources, street networks and street canyons. It is intended for regulatory and planning purposes.

MUKLIMO - The micro-scale urban climate model MUKLIMO is a two-dimensional, numerical, prognostic grid-point model for calculating atmospheric conditions in the area of block structures. It was developed during 1980-1983 in the framework of the project "Numerische Simulation des Stadtklimas" sponsored by the Umweltbundesamt, and is described in "A micro-scale urban climate

model". The PC version is specially programmed to calculate the dispersion of vehicle exhaust. In contrast to the original version, the PC version is limited to the calculation of wind fields, turbulent exchange coefficients, and pollutant dispersion. However, there are additional program parts that make it possible to model porous buildings as well as forests.

MUKLIMO3 - This model is the three-dimensional version of the original model MUKLIMO.

MUSE (Greece) - A photochemical atmospheric dispersion model developed by Professor Nicolas Moussiopoulos at the Aristotle University of Thessaloniki in Greece, it is intended for the study of photochemical smog formation in urban areas and the assessment of control strategies on a local-to-regional scale. It can simulate dry deposition and the transformation of pollutants can be treated using any suitable chemical reaction mechanism.

NAME -The Numerical Atmospheric-dispersion Modeling Environment is a local-to global-scale model developed by the UK's Met Office. It is used for: the forecasting of air quality, air pollution dispersion, and acid rain; tracking radioactive emissions and volcanic ash discharges; the analysis of accidental air pollutant releases and assisting in emergency response; and long-term environmental impact analysis. It is an integrated model that includes boundary layer dispersion modeling.

Non-road Vehicle and Engine Emission Modeling (US Environmental Protection Agency, Office of Mobile Sources) models non-road vehicle and engine emissions. It is a large file intended for professional mobile source emission modelers, such as state air quality officials and consultants.
download

Non-road Vehicle and Engine Emission Modeling for Tier 2 Proposed Rule (US Environmental Protection Agency, Office of Mobile Sources) models emissions from non-road vehicles. It is a draft model for the Tier 2 Proposed Rule.
download

OBODM By (US Environmental Protection Agency, Office of Air Quality Planning and Standards [OAQPS]) -This model is intended for use in evaluating

the potential air quality impacts of open burning and detonation (OB/OD) of obsolete munitions and solid propellants.
download

OCD (US Environmental Protection Agency, Office of Air Quality Planning and Standards [OAQPS]) - Offshore and Coastal Dispersion Model is a straight-line Gaussian model developed to determine the impact of offshore emissions from point, area, or line sources on the air quality of coastal regions. OCD incorporates overwater plume transport and dispersion as well as changes that occur as the plume crosses the shoreline. Hourly meteorological data are needed from both offshore and onshore locations.
download

OML (Denmark) - A model for dispersion calculations of continuous neutral or buoyant plumes from single or multiple, stationary point, and area sources, this has some simple methods for handling photochemistry (primarily for NO_2) and for handling complex terrain. The model was developed by the National Environmental Research Institute of Denmark, which is a part of Aarhus University. See the OML home page for further reference. **ONM9440** (Austria) - A Gaussian dispersion model for continuous, buoyant plumes from stationary sources for use in flat terrain areas, this includes plume depletion by dry deposition of solid particulates.

OSPM (Denmark) - The Operational Street Pollution Model is a practical street pollution model developed by the Department of Atmospheric Environment at the National Environmental Research Institute of Denmark. For almost 20 years, OSPM has been routinely used in many countries to study traffic pollution, perform analyses of field campaign measurements, study the efficiency of pollution abatement strategies, carry out exposure assessments, and as reference in comparison to other models. OSPM is generally considered to be state-of-the-art in applied street pollution modeling.

OZIPR (US Environmental Protection Agency, Office of Air Quality Planning and Standards [OAQPS]) is a one-dimensional photochemical box model that is an alternative version of the OZIP model dealing with air toxic pollutants.
download

PART5 (Highway Vehicle Particulate Emission Modeling Software) (US Environmental Protection Agency, Office of Mobile Sources)is a particulate emission factor model.
download

Percent View (Lakes Environmental Software) is a utility that generates the percentile concentrations for the results of the air model ISCST3.
download

PLUVUEII (US Environmental Protection Agency, Office of Air Quality Planning and Standards [OAQPS]) is a model used for estimating visual-range reduction and atmospheric discoloration caused by plumes resulting from the emissions of particles, nitrogen oxides, and sulphur oxides from a single source. The model predicts the transport, dispersion, chemical reactions, optical effects and surface deposition of point- or area-source emissions.
download

POLGRAPH (Portugal) - This model was developed at the University of Aveiro in Portugal by Professor Carlos Borrego to evaluate the impact of industrial pollutant releases and for air quality assessments. It is a Gaussian plume dispersion model for continuous, elevated point sources to be used on a local scale over flat or gently rolling terrain.

PROKAS-V (Germany) - A Gaussian dispersion model for evaluating the atmospheric dispersion of air pollutants emitted from vehicular traffic on a road network of line sources on a local scale.

Puff is a volcanic ash-tracking model developed at the University of Alaska Fairbanks. It requires NWP wind field data on a geographic grid covering the area over which ash may be dispersed. Representative ash particles are initiated at the volcano's location and then allowed to advect, diffuse, and settle within the atmosphere. The location of the particles at any time after the eruption can be viewed using the post-processing software included with the model. Output data is in net CDF format and can also be viewed with a variety of software.

PUFF-PLUME is a Gaussian chemical/radionuclide dispersion model that includes wet and dry deposition, real-time input of meteorological observations and forecasts, dose estimates from inhalation and gamma shine, and puff or plume dispersion modes. It is the primary model used for emergency response for the atmospheric release of radioactive materials at the Savannah River Site of the United States Department of Energy. It was first developed by Pacific Northwest National Laboratory (PNNL) in the 1970s.

RADM (France) - The Random-walk Advection and Dispersion Model was developed by ACRI-ST, an independent research and development organization in France. It can model gas plumes and particles (including pollutants with exponential decay or formation rates) from single or multiple stationary, mobile or area sources. Chemical reaction, radioactive decay, deposition, complex terrain, and inversion conditions are accommodated.

REMSAD - The Regional Modeling System for Aerosols and Deposition calculates the concentrations of both inert and chemically reactive pollutants by simulating the atmospheric processes that affect pollutant concentrations over regional scales. It includes processes relevant to regional haze, particulate matter and other airborne pollutants, including soluble acidic components and mercury.

REWIMET-A is a hydrostatic three-layermeso-scale wind field simulation for applications in areas with a horizontal extension between 20 and 200 km; horizontal resolution ranges from 2 to 10 km. The model calculates time-dependent horizontal wind components and potential temperature as well as layer averages. The depth of the mixing layer is predicted; vertical velocity and the Exner function are determined diagnostically. The model considers the extensive stratification of temperature, the horizontal pressure gradient, and surface temperature. The model considers topography (orography and land use as well as inhomogeneous terrain height, roughness, and surface temperature).

RFG Computer Model (Complex Model) (US Environmental Protection Agency, Office of Mobile Sources) models reformulated gasoline (RFG) emissions.
download

RFG Computer Model (Simple Model) (US Environmental Protection Agency, Office of Mobile Sources) models reformulated gasoline (RFG) emissions.
download

RIMPUFF (Denmark) - A local- and regional-scale real-time puff diffusion model developed by the Risø National Laboratory for Sustainable Energy at the Technical University of Denmark. RIMPUFF is an operational emergency response model in use for assisting emergency management organisations dealing with chemical, nuclear, biological, and radiological (CBRN) releases into the atmosphere. RIMPUFF is in operation in several European national emergency centres for preparedness and prediction of nuclear accidental releases (RODOS, EURANOS, ARGOS), chemical gas releases (ARGOS), and also serves as a decision support tool during active combat of airborne transmission of various biological infections.

RTDM3.2 (US Environmental Protection Agency, Office of Air Quality Planning and Standards [OAQPS]) -The Rough Terrain Diffusion Model is a sequential Gaussian plume model designed to estimate ground-level concentrations in rough or flat terrain in the vicinity of one or more co-located point sources.
download

SAFE AIR II (Italy) - The Simulation of Air pollution From Emissions II was developed at the Department of Physics at the University of Genoa to simulate the dispersion of air pollutants above complex terrain at local and regional scales. It can handle point, line, area, and volume sources as well as continuous plumes and puffs. It includes first-order chemical reactions and plume depletion by wet and dry deposition, but it does not include any photochemistry.

Screen View (Lakes Environmental Software)- A user-friendly interface for the US EPA screening model, SCREEN3, this US EPA-approved model can be used to calculate conservative or worst-case estimates of ground level concentrations for a single source. It can model scenarios with simple or complex terrain, with or without building downwash, and give results at discrete or automated distances.
download

SCREEN3 (US Environmental Protection Agency, Office of Air Quality Planning and Standards [OAQPS]) is a single-source Gaussian plume model that provides maximum ground-level concentrations for point, area, flare, and volume sources, as well as concentrations in the cavity zone and concentrations due to inversion break-up and shoreline fumigation. SCREEN3 is a screening version of the ISC3 model.
download

SDM (US Environmental Protection Agency, Office of Air Quality Planning and Standards [OAQPS]) -The Shoreline Dispersion Model is a multiple-point Gaussian dispersion model that can be used to determine ground level concentrations from tall stationary point-source emissions near a shoreline.
download

SEVEX (Belgium) - The SEVesoEXpert model simulates the accidental release of toxic and/or flammable material over flat or complex terrain from multiple pipe and vessel sources or from the evaporation of volatile liquid spill pools. Accidental releases may be continuous, transient or catastrophic. The integrated model can handle denser-than-air gases as well as neutral gases. It does not handle multi-component material, nor does it provide for chemical transformation of releases.

SLAB (US Environmental Protection Agency, Office of Air Quality Planning and Standards [OAQPS]). This model treats denser-than-air releases by solving one-dimensional equations of momentum, conservation of mass, species, and energy, and the equation of state. It handles release scenarios including ground-level and elevated jets, liquid pool evaporation, and instantaneous volume sources.
download

STACKS (The Netherlands) - A Gaussian plume dispersion model for point and area buoyant plumes to be used over flat terrain on a local scale, it includes building effects, NO_2 chemistry and plume depletion by deposition. It is used for environmental impact studies and the evaluation of emission-reduction strategies.

STOER.LAG (Germany) - A dispersion model designed to evaluate accidental releases of hazardous and/or flammable materials from point or area sources in

industrial plants, this model can handle neutral and denser-than-air gases or aerosols from ground-level or elevated sources. The model accommodates building and terrain effects, the evaporation of volatile liquid spill pools, and the combustion or explosion of flammable gas-air mixtures (including the impact of heat and pressure waves caused by a fire or explosion).

SYMOS'97 (Czech Republic)-A model developed by the Czech Hydrometeorological Institute, for dispersion calculations of continuous neutral or buoyant plumes from single or multiple point, area or line sources, it can handle complex terrain and - can also be used to simulate the dispersion of cooling tower plumes.

TAPM - An advanced dispersion model that was developed by Australia's Commonwealth Scientific and Industrial Research Organisation (CSIRO), it is integrated with a pre-processor for providing meteorological data inputs. It can handle multiple pollutants and point, line, area, and volume sources on a local, city, or regional scale. Capabilities include building effects, plume depletion by deposition, and a photochemistry module.

TCAM is a multiphase three-dimensional Eulerian-grid model designed by the ESMA group at the University of Brescia for modeling the dispersion of pollutants at medium scale. Real conditions are idealized in two dimensions: model structures and atmospheric conditions are fixed along the *y*-axis variables depend only on one horizontal coordinate and the vertical coordinate. This assumption is a good approximation for long roadways with uniform margins on both sides, especially when atmospheric stream flow towards the roadway occurs at small angles; however, the influence of intersections is not considered. framework of the model, *i.e.*, grid structure, height and contours of obstacles, location and amount of emissions of sources, wind speed, *etc.*, are defined by the user in an input file.

TSCREEN (US Environmental Protection Agency, Office of Air Quality Planning and Standards [OAQPS])- The Toxics Screening Model is a Gaussian model for analyzing toxic emissions and their subsequent dispersion from one of many different types of possible releases for superfund sites. It contains 3 models: SCREEN3, PUFF, and RVD (Relief Valve Discharge).
download

UAM-V - The Urban Air shed Model was a pioneering effort in photochemical air quality modeling in the early 1970s and has been used widely for air quality studies focusing on ozone.

UDM - The Urban Dispersion Model is a Gaussian-puff-based model for predicting the dispersion of atmospheric pollutants in the range of 10m to 25 km within the urban environment. It was developed by the Defense Science and Technology Laboratory for the UK Ministry of Defence. It handles instantaneous, continuous, and pool releases, and can model gases, particulates, and liquids. The model has a three-regime structure: single building (area density < 5%), urban array (area density > 5%), and open. The model can be coupled with the US SCIPUFF model to replace the open regime and extend the model's prediction range.

UDM-FMI (Finland) - This model was developed by the Finnish Meteorological Institute (FMI) as an integrated Gaussian urban-scale model intended for regulatory pollution control. It handles multiple point, line, area, and volume sources, and it includes chemical transformations (for NO_2), wet and dry deposition (for SO_2), and downwash phenomena, but does not include building effects.

VALLEY (US Environmental Protection Agency, Office of Air Quality Planning and Standards [OAQPS])is a steady-state, complex terrain, univariate Gaussian plume dispersion algorithm designed for estimating either 24-hour or annual concentrations resulting from emissions from up to 50 point and area sources. download

VDI 3782 Bl.1 is a Gaussian dispersion model for air quality policies that simulates dilution and transmission of emitted substances *via* the statistical theory of turbulence. Emission data and meteorological parameters are given as input Scattering information was obtained in experimental dispersion investigations, making this an empirical dispersion model with relatively short calculation times. The model is particularly used to determine emissions, statistical indicators such as averages and percentiles.

VDI 3945 Bl.1- In contrast to the Gaussian plume model (VDI 3782), the Gaussian cloud model (puff model) is a case model that describes the temporal

course of concentration distribution. The model assumes that pollution caused by a point source forms a puff that enlarges with time and moves with the wind, an assumption with the advantage - that the emission need not be constant.

VISCREEN (US Environmental Protection Agency, Office of Air Quality Planning and Standards [OAQPS]) calculates the potential impact of a plume of specified emissions for specific transport and dispersion conditions.
download

WINMISKAM is a Windows version of the micro-scale climate and dispersion model MISKAM. In addition to the functions of MISKAM, it is also possible to calculate statistical indicators of air pollution.

List of Weather Databases

1. **WorldClimate.com**:

   Contains over 85,000 records of world climate data (historical weather averages) from a wide range of sources
   Web site: http://www.worldclimate.com/

2. **NCDC:** National Climatic Data Center.

   NCDC is the world's largest active archive of weather data. NCDC produces numerous climate publications and responds to data requests from all over the world.
   Web Site: http://www.ncdc.noaa.gov/oa/ncdc.html

3. **WMO:** The World Meteorological Organization (WMO) is a specialized agency of the United Nations. It is the UN's authoritative voice on the state and behaviour of Earth's atmosphere, its interaction with the oceans, the climate it produces, and the resulting distribution of water resources.
   Web Site: http://www.wmo.int

4. **Climate-Charts:** Climate data and sunrise/sunset displayed in charts and tables for 149 countries and regions and more than 12,000 specific locations.
   Web Site: http://www.climate-charts.com/

5. **WeatherBase:** Travel weather, climate averages, forecasts, current conditions and norms for 26,939 cities worldwide. Web Site: http://www.weatherbase.com/

6. **ClimWat:** Climwat is a climatic database to be used in combination with the computer program CROPWAT. It includes data from a total of 3262 meteorological stations from 144 countries. FAO Natural Resources and Environment.
   Web Site:http://www.fao.org/nr/water/infores_databases.html

7. **WeatherOnline:** Weather around the world.
   Web Site:http://www.weatheronline.co.uk/

8. **Climate Change Knowledge Portal:** The Climate Change Knowledge Portal (CCKP) Beta is a central hub of information, data and reports about climate change around the world. Here you can query, map, compare, chart and summarize key climate and climate-related information.
   Website: http://sdwebx.worldbank.org/climateportal/index.cfm

9. **IRI/LDEO Climate Data Library:** The IRI/LDEO Climate Data Library contains over 300 datasets from a variety of earth science disciplines and climate-related topics. It is a powerful tool that offers the following capabilities:

   - Access any number of datasets;

   - Create analyses of data ranging from simple averaging to more advanced EOF analyses using the Ingrid Data Analysis Language;

   - Monitor present climate conditions with maps and analyses in the Map Room;

   - Create visual representations of data, including animations;

   - Download data in a variety of commonly-used formats, including GIS-compatible formats.

   Website: http://iridl.ldeo.columbia.edu/

10. **The Federal Ministry of Transport, Building and Urban Development (Germany):** The Deutscher Wetterdienst is a public institution with partial legal capacity under the Federal Ministry of Transport, Building and Urban Development.
    Website: http://www.dwd.de

11. **UNDP Climate Change Country Profiles:** These country-level climate data summaries are intended to address the climate change information

gap for developing countries by making use of existing climate data to generate a series of country-level studies of climate observations and multi-model projections made available through the WCRP CMIP3.
Website: http://www.geog.ox.ac.uk

12. **Environmental Data Explorer**: The Environmental Data Explorer is the authoritative source for data sets used by UNEP and its partners in the Global Environment Outlook (GEO) report and other integrated environment assessments. Its online database holds more than 500 different variables, as national, sub-regional, regional, and global statistics or as geospatial data sets (maps), covering themes like freshwater, population, forests, emissions, climate, disasters, health, and GDP. Display them on-the-fly as maps, graphs, data tables or download the data in different formats.
Website: http://geodata.grid.unep.ch/

MISCELLANEOUS

13. **ClimateData.eu:** Climate database for Europe and Africa.
Web Site: http://www.climatedata.eu/

14. **CliFlo**: Web system providing access to New Zealand's National Climate Database.
Web Site: http://cliflo.niwa.co.nz/

15. **Canadian National Climate Data and Information Archive:** Locate climate data for many Canadian cities using the interactive map of Canada.
Web Site: http://www.climate.weatheroffice.gc.ca

16. **US Climate data:** Climate database for the U.S.
WebSite: http://www.usclimatedata.com/

17. **SERVIR:** Regional visualization and monitoring system for Mesoamerica.
Website: http://www.servir.net

Index

A

Advection: 25-27-42-55-77-81-105-106-113-159-162-193-196-207
Advection-diffusion equation: 159-165-166-167-170-202
AERMOD: 88-94-142-143-144-145-150-185-186
Aerogenerator: 174-175-176-181
AERSCREEN: -142-147
air pollution modeling: 114-134
air quality management: 154-185
Albedo: 3-37-145
Analytical solutions: 153-158
atmospheric boundary layer: 3-24-110-120-122-129-145-153-160-192
atmospheric dispersion: 49-112-129-154-162-188-189-190-192-193-194-201-204-206
atmospheric downwash: 134
atmospheric stability: 3-14-21-34-49-99-112-116-135-157-159-193
Atmospheric Temperature: 124-174-183
atmospheric turbulence: 18-26-136-153-174

B

baroclinic condition: 42-50-56
barotropic condition: 42-50-52
Boundary Conditions: 48-51-71-73-78-158-160-162-163-167-170
Bowen gradient Richardson number: 3
Box Model: 112-136-191-198-205
buoyancy frequency: 17

C

CALPUFF: 142-147-150-189
Coast valley breeze: 57
coastal breeze: 116
coastal valleys: 127

P

Pasquill classification 112
Planetary Boundary Layer 79-115-130-144-183-186
Plume fumigation 139-148-150-193
pollutant concentration 92-95-135-138-140-143-144-154-163-190
potential temperature 14-18-20-29-48-54-77-80-114-117-119-202-207
Prognostic methods 111

R

raob data 70
RASS 110-127
refractivity index 110
Remote sensing 122-129-174-182
Richardson number 117
Rossby number 44-47

S

Scattering term 125
s-coordinate system 42
Screening Models 142
Showalter Index 21-23
signal-to-noise ratio 110
Snodar 183
Sodar calibration 175
Sodar 127-174-176-179
Spatial Discretization 57-77
speed patterns 176
Stable Boundary Layer 27-32-111-113-139-144
Surface Energy Budget 24
synoptic winds 116

T

Thermal Bubble 180